RADIATION AND ENERGY BUDGETS OF ALPINE TUNDRA, SCOUT MOUNTAIN, SOUTHERN BRITISH COLUMBIA, CANADA

by

Ian Robert Saunders

B.Sc. (Hons), University of East Anglia, 1981

M.Sc., Simon Fraser University, 1985

THESIS SUBMITTED IN PARTIAL FULFILLMENT OF

THE REQUIREMENTS FOR THE DEGREE OF

DOCTOR OF PHILOSOPHY

in the Department

of

Geography

SIMON FRASER UNIVERSITY

June 1990

APPROVAL

Name: Ian Robert Saunders

Degree: Doctor of Philosophy

Title of Thesis: Radiation and energy budgets of alpine tundra, Scout Mountain, southern British Columbia,Canada

Examining Committee:

Chairman: R. Hayter
Professor

W.G. Bailey
Associate Professor
Senior Supervisor

R.D. Moore
Assistant Professor

Dr. I. Hutchinson
Associate Professor
Department of Geography
Simon Fraser University

W.R. Rouse
Professor
External Examiner
Department of Geography
McMaster University

Date Approved: June 11, 1990

PARTIAL COPYRIGHT LICENSE

I hereby grant to Simon Fraser University the right to lend my thesis, project or extended essay (the title of which is shown below) to users of the Simon Fraser University Library, and to make partial or single copies only for such users or in response to a request from the library of any other university, or other educational institution, on its own behalf or for one of its users. I further agree that permission for multiple copying of this work for scholarly purposes may be granted by me or the Dean of Graduate Studies. It is understood that copying or publication of this work for financial gain shall not be allowed without my written permission.

Title of Thesis/Project/Extended Essay

Radiation and energy budgets of alpine tundra, Scout Mountain, southern British Columbia, Canada

Author:

(signature)

Ian Saunders

(name)

August 8, 1990

(date)

ABSTRACT

Two seasons of radiation and energy budget measurements from October 1986 to July 1987 and April to May 1988 at Scout Mountain, southern British Columbia, Canada, encompassed a broad range of atmospheric and surface conditions. Snow cover exerted a strong influence on energy and mass transfers at all time scales considered. In winter and early spring, radiation transfers were strongly suppressed by the high albedo and limiting surface temperatures. In late spring and summer, atmospheric transmissivity generally governed the behaviour of the radiation budget. Atmospheric longwave radiation for cloudy and cloudless skies was modelled using several published equations. Two variants of the Stefan–Boltzmann equation gave reliable estimates of both atmospheric and terrestrial longwave radiation. Net radiation was modelled using flux-by-flux and empirical methods.

Energy budgets displayed a wide range of regimes consequent on the surface energy and moisture availability. For all days with a snow-free surface, the mean Bowen ratio was about 1.00. Both energy- and moisture-limiting evaporation regimes, as defined by the McNaughton–Jarvis coupling coefficient, occurred at hourly and daily timescales. The tundra surface dessicated rapidly due to the efficient drainage, limited soil moisture storage capacity and the influence of quick-drying rock surfaces. Thus it was the frequency, and not the magnitude, of precipitation which was of greater importance to maintaining evaporation. Hourly surface resistances, derived by residual from the Penman–Monteith combination model, demonstrated the lack of efficiency in the transfer of subsurface moisture to the atmosphere during periods of dessication. Sensible and latent heat flux modelling included eddy correlation, Bowen ratio–energy budget (BREB), Ohm's Law, aerodynamic and Priestley–Taylor methods. The use of eddy correlation sensible heat measurements was found to be a superior determinant of the evaporative flux. From an operational perspective, the simpler methods demonstrated promising performances. In this respect, the Ohm's Law (for sensible heat) and Priestley–Taylor (for latent heat) models are worthy of further investigation. Future research needs to address the difficulty in surface parameterization in alpine environments, particularly moisture availability and temperature.

For Brian

ACKNOWLEDGEMENTS

I wish to thank all members of my examining committee for their thoughts and comments so generously given. These fine people are: Bill Bailey, Dan Moore, Ian Hutchinson and Wayne Rouse. In particular, as my senior supervisor Bill provided superlative support throughout, and I will always be in his debt (which is just the way he likes it). The dedication to Brian Sagar reflects my gratitude to him for his inputs to my work, and I only wish I was able to offer my thanks in person.

Field assistance *par excellence* was provided by Young Jimmy Bowers, with contributions from Susan Smythe and Catherine Boniface during the final shutdown. Susan also performed some useful plant identifications. A great deal of moral support came from Lesley Cerny, Elisabeth Rodewald and Betty Bernoth. A great deal of alimentary support came from the Smythe family, Achsah, Royle and Susan. Also, Ted Weick tells me that he was indispensable to my research.

Permission to work in Catherdral Provincial Park was granted by the B.C. Ministry of Environment and Parks, with Harold Schmidt being especially helpful. Accommodation and transport within the park was arranged with Cathedral Lakes Resort, and in particular the assistance provided by Tom Fleet and John Murai is gratefully acknowledged.

Financial assistance for the work was largely from NSERC Operating Grant A2614 (to W. G. Bailey). Further funding through Simon Fraser University scholarships and fellowships was invaluable. In particular, the Bert Henry Memorial Graduate Scholarship enabled a thorough search for a suitable field site to be undertaken, and the George and Ada Isabelle Steele Scholarship was instrumental in financing the second, 1988, fieldwork session.

TABLE OF CONTENTS

LIST OF TABLES

LIST OF FIGURES

CHAPTER I

INTRODUCTION

In a recent review of micro- and mesoclimatology, Smithson (1989) reported mountain environments as being popular for meteorology and climatology research. The increasing interest in mountain environments is reflected by the recent growth of research activity in all geographical disciplines (Slaymaker, 1983 and 1984; Ives, 1985 and 1986). The surface transfers of radiation, energy and mass are explicitly related and of importance to climatic, hydrologic, geomorphologic and biologic processes. The measurement and modelling of radiation and energy budgets is therefore of value for a wide range of applications. The fact remains, however, that the physical climatology of alpine environments is relatively poorly known, especially with regard to the controlling processes. Even after more than a century of global solar radiation measurements from alpine locations in Europe, little effort has been made to determine the other components of the radiation budget (Müller, 1985).

Two decades ago, very little was known about energy budgets in mountainous environments, especially in non-glacierized basins. Mountain climate research tended to be focussed on larger scale problems such as local winds and mesoscale airflow, or changes in temperature and precipitation with altitude (Flohn, 1974; Barry, 1981). In North America, there has been minimal alpine radiation and energy budget research in alpine terrain, in spite of the importance of the Western Cordillera to the hydrometeorology of the whole continent. In Canada, the need for mountain research programs has been recognized (Eley, 1987) but little action has been taken.

Most mountain research in North America has focused on meso- and macroscale airflow modelling with little regard for the surface-atmosphere interactions. The heterogeneity and complex topography of mountain surfaces dictate that these larger scale approaches are of limited utility when attempting to understand physical climatology at the surface. The physically-based approaches employed in microscale heat and mass transfer measurement explicitly recognize the controlling processes.

The term "alpine" has been used to define various mountain environments. Löve (1970) suggested that it be reserved for treeless terrain above the krummholz zone and this

recommendation is followed here. Climatologically, the alpine environment is one of the least understood on earth. Despite many observations of global solar radiation from mountains around the world, details of surface radiation, energy and mass transfers have until recently remained sketchy. Field experiments in Europe and North America during the last decade have begun to elucidate some aspects of the physical climatology of alpine tundra, but as yet there is insufficient information to categorically define an alpine tundra climatology.

Several reasons may account for this apparent lack of research activity in mountainous regions. Not least of these are the logistical problems encountered, including access to the alpine zone, maintenance of instruments in extreme weather conditions and the attendant difficulties for personnel. Recent developments in climatological equipment and computerized data aquisition systems have greatly facilitated remote data collection, and this is reflected by the increase in research efforts in mountainous regions. Except for the European Alps, most alpine areas of the world tend to be remote, and require experiments to be self-contained.

Similar arguments could be applied to Arctic research, and yet there is an abundance of studies from northern environments. In Canada, the impetus for Arctic research was doubtlessly enhanced by the financial inputs resulting from the petroleum industry's activities in the North. More recently, emphasis has been placed on northern studies as a result of the increasing awareness and attention accorded to native peoples by federal governments.

Mountainous regions are increasingly a focus of attention for geographers, as exemplified by the publication of journals and books in the field (Ives, 1986). In the atmospheric sciences, complex-terrain issues have been addressed in a number of large experiments from mountain ranges in Europe and North America, most recently at Brush Creek, Colorado (Clements *et al.*, 1989). These experiments have been important in focusing research efforts to such problems as airflow modelling in mountain valleys and plume dispersion, but there are no parallels to this type of experiment in the field of mountain microclimatology.

OVERVIEW OF THE PRESENT STUDY

Objectives

In light of the opening comments, the scope for research in alpine climatology can clearly be seen to be broad. To date, research in the physical climatology of alpine environments has focused on snow and ice surfaces. For a more complete understanding of the mountain environment, consideration of tundra, rock and meadow surfaces is required.

The objectives of the present study, therefore, were to describe the radiation, energy and mass transfers of an alpine tundra surface for the full range of seasonal conditions and to examine the utility of both physically-based and empirical modelling. The approach taken was to include descriptive analyses of radiation and energy transfers which included explicit consideration of the controls. This was complemented by modelling of selected budget parameters, with emphasis placed on models with simple data requirements in recognition of the difficulty in maintaining instruments in mountain environments.

The value of modelling lies in the dual abilities of models to contribute to interpretations of relevant phenomena (as exemplified by the use of the Penman-Monteith combination model to derive surface resistance) and to enable the behaviour of those phenomena to be predicted. (for example, to derive radiation and energy fluxes from ambient atmospheric and surface conditions).

Modelling experiments were biased towards the evaluation of physically-based approaches to flux estimation. The value of physically-based models lies in their ability to account for atmospheric and surface controls on climatic parameters. In concluding a critique of hydrological modelling, Beven (1989) proposed that the combination of field measurements and physically based models offers a sound approach to examining real-world processes. This was adopted for the modelling of turbulent heat fluxes, but not the longwave and net radiation fluxes.

Thesis Organization

Chapters II and III are general reviews of alpine climate research. Chapter IV describes radiation budgets at the study site. Modelling of longwave radiation and net radiation is covered in Chapters V and VI respectively. Chapter VII describes the energy budget and is followed by two chapters devoted to turbulent heat flux modelling (Chapter VIII: sensible heat; Chapter IX: latent heat). The final chapter summarizes the salient conclusions and contributions of the work, and examines possible future research directions.

The Field Site

Data were derived exclusively from Scout Mountain in the Okanagan Range of the eastern Cascade Mountains (49° 05' N, 120° 12' W, Figures 1.1 and 1.2). The site was at 2350 m above mean sea level (a.m.s.l.), which is about 200 m above the local forest line. Geologically, Scout Mountain consists of Princeton Basalt of Tertiary age underlain by the Jurassic plutonic Lakeview Granodiorite (Rice, 1947; Melcon, 1975). At the field site, only the basalt is in evidence at the surface. The area was covered by glacial ice up to an elevation of approximately 2600 m a.m.s.l. during the Wisconsinan glaciations of the late Pleistocene epoch.

The surface of the field site is a 1–2° slope facing southwest and consists of sorted patterned ground typical of periglacial environments (Figure 1.2). The surface microrelief includes stone polygons of 2 – 3 m diameter with cores of vegetated soils (Figure 1.3). The polygons themselves support no well developed vegetation or soil, and many consist of open–framework boulders. The presence of lichens only on the upper surfaces of the rocks in the polygons on Scout Mountain suggests that the patterned ground is inactive.

Scout Mountain lies within the drainage basin of the Ashnola River, which drains into the Similkameen River and ultimately into the Columbia River in Washington State. The hydrologic regime of the area is characterized by its position in the rain shadow of the coastal mountain ranges. In the alpine areas much of the precipitation falls as snow, and rainfall is confined to summer months. The combination of the strong winds and cold, dry winter snowfalls dictate that most snow is quickly removed from the tundras in the Okanagan Range and deposited on leeward slopes (Figure 1.4).

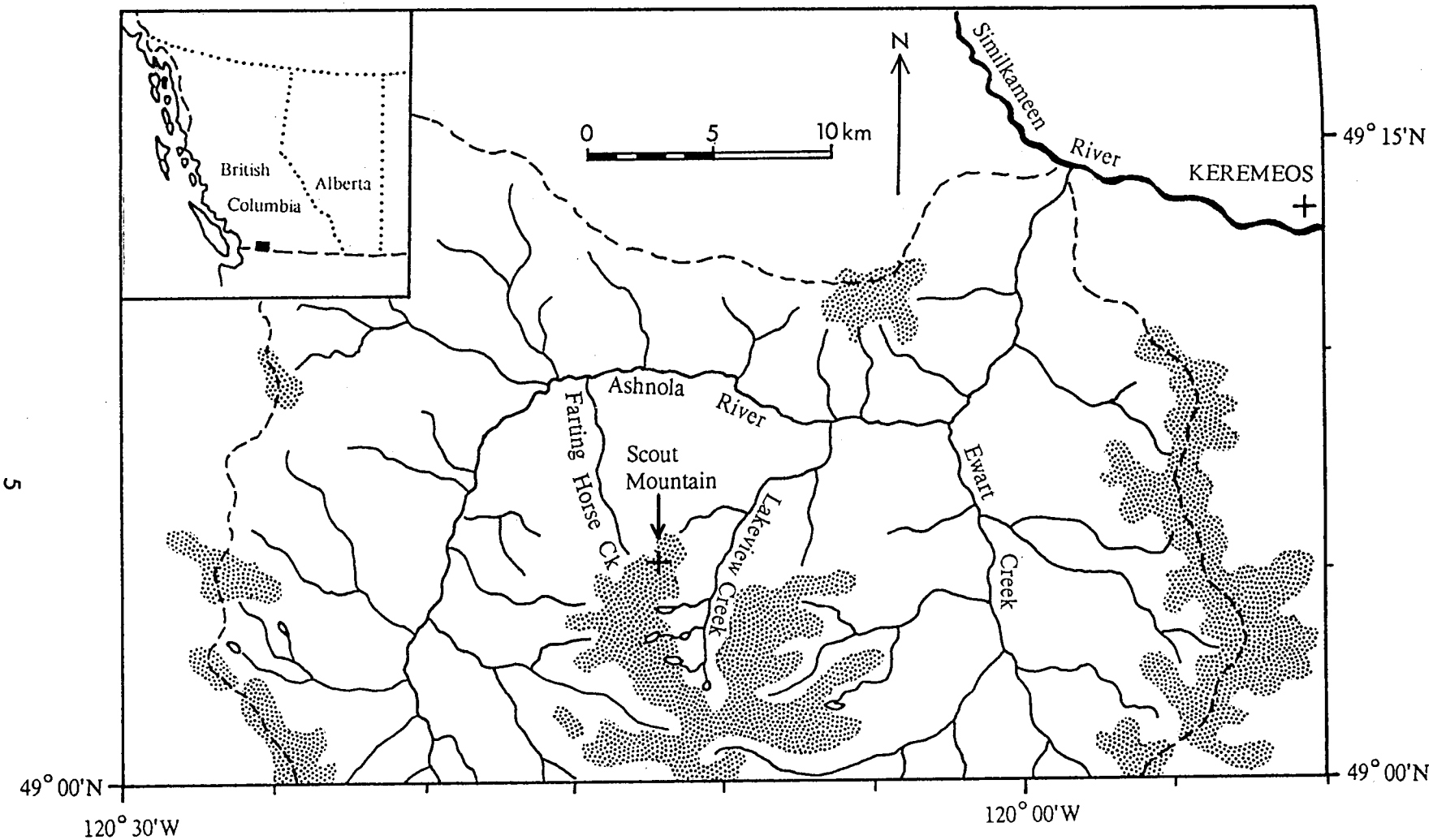

Figure 1.1. Location map showing western Canada (inset), Ashnola River basin north of 49° N and the study site at Scout Mountain. Shaded areas denote land above treeline.

Figure 1.2. View of Scout Mountain field site from the north, June 1987.

Figure 1.3. Close-up view of the tundra surface immediately west of the field site, July 1987.

Figure 1.4. View of Scout Mountain field site from the northwest, February 1987.

There is no runoff nor permanent standing water at the site. One permanent pond and several ephemeral ponds (all fed exclusively by groundwater or throughflow) occur to the south, and are associated with the basalt–granodiorite contact. Several springs at the base of Scout Mountain feed into small distributaries (e.g. Farting Horse Creek, Lakeview Creek) which ultimately feed the Ashnola River. The nearest operational river gauging station to the field site, at the Ashnola–Similkameen confluence 23 km distant, records low flows in the fall–winter season and peak floods in May or June.

The soil at the field site belongs to the Apex Series of Orthic Sombric Brunisols (Green and Lord, 1979). A compact hummocky turf lies above an organic–rich A horizon 50–100 mm in depth. Most of the grasses, sedges and flowers grow on the hummocks. Below the A horizon is 0.5 – 1.0 m of sandy mineral material with many rock fragments entrained. Rocks beneath this layer resisted penetration. Several bedrock outcrops occur on the sides of Scout Mountain, suggesting that the surficial material is not deep.

The vegetation at the site is characterized by *Carex scirpoidea* communities as described by Douglas and Bliss (1977). Alpine flowers bloom in late June to early July at Scout Mountain The most prominent flowering plants are Late Yellow Locoweed (*Oxytropis campestris* (L.) DC) and Cinquefoil (*Potentilla sp.*). Most vegetation was less than 100 mm in height. A detailed examination of the alpine flora of Lakeview Mountain, which lies 5 km to the southeast of Scout Mountain, is reported by Ratcliffe and Turkington (1987).

Surface cover at Scout Mountain was assessed through a systematic point survey along eight 200 m transects radiating from the microclimate site along the points of the compass. Vegetated areas bounded by stone polygons accounted for 43% of the surface area, 21% was occupied by the stone polygons themselves, core–polygon boundaries accounted for 21% of the points and the remaining 15% were unclassified. With regard to actual surface type, 23% was unvegetated rock, 29% comprised grass–sedge communities, 25% was mat plants and the remaining 23% comprised some combination. Lichens occured throughout the site regardless of specific surface type.

Weather Conditions During the Field Seasons

To gauge the temporal representativeness of the Scout Mountain data, climatological data from local weather stations is presented in Tables 1.1 and 1.2. Based upon the record at Keremeos (Figure 1.1), temperatures in late 1986 were about normal. Winter and spring of 1987 were about 2°C warmer than normal. June and July 1987 were again about normal. A similar pattern occurred in 1988, with March and April about 1°C warmer than normal, and May 0.5°C cooler.

Winter snowfall in 1987 was substantially less than normal in the Similkameen basin, and the warm spring temperatures brought about an early depletion of the snowpack. In 1988, a dry, mild winter was followed by a stormy spring which resulted in above-average precipitation in the Similkameen basin. Despite this, the accumulated snowpack remained insubstantial.

In summary, therefore conditions during both fieldwork periods at Scout Mountain were generally warmer and drier than normal. The data collected, however, were derived from a wide range of atmospheric and surface conditions.

Table 1.1. Monthly mean temperature from Keremeos, Mount Kobau and Scout Mountain.

Year	J	F	M	A	M	J	J	A	S	O	N	D	Year
Keremeos[1]													
1951–80	-3.4	1.0	5.0	10.0	14.7	18.2	21.6	20.9	16.4	9.7	2.8	-1.5	9.6
1986	-0.3	-0.3	7.7	8.9	14.5	19.3	19.0	23.1	14.0	10.4	2.1	-1.3	9.8
1987	-1.5	3.0	7.2	12.6	15.3	20.7	21.1	20.5	18.4	10.8	5.1	-1.3	11.0
1988	-3.7	1.5	6.0	11.2	14.2	17.7	21.2	20.3	16.2	11.9	3.6	-2.0	9.8
Scout Mountain													
1986											-7.4	-6.1	
1987	-7.7	-7.1	-6.0	-1.8	1.7	8.1	7.3						
1988				-2.3	2.5								
Mount Kobau[2]													
1951–80	-8.5	-6.0	-5.4	-1.3	4.1	8.2	12.2	12.1	7.8	2.2	-4.6	-7.6	1.1

1. Keremeos is 30 km northeast of Scout Mountain at 430 m amsl.
2. Mount Kobau is 40 km east of Scout Mountain at 1862 m amsl. No climate data for 1986–88 was recorded at this station.
Source of data: Environment Canada, Atmospheric Environment Service

Table 1.2. Monthly snow course data from the Similkameen River basin in 1986–88, with 1935–85 normals.

	Feb 1	Mar 1	Apr 1	May 1	May 15	Jun 1
Mount Kobau[1]						
1935–85	220	271	327	339	269	126
1986	155	219	260	330	336	144
1987	147	199	248	221	0	0
1988	225	239	284	236	154	6
Lost Horse Mountain[2]						
1935–85	166	205	242	261	229	102
1986	149	195	229	280	306	110
1987	110	143	173	94	4	0
1988	74	92	160	136	67	6

1. Mount Kobau snow course is 40 km west of Scout Mountain at 1810 m amsl
2. Lost Horse Mountain snow course is 20 km north of Scout Mountain at 1920 m amsl.
All values are mm water equivalent.
Source of data: British Columbia Ministry of Environment, Snow Survey Bulletin

CHAPTER II

REVIEW OF RADIATION BUDGET RESEARCH IN ALPINE ENVIRONMENTS

INTRODUCTION

Relatively little research has been directed to radiation and energy budgets of alpine environments (Barry, 1981; Müller, 1985). Most work has concentrated on snow and ice surfaces, and has been glaciological or hydrological in purpose. This review considers the state of knowledge of alpine radiation budget research from a North American perspective and focusses upon tundra surfaces. Previous reviews of alpine climatology by Karrasch (1973), Barry (1981) and Müller (1985). contained strong European biases and concentrated more on snow/ice surfaces. In North America, the combination of relatively recent (compared to Europe) colonization and the problems in accessing the alpine zone (most of which remains remote wilderness) have limited the research productivity.

THEORETICAL BACKGROUND

The driving force behind radiation transfers at the earth's surface is the input of solar radiation. At any given location this is a function of latitude, time of day, time of year and the solar constant. Atmospheric attenuation of solar radiation is achieved by scattering, reflection and absorption by constituent gases, water vapour, particulate matter and clouds. The resulting irradiance at the earth's surface, the global solar radiation ($K\downarrow$), depends upon the atmospheric transmissivity (t) and the extraterrestrial radiation (K_{EX})

$$K\downarrow = K_{EX} t \ . \qquad (2.1)$$

Surface absorption of solar radiation (K^*) depends upon the albedo (α)

$$K^* = K\downarrow (1-\alpha) = K\downarrow - K\uparrow \qquad (2.2)$$

where $K\uparrow$ is the reflected solar radiation flux. Numerous global solar radiation models have been developed. Calculating the direct-beam irradiance for any slope is essentially a geometrical problem and several algorithms have been developed (e.g. Garnier and Ohmura, 1968; Isard, 1983). The diffuse-beam component of solar radiation is harder to model

because cloud cover is problematic and assumptions of isotropy are invalid. Recent developments in anisotropic modelling circumvent these problematic assumptions (Hay and McKay, 1985). The potential to model the solar radiation in mountainous regions is therefore available, but few complete studies exist. Direct-beam models for mountains have been reported by Swift (1976), Dozier (1980), Munro and Young (1982) and Isard (1986). Only Dozier modelled diffuse-beam radiation.

The longwave radiation budget comprises an atmospheric ($L\downarrow$) and a terrestrial ($L\uparrow$) component

$$L^* = L\downarrow - L\uparrow = L\downarrow - [\epsilon_0 \sigma T^4 + (1-\epsilon_0) L\downarrow] \qquad (2.3)$$

where L^* is net longwave radiation, ϵ_0 is the surface emissivity, σ is the Stefan-Boltzmann constant and T_0 is surface temperature. In reality, most natural surfaces have emissivities close to unity and therefore $(1-\epsilon_0) L\downarrow$ becomes a negligible term.

Emissivity does vary with surface type, but is conservative. For tundra, $\epsilon_0 = 0.90$–0.99 and for grass, $\epsilon_0 = 0.90$–0.95 (Oke, 1987). Snow and ice emissivities exhibit a wider range, but measurements suggest that generally they are close to unity: $\epsilon_0 = 0.94$–0.99 for snow and $\epsilon_0 = 0.97$ for ice (Warren, 1982; Price and Petzold, 1984; Müller, 1985). Snow emissivity is a very stable property, being insensitive to changes in grain size, impurities, depth, density or liquid water content.

In attempting to avoid the difficulties in measuring $L\downarrow$, several empirical methods have been developed which use standard screen-level climate data. For cloudless skies, commonly employed methods are those of Brunt (1932), Swinbank (1963), Idso and Jackson (1969), Brutsaert (1975) and Idso (1981). The Swinbank and Idso-Jackson models require only air temperature (T). The remaining models require vapour pressure (e) to be measured. None of these models were developed from specifically alpine data, although those of Idso and Jackson (1969) and Idso (1981) included cold-temperature data. Current longwave radiation research in alpine environments has not conclusively validated the use of any of these models. Problems have included the strong surface gradients of temperature and vapour pressure which destroy the representativeness of screen-level measurements (LeDrew, 1975a), and the presence of temperature inversions found over alpine snow and ice surfaces. Some

of the models do not perform well below 0°C (Aase and Idso, 1978), which is an important consideration in high mountains where freezing temperatures are common.

The complete radiation budget equation sums the solar and longwave radiation exchanges

$$Q^* = K^* + L^* = (K\downarrow - K\uparrow) + (L\downarrow - L\uparrow) \qquad (2.4)$$

where Q^* is net radiation absorbed (when positive) or lost (when negative) at the surface. Longwave radiation exchanges are diurnally less variable than solar, so changes in Q^* are predominantly controlled by $K\downarrow$. The exception to this lies in the case of highly reflective surfaces and for surfaces with changing albedo. In these cases using K^* rather than $K\downarrow$ should improve correlation (e.g. Wagner, 1980), but this approach is statistically invalid, because the two are not fully independent. Empirical relations between Q^* and $K\downarrow$ have been developed mostly for grass or agricultural crops (Davies, 1967; Fritschen, 1967; Gay, 1971) and are useful because Q^* is measured at far fewer locations than $K\downarrow$. Comparable alpine data have been presented by Terjung *et al.* (1969a) and Bailey *et al.* (1989). There are concerns regarding the use of $Q^* = f(K\downarrow)$ models with respect to season and latitude. At times of low solar irradiance, either in mid-latitude winters or in high latitudes, the control of solar radiation in determining net radiation decreases, and at sufficiently low solar radiation levels $Q^* = f(K\downarrow)$ models become unreliable.

RADIATION MEASUREMENTS IN ALPINE ENVIRONMENTS

Alpine environments are often characterized by heterogeneous surfaces complicated by an infinity of slope angle-azimuth combinations. In a review of alpine microclimate research, the surface controls on climate inherent in radiation and energy budgets dictate that data need to be stratified by surface type to render intercomparisons realistic. The limited number of alpine microclimate studies suggest that categories must be broadly defined. In this review, data includes both snow-free and snow/ice surfaces. Snow-free surfaces include meadow, tundra, blockfields ("*felsenmeer*") and moraines. Meadows are predominantly grassy, and in many cases are subalpine rather than strictly alpine. Many meadow sites in Europe have been disturbed by grazing and cultivation. Tundra includes those surfaces with sparse

vegetation cover of lichens, mosses and some vascular plants, and is characteristically rocky.

The field measurement of radiation budget components requires that several site criteria be met before theory is applied. Unless the object is to determine terrain effects on the radiation budget, the ideal site is one with surface homogeneity and a minimum of obstructions to the atmospheric hemisphere. It is typically difficult to satisfy both requirements in mountainous regions. Some mountain radiation studies have focussed on the modifications to the radiation budget induced by surrounding terrain (Ohmura, 1970; Marcus *et al.*, 1981; Olyphant, 1986a; Marks and Dozier, 1979).

Measurement of all the radiation budget components is generally straightforward when employing radiometers. Discussions of instrumentation can be found in Latimer (1972), Szeicz (1975), Oke (1987) and Walton (1982). Errors in direct measurement tend to be small (within ±10%) but increase when residuals are involved.

Solar Radiation

The majority of radiation budget work undertaken in alpine environments has been accomplished in the European Alps. Many of the early radiation measurements from high mountains were taken during attempts to determine the solar constant and to quantify the greater radiative fluxes perceived in the alpine. Increases in solar radiation with altitude have been discussed in detail by Sauberer and Dirmhirn (1958) and Barry (1981). In summary, $K\downarrow$ increases exponentially with altitude in both cloudless and cloudy weather. Diffuse-beam solar radiation decreases with altitude in cloudless conditions, but increases with cloudy conditions.

Müller's (1985) review of European data is the most exhaustive to date. Despite more than a century of measurements and relatively easy access to alpine terrain in Europe, few high quality measurements of radiation transfers exist, with the exception of direct-beam and global solar radiation. Longwave and net radiation transfers have rarely been measured, and non-glacial experiments are uncommon.

For cloudless skies, results of every alpine radiation budget experiment confirm theoretically-predicted high values of $K\downarrow$ in the alpine zone. The predominance of cloudless-sky data in alpine solar radiation studies unfortunately disguises the fact that

Table 2.1. Selected alpine radiation budget results: snow-free surfaces.

Author	Location	Site & altitude	Measurement period	Conditions	K↓	K↑	K*	α	L↓	L↑	L*	Q*
Aufdemberge (1974)	Chitistone Pass, Alaska 61° N, 139° W	Moss-lichen tundra. 1770m	July (10d)	Various	19.4	3.7	15.7	0.20	24.1	29.8	-5.7	10.0
Bailey *et al.* (1989)	Plateau Mountain, Alberta 50° N, 114° W	Fellfield. 2480m	Jun-Jul (30d)	Mostly cloudless	25.8	4.4	21.4	0.17	20.9	30.1	-9.1	12.2
Gates and Janke (1966)	Niwot Ridge, Colorado 40° N, 106° W	Tundra. 3500m	July (1d)	Partly cloudy	33.7	6.8	26.9	0.20	28.7	34.9	-6.2	20.7
			Sept (1d)	Cloudless	27.7	4.5	23.2	0.16	28.7	33.9	-5.2	18.0
Halbsguth *et al.* (1984)	Dischma valley, Switzerland 46° N, 10° E	Subalpine grass meadow. 1970m	August (10d)	Cloudless	26.2	5.9	20.4	0.23	27.8	33.0	-5.2	14.0
				Cloudy	18.8	4.7	14.1	0.25	28.1	31.9	-3.8	10.3
Kraus (1971a)	Imja Khola, Nepal 30° N, 89° E	Moraine. 4750m	April (9d)	Various	25.2	4.1	21.1	0.16	21.4	28.5	-7.1	13.9
LeDrew (1975b)	Niwot Ridge, Colorado 40° N, 106° W	Tundra. 3500m	Jun-Aug (62d)	Various	21.3	3.6	17.7	0.17	25.7	34.1	-8.5	12.5
Terjung *et al.*, (1969a)	White Mountains, California 38° N, 118° W	Felsenmeer. 4270m	July (1d)	Cloudless	40.6	8.1	32.5	0.20	N/A[1]	N/A	-8.4	24.1
Terjung *et al.*, (1969b)	White Mountains, California 38° N, 118° W	Tundra. 3600m	July (1d)	Cloudless (daytime only)	41.1	11.9	29.1	0.29	13.0	19.7	-6.7	22.4

All flux densities are daily means, units $MJ\,m^{-2}d^{-1}$.
1. Not available.

mountain ranges experience more cloud cover than non-mountainous terrain. Gates and Janke's (1966) provocative image of dawn breaking over alpine tundra with the "intensity of an avalanche" should be contrasted with the common observation that mountainous regions are characterized by overcast conditions for much of the time.

Data in Table 2.1 show that tundra, moraine and fellfield surfaces are broadly similar, and are characterized by albedos of about 0.15 to 0.20. Subalpine grass meadows are slightly more reflective at 0.25 (Halbsguth *et al.*, 1984). The difference in surface roughness, texture and colour of these surfaces might be expected to give different diurnal albedo trends, but no field research has confirmed this.

A majority of alpine radiation budget studies have been performed on snow and ice surfaces. This is partly because many are more glaciological and hydrological than climatological in purpose. Additionally, in rugged mountain terrain, snow and ice fields are often the most practical sites available for instrumentation. Reviews of snow and ice radiation budget research include those of Male and Granger (1981), Barry (1983) and Dozier (1987). Müller's (1985) review of European work concentrates almost exclusively on glacier surfaces. Table 2.2 summarizes the results of these studies for snow and ice surfaces.

Snow and ice radically affect the radiation budget. The range of albedos possible on glacier surfaces ranges from 0.85 for fresh dry snow to a low value of 0.15 for very dirty ice (Müller, 1985). A concomitant wide range in glacier radiation regimes follows this variability. Snow surface albedo depends upon the wavelength, zenith angle, grain size, impurity content and cloud cover, and there are spectral dependencies for some of these variables (Choudhury and Chang, 1981; Warren, 1982). Generally speaking, however, the effects of all these factors are small. Daily and seasonal variations in snow albedo have sometimes, however, been explained by invoking changing snow properties (e.g. Ambach and Hoinkes, 1963; Dirmhirn and Eaton, 1975).

The prime objective of many glaciologically-oriented radiation budget studies has been to determine relations between radiation and ablation. Often only $K\downarrow$ is used as input data (e.g. Goodison, 1972) but the variable nature of glacier albedos suggest that K^* is the more logical determinant for ablation modelling since it accounts for albedo changes (Munro and Young, 1982). Even though $K\downarrow$ decreases following the summer solstice, K^* increases due to

Table 2.2. Selected alpine radiation budget results: snow and ice surfaces.

Author	Location	Site & altitude	Measurement period	Conditions	K↓	K↑	K*	α	L↓	L↑	L*	Q*
Aguado (1985)	Soda Springs, California 39° N, 120° W	Subalpine snowpack 2100m	April–June (120d)	Mean for 3 seasons	27.4	12.9	14.5	0.47	N/A[1]	N/A[1]	−6.5	8.0
Aufdemberge (1974)	Capps Glacier, Alaska 61° N, 139° W	Ice. 1740m	July (10d)	Various	19.5	6.1	13.5	0.32	25.8	26.4	−0.6	13.0
Brazel and Marcus (1979)	Mt. Logan, Yukon 61° N, 140° W	Snowfield. 5370m	July (22d)	Various	32.2	28.8	3.4	0.89	13.8	22.1	−8.3	−4.9
Lougeay (1970)	Seaward Glacier, Yukon 60° N, 139° W	Glacier: snow. 1700m	July (9d)	Cloudless	31.4	23.2	8.2	0.74	28.8	25.2	3.6	11.8
				Mostly cloudy	22.9	17.8	5.1	0.78	30.5	25.9	4.6	9.8
Munro (1975)	Peyto Glacier, Alberta 52° N, 117° W	Glacier: ice. 2280m	August (35d)	Various	21.4	5.3	16.2	0.25	22.4	27.3	−4.8	11.4
Sauberer and Dirmhirn (1953)[2]	Sonnblick, Austria 47° N, 13° E	Glacier. 3000m	Jan–Dec.	Dec., cloudless	7.3	5.8	1.5	0.80	15.0	23.8	−8.9	−7.5
				Dec., overcast	3.4	2.7	0.7	0.80	20.3	22.8	−2.5	−1.8
				June, cloudless	35.2	14.1	21.1	0.40	19.5	27.7	−8.1	13.0
				June, overcast	17.4	7.0	10.4	0.40	26.4	27.0	−0.6	9.9
Wagner (1979, 80)	Hintereisferner, Austria. 47° N, 11° E	Glacier: snow. 2960m	July–Sept. (92d)	July	26.4	16.9	9.4	0.64	22.6	26.7	−4.1	5.3
				Aug.	18.9	10.7	8.1	0.57	23.9	27.1	−3.2	4.9
				Sept.	18.5	8.1	10.3	0.44	20.1	25.7	−4.9	5.5
Wendler and Ishikawa (1973)	McCall Glacier, Alaska. 69° N, 142° W	Glacier. 1730m	July (11d)	Ice	19.5	6.4	13.1	0.33	N/A	N/A	−6.9	6.2
		Glacier. 2140m		Snow	19.5	11.4	8.1	0.59	N/A	N/A	−4.4	3.7

All flux densities are daily means, units $MJ\,m^{-2}d^{-1}$.
1. Not available.
2. Data from Sauberer and Dirmhirn (1953) are selected from long-term estimates.

the darkening of the glacier surface as the previous winter's snow melts off to reveal bare ice (Wagner, 1979).

Longwave Radiation

Fewer measurements of longwave than solar radiation have been reported from the alpine environment, and again most are from the European Alps (Tables 2.1 and 2.2). Data reviewed by Barry (1981) confirm that the decrease in temperature and atmospheric mass at greater altitudes leads to smaller $L\downarrow$ fluxes. This is offset by smaller $L\uparrow$ losses (colder surface temperatures, greater persistence of snow cover) such that L^* changes little with altitude (Sauberer and Dirmhirn, 1958).

Studies over alpine tundras and glaciers demonstrate that the typical daily progression of $L\downarrow$ contains an early morning minimum and an afternoon maximum, in response to atmospheric temperature and vapour pressure (e.g. Aufdemberge, 1974; Wagner, 1980; Bailey *et al.*, 1989). In this respect, the alpine longwave radiation exchanges are no different than non-alpine.

Atmospheric longwave radiation modelling in alpine environments has received little attention compared to the numerous efforts at simulating solar fluxes. Most studies have attempted to derive relations which estimate $L\downarrow$ for cloudless skies only (termed $L\downarrow_0$). Corrections to convert $L\downarrow_0$ to $L\downarrow$ were given for the Alps by Müller (1985) for three cloud types and were a few percent greater than the more common correction of Bolz (1949). No comparable North American data exist.

Three $L\downarrow_0$ modelling experiments have been independently undertaken in the alpine tundra zone at Niwot Ridge, Colorado. LeDrew (1975a) evaluated four $L\downarrow_0$ models (Brunt, Idso-Jackson, McDonald, Monteith) with disappointing results, and empirically adapted Brunt's (1932) model to his data. Curiously, Brazel and Hyers (1981) used LeDrew's (1975a) model at the same site yet found it overestimated by 20%. The same authors had satisfactory results from the Idso-Jackson (1969) and Brutsaert (1975) equations. Lougeay and Brazel (1982) had good results from the Idso-Jackson model at Niwot Ridge, and adequate results from LeDrew's (1975a) and Marks and Dozier's (1979) models.

Marks and Dozier (1979) adapted Brutsaert's (1975) model to the alpine environment of Sierra Nevada for snowmelt modelling purposes. They attempted to convert air temperature and vapour pressure data from the alpine zone to sea-level equivalents using assumptions of constant environmental lapse rates and relative humidity. Under cloudless skies, adequate results were obtained, but under cloudy conditions and low temperatures or vapour pressures, performance was much less satisfactory. The model was subsequently found by Lougeay and Brazel (1982) to consistently underestimate. The results obtained by Dobesch (1980) contradicted those of Marks and Dozier (1979). Using European alpine data, Dobesch found the Swinbank and Monteith models to work well under cloudy conditions but not on cloudless days. Dobesch also used the models, without corrections, for cloudy skies, and achieved acceptable results. Considering that these models were originally developed for cloudless skies and that $L\downarrow$ must increase with increasing cloud, these results must be viewed with caution.

Longwave radiation exchanges over snow and ice are constrained by the limiting surface temperature of 0°C, which means that $L\uparrow \leq 316\ W\ m^{-2}$. As a result, L^* tends to be greater for a given value of $L\downarrow$ over a snow/ice surface than over snow-free terrain. Since net solar radiation is decreased by the high albedo of snow, longwave radiation therefore has the potential to play an increasingly important role in the radiation budget, especially with cloud cover (Lougeay, 1970; Ambach, 1974). Relationships between L^* and cloud cover have been reported from alpine glaciers by Ambach and Hoinkes (1963) and Wagner (1980). The dominance of L^* over K^* may even occur in cloudless conditions if the snow surface is sufficiently reflective (Brazel and Marcus, 1979).

Since high albedos and cloud cover are more common in alpine areas than non-alpine areas, the exchanges of longwave radiation assume a greater relative importance in alpine radiation budgets. Positive values of L^*, such as those of Lougeay (1970), have not been commonly observed, but conceivably occur whenever a warm air mass overlies a cold snow or ice surface and solar fluxes are small.

Net Radiation

In general, net radiation is observed to decrease with altitude, largely due to the longer snow cover duration. This is confirmed by hypothetical modelling of a 'typical' alpine glacier (Müller, 1985). Few studies pertaining solely to Q^* have been done in mountain environments and none are specifically alpine. In pointing out the importance of Q^* to climatological modelling, Flohn (1974) called for efforts to correct this deficiency, but as yet little progress appears to have been made. Net radiation has been modelled empirically in North American mountains by Storr (1972) and Bailey *et al.* (1989) in the Rocky Mountains of Alberta, by Terjung *et al.* (1969a) in the White Mountains of California and by Isard (1989) in the Rocky Mountains of Colorado. All three studies presented relations between Q^* and $K\downarrow$, and for surfaces with similar albedos at similar latitudes such relations can be expected. When data in Table 2.1 are plotted, a relation comparable to the well-known Davies (1967) equation emerges (Figure 2.1).

DISCUSSION

In attempting to characterize the radiation regime of alpine environments, most authors have resorted to valley-mountain comparisons. These mask many details of the high mountain environment. In view of the fact that global solar radiation can be readily modelled, it seems disappointing to find that the great majority of field measurments are of this component. By comparison, the longwave and net radiation components have been largely ignored. The slower development of longwave and net radiation sensors has undoubtedly played a role, although the introduction of pyrgeometers and net pyrradiometers in the last three decades has not resulted in increased radiation budget research as much as might have been hoped. Cloudless sky $L\downarrow$ modelling in the alpine is generally satisfactory, although results have been erratic in some studies. LeDrew (1975a) suggested that the more extreme gradients between an alpine surface and the free atmosphere above were responsible for negating the validity of the standard $L\downarrow$ models. It is also more difficult to obtain high quality longwave radiation measurements. These difficulties help explain the fact that three independent studies from the same field site reported contradictory results.

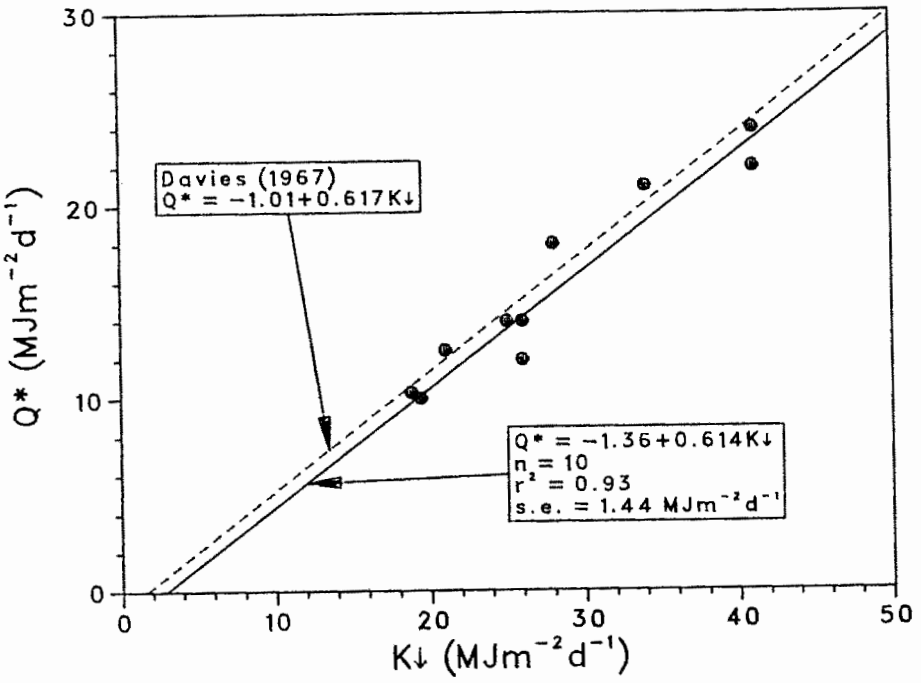

Figure 2.1. Relations between mean daily global solar radiation (K↓) and net radiation (Q*) for the snow-free tundra data listed in Table 2.1. The linear regression line and the relation of Davies (1967) are shown.

Two problems need to be overcome in alpine longwave radiation modelling: inclusion of (1) cloud cover, and (2) the sub-zero temperature domain. Mountains are often cloudier than surrounding lowlands, and serious attention needs to be given to cloudy sky radiation budgets. In particular, attention needs to be given to longwave radiation. Temperature ranges of existing $L\downarrow$ models tend not to include the commonly-experienced cold temperatures of alpine terrain. Efforts are required to ascertain the utility of models in sub-freezing conditions at high altitude. The problems of $L\downarrow$ modelling in the alpine environment could possibly be circumvented by concentrating on $L\uparrow$ instead. Surface temperature estimations from air temperature or radiation data could be used in the Stefan-Boltzmann equation to estimate $L\uparrow$.

Empirical relations between $K\downarrow$ and Q^* for snow-free alpine surfaces corresponded very closely to that of Davies (1967). This confirms the measurements reporting increased solar radiation loading at high altitudes to be offset by greater longwave radiation losses. Thus the alpine radiation budget behaves conservatively, a fact somewhat masked by the concentration of research in the solar aspects of alpine radiation budgets. Empirical $Q^* = f(K\downarrow)$ relations need to be modified if they are to be used in the alpine environment over time periods which involve surface changes. These relationships become unusable as soon as snow accumulates on the ground, and this can happen at any time of the year in the alpine zone. The inclusion of either albedo or K^* is needed, but then modelling integrity is sacrificed by the fact that $Q^* = f(K^*)$. Flux-by-flux modelling would avoid these problems, but apparently no research has been directed towards this topic for the alpine environment.

Most of the field data discussed have been derived from horizontal surfaces. Even though sloping surfaces abound in mountainous terrain, relatively few research advances have been made towards determining complete radiation budgets from sloping surfaces. Direct-beam solar radiation can be relatively easily modelled for slopes, but the remaining radiation budget components are difficult to determine. Problems arise in complex terrain as a result of topographic shading or enhancement of radiation fluxes, which complicate modelling. In North America the major field research efforts addressing slope radiation budgets have been concentrated in Colorado as part of the U.S. Department of Energy's Atmospheric Studies in Complex Terrain (ASCOT) program. The topographic influence extends to all components of the radiation budget, although $L\downarrow$ tends to be conservative (Whiteman *et al.*, 1989a). Strong

diurnal trends in $K\downarrow$, $K\uparrow$, $L\uparrow$ and Q^* characterize cloudless days, but details of cloudy-sky scenarios are unresearched. It remains to be seen to what extent the greater cloud cover associated with mountainous areas suppresses the topographic enhancement of surface radiation budgets. Initial studies suggest that the topographically-induced heterogeneity in solar radiation inputs are offset by the diffusing effects of clouds (Isard, 1989), and topographic enhancement of longwave radiation in cirques may also produce a similar net result (Brazel and Marcus, 1987).

CHAPTER III

REVIEW OF ENERGY BUDGET RESEARCH IN ALPINE ENVIRONMENTS

INTRODUCTION

Although climate data have long been collected in mountainous regions, only a minority proportion has been derived from the alpine zone (above treeline). There have been relatively few complete energy budget studies, and most of these have been performed over snow/ice surfaces, being glaciological or hydrological in purpose, There are presently only a few studies relating to alpine tundra environments, mostly from North America. With the recent increase of interest in mountain environments for climatological, hydrological and recreational purposes, it is timely to review the progress to date.

The scarcity of high quality energy budget modelling from alpine tundra environments is probably due to a combination of logistical problems (discussed in the previous chapter) and theoretical/experimental limitations. It is difficult to find sites suitable for alpine energy budget research which meet all theoretical demands. Many mountain research sites are inaccessible, especially in winter, and the working conditions are more extreme for both the researcher and the instrumentation. Most of the data refer to mid-latitude mountains.

THEORETICAL BACKGROUND

The sparse vegetation which characterizes alpine tundra surfaces dictates that energy storage in the canopy and the energy used in photosynthesis will be negligible. In the absence of snow cover, the need for conservation of energy at the surface dictates that

$$Q^* + Q_G + Q_H + Q_E + Q_R + Q_A = 0 \qquad (3.1)$$

where Q^* is net radiation, Q_G is ground heat flux, Q_H and Q_E are vertical turbulent fluxes of sensible and latent heat, Q_R is energy from rainfall and Q_A is horizontal advection. For snow or ice, the change in heat storage (ΔQ_S) and the energy used in melting (Q_M) are also considered. The convention adopted here is that energy fluxes are positive when directed towards the surface.

For a spatially uniform surface, $Q_A = 0$. The input of energy from rainfall is generally an order of magnitude less than the other energy fluxes. Therefore, Equation (3.1) simplifies to

$$Q^* + Q_G + Q_H + Q_E = 0 \qquad (3.2)$$

Net Radiation and Ground Heat Flux

Measurement of net radiation is generally a simple task with a pyrradiometer. Evaluation of ground heat flux is typically accomplished with buried flux transducers. The flux divergence between the surface and the plates needs to be accounted for (Fuchs and Tanner, 1968; Wilson and McCaughey, 1971). This requires knowledge of the volumetric mineral, organic and water contents. Ground heat flux is therefore given as

$$Q_G = Q_{Gz} + Cz\frac{\Delta T}{\Delta t} \qquad (3.3)$$

where Q_{Gz} is the heat flux measured by the transducer at depth z, $\Delta T/\Delta t$ is the change in the temperature of the soil layer 0–z with respect to time, and soil heat capacity (C) is given by

$$C = C_M x_M + C_O x_O + C_W x_W \qquad (3.4)$$

where C is heat capacity and x is volume fraction, and subscripts m, o and w denote mineral, organics and water. The heat storage of pore air is negligible and has been omitted from Equation (3.4).

The inherent variability of soil dictates that ground heat flux measurements need to be adequately replicated in an attempt to obtain a representative value. This is especially problematic in most alpine areas due to the poorly developed soils and the presence of periglacial patterned ground.

Turbulent Flux Densities

Several different methods have been employed to determine the vertical turbulent fluxes in alpine terrain. These include the aerodynamic method, Bowen ratio–energy budget (BREB) method, Ohm's Law, bulk aerodynamic method and eddy correlation. However, they will not all be derived here. Detailed derivations of each method can be found in Thom (1975), Brutsaert (1982) and Oke (1987). Of importance to this review are the assumptions implicit in the use of these models in alpine environments.

Both the aerodynamic and BREB methods are derived from mass transfer equations

$$Q_H = \rho c_p K_H \frac{\partial T}{\partial z} \tag{3.5}$$

and

$$Q_E = \frac{\rho c_p}{\gamma} K_V \frac{\partial e}{\partial z} \tag{3.6}$$

where ρ is air density, c_p is specific heat of air at constant pressure, γ is the psychrometric coefficient, K_H and K_V are eddy diffusivities of heat and water vapour, T is air temperature, e is vapour pressure and z is height above the surface.

(a) Aerodynamic Method

From Thom (1975)

$$Q_H = \rho c_p k^2 (z-d)^2 \frac{\partial u}{\partial z} \frac{\partial T}{\partial z} (\Phi_M \Phi_H)^{-1} \tag{3.7}$$

and

$$Q_E = \frac{\rho c_p}{\gamma} k^2 (z-d)^2 \frac{\partial u}{\partial z} \frac{\partial e}{\partial z} (\Phi_M \Phi_V)^{-1} \tag{3.8}$$

where k is von Karman's constant (0.41), d is the zero–plane displacement, u is wind speed and the Φ–functions are corrections for non–neutral stability, derived semi–empirically from the Richardson number (Dyer and Hicks, 1970; Dyer, 1974). Most alpine studies using the aerodynamic method have not included corrections for stability and may therefore be erroneous (e.g. Terjung *et al.*, 1969b).

(b) Bowen Ratio–Energy Budget (BREB) Method

The Bowen ratio (β) is defined as the ratio between sensible and latent heat flux densities (Bowen, 1926). This approach avoids some of the rigours of the aerodynamic method by assuming similarity between the eddy diffusivities for heat and water vapour. By dividing Equation (3.5) by (3.6) the Bowen ratio is derived and the need for vertical profiles of wind speed is eliminated

$$\frac{Q_H}{Q_E} = \gamma\frac{\Delta T}{\Delta e} = \beta \qquad (3.9)$$

and substituting (3.9) into (3.2) gives

$$Q_E = -\frac{(Q^*+Q_G)}{1+\beta} \qquad (3.10)$$

Success of the Bowen ratio method assumes that the transfer coefficients for heat and water vapour are equal. The experimental work of Dyer (1967) and Swinbank and Dyer (1967) confirms the practical validity of this assumption.

The psychrometric coefficient (γ) is dependent upon air pressure and temperature, and so changes with altitude

$$\gamma = \frac{c_p P}{0.622 L_v} \qquad (3.11)$$

where P is atmospheric pressure and L_v is the latent heat of vaporization. If not corrected for alpine conditions, significant errors are possible (Storr and Den Hartog, 1975).

(c) Ohm's Law Method

Exploiting the Ohm's Law relation between potential difference, flux density and resistance, the turbulent fluxes can be defined as

$$Q_H = \rho c_p \frac{(T_z - T_0)}{r_{aH}} \qquad (3.12)$$

and

$$Q_E = \frac{\rho c_p}{\gamma} \frac{(e_z - \epsilon_0)}{r_{aV}} \qquad (3.13)$$

where T_z and e_z are, respectively, air temperature and vapour pressure at height z, T_0 and ϵ_0 are the surface values and r_{aH} and r_{aV} are the aerodynamic resistances to transfer of

heat and vapour. In accordance with the similarity between eddy diffusivites for heat and vapour, r_{aH} and r_{aV} are assumed to equal a common value, r_a.

Momentum is transferred at the surface in part by bluff-body effects for which there are no parallels for heat and vapour transfer. Therefore, r_a is equal to that for momentum (r_{aM}) plus an excess resistance to account for the bluff-body effects (r_b)

$$r_a = r_{aM} + r_b \tag{3.14}$$

Combining the mass transfer equation for momentum with the stability-corrected equation defining the logarithmic wind profile, Thom (1975) shows that

$$r_{aM} = \frac{(\ln(z/z_0) + \Phi_M)^2}{k^2 u} \tag{3.15}$$

where z_0 is the roughness length. Bluff-body resistance can be determined from (Thom, 1972)

$$r_b = 6.266\, u_*^{-0.667} \tag{3.16}$$

For relatively smooth surfaces, such as tundra, the magnitude of r_b is much less than that of r_{aM} and can be ignored without incurring large errors.

Further, calculation of the stability correction (Φ_M) can be avoided (Bailey and Davies, 1981). Avoiding the calculation of r_b and Φ_M eliminates the need to measure wind profiles and the data requirements consequently become more simple.

(d) Bulk Aerodynamic Method

Analagous to the Ohm's Law approach, the bulk aerodynamic method replaces the aerodynamic resistances with transfer coefficients for heat (D_H) and vapour (D_V) and for neutral stability are expressed as

$$Q_H = \rho c_p D_H (T - T_0) \tag{3.17}$$

and

$$Q_E = \frac{\rho c_p}{\gamma} D_V (e - e_0) \tag{3.18}$$

where

$$D_H = D_V = \frac{k^2 u}{(\ln(z/z_0))^2} \qquad (3.19)$$

which is simply the inversion of Equation (3.15). For non-neutral conditions, stability corrections are included.

(e) Eddy Correlation Method

The utility of measuring vertical wind speed fluctuations from eddies and relating this to heat and mass transfers in the boundary layer was first demonstrated by Swinbank (1951) and is succinctly derived by Oke (1987). Assuming that fluctuations in air density are zero and that measurements are made over uniform terrain

$$Q_H = \rho c_p \overline{(w' T')} \qquad (3.20)$$

where $\overline{(w' T')}$ is the time-averaged product of the instantaneous covariances of vertical wind speed (w) and air temperature (T). A similar relation can be derived for latent heat transfer.

Advantages of the eddy correlation method arise from it's simplicity. Only one level of measurement is required and any timescale beyond a minimum averaging period of about 15 minutes is valid (Brutsaert, 1982).

Snowpack Heat Fluxes

Changes in snowpack heat storage can be determined if temperature, ice content and water content are known (Anderson, 1976). Measurement of the liquid water content of snow is difficult for the short time intervals commonly used in energy budget studies (30-60 minutes). The freezing calorimetry, alchohol calorimetry and dilution methods give comparable results (Boyne and Fisk, 1987).

Without direct measurement of melt production within the snow, the evaluation of melt energy (Q_M) is usually accomplished by treating it as a residual in the energy budget equation. This requires reliable measurements of all the other components and suffers from

the susceptibility of accumulated errors in the measured terms.

Methodological Problems

The field measurement of the energy budget components requires that certain criteria are met before theory can be appropriately applied. The important attributes of a site are that it be spatially homogeneous to minimise horizontal advection, and that it has sufficient upwind fetch. The difficulty in finding and accessing sites with these attributes in rugged alpine terrain is undoubtedly an important factor in restricting the number of alpine energy budgets in many mountain areas. Fetch requirements have not been rigidly specified. However, a 1:100 height:fetch ratio is commonly adopted as a working minimum value, although values as low as 1:20 have been found to be satisfactory (Heilman *et al.*, 1989). Unless fetch is very great, energy budget measurements must therefore be made close to the surface. The gradients of temperature, vapour pressure and wind speed can be small and consequently very accurate measurements are required if errors are to be minimised. This problem is more acute when using the aerodynamic method.

In general, advective influences (Q_A) have not been measured in alpine experiments. Brazel (1974), LeDrew (1975b) and Isard and Belding (1989) invoked sensible heat advection as reasons for non-closing energy budgets but made no attempt at quantitative verification. Olyphant and Isard (1988) quantified sensible heat advection, finding it to be nearly negligible over tundra but, as could be expected, an important source of heat to the upwind/leading edge of snow patches.

ENERGY BUDGET MEASUREMENTS IN ALPINE ENVIRONMENTS

Snow-free Surfaces

Summer microclimate experiments from alpine tundra have been reported by several authors (Table 3.1). Additionally, minor contributions have come from biological and ecological studies (e.g. Bliss, 1956; Douglas and Bliss, 1977), but these are generally of poorer quality and the data have been excluded from this review. Several of these experiments raise concerns regarding data quality. Problems of surface inhomogeneity were encountered by Terjung *et al.* (1969b), Brazel (1974) and Aufdemberge (1974). Rott (1979) had marginal

Table 3.1. Selected alpine energy budget results: snow-free surfaces.

Author	Location	Site & altitude	Measurement period	Methods used	Conditions	Q^*	Q_G	Q_H	Q_E	Bowen ratio
Aufdemberge (1974)	Chitistone Pass, Alaska 61° N, 141° W	Moss-lichen tundra. 1770m	July (10d)	Aerodynamic	Various	10.0	−2.1	−2.7	−5.2	0.52
Bowers and Bailey (1987, 1989)	Plateau Mountain, Alberta 50° N, 114° W	Fellfield. 2480m	June–July (30d)	Bowen ratio	Mostly cloudless	12.2	−1.1	−6.3	−5.1	1.26
Brazel (1974)	Chitistone Pass, Alaska 61° N, 141° W	Moss-lichen tundra. 1770m	July–August (10d)	Aerodynamic	Cloudless	10.1	−0.5	−6.7	−2.9	2.31
					Cloudy/wet	4.8	−0.5	−7.3	3.0	−2.43
					Cloudy/dry	7.2	−0.1	−0.1	−7.0	0.01
Häckel (1978)	Rotwand, FRG 48° N, 9° E	Subalpine grass meadow. 1400m	July (1d)	Bowen ratio	Cloudless	14.2	−1.3	−6.8	−6.1	1.11
Halbsguth *et al.* (1984)	Dischma valley, Switzerland 46° N, 10° E	Subalpine grass meadow. 1970m	August (10d)	Bowen ratio	Cloudless	14.0	−1.3	−3.2	−9.3	0.34
					Cloudy	10.4	−0.3	−0.3	−7.4	0.04
Kraus (1971a)	Imja Khola, Nepal 30° N, 89° E	Moraine. 4750m	April (9d)	Aerodynamic	Various	13.9	−0.5	−8.3	−5.1	1.63
LeDrew (1975a)	Niwot Ridge, Colorado 40° N, 106° W	Grass-sedge tundra. 3500m	June–August (44d)	Hydrologic (lysimeter)	July	12.5	−1.7	−7.0	−5.4	1.30
Rott (1979); Staudinger and Rott (1981)	Obergurgl, Austria 47° N, 11° E	Subalpine grass meadow. 1960m.	July–Sept.	Bowen ratio	Cloudless	10.9	−0.9	−0.9	−9.7	0.09
		Alpine grass-sedge tundra. 2580m			Cloudless	13.4	−1.1	−4.0	−8.3	0.48
Terjung *et al.* (1969b)	White Mountains, Calilfornia 38° N, 118° W	Grass-sedge tundra. 3600m	July (1d)	Aerodynamic, Bowen ratio	Cloudless	22.6	−2.5	−6.7	−13.8	0.49

All flux densities are daily means, units $MJ\,m^{-2}d^{-1}$.

Table 3.2. Selected alpine energy budget results: snow and ice surfaces.

Author	Location	Site & altitude	Measurement period	Methods used	Conditions	Q^*	Q_H	Q_E	Q_M	Q_P	Bowen ratio
Ambach and Hoinkes (1963)	Kesselwandferner, Austria 47° N, 11° E	Snowfield. 3240m	Aug.–Sept. (28d)	Aerodynamic	Various	2.4	1.5	−0.1	−3.9	--	−11.0
Aufdemberge (1974)	Capps Glacier, Alaska 61° N, 139° W	Glacier: ice. 1740m	July (10d)	Aerodynamic	Various	12.9	1.9	1.1	−16.0	Negl.	1.7
Brazel and Marcus (1979)	Mt. Logan, Yukon 61° N, 140° W	Snowfield. 5370m	July (23d)	Aerodynamic	--	−4.9	0.5	4.4	-	Negl.	0.1
Fohn (1973)	Peyto Glacier, Alberta 52° N, 117° W	Glacier: ice. 2280m	July (14d)	Aerodynamic/ evaporation pans	Various	6.9	7.3	0.6	−14.8	--	12.2
Lougeay (1970)	Seaward Gl., Yukon 60° N, 140° W	Glacier: snow. 1700m	July (9d)	Aerodynamic	Cloudless Cloudy	11.8 9.8	0.9 −0.03	−0.8 −0.1	−11.9 −9.8	-- --	−1.1 0.3
Moore (1983b)	Southern Alps, New Zealand 44° S, 170° E	Snow. 1450m Snow. 1550m	Oct.–Nov. (13d)	Bulk aerodynamic	Maritime Rain–shadow	1.7 2.4	6.0 10.3	2.7 0.5	−10.6 −13.2	0.2 0.0	2.2 20.6
Munro (1975)	Peyto Glacier Alberta 51° N, 117° W	Glacier: ice. 2280m	Aug. (35d)	Aerodynamic	Cloudless	11.4	3.7	0.9	−16.0	--	4.1
Wendler and Ishikawa (1973)	McCall Glacier, Alaska 69° N, 142° W	Glacier: ice. 1730m Glacier: snow. 2140m	July (11d)	Bowen ratio	Various	6.2 3.7	4.9 2.2	−0.4 −2.3	−9.9 −3.5	-- --	−12.3 −1.0

All flux densities are daily means, units $MJ\,m^{-2}d^{-1}$.

fetch requirements. Methodological problems have included insufficient measurement frequency (Aufdemberge, 1974; LeDrew, 1975b) and instrument error or failure (Terjung *et al.*, 1969b). The results of Terjung *et al.* (1969b) and Häckel (1978) refer to measurement periods of one day or less.

The data show that alpine energy budgets are variable in both nature and magnitude. This is to be expected, since the sites tabulated range from moist meadow (Rott, 1979; Halbsguth *et al.*, 1984) to dessicated fellfield (Bowers and Bailey, 1987; 1989). Mean net radiation for cloudless conditions is 12 ± 2 MJ $m^{-2}d^{-1}$ for most of the data. The very high values of Terjung *et al.* (1969b) were derived under an extremely transparent atmosphere, and probably represent the upper extreme for mid-latitude mountains.

Examination of Table 3.1 reveals little to suggest that alpine energy budgets are radically different from other comparable surfaces, such as grass or agricultural crops, except perhaps in the magnitude of fluxes. For given cloud and soil moisture conditions, alpine energy budget components appear to behave similarly to those from other environments. The moister sites are typified by lower Bowen ratios than the drier locations, as is expected. However, the generalized nature of the information in Table 3.1 masks some characteristics of alpine energy budgets, such as the wide variability of data and the multitude of micro- and topoclimates typical of the alpine zone. Of further interest is the strong *positive* latent heat flux (i.e. condensation) found by Brazel (1974) during cloudy, wet conditions. The persistence of cloud in mountains may mean that positive Q_E may occur with regularity in the alpine zone. A further characteristic of alpine tundra surfaces may be found in the severe surface heating associated with strong radiative fluxes, unparalleled in non-alpine environments (Terjung *et al.*, 1969b; Rott, 1979).

A further typicality of alpine energy budgets lies in the nature of the soil moisture regime. Soil moisture availability in the alpine zone is generally limited by the coarse soil texture and shallow root systems which allow quick drainage and limit the potential reservoir for vascular plants. In these instances, evaporation is only strong immediately following snowmelt or rainfall. The subsequent change from an evaporating regime to a dry regime may occur rapidly. Without continual moisture input at the surface, the tundra therefore becomes dessicated, with high Q_H and β (e.g. Kraus, 1971a; LeDrew, 1975b; Bowers and

Bailey, 1987; 1989). In areas where soil and vegetation development is better, such as subalpine meadows, evaporation experiences less restriction than in alpine tundra (Halbsguth *et al.*, 1984). Comparisons between adjacent meadow and tundra surfaces were well illustrated by Rott (1979) and Staudinger and Rott (1981). These authors summarized the meadow evapotranspiration regime as energy-limiting and the tundra regime as moisture-limiting. This appears to be a valid generalization for the alpine environment.

In North America, alpine climates have been documented for a maritime regime (Chitistone Pass, Alaska) and drier, rain shadow regimes (Niwot Ridge, Colorado and Plateau Mountain, Alberta). The energy budget characteristics at each site are superimposed on the regional climate. The Chitistone Pass work illustrates a range of energy regimes forced by the synoptic weather. Brazel (1974) documents energy budgets for three broad regimes and recognizes the importance of regional weather patterns in influencing energy exchanges. Similar results are found for the same site by Aufdemberge (1974). Of significance is the changing Bowen ratio, reflecting the surface's response to the weather, and in particular the observation that cloudless conditions, although perhaps representing an ideal scenario, are not the norm for maritime mountains.

The Niwot Ridge and Plateau Mountain energy budgets show regimes with less variation than the Chitistone Pass work. They are generally moisture-limiting regimes and as such exert control on the vegetation growth (Greenland *et al.*, 1984). Topographic influences on the spatial patterning of energy transfers is limited by cloud cover (Isard, 1989). Typically, dessicated conditions persist, with Bowen ratios greater than unity. Periodic precipitation events stimulate evaporation for limited periods. At other times the need for the preservation of soil moisture appears to exert a strong control. For example, Bowers and Bailey (1989) document changes in surface resistance (derived from the Penman-Monteith combination model) which illustrate an increasing restriction on moisture release by plants from late morning onwards.

Alpine energy budget research has generally been of a descriptive nature and to date there have been few attempts at determining aerodynamic characteristics of the surface, or at modelling. Four studies have examined the relation of Φ_H to stability parameters for alpine or subalpine sites, using z/L (where L is the Monin-Obukhov length (Thom, 1975)) or the

Richardson Number (Ri). In testing the validity of boundary layer theory at an alpine tundra site, Rott (1979) reported that the stability function (for daytime unstable cases) correlated well with (z/L) within the limits previously defined by Pruitt *et al.* (1973) for a grass surface. Halbsguth *et al.* (1984) found similar results in a subalpine grass meadow. LeDrew's (1975b) unsuccessful attempt to find a Φ_H–Ri relation was attributed to advection, but the instrument and logistical deficiencies of the experiment may also have contributed (Q_H was calculated as a residual from lysimeter data and uncorrected Q_G). Kraus (1971b) found that Φ_H increased more rapidly with z/L for an alpine moraine than a lowland grass field, probably due to the greater roughness of the moraine. Given sufficient fetch and homogeneity, therefore, alpine and subalpine surfaces behave in a theoretically predictable manner which differs little from their non-alpine counterparts.

Snow and Ice Surfaces

Alpine environments are characterized by the presence of both permanent and seasonal snow and ice. Many glacier and snowmelt studies utilize an energy budget approach to determine melt. Indeed, a majority of glacier energy budget studies are glaciological in purpose. Melt is usually calculated by estimating Q^*, Q_H, Q_E and ΔQ_S and then calculating the residual energy, Q_M, left over to produce melting (see Equation 3.1). The heat input from rain-on-snow events, Q_R, may also be included. Latent heat is usually insignificant at timescales longer than a day, but may be an important control for diurnal energy regimes (Lang, 1981).

Most glacier energy balance studies are from alpine or arctic environments, whereas a large proportion of snowmelt research includes forest or prairie studies. For a given snowpack thickness, alpine tundra energy balances probably show more similarity to treeless prairies than to forests. Trees in the forest environment alter the surface radiation and energy regimes in a way which differs from prairie and alpine cases. Snow and ice energy budgets have been discussed by Flohn (1974), Munro (1975), Male and Gray (1975; 1981), Male (1980), Male and Granger (1981), Paterson (1981), Barry (1981), Dozier (1987) and Morris (1989). Table 3.2 lists selected alpine data.

The high albedo of snow ensures that K^* and Q^* are minimised. Energy fluxes are perforce small. Unlike snow-free surfaces, Q_H is often a source of energy to the snow

surface; Q_E may be either a source or sink. A principal factor which determines the behaviour of the energy budget of snow is whether or not snowpack temperature increases sufficiently to initiate melting. The transition from a non-melting to melting snowpack generally occurs in the spring as a result of increasing $K\downarrow$, decreasing albedo and warmer temperatures. Snowpack energy balances may then be characterized by diurnal melting, as Q_M becomes a heat sink following a morning warm-up period (Granger and Male, 1978).

Most melt studies show Q^* to be the dominant source of energy in alpine and non-alpine snowpacks. The studies which have shown Q_H or Q_E to be dominant heat sources to a snowpack have been typified by conditions of heavy cloud and warm maritime air masses (Prowse and Owens, 1982; Moore, 1983a).

The difficulties in measuring small temperature and humidity gradients in the alpine environment often become even more acute over a snow or ice surface due to the lack of surface heating. Other methods of flux determination using single-level measurements of temperature and vapour pressure have been used, most popularly the bulk aerodynamic and eddy correlation methods (Munro, 1990). Bulk aerodynamic formulae have been used with some success for melting snow surfaces, where T_0 and ϵ_0 are assumed. Moore (1983b) provides a full discussion of the method with a table of z_0 values for different snow conditions. Intercomparisons have been performed between the bulk aerodynamic method and energy balance (Hay and Fitzharris, 1988) and eddy correlation (Munro, 1989) methods. Hay and Fitzharris' work showed larger percentage errors for the bulk aerodynamic estimates of hourly ablation but smaller errors for larger timescales. Munro demonstrated that the bulk aerodynamic method is capable of estimating hourly sensible heat fluxes to within 20 $W m^{-2}$ if careful consideration is given to roughness lengths. Other eddy correlation measurements over snow surfaces have been limited in number. A pioneer four-hour experiment by Hicks and Martin (1972) demonstrated the utility of the method for snow. A more extended study by McKay and Thurtell (1978) on a snow-covered field confirmed the importance of Q_H as a source of energy. Typically, no diurnal periodicity was found in Q_H or Q_E due to the strong control of the synoptic air mass on the surface energy.

Surface snowmelt energy budgets have been found to respond to mesoscale air mass characteristics. For example, relations between 85 kPA temperature and surface sensible heat

fluxes were found for a prairie snowpack (Granger and Male, 1978). Such an approach to surface energy budgets in mountains might suffer from (1) the orographic alteration of the air mass, (2) the fact that many mountain surfaces are physically above the 85 kPa level and (3) local problems in the temperature structure of the lower atmosphere created by topography. For seasonal appraisals of surface energy budgets, however, synoptic-scale forcing is apparent. Seasonal mass balances of alpine glaciers respond to weather patterns at this scale (Hay and Fitzharris, 1988).

Most studies find that the heat input from rain Q_R is negligible in seasonal energy budgets. Under conditions of heavy warm rainfall, Q_R can become a source of energy which is at least measureable (Anderton and Chinn, 1978; Moore and Owens, 1984) and which may contribute up to 20% of the heat input to the snowpack during storms (Fitzharris *et al.*, 1980).

DISCUSSION

Current theory is able to model energy budgets of homogeneous surfaces if suitable data can be collected. The problems of energy budget research in the alpine tundra environment lie with the heterogeneous surfaces and the logistical difficulties in generating quality field data. Recent work from alpine sites has illustrated that high quality field research and results can be achieved in the summer months. Logistically speaking, extending such work into the colder and snowier seasons presents difficulties, and few efforts have been made in this direction.

The theoretical and methodological requirements for turbulent flux evaluation have rarely been fully met in alpine studies, and the first step in improving data quality from this environment must lie in overcoming these limitations. Quality rather than quantity is preferable. Coupled with this is the need to provide unambiguous surface specification at measurement sites in order to validate comparisons from different studies and aid in interpolation of results.

Most alpine tundra research has been conducted in the summer. One of the problems of energy flux estimation in the alpine zone has been the cold conditions. The main

logistical issue is the calculation of vapour pressure when wet-bulbs are frozen. This hinders the determination of vapour pressure. Recent research has demonstrated the feasibility of anti-freeze solutions (Fritschen and Simpson, 1989) but even so these do not accommodate very low temperatures (< -10°C). Research efforts concentrating on the evaluation of Q_H under such conditions are therefore a priority. Possibly the bulk aerodynamic or Ohm's Law analogue methods (Thom, 1975) could offer practical alternatives to the more traditional profile methods. Given that data collection in the alpine zone is more difficult, modelling approaches which are simple, yet based on firm physical grounds, are likely to be the most valuable for operational applications.

Generalizations are hard to define with such limited data. The definition of "typical" alpine surface climates is problematic as a result of limited field data and the multitude of microclimates found. Energy partitioning in the alpine zone has been seen to be dependent upon both the effects of macroscale weather and microscale variations in the surface soil moisture regime. In addition there are temporal variations. Evaporation tends to be energy-limiting in moist meadows and moisture-limiting in the dry tundra zone. Spatial heterogeneity of surface types may increase the importance of advective heat fluxes, particularly when snow and snow-free surfaces co-exist.

Several aspects of the alpine tundra energy budget regime appear to be associated with a defined alpine climate. Taken individually they are not unique to the alpine tundra - their collective association is the important aspect. High radiant fluxes, strong surface heating and extreme vertical temperature gradients are common in alpine tundra when atmospheric conditions allow them. Of critical importance in alpine energy partitioning is the sub-surface soil moisture regime, which appears at times to be strongly controlled by physiological activity. Bowers and Bailey (1989) described this mechanism of control on surface water loss. In contrast, Körner and Mayr's (1981) measured decreasing stomatal resistance with altitude, but appeared to be working at wetter sites where moisture availability was not a problem.

As with radiation budgets, energy budgets of sloping surfaces remain a largely untouched research problem, and nowhere is this more important than in mountainous regions. No alpine sloping surface research has been undertaken. The closest analogies are energy budgets from a topographically simple valley in Colorado (Whiteman *et al.*, 1989b).

Energy budget components were found to be strongly affected by the topographic dependence of vegetation and soil moisture. In turn, the sensible heat flux drove slope and valley winds. The infinite number of permutations of slope angle, azimuth and surface type in the alpine environment attest to the complexity of high mountain climates (and the related research problems) and suggest a rich potential for future research.

Physiological and ecological similarities between Arctic and alpine tundra suggest that climatic data should at least be comparable between the two. Indeed, in a review of tundra characteristics, Lewis and Callaghan (1976) combined the two. Given that the Arctic has seen more research than the alpine, it offers the potential transfer of Arctic results to alpine environments. The only serious comparison between the radiation and energy budgets of the Arctic and alpine environments has been that of LeDrew and Weller (1978) using data from Barrow, Alaska, and Niwot Ridge, Colorado. Not suprisingly, many of the differences between the two data sets result from the great latitudinal difference (71° N and 40° N respectively), rather than the altitudinal difference (sea level and 3500 m a.m.s.l.). Alpine climate seemed to show greater temporal variability due to the more dynamic nature of the cloud cover; in consequence, more extreme values of $K\downarrow$ were produced. The intercomparison of factors affecting plant development in the Arctic and alpine environments by Bliss (1956) arrived at similar conclusions. The alpine was considered to be the more severe environment, with stronger winds, radiation loading, surface temperatures and greater dessication.

CHAPTER IV

RADIATION BUDGETS OF ALPINE TUNDRA, SCOUT MOUNTAIN, SOUTHERN BRITISH COLUMBIA, CANADA

INTRODUCTION

The review in Chapter II demonstrated that despite the numerous measurements of global solar radiation in high mountain locations, experiments encompassing the complete radiation budget for non-glacierized surfaces are relatively rare. Knowledge of longwave and net radiation transfers is limited and many studies are derived from very short periods of measurement (Barry, 1981; Price, 1981; Müller, 1985). Repeated calls for further information on alpine radiation fluxes have not been fully addressed (Terjung *et al.*, 1969a; Storr, 1972; Flohn, 1974).

In the western cordillera of Canada, climate measurements are preferentially made in valleys, which although having the advantage of accessibility, are not representative of adjacent alpine terrain. Despite the predominance of mountain ranges in this region, there are no operational climate stations which record radiation flux densities in the alpine zone (Environment Canada, 1982). Addressing this paucity of knowledge, the present study measured radiation budgets at an alpine tundra site in British Columbia over a total period of twelve months. A wide range of atmospheric and surface conditions were experienced, enabling an improved insight into the controlling factors governing the radiation transfers of the alpine tundra environment at hourly, daily and monthly time scales.

THEORETICAL BACKGROUND

The radiation budget at any place or time was defined in Chapter II as

$$Q^* = K^* + L^* = (K\downarrow - K\uparrow) + (L\downarrow - L\uparrow) \qquad (4.1)$$

where $K\downarrow$ and $K\uparrow$ are global solar and reflected solar radiation. The longwave radiation fluxes consist of atmospheric ($L\downarrow$) and terrestrial ($L\uparrow$) components. The sum of net solar (K^*) and net longwave (L^*) radiation gives the net radiation (Q^*). For this study, the

transmissivity of the atmosphere was derived from

$$t = K\downarrow / K_{EX} \qquad (4.2)$$

where K_{EX} is the extraterrestrial radiation. When using measured $K\downarrow$ in the field to determine t, multiple reflections between the surface and the atmosphere are also included. However, unless both the surface albedo and the cloud albedo are very high, the errors involved are not dissimilar to the measurement errors (although represent a bias). Surface albedo was derived from

$$\alpha = K\uparrow / K\downarrow \qquad (4.3)$$

EXPERIMENTAL PROCEDURE

The measurement site was on Scout Mountain (49° 05' N, 120° 12' W) at an altitude of 2350 m a.m.s.l., about 200 m above the local treeline. The site was approximately horizontal and consisted of tundra with inactive patterned ground (Figure 1.2). Details of the site were provided in Chapter I.

Extraterrestrial radiation was calculated from Garnier and Ohmura's (1968) method combining Fuggle's (1970) algorithm with radius vector and the equation of time (Robinson, 1966). The site was assumed to be horizontal for the purposes of measurement and modelling. All components of the radiation budget were measured directly or calculated by residual on an hourly basis for the periods November 1986 to July 1987, and April to May 1988.

Global solar and reflected solar radiation were measured with an Eppley PSP Precision pyranometer and an inverted Middleton CN-7 pyranometer. Net radiation was measured with Middleton CN-1 net pyrradiometer. The lower dome on a further CN-1 was replaced with a black-box cavity to measure incoming all-wave radiation from which $L\downarrow$ could be determined by residual. An Eppley pyrgeometer directly measured $L\downarrow$ during July 1987 and April to May 1988. Terrestrial longwave radiation was not directly measured in 1986-87, but was measured in 1988 with a second Eppley pyrgeometer. Based upon manufacturer's calibrations for the radiometers and data aquisition systems, the errors in radiation flux

densities were $\leq \pm 5\%$, which is characteristic of instruments of this sort (Latimer, 1972; Hay and Wardle, 1982). Inversion of radiometers to measure $K\uparrow$ and $L\uparrow$ may have increased the errors (Fuquay and Buettner, 1957).

Net pyrradiometer domes were manually dessicated and sealed, since no satisfactory method of unattended aspiration was found. Blowing snow and rime formation dictated the necessity for regular replacement of domes, as also noted by Walton (1982). The performance of the net pyrradiometer with black-body cavity was unreliable during the 1986-87 season, and much of the longwave radiation data were subsequently rejected. The 1988 data set is of high quality throughout.

All radiation instruments were mounted on the same mast and arranged for minimum mutual disturbance. Sensor height was about 1.4 m, with a concomitant viewed area of 15 m radius for down-facing sensors (Latimer, 1972). Horizon obstruction to solar radiation was minimal, and only significant for a few days before and after the winter solstice. At this time the sun was partially obscured by a mountain 1 km to the southwest for the last hour of the day.

All data were collected and stored using Campbell Scientific CR21 and 21X dataloggers which recorded sensor signals at 10 s intervals and stored hourly means. Daily data were derived from the hourly measurements. Two data losses of several days each occurred in January, 1987 (longwave radiation only) and March, 1987 (all radiation data), resulting from accidental erasure of data.

The instruments were serviced daily for periods ranging from a few days (winter) to several weeks (summer). Data quality at these times is good, especially considering the remoteness and harshness of the environment. Some problems were encountered with the sensors, almost exclusively at times when the site was unattended. The most severe problem was rime ice formation on the radiometer domes. Such conditions could be recognized in the data set, since albedo became radically greater than unity as the $K\downarrow$ dome became more obscured than the $K\uparrow$ dome. Snow was less of a problem than rime. Snow usually fell as dry flakes or pellets which did not adhere to the radiometer domes.

From a total of nearly twelve months of continuous operation, 300 days (85%) were used in daily and monthly radiation budget description and analysis. As could be expected, most of the unusable data occured in the winter when conditions were most inclement. More longwave data is missing than solar, as a result of the problems with the black-body cavity.

MEASUREMENT RESULTS

Hourly Radiation Budget

At the hourly timescale, the daytime radiation trends were generally dominated by solar radiation, although in mid-winter the longwave radiation fluxes were often of larger magnitude. Most days were cloudy or partly cloudy, and many showed wide-ranging variations in radiation fluxes caused by changing cloud cover. Completely cloudless days accounted for only 11% of the total of 334 usable days of data. Although a minority case, the cloudless-day situation will be described first.

The radiation budgets for December 10, 1986 and May 21, 1988 were good examples of the extreme cases typical of winter and summer (Figures 4.1 and 4.2). The differences in solar radiation flux densities are clear: global solar radiation reaches a maximum of about $320\,W\,m^{-2}$ in the December case compared to nearly $1000\,W\,m^{-2}$ in the May example. Mean daily transmissivities are similar: 0.70 and 0.76 respectively. Hourly transmissivity varies with solar elevation. The topographic blocking of the sun is evidenced for the last hour of the day, when the transmissivity is halved (Figure 4.1).

Several spot measurements of diffuse solar radiation were made on cloudless days at Scout Mountain by temporarily shielding the Eppley pyranometer. Invariably the ratio of diffuse-beam radiation to global solar radiation was about 1:6 or 0.17. This can be compared with values from other alpine areas. Sauberer and Dirmhirn (1953) modelled values of 0.08-0.14 at 3000 m a.s.l. in the Alps, Bishop *et al.* (1966) measured 0.14 at 5000 m a.s.l. altitude in the Himalayas, and a value of 0.13 was found in the White Mountains of California (Terjung *et al.*, 1969a). The Scout Mountain value of 0.17 is slightly greater than these measurements, and is probably due to the lower altitude (2350 m a.m.s.l.) of the measurement site. Possible, though unlikely, is the added effect of pollutants from the urban areas upwind to the west (Vancouver and Seattle).

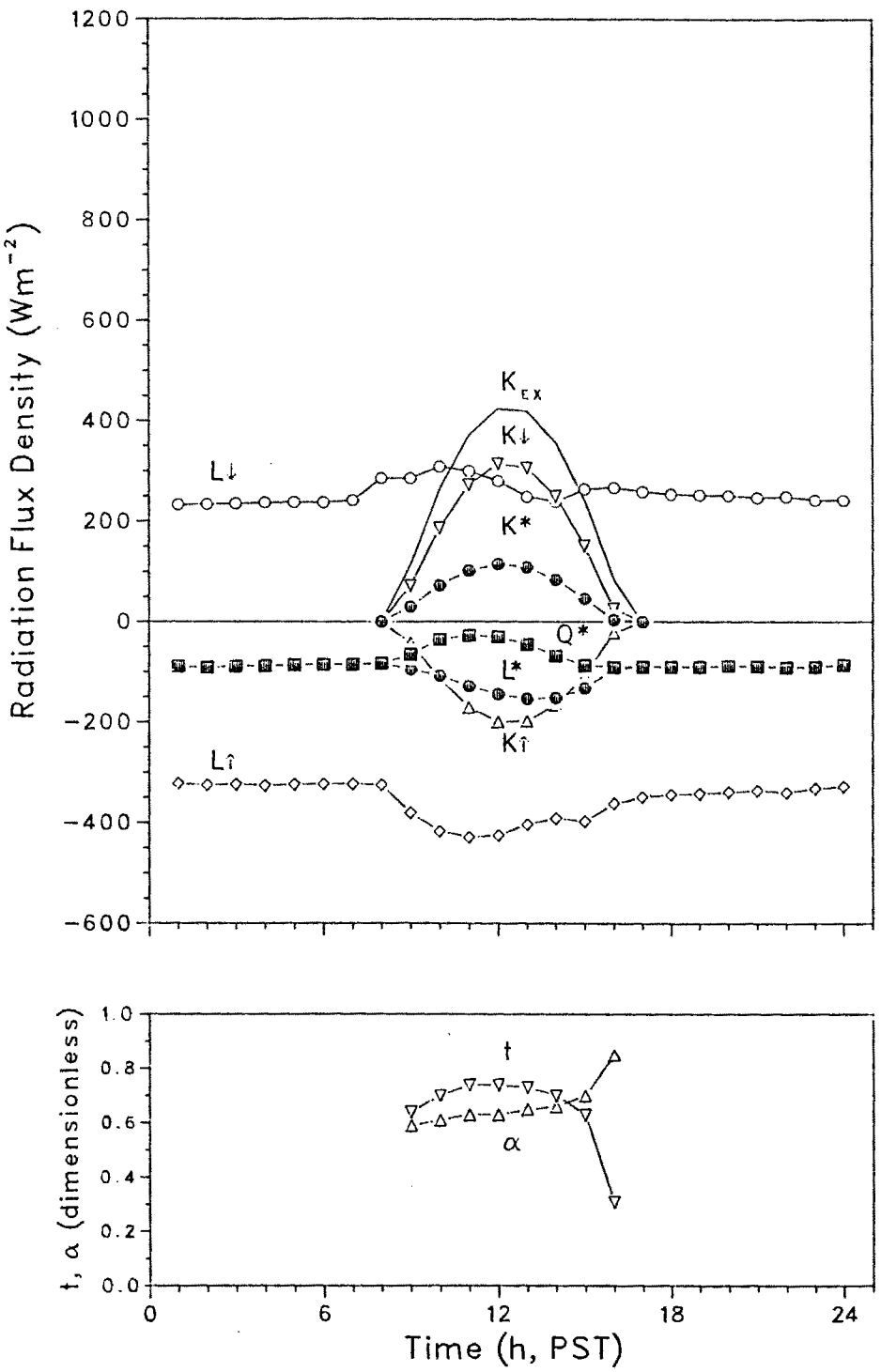

Figure 4.1. Hourly radiation flux densities measured at Scout Mountain on December 10, 1986 for a snow-covered surface and cloudless skies.

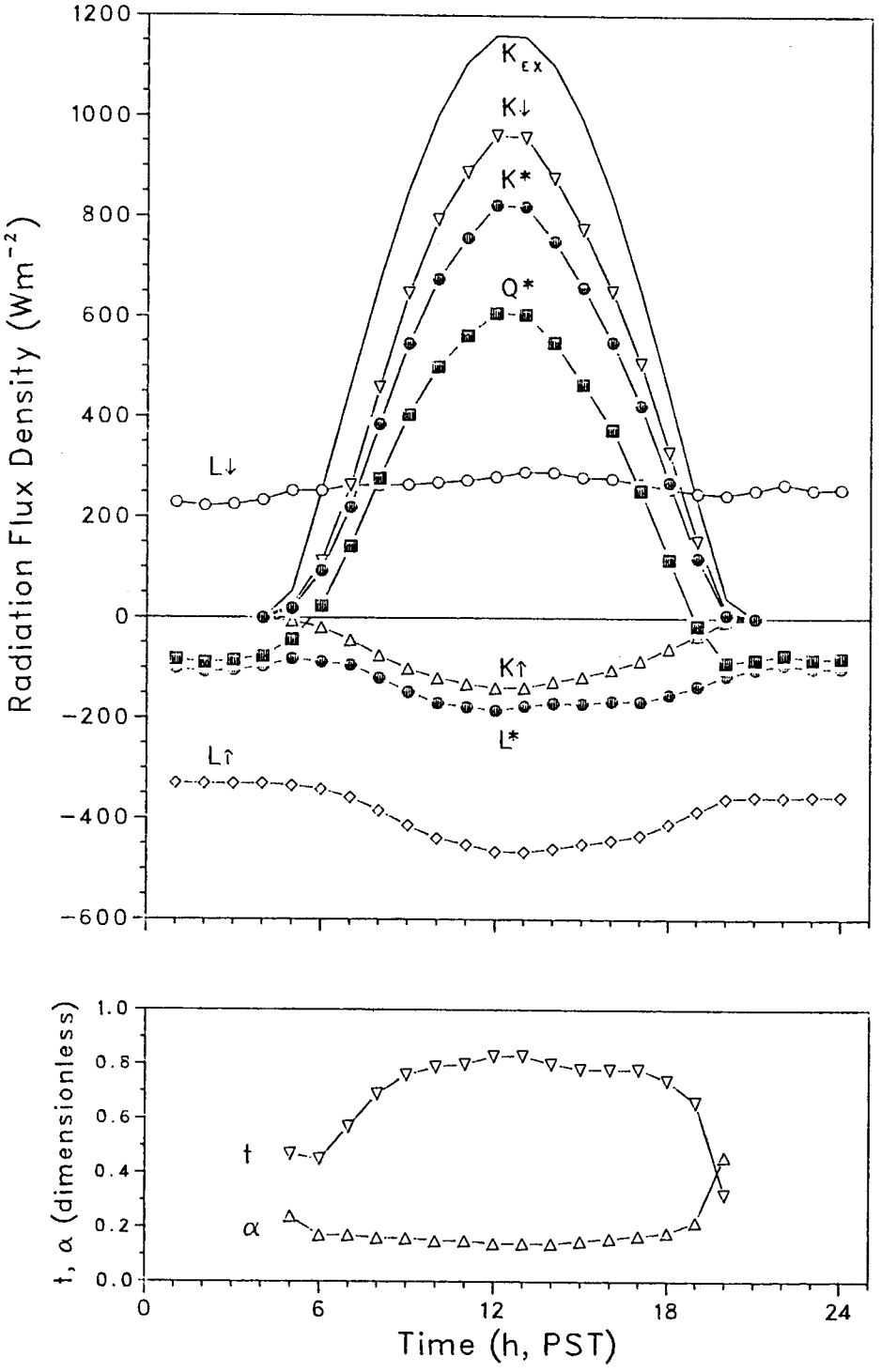

Figure 4.2. Hourly radiation flux densities measured at Scout Mountain on May 21, 1987 for a snow-free surface and cloudless skies.

The difference in albedo between the winter snow cover and the summer tundra resulted in very different net solar radiation values: maximums of 100 and 851 W m^{-2} occurred. In the December case, K^* was not sufficiently large to cause net radiation to become positive. In May, Q^* was strongly controlled by K^* throughout the daytime. Slight increases in albedo were noted at low solar elevations on days without heavy cloud cover. Similar phenomena have been noted in other alpine studies (Terjung *et al.*, 1969a; Bowers, 1988; Bailey *et al.*, 1989). Possible explanations for this are direct-beam solar radiation striking the inverted pyranometer dome (Fritschen, 1967), trapping of incident radiation in ground-surface interstices at higher solar elevations (Coulson and Reynolds, 1971), the specular nature of reflection of most natural surfaces at low solar angles (Oke, 1987) and errors in sensor levelling. Alpine snow surfaces have also also been found to show similar diurnal albedo trends, attributed to changing snow crystal structure and water content (Ambach and Hoinkes, 1963; Wagner, 1979). None of these explanations can be excluded at Scout Mountain.

Night-time longwave radiation fluxes were remarkably similar for both the cloudless days depicted in Figures 4.1 and 4.2, but the greater daytime surface heating on the summer day resulted in greater daytime radiative heat losses. Although the diurnal trend of net radiation was strongly governed by solar radiation in both cases, the magnitude of the longwave radiation dominated the overall radiation budget in winter.

Cloudy or partly cloudy skies accounted for most days of data. The erratic behaviour of the solar and net radiation fluxes on April 28, 1988 (Figure 4.3) are characteristic of showery conditions with sunny breaks. Large variations in transmissivity occurred as cloud cover changed, being 0.30-0.40 during precipitation events and increasing to 0.80 during sunny spells. Albedo was relatively constant but did display a small response around midday to small accumulations of fresh snow. Longwave radiation did not vary greatly, although small changes in L^* can be attributed to cloud variations. For example, at 1500 h when transmissivity is high, L^* decreases due to lack of an insulating cloud cover, and the reverse situation occurs at 1200-1300 h.

A typical cloudy day is shown in Figure 4.4 for April 20, 1987. Cloud cover was mostly 10/10 altocumulus and altostratus in varying thicknesses. This is reflected by the

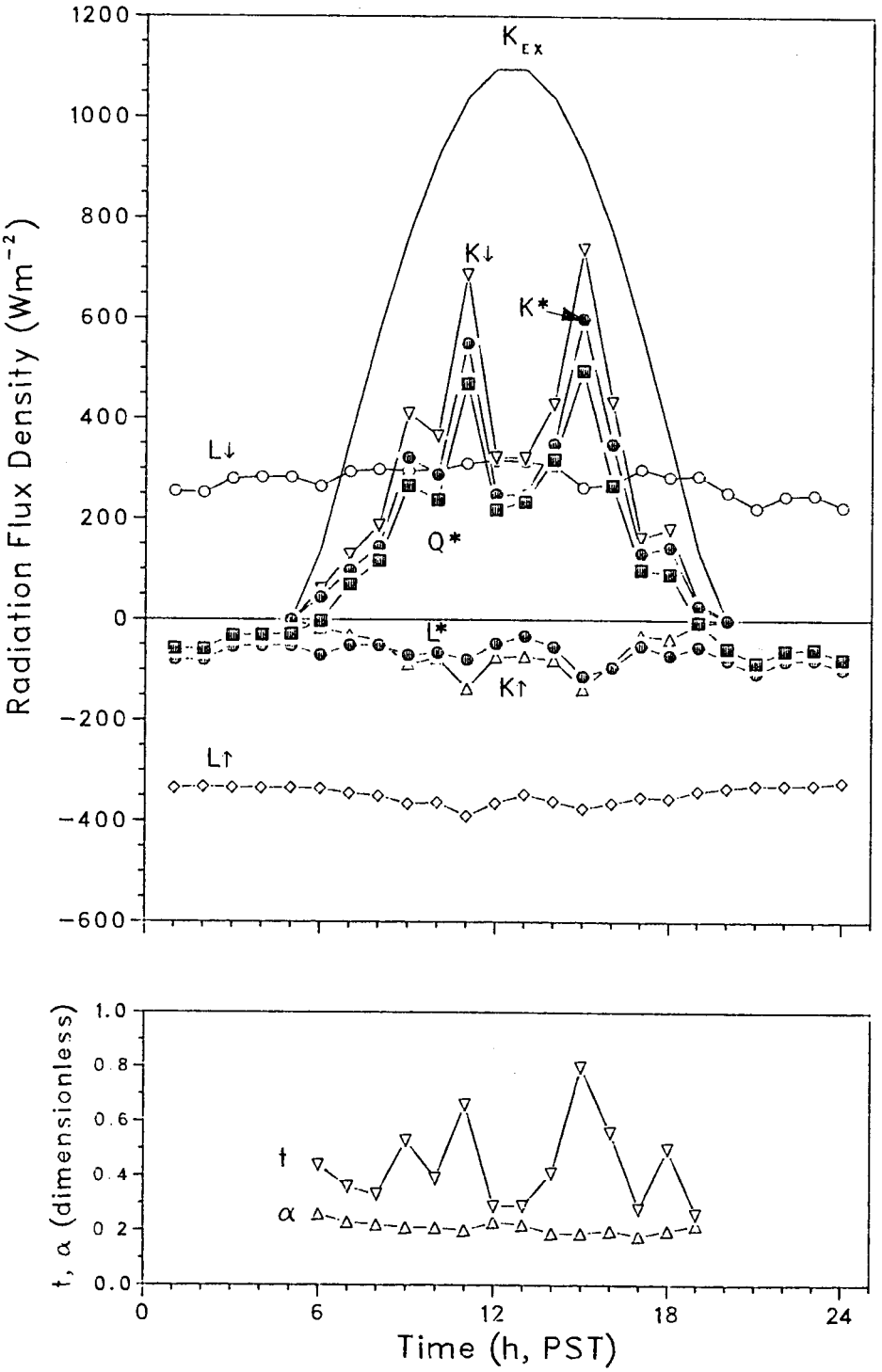

Figure 4.3. Hourly radiation flux densities measured at Scout Mountain on April 28, 1988 for a snow-free surface and intermittent cloud.

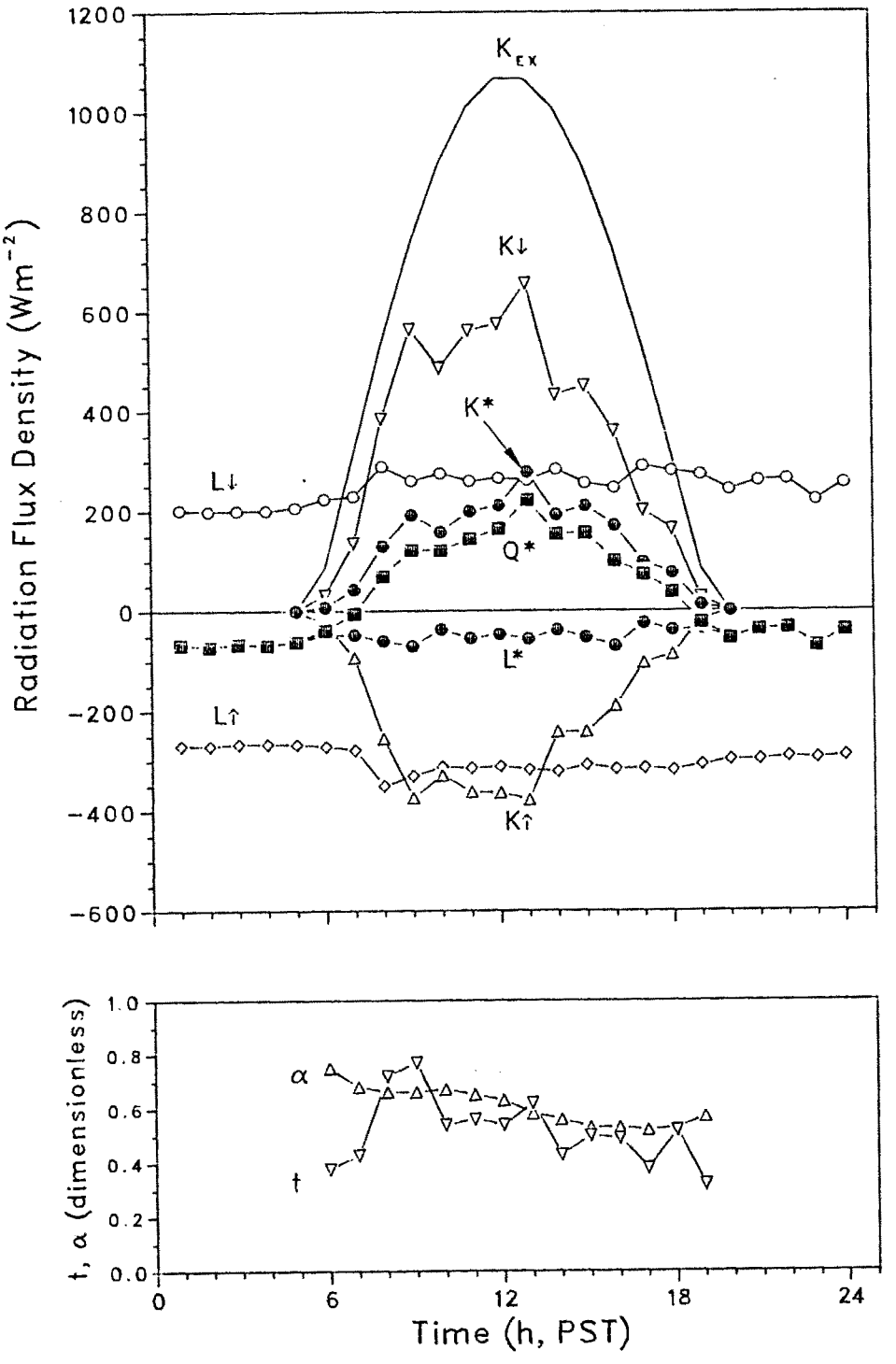

Figure 4.4. Hourly radiation flux densities measured at Scout Mountain on April 20, 1987 for snowmelt conditions and high overcast cloud.

conservative nature of transmissivity and the solar and net radiation flux densities. The longwave radiation fluxes are essentially constant and net longwave radiation does not exceed $-100\ W\,m^{-2}$. This day occurred during a period of melting and the decrease in albedo over the day from 0.75 to 0.50 is clearly exhibited.

Heavy overcast skies and precipitation frequently occurred at Scout Mountain. A typical day with such conditions was June 16, 1987, characterized by snowfall from morning nimbostratus followed by a decrease in cloud height which gave fog at the site in the afternoon (Figure 4.5). Transmissivity only once rose above 0.25. Albedo showed the effects of the snow shower in late morning, with a sudden increase from the tundra value of 0.16 to nearly 0.50. The snow quickly melted. Such events are common at any time in the alpine environment. Longwave radiation exchanges were limited by the presence of cloud, and net losses were less than $-50\ W\,m^{-2}$ throughout the entire 24-hour period.

It is common for mountain ranges to generate their own cloud cover. Figure 4.6 shows the radiation budget for May 10, 1988, a typical warm spring day which began with cloudless skies then developed convective cumulus over the higher parts of the Cascade Mountains while leaving much of the lower-lying country to the north and east with little or no cloud. A complete cumulus cover had developed over Scout Mountain by 1500 h. The trend in transmissivity is characteristic of such days, decreasing from about 0.80 to low values of 0.20 – 0.40 in a few hours. The solar and net radiation trends are markedly affected, and to a lesser degree so is longwave radiation. The afternoon cloud limits solar radiation inputs and enhances longwave radiation inputs such that both K^* and L^* tend towards smaller magnitudes. Similar diurnal trends are seen in many mountainous regions.

Daily Radiation Budget

Daily totals of global solar radiation varied greatly at Scout Mountain (Figure 4.7 and 4.10). This was a result of the seasonal changes in earth-sun relationships and daily changes in the atmospheric transmissivity induced by synoptic and local weather patterns.

Transmissivity was generally in the range 0.20 to 0.80 (Figures 4.8 and 4.10). The central tendency of the data was approximated by $t = 0.50$. Days when $t > 0.80$ occurred exclusively in winter. The colder atmosphere of this season restricts both the water vapour

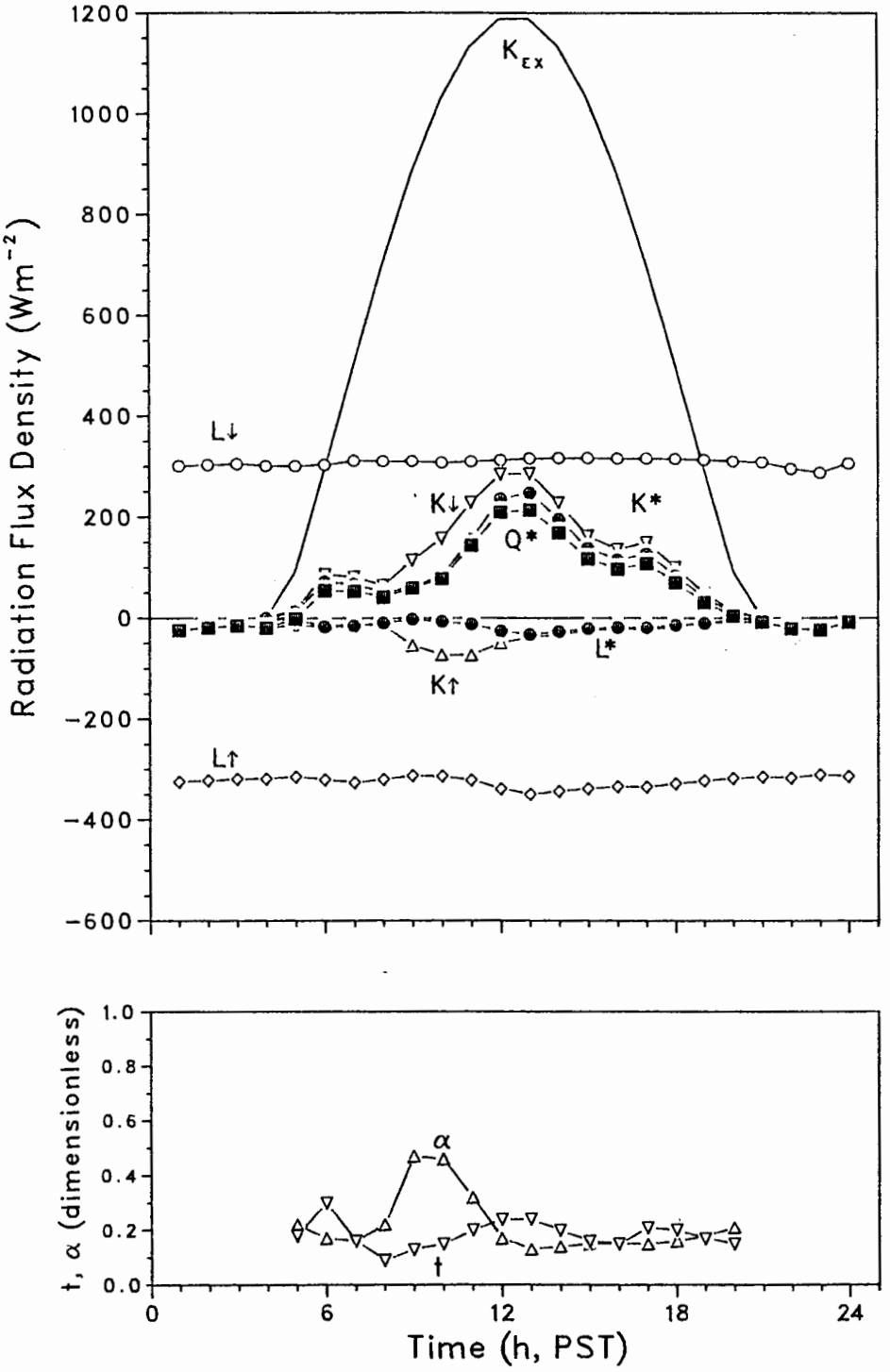

Figure 4.5. Hourly radiation flux densities measured at Scout Mountain on June 16, 1987 for heavy overcast skies with mid-morning snowfall.

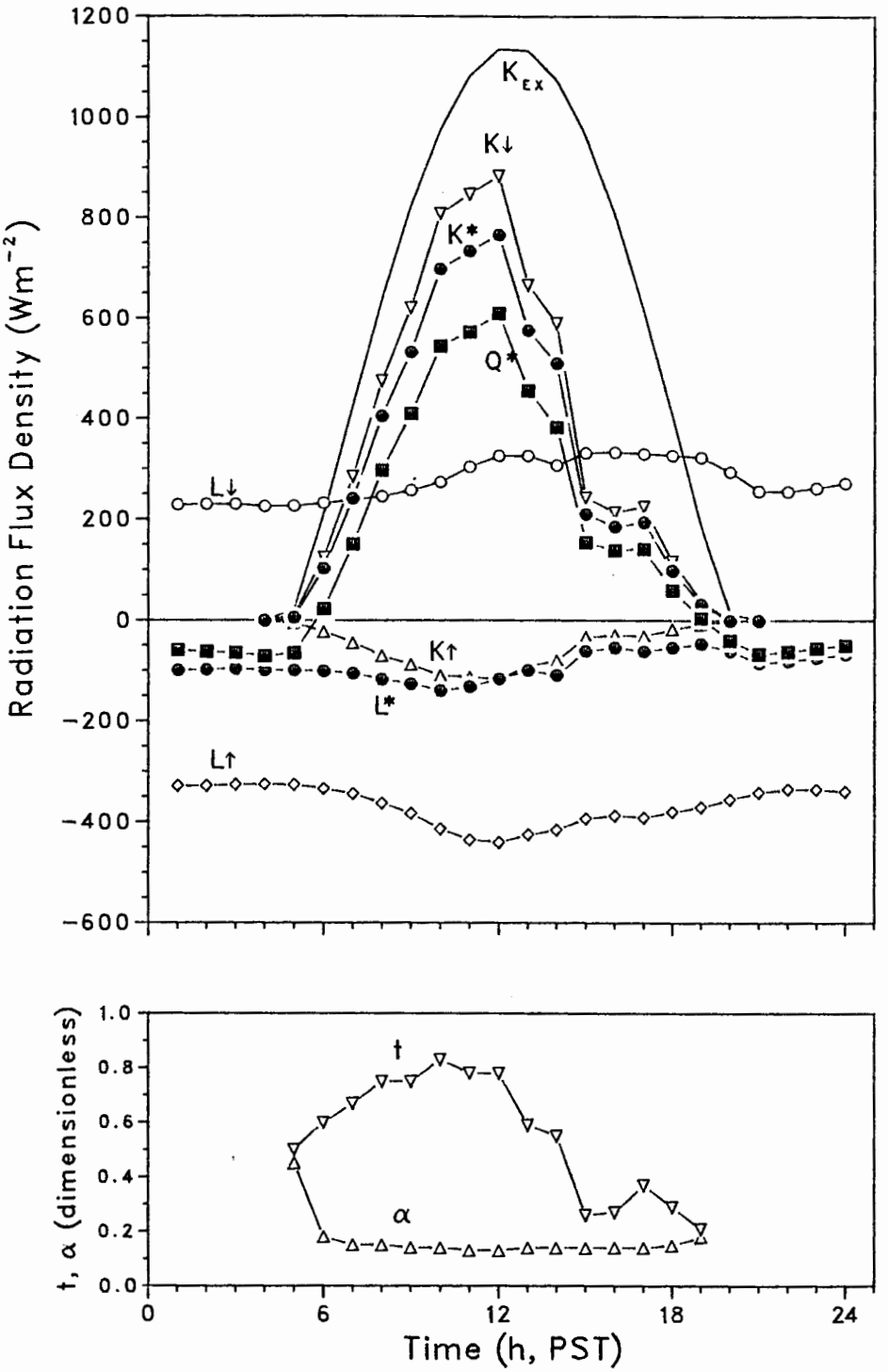

Figure 4.6. Hourly radiation flux densities measured at Scout Mountain on May 10, 1988 for a snow-free surface with afternoon convective cumulus development.

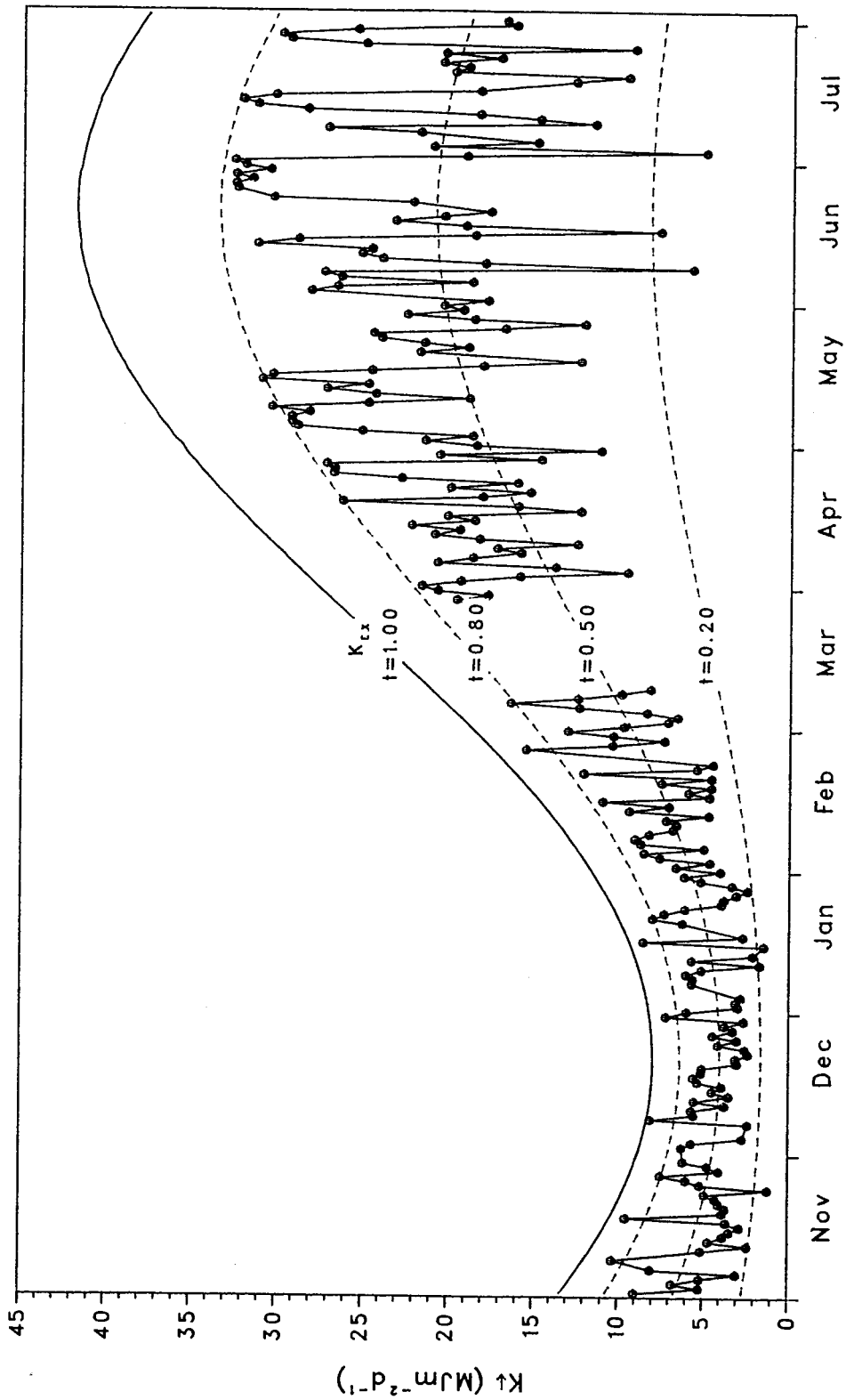

Figure 4.7. Daily totals of K_{EX} and K↓ for November 1987 to July 1987. Dashed lines show different values of $K\downarrow/K_{EX}$.

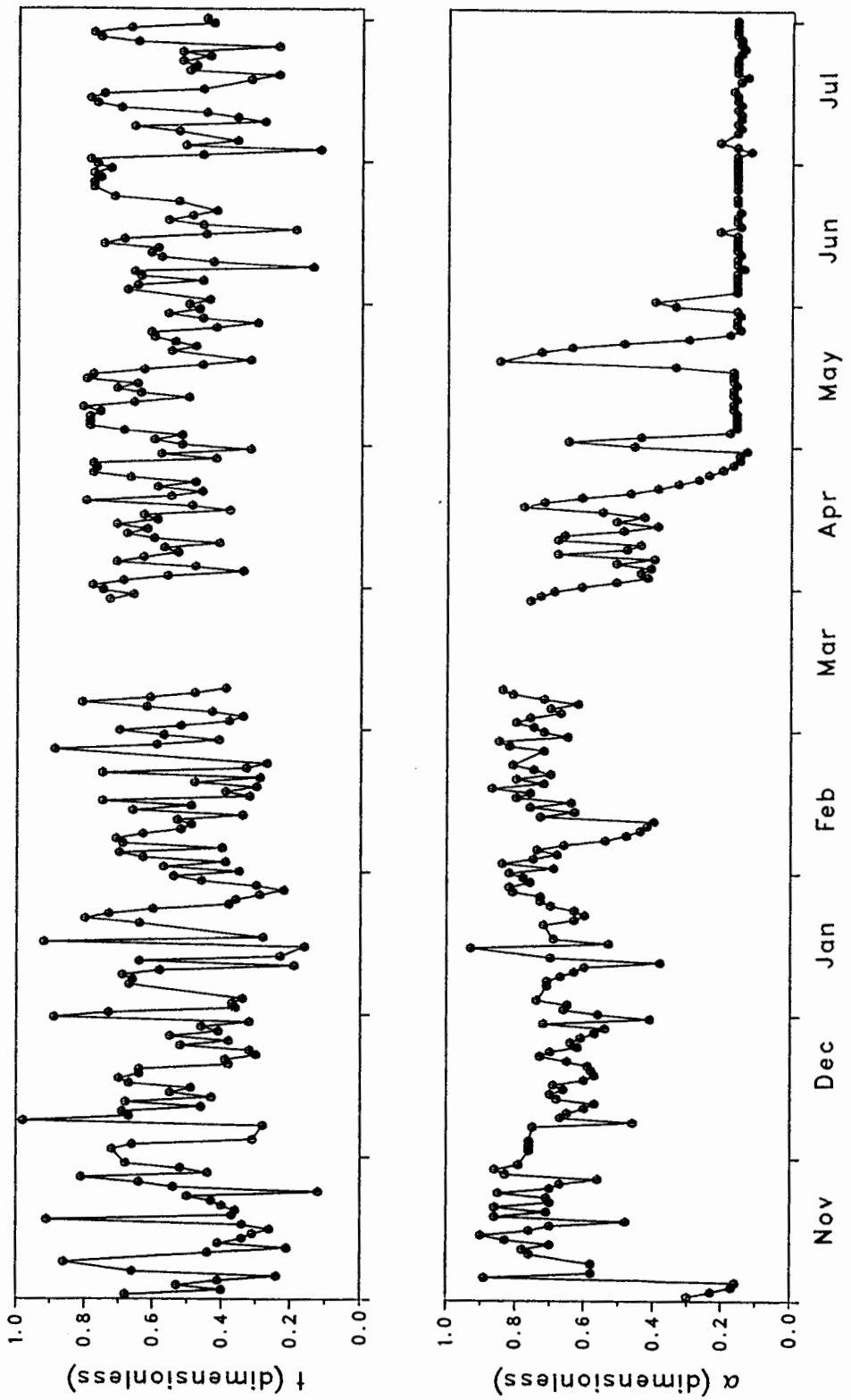

Figure 4.8. Daily t and α for November 1986 to July 1987.

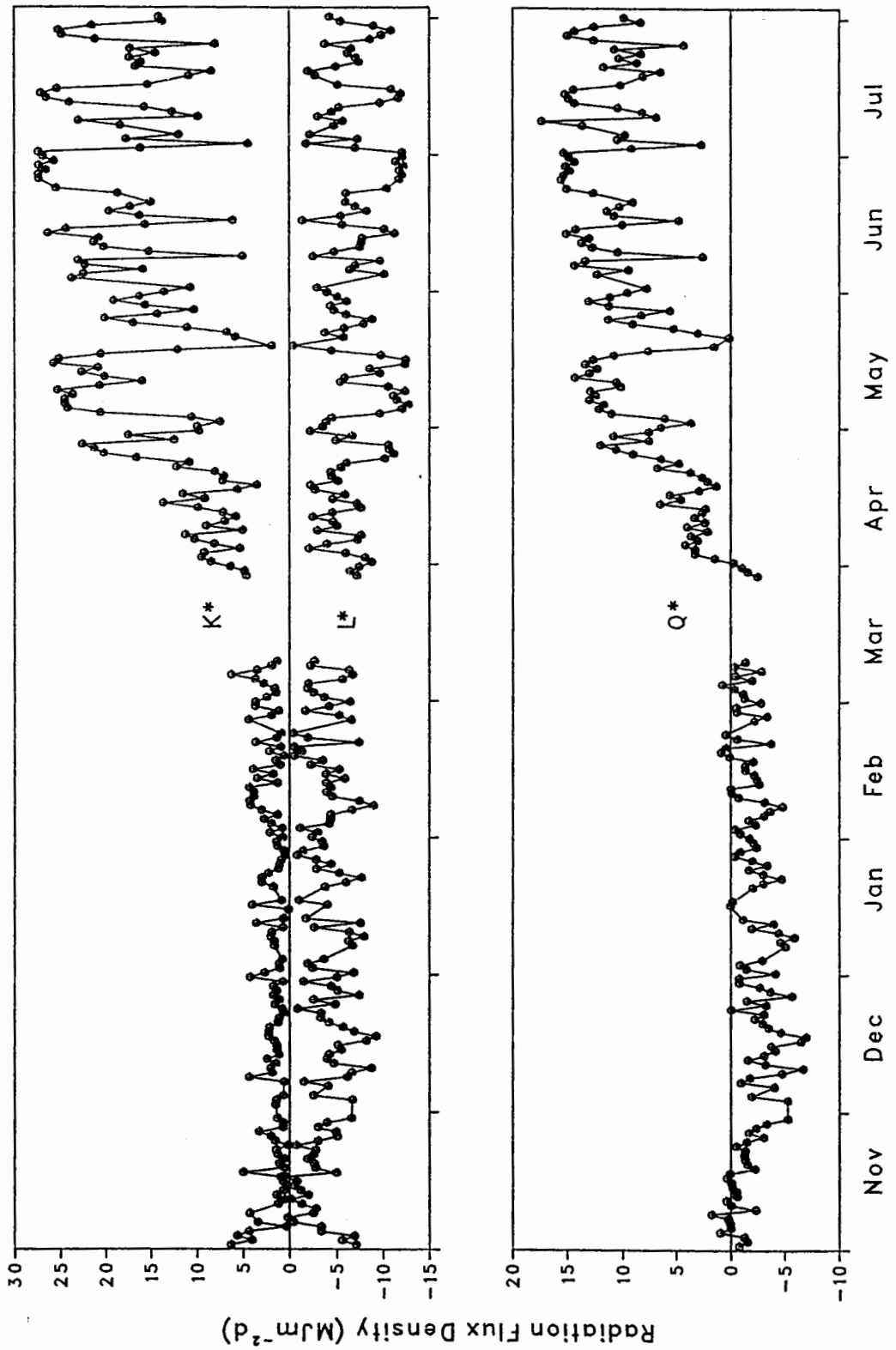

Figure 4.9. Daily totals of K*, L* and Q* for November 1986 to July 1987.

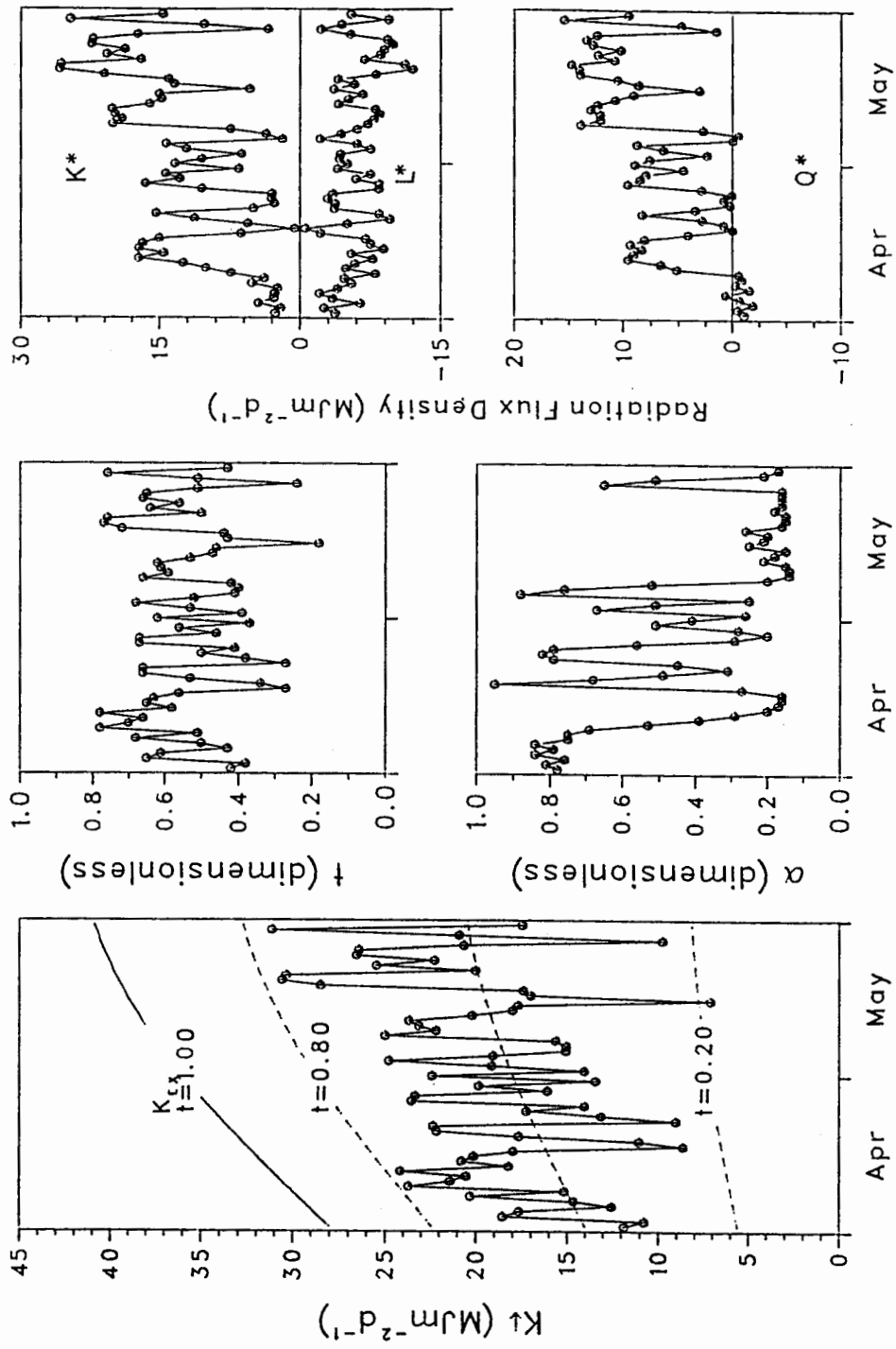

Figure 4.10. Daily K_{EX}, K↓, K↑, t, α, K*, L* and Q* for April to May 1988.

content and the convective input of pollutants, thus contributing to higher transmissivities. The increased frequency of temperature inversions typically found in southern British Columbia may also play a role by trapping pollutants and aerosols in the valleys. The maximum measured transmissivity of 0.98 (December 8, 1986) is too high to be a consequence of greater atmospheric transparency, however. Multiple reflections between the ground and cloud cover are the probable explanation, and one which is supported by the fact that extreme transmissivities were only measured when the surface was snow-covered.

Transmissivity was rarely less than 0.20. This probably resulted from the reduced optical path length as a consequence of high altitude (Haurwitz, 1948) but in the absence of comparable data from local lowland sites this cannot be verified for the Scout Mountain data.

Albedo, like transmissivity, exerted a highly variable control on the daily radiation budget for most of the two field seasons (Figures 4.8 and 4.10). Generally, it was high (0.60 - 0.80) in winter and low (about 0.17) in summer, as is typical for a surface with seasonal snow cover. Of interest at Scout Mountain was the variability in α during the snow months. Even in midwinter, α varied from day to day and was rarely constant for more than three days. This variability was due to the very thin snowpack at Scout Mountain, which often changed rapidly with radiation input, wind and storm activity. Rarely was the snow sufficiently deep to cover all the rocks and vegetation at the site. Additionally, aeolian erosion and deposition of the snow formed continually-changing sastrugi (Figure 1.4), whose alignment have been shown to affect surface reflectivity (Wendler and Kelley, 1988).

Only the first complete melting of the winter snow cover resulted in a progressive decline in albedo. Melting was complete within a week in both years (late April 1987 and early April 1988). This rapid decline in snow cover and the consequent effect on albedo is characteristic of thin snowpacks in Arctic tundra (Rouse, 1984a) and prairie settings (Gray and Landine, 1987). After the winter snow cover had melted, subsequent fresh snowfalls melted quicker and albedo showed very rapid changes (such as in late April to early May, 1988). Even in summer, occasional snowfalls increased α, otherwise daily values were relatively constant at 0.16 to 0.17. Although all the lower albedo values measured (e.g. α = 0.14 on July 3, 1987) were associated with rainfall, rain often had little or no effect.

Daily variations of longwave radiation transfers were not as marked as those of solar radiation. This resulted in a very conservative net longwave radiation flux at both seasonal and daily timescales (Figures 4.9 and 4.10). Deviations of L* from the mean were about 4 MJ $m^{-2}d^{-1}$ compared to 15 MJ $m^{-2}d^{-1}$ for K*. Daily L* was generally greater in magnitude than K* during the winter snow months but the reverse was true for April to July.

Daily net radiation totals thus displayed strong seasonality, controlled by the presence or absence of the winter snow cover. A winter longwave–dominated regime characterized by small net radiation losses gave way to a summer solar–dominated regime with much greater positive net radiation (Figure 4.9). In the winter, the presence of a snow cover led to suppressed radiation transfers regardless of atmospheric conditions. This persisted into early spring, and Q* remained negative despite the seasonal increase in solar radiation inputs. Although the snow cover was always very thin, the frequency of snow storms was sufficient to maintain minimal absorption of solar radiation, and Q* did not become positive in the spring until there were a few consecutive snowfall–free days (which occurred in early April in both years). In the summer, the radiation budget was consequent on controls from both the surface and the atmosphere; when snow cover was absent (for example, throughout July 1987) atmospheric transmissivity was the dominant control.

Monthly Radiation Budget

Mean daily radiation flux densities for each month of measurement at Scout Mountain are given in Table 4.1 and Figures 4.11 and 4.12. The trend of global solar radiation closely followed that of extraterrestrial radiation as a result of the conservative changes in transmissivity (Figure 4.11). The solar radiation input was about 2 MJ $m^{-2}d^{-1}$ less in the spring of 1988 than in 1987. Atmospheric transmissivity displayed no strong seasonal trend, but was less in 1988 due to greater cloud cover from increased storm activity. The role of winter snow in controlling seasonal solar radiation transfers is clear: the winter albedo values of 0.60 to 0.70 declined during April to May to the summer value of about 0.17. The stormier weather in April to May 1988 resulted in more snowfall than the same period in 1987, resulting in higher albedoes.

Net solar radiation was very small (less than 5 MJ $m^{-2}d^{-1}$) all winter, but showed a dramatic increase from May onwards as the snow cover disappeared (Figure 4.12). The value

Table 4.1. Mean daily radiation flux densities measured at Scout Mountain, November 1986 to July 1987 and April to May 1988.

Month	K_{EX}	K↓	K↑	K*	t	α	L↓	L↑	L*	Q*
Nov 1986	11.10	5.14	3.14	1.99	0.48	0.61	22.48	25.19	−2.74	−1.00
Dec 1986	8.12	4.45	2.76	1.69	0.55	0.62	22.15	27.08	−4.96	−3.34
Jan 1987	9.88	4.63	3.12	1.52	0.47	0.67	20.77	24.28	−3.98	−2.41
Feb 1987	14.75	7.62	5.18	2.45	0.52	0.68	20.71	24.73	−4.02	−1.57
Mar 1987	21.48	12.49	9.08	3.42	0.58	0.73	20.86	25.57	−4.71	−1.29
Apr 1987	32.00	18.63	8.13	10.51	0.58	0.44	21.80	27.65	−5.85	4.67
May 1987	38.84	22.90	6.03	16.87	0.59	0.26	22.33	29.77	−7.43	9.43
Jun 1987	41.72	24.23	4.00	20.23	0.58	0.17	25.09	33.37	−8.03	12.02
Jul 1987	39.69	20.66	3.24	17.41	0.52	0.16	25.83	32.42	−6.59	10.83
Apr 1988	32.00	17.32	9.00	8.32	0.54	0.52	23.03	28.59	−5.37	3.44
May 1988	38.84	20.85	5.68	15.17	0.54	0.27	22.92	29.44	−6.52	9.27

All values are $MJm^{-2}d^{-1}$, except t and α which are dimensionless.

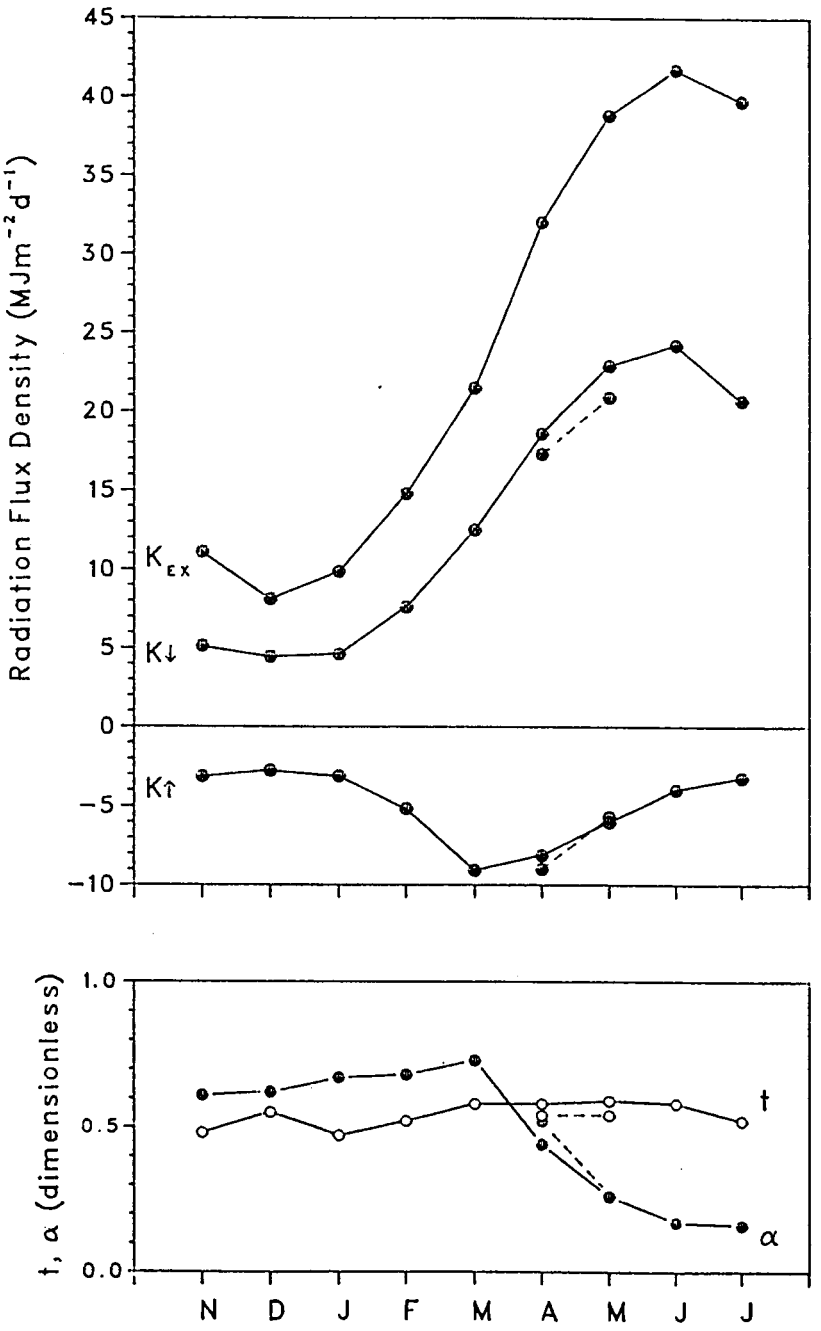

Figure 4.11. Monthly mean daily K_{EX}, K↓, K↑, t and α for November 1986 to July 1987 (solid lines) and April to May 1988 (dashed lines).

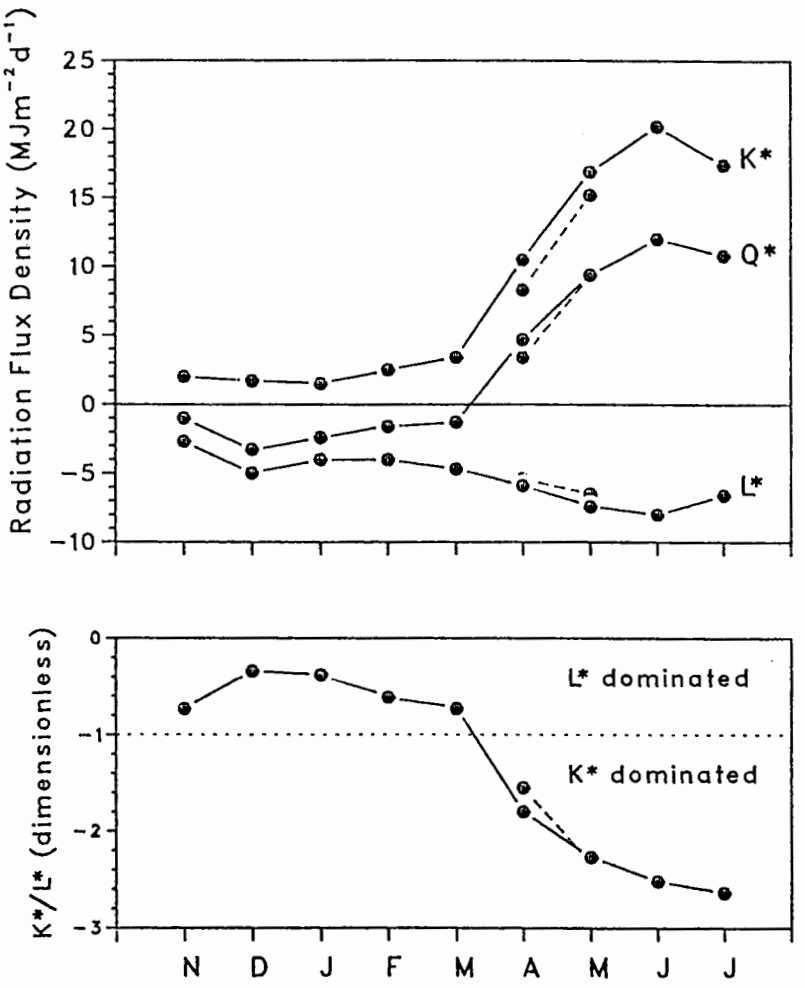

Figure 4.12. Monthly mean daily K*, L* and Q* for November 1986 to July 1987 (solid lines) and April to May 1988 (dashed lines).

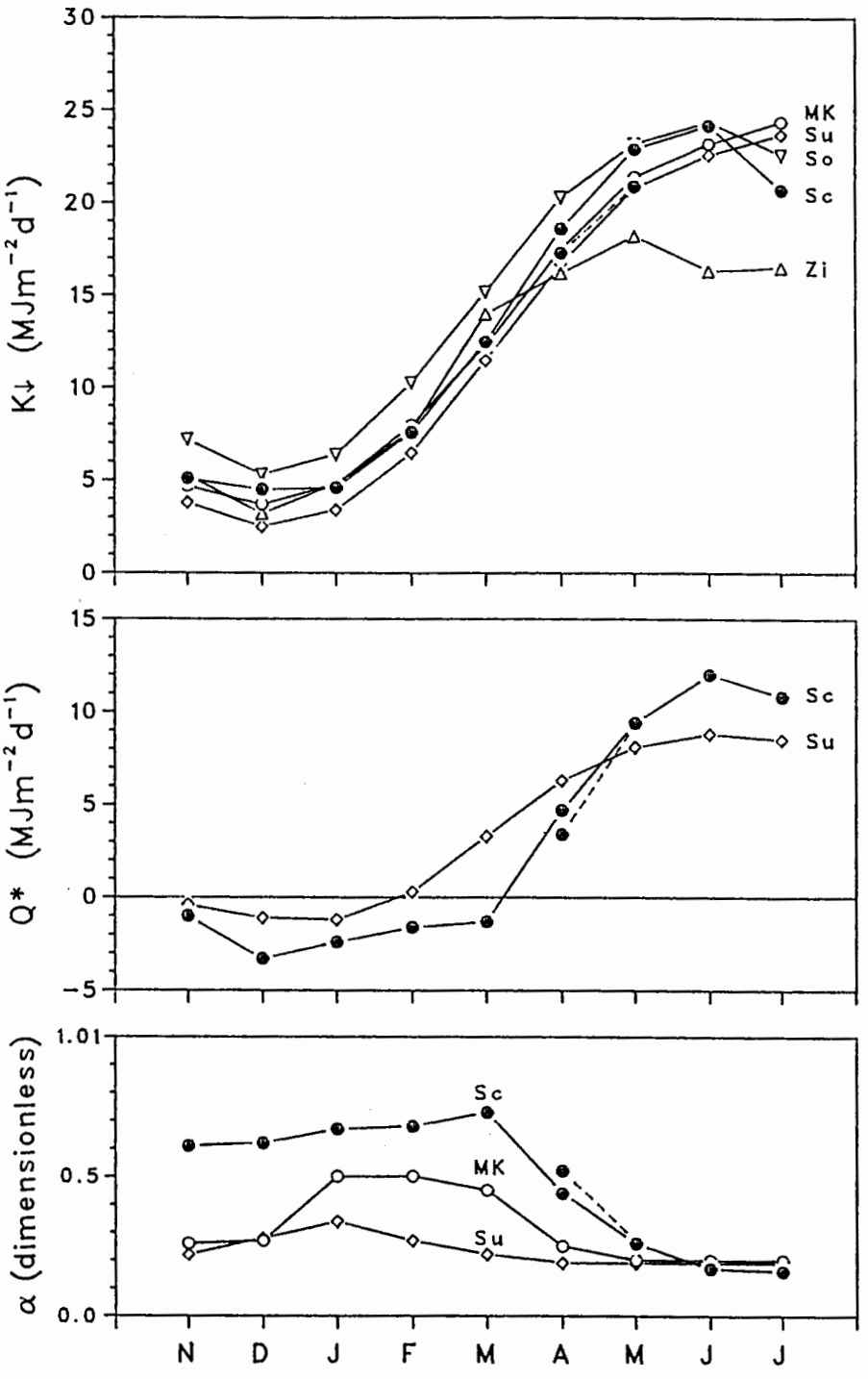

Figure 4.13. Monthly mean daily K↓, Q* and α for three British Columbian locations (Sc: Scout Mountain; MK: Mount Kobau; Su: Summerland) and two Austrian locations (So: Sonnblick; Zi: Zirbitzkogel). Dashed lines are Scout Mountain 1988 data.

of K^* in 1988 was about 2.0 MJ $m^{-2}d^{-1}$ less than that in 1987 due to the higher albedo. Longwave radiation transfers were more conservative than solar radiation transfers and displayed trends commensurate with seasonal temperatures. Winter snow cover suppressed longwave radiative losses, and L^* was consequently smaller than in the summer (Figure 4.12).

Net radiation was small and negative for the snow season and strongly positive during the summer, reflecting the seasonal control of albedo and the dominance of solar radiation in the radiation budget in summer. The relative contributions of solar and longwave radiation, as described by K^*/L^*, show that a winter L^*-dominated regime changes to a summer K^*-dominated regime between March and April (Figure 4.12 and Table 4.1). Based upon these observations, therefore, longwave radiation appears to exert an important control on daily and monthly net radiation for about half of the year.

Figure 4.12 compares Scout Mountain data with local weather station normals from Summerland (50° N, 120° W) and Mount Kobau (49° N, 120° W), respectively 70 and 40 km distant and 454 and 1862 m amsl. Two Austrian sites from similar latitudes are included for comparison: Sonnblick (47° N, 13° E, 3100 m amsl) and Zirbitzkogel (47° N, 12° E, 2500 m amsl) (data from Sauberer and Dirmhirn, 1958). As could be expected, $K\downarrow$ at Scout Mountain was generally greater than the local stations in 1986–87 as a result of its higher altitude, but the 1988 data show little difference from the Mount Kobau normals. The greatest difference between the data sets occurs in July, when $K\downarrow$ at Scout Mountain was markedly less than the long-term means of the two weather stations, and suggests unseasonably heavy cloud cover. Apart from July, Scout Mountain data showed similar trends to all the other data except that for Zirbitzkogel, which appears to experience spring and summer cloud cover.

A clear difference between the alpine radiation climate at Scout Mountain and nearby lowlands at Summerland is illustrated by the net radiation trends for each site (Figure 4.12). The longer duration of snow in the alpine zone kept net radiation low in the winter and spring months, but more intense radiation loading at the higher altitude in the summer led to an alpine Q^* magnitude which exceeded the lowland values. The effects of the alpine snow cover are also clearly apparent in the graph for albedo.

DISCUSSION

The Scout Mountain radiation budgets correlated well with the generalized fellfield regimes described by Lewis and Callaghan (1976). A winter snow period characterized by limited radiation flux magnitudes was followed by a short snowmelt period which led to a summer regime characterized by much greater absorbed solar and emitted longwave radiation from a snow-free tundra surface. The primary control on the radiation budget in winter and spring was the presence of the snow cover. In summer, atmospheric controls played the major role. Thus the radiation budget showed two seasonal regimes separated by a short transition period.

Based upon appearances alone, there is little in the figures which individually can be labelled as being uniquely alpine. The controls of the radiation budget depicted could result from any mid-latitude location which experiences seasonal snow cover. Those components which help to define alpine radiation budgets can be seen, such as the high transmissivities on cloudless days, the local orographic cloud effects, the responsiveness of albedo to snow cover, the conservative nature of longwave radiation fluxes, and the marked seasonal trend of net radiation. The collective association of all these defines the alpine radiation budget. Additionally, the greater variability in transmissivity in the alpine zone induced by local orographic cloud has been used to distinguish alpine tundra radiation budgets from those of Arctic tundra (LeDrew and Weller, 1978).

A further characteristic of the alpine radiation budget at Scout Mountain, and probably typical of dry alpine tundras in general, is the erratic nature of the albedo. Although almost consistently high throughout the winter months, albedo did fluctuate from day to day. In spring, once the winter snow cover had been depleted, albedo varied widely due to changes in snow cover resulting from storm precipitation and radiative and wind-induced snowpack depletion. This contrasts with the more strictly delineated seasonal albedo trends found in Arctic tundra (Lewis and Callaghan, 1976; Rouse, 1984a). In the latter cases, albedo is depicted as decreasing from winter values to snow-free values within a few days, and remaining low thereafter. The variability of the alpine tundra albedo hinders the development of albedo decay models found for other environments such as prairie regions (Gray and Landine, 1987).

As could be anticipated, longwave radiation transfers tended to be very conservative. In terms of its magnitude and contribution to net radiation, longwave radiation was most important during the winter. With the increases in solar radiation inputs and decreased snow cover in spring and summer, longwave radiation became of secondary importance. Overall, therefore, net radiation at Scout Mountain responded to a variety of controls operating at a wide range of spatial and temporal scales.

CHAPTER V

MODELLING LONGWAVE RADIATION IN AN ALPINE TUNDRA, SCOUT MOUNTAIN, SOUTHERN BRITISH COLUMBIA, CANADA

INTRODUCTION

The review of alpine radiation budget research in Chapter II concluded that the longwave component has received relatively little attention. Although longwave radiation is often of secondary importance in the radiation budget, its relative contribution to net radiation increases when a snow cover exists and when topographic influences are of importance. The previous chapter demonstrated that longwave radiation transfers are important controls on net radiation during the winter months. Even in summer, longwave radiation can play a significant role in the mountain radiation budget, where appreciable increases in longwave radiation receipt occur due to terrain emittance. This study examined modelling approaches to all three components of the longwave radiation budget at an alpine tundra in southern British Columbia, Canada. For atmospheric longwave radiation, several published empirical models, as well as variants of the Stefan–Boltzmann equation, were tested. Terrestrial longwave radiation was modelled using air and surface temperatures. Net longwave radiation was derived from both a combination of the above approaches and other, empirical, methods.

THEORETICAL BACKGROUND

The longwave radiation budget is described by

$$L^* = L\downarrow - L\uparrow \qquad (5.1)$$

where $L\downarrow$ is atmospheric longwave radiation, $L\uparrow$ is terrestrial longwave radiation, and L^* is the net longwave radiation. Terrestrial longwave radiation is defined by the Stefan–Boltzmann equation

$$L\uparrow = \epsilon_0 \sigma T_0^4 + (1-\epsilon_0)L\downarrow \qquad (5.2)$$

where ϵ_0 is surface emissivity, σ is the Stefan–Boltzmann constant and T_0 is surface

temperature (in Kelvin). The difficulties in measuring atmospheric temperature and emissivity prevent the direct application of Equation (5.2) to determine $L\downarrow$.

In alpine tundra, both snow and snow-free surfaces need to be considered. Both of these surface types have been found to behave similarly to blackbody radiators. Oke (1987) lists tundra emissivities as 0.90 to 0.99, and those for snow and ice range from 0.94 to 0.99 (Warren, 1982; Price and Petzold, 1984; Müller, 1985). These high emissivities dictate that reflected longwave radiation $(1-\epsilon_0)L\downarrow$ is of small importance and neglecting to consider it will generally result in errors of less than 5% (although these will be biased). This degree of error is smaller than the measurement accuracy of most pyrradiometers.

In practice, determination of realistic values of ϵ_0 and T_0 for the earth's surface and the atmosphere can be difficult. Empirical relations between an "effective emissivity" for the atmosphere (ϵ_A) and screen-level data have been used in an attempt to circumvent this problem. This approach implicitly includes the assumption that screen-level measurements are representative of the overlying atmosphere. Although this might appear a tenuous assumption to make, much of the effective mass of the atmosphere which contributes to $L\downarrow$ lies close to the surface, and therefore screen-level data are viable surrogates (Davies and Idso, 1979). Most methods have been developed and tested only for atmospheric longwave radiation from cloudless skies ($L\downarrow_0$). Some models require only air temperature as input data, others need vapour pressure and some require both. The inclusion of vapour pressure presents two difficulties. Firstly, it requires measurement, which is not always a standard operational procedure, and secondly, it is not totally independent of air temperature.

Atmospheric Longwave Radiation Models

Several models have been derived to estimate cloudless-sky atmospheric longwave radiation ($L\downarrow_0$) from screen-level data. Several of the most widely-used are reviewed below.

1. Models Using Temperature.

Temperature-only models have the advantage of simple data requirements. Implicit in these models is the assumption that relations between temperature and vapour pressure vary systematically. Intercomparisons of $L\downarrow$ models from non-alpine locations show that they tend to perform poorer than models which include vapour pressure (Aase and Idso, 1978; Hatfield

et al., 1983).

There are two models which require only air temperature as input data, that of Swinbank (1963)

$$L\downarrow_0 = 1.20\sigma T^4 - 171 \qquad (W m^{-2}) \qquad (5.3)$$

and that of Idso and Jackson (1969)

$$L\downarrow_0 = \sigma T^4 (1 - 0.261 \exp(-7.77 \times 10^{-4}[273 - T])) \qquad (W m^{-2}) \qquad (5.4)$$

where T is screen-level air temperature (in Kelvin). Swinbank's model was not developed with sub-zero temperatures (although it was tested for such conditions in this study), nor was it verified with alpine data. Idso and Jackson's equation attempted to include the behaviour of water vapour emittance over a wide range of temperatures, and its verification included cold-temperature data from the Arctic.

2. Models Using Vapour Pressure.

Several models which use vapour pressure have been developed. Commonly used are those of Brunt (1932),

$$L\downarrow_0 = \sigma T^4 \ (0.61 + 0.05\sqrt{(e/100)}) \qquad (W m^{-2}) \qquad (5.5)$$

Brutsaert (1975)

$$L\downarrow_0 = \sigma T^4 \ (0.575 (e/100)^{0.143}) \qquad (W m^{-2}) \qquad (5.6)$$

and Idso (1981)

$$L\downarrow_0 = \sigma T^4 \ [0.70 + 5.95 \times 10^{-5} (e/100) \exp(1500/T)] \qquad (W m^{-2}) \qquad (5.7)$$

where e is screen-level vapour pressure measured in Pascals. Some studies using these models have empirically adjusted the coefficients for particular locations, such as LeDrew's (1975a) interpretation of Brunt's model. This study used the original published values of the coefficients.

3. Cloud Observations.

Cloudy-sky longwave radiation has received less attention than the cloudless situation. The increased atmospheric longwave radiation emitted by clouds results in the need for a correction for $L\downarrow_0$. The most common approach has been that derived from Bolz (1949)

$$L\downarrow = L\downarrow_0 (1+an^2) \qquad (5.8)$$

where n is the proportion of cloud cover ($0 \leq n \leq 1$) and the variable a is contingent on cloud type (Oke, 1987).

PREVIOUS ALPINE RESEARCH

There are few studies pertaining to longwave radiation from the alpine environment (Barry, 1981; Müller, 1985). Previous research has concentrated on cloudless-sky emittance of atmospheric longwave radiation. The terrestrial and net longwave radiation components have not seen comparable levels of research activity. The exception to this has been the interest shown in terrain enhancement of incoming longwave radiation (Marks and Dozier, 1979; Marcus *et al.*, 1981; Olyphant, 1986a; Brazel and Marcus, 1987). This work shows some bias towards glaciological applications (ablation and mass balance measurements).

Previous alpine longwave radiation research was reviewed in Chapter II. That review suggested that longwave radiation research in alpine environments has reached few firm conclusions. No general concensus of the relations between longwave radiation fluxes and screen-level data have emerged, even for repeated experiments at the same site in the same season. The effects of cloud have not been satisfactorily modelled. To address these problems, research needs to be directed towards further validation of empirical models for both cloudless and cloudy conditions.

EXPERIMENTAL PROCEDURE

Field Data Collection

The field site (described in Chapter I) was on Scout Mountain (49° 05'N, 120° 12'W) at an altitude of 2350 m a.m.s.l., about 200 m above the local treeline. The site was approximately horizontal and consisted of grass-sedge tundra with inactive patterned ground. Hourly means of radiation budget components were measured during two field seasons from November 1986 to July 1987 and from April to May 1988. Daily (24 hour) flux density totals were derived from the hourly data. An Eppley pyrgeometer was used to measure $L\downarrow$ in July 1987 and April to May 1988. A second was used for $L\uparrow$ measurements in April to May 1988. For November 1986 to July 1987, $L\downarrow$ was also derived by residual using a net pyrradiometer with a black body cavity, but problems with the instrument caused most of the hourly data to be rejected. Surface temperature for snow-free tundra was measured with two thermocouple arrays. Air temperature was measured with shielded, apsirated thermocouples. All cloud cover data was estimated from field observations. Further details of instrumentation were provided in Chapter IV.

Intercomparisons

Comparative modelling between observed (O) and predicted (P) radiation flux densities focussed on assessing the errors between them. The mean absolute error (MAE), mean bias error (MBE), root mean squared error (RMSE) and the index of agreement (d) were calculated employing Willmott's (1981) formulae. The MAE is the mean difference between the absolute values of O and P and the MBE is the mean difference between their true values. The RMSE defines the root of the averaged squared differences between O and P and d is a dimensionless index which reflects the degree of predictive accuracy from the independent variable. Good agreement between O and P is indicated by values of d in excess of about 0.80. Linear regressions were also performed, although their limited diagnostic value for meteorological model assessment (Willmott, 1982) was recognized.

Validation of Bolz's Correction Factor

The correction factor (Equation 5.8) derived from Bolz (1949) was validated for the Scout Mountain data before being used in modelling procedures. Measured $L\downarrow$ was graphed against σT^4 for cloudless and cloudy-sky data (Figure 5.1). The cloudless-sky data are approximately linear within the range $0.65 < \epsilon_A < 0.80$. The scatter of the cloudy-sky data is apparent, and results from the wide range of permutations of cloud cover and type ranging from cirroform clouds to fog. Those data which are for cirroform clouds and/or small percentages of cloud cover coincide with the cloudless-sky data. Since emissivity cannot exceed unity, those data in Figures 5.1 and 5.2 which lie above the line $\epsilon_A > 1.00$ must result from errors in either measured $L\downarrow$ or T.

When Bolz's (1949) correction factor is applied to these data, most of the cloudy-sky data are relocated to correspond closely with the cloudless-sky data, and general linearity occurs (Figure 5.2). This supports the use of the cloud cover correction at Scout Mountain. The linearity of the data in Figure 5.2 is approximated by an effective emissivity of 0.75. Accepting this, the utility of using

$$L\downarrow_0 = 0.75\sigma T^4 \qquad (5.9)$$

was examined by including it with the other empirical models described above.

Results for Cloudless Skies

1. Hourly data.

Results of model intercomparisons for cloudless skies are summarized in Table 5.1. The results from the Brunt, Idso and Equation (5.9) methods are shown in Figures 5.3, 5.4 and 5.5 respectively. All models worked reasonably well, with d values greater than 0.80 and errors (MAE, MBE, RMSE) of the order of $\pm$ 15 W m^{-2}. The exception to these generalizations was the Swinbank model, which produced poorer results. Considering all the error terms (MAE, MBE, RMSE) and the indexes of agreement, the best results were those of Brunt and Brutsaert equations. The performance of Equation (5.9) compared favourably with the other models. Considering the similar results of all models (excepting Swinbank's), the additional measurement of vapour pressure necessary for use with the Brunt, Brutsaert

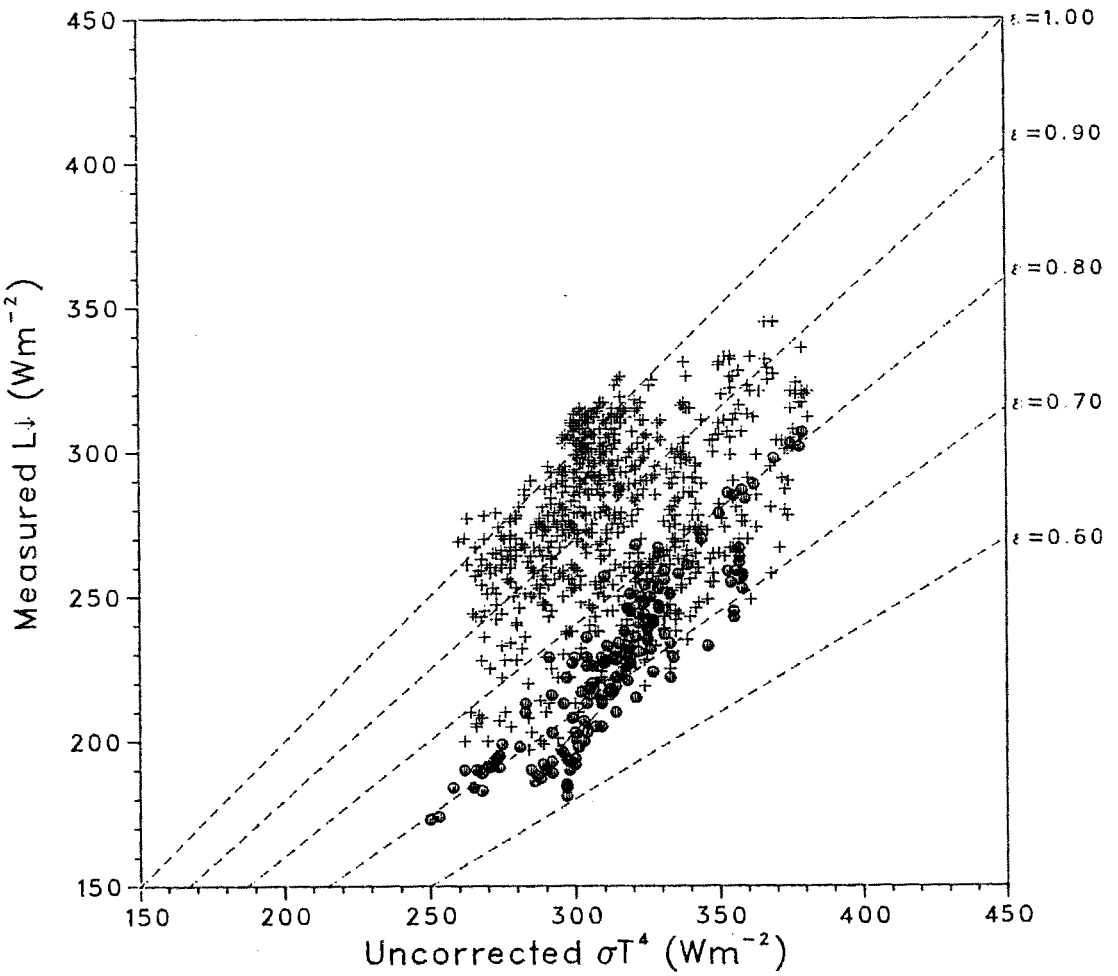

Figure 5.1. Hourly measured L↓ versus σT^4 uncorrected for cloud cover, for cloudless skies (•) and cloudy (+) skies. Dashed lines show $L\downarrow = \epsilon \sigma T^4$ for several values of ϵ.

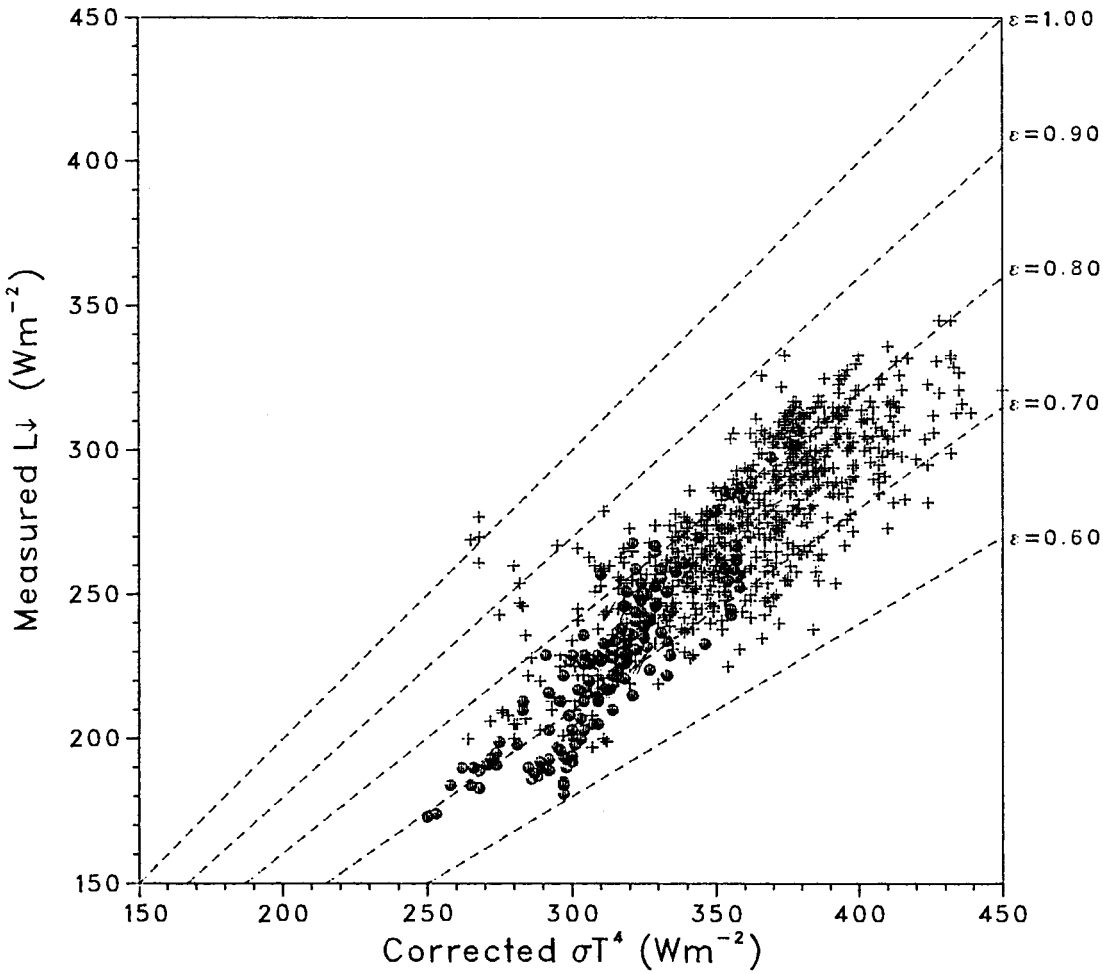

Figure 5.2. Hourly measured L↓ vs σT^4 corrected for cloud cover, for cloudless skies (•) and cloudy (+) skies. Dashed lines show $L\downarrow = \epsilon \sigma T^4$ for several values of ϵ.

Table 5.1. Observed hourly and daily atmospheric longwave radiation flux densities for cloudless and cloudy skies compared to that predicted by the models of Swinbank (1963), Idso and Jackson (1969), Brunt (1932), Brutsaert (1975), Idso (1981) and Equations (5.9) and (5.10) of this study.

Model	n	$\bar{O}$	$\bar{P}$	s_o	s_p	r^2	a	b	MAE	MBE	RMSE	d
Cloudless skies - hourly data												
Swinbank	165	227	205	29	32	0.81	58	0.824	23	−22	26	0.84
Idso–Jackson	165	227	232	29	19	0.81	−89	1.363	12	5	15	0.90
Brunt	165	227	224	29	23	0.80	−28	1.139	11	−3	13	0.93
Brutsaert	165	227	222	29	27	0.76	21	0.926	12	−5	15	0.93
Idso	165	227	240	29	23	0.79	−43	1.128	16	13	18	0.88
Equation (5.9)	165	227	235	29	20	0.81	−83	1.319	13	8	16	0.89
Cloudless skies - daily data												
Swinbank	13	22.36	21.10	1.91	2.93	0.82	9.83	0.594	1.40	−1.17	1.82	0.83
Idso–Jackson	13	22.36	22.05	1.91	1.76	0.82	0.63	0.986	0.68	−0.35	0.87	0.93
Brunt	13	22.36	21.76	1.91	2.17	0.86	0.45	0.817	0.86	−0.61	1.03	0.92
Brutsaert	13	22.36	21.93	1.91	2.52	0.86	6.87	0.706	0.90	−0.42	1.10	0.92
Idso	13	22.36	23.03	1.91	2.13	0.86	3.13	0.835	0.81	0.66	1.03	0.93
Equation (5.9)	13	22.36	22.42	1.91	1.83	0.82	1.03	0.952	0.63	0.02	0.80	0.94
Cloudy skies - hourly data												
Swinbank	775	277	236	29	34	0.48	136	0.595	41	−41	48	0.62
Idso–Jackson	775	277	267	29	24	0.65	16	0.977	16	−10	20	0.86
Brunt	775	277	259	29	27	0.63	57	0.849	21	−18	25	0.81
Brutsaert	775	277	258	29	31	0.60	90	0.724	23	−19	28	0.79
Idso	775	277	277	29	28	0.65	47	0.831	14	0	18	0.89
Equation (5.9)	775	277	271	29	25	0.65	19	0.949	15	−6	18	0.88
Cloudy skies - daily data												
Equation (5.10)	21	26.47	25.83	0.98	1.29	0.61	11.06	0.596	0.80	−0.63	1.02	0.79

Means of observed ($\bar{O}$) and predicted ($\bar{P}$) values, their standard deviations (s_o, s_p) coefficients of determination (r^2), constant (a) and slope (b) of regression equations are all derived from SPSSX statistical program packages for n valid cases. Measures of difference, mean absolute error (MAE), mean bias error (MBE), root mean square error (RMSE) and index of agreement (d) are derived from the methods of Willmott (1981). Units for $\bar{O}$, $\bar{P}$, s_o, s_p, a, MAE, MBE, and RMSE are $W m^{-2}$ (hourly data) and $MJ m^{-2} d^{-1}$ (daily data). Values for r^2, b and d are dimensionless.

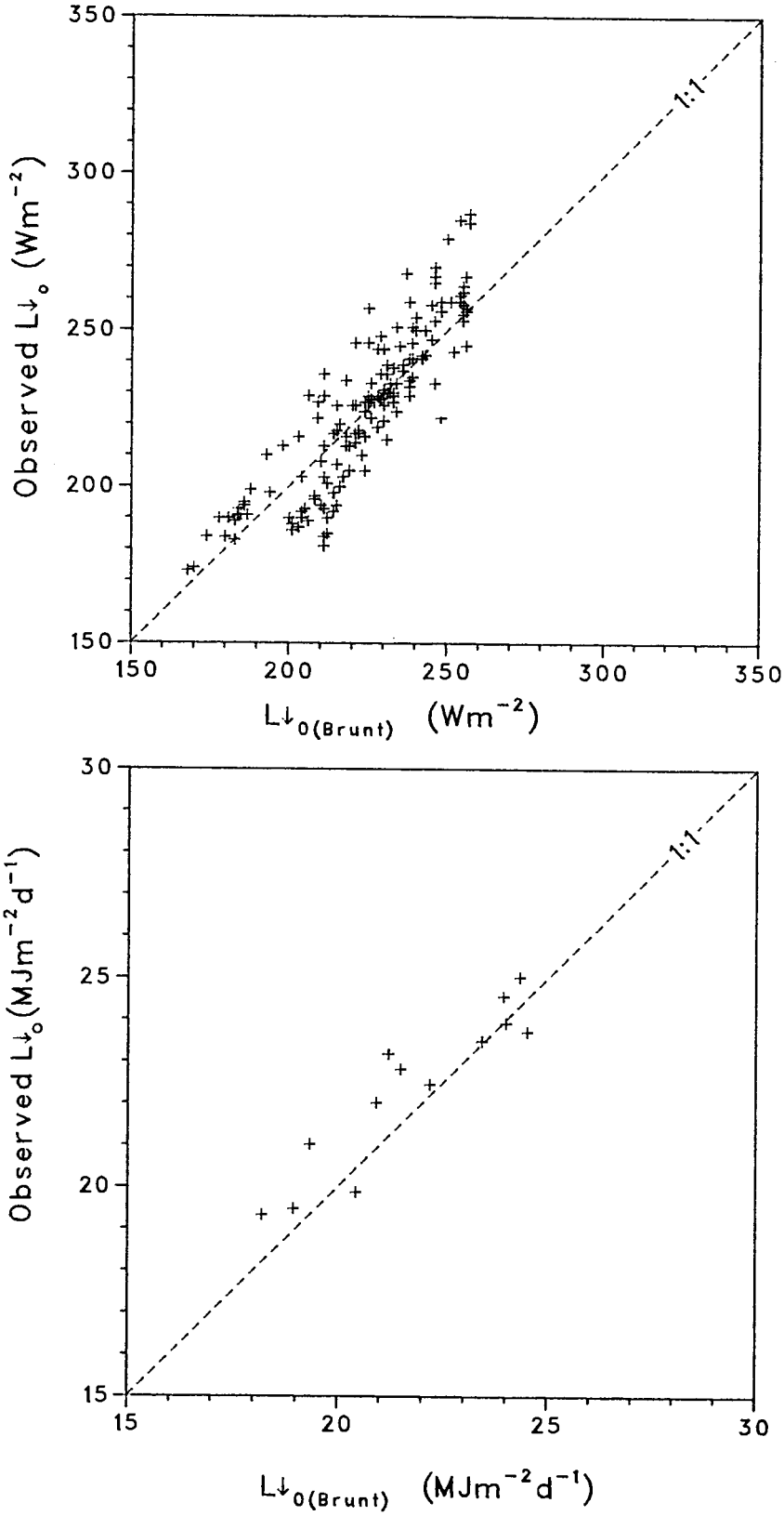

Figure 5.3. Hourly and daily observed $L\downarrow_0$ versus $L\downarrow_0$ modelled with Brunt's (1932) equation.

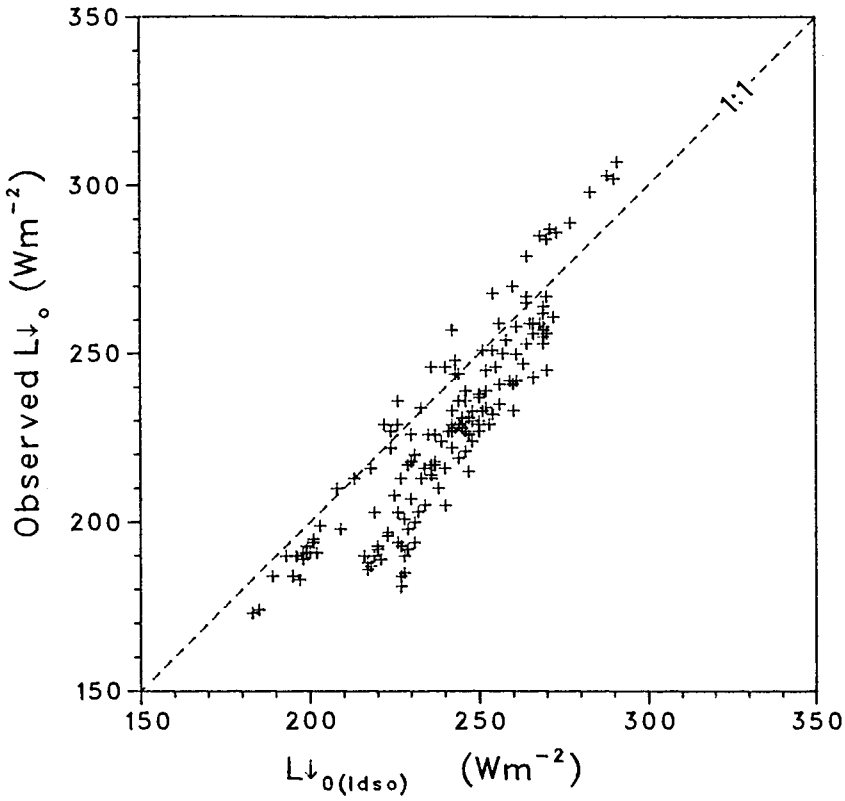

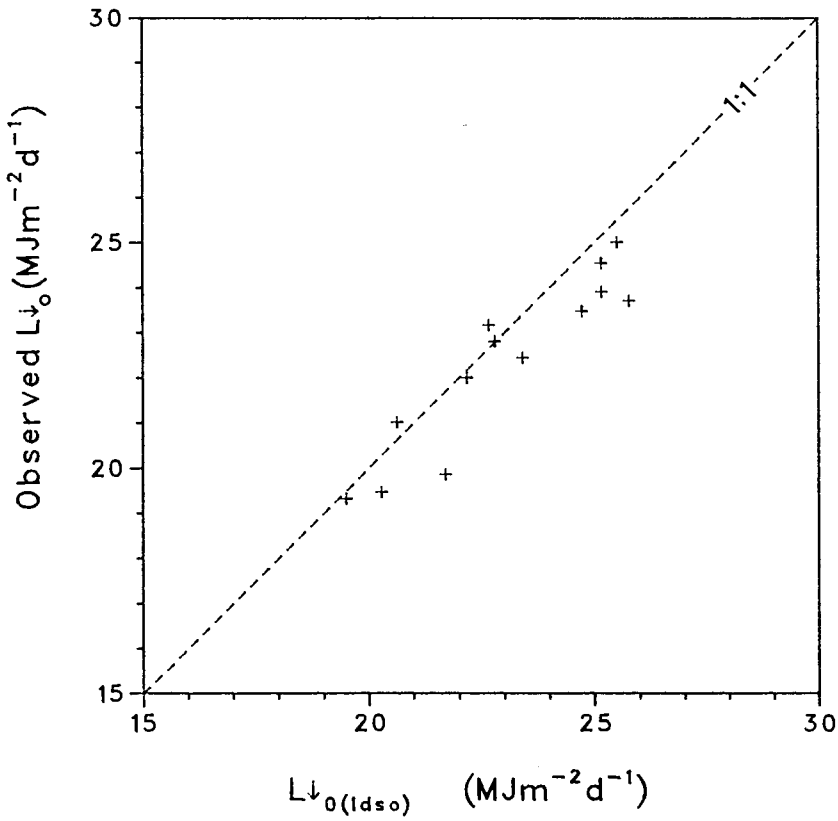

Figure 5.4. Hourly and daily observed $L\downarrow_0$ versus $L\downarrow_0$ modelled from Idso's (1981) equation.

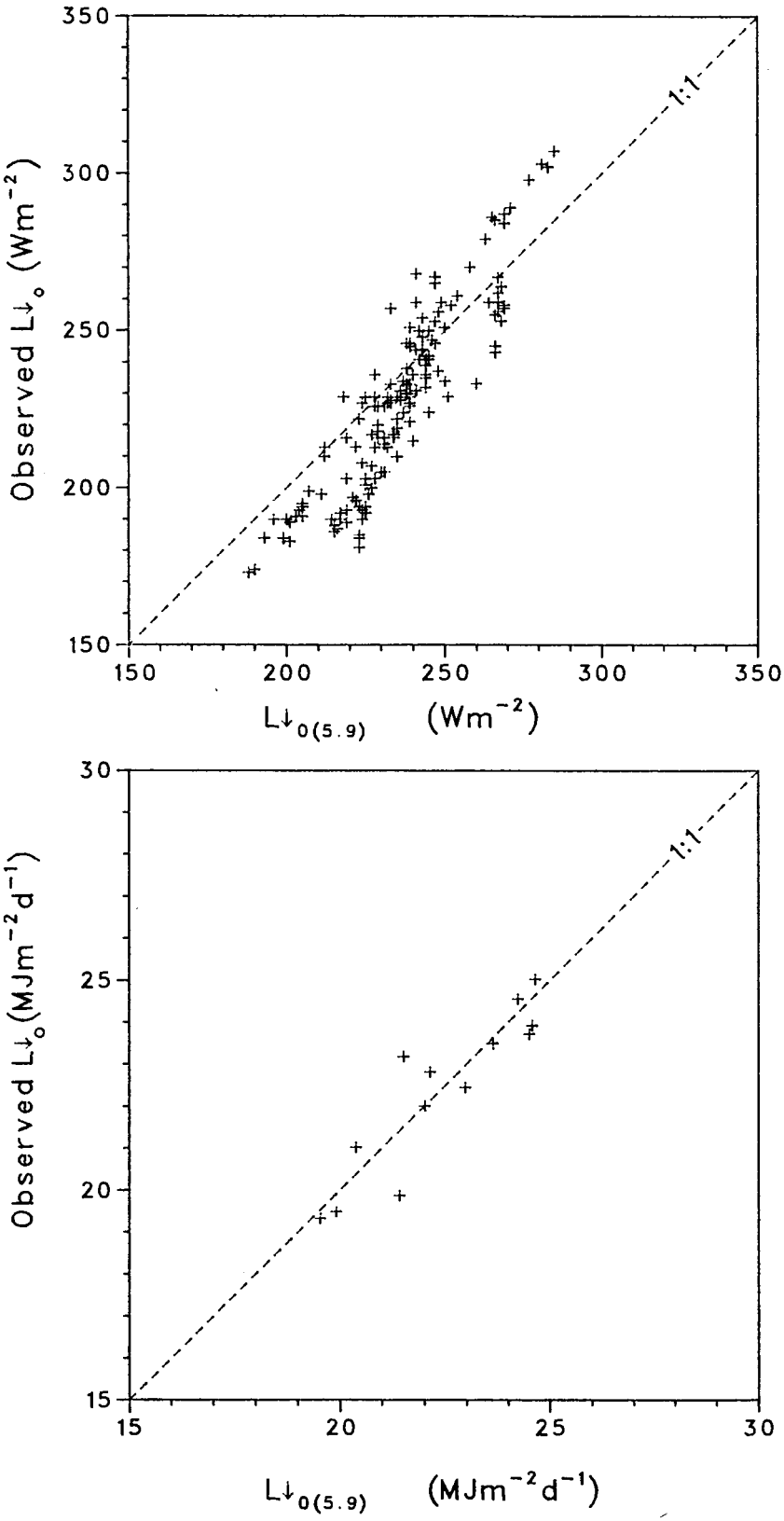

Figure 5.5. Hourly and daily observed $L\downarrow_0$ versus $L\downarrow_0$ modelled with Equation (5.9).

and Idso models did not appear worthwhile.

2. Daily data.

Results for the daily data mimicked that for the hourly data (Table 5.1). Excepting the Swinbank equation, all models produced indexes of agreement greater than 0.90 and RMSE values about 1.00 $MJ\,m^{-2}d^{-1}$. The Brunt, Idso and Equation (5.9) results are shown in Figures 5.3, 5.4 and 5.5 respectively. The best predictor of daily $L\downarrow_0$ was Equation (5.9), which predicted $L\downarrow_0$ with virtually no bias (MBE=0.02 $MJ\,m^{-2}d^{-1}$).

Results for Cloudy Skies

1. Hourly data.

For cloudy skies and hourly data, all models performed less well than for cloudless skies (Table 5.1). None of the models produced indexes of agreement greater than 0.90, and MAE's, MBE's and RMSE's were generally larger than those for the cloudless-sky data. The Swinbank equation seriously underestimated $L\downarrow$ (MBE = −41 $W\,m^{-2}$) and the Brutseart equation also performed poorly (d = 0.79). All regressions were poor. The RMSE's indicated that the Idso-Jackson model, the Idso model and Equation (5.9) were capable of predicting $L\downarrow$ to ± 20 $W\,m^{-2}$. As with the cloudless-sky data, no difference between temperature-only approaches and the other models were apparent (Swinbank model excluded).

The poorer performance of the models for cloudy skies must include the effects of subjectivity in the determination of cloud cover and type. Only one-layer cloud estimations were included in the analyses, and no weighting factors were applied to account for the location of the cloud in the sky hemisphere. There are thus several possible sources of error in the results. However, the linearity of the cloud-corrected data (Figure 5.2) suggests that the errors resulting from subjective cloud observations were not excessive.

2. Daily data.

For daily data, the estimation of realistic values of cloud cover was problematic, and a different approach was adopted. Exploiting the fact that cloud cover enhances $L\downarrow$ while reducing atmospheric transmissivity (t), an empirical relation was derived between cloudy-sky atmospheric longwave radiation to $L\downarrow_0$ and t from the 1988 data set:

$$L\downarrow = 10.76 + 0.87\,L\downarrow_0 - 9.82\,t \qquad (MJ\,m^{-2}d^{-1}) \qquad (5.10)$$

$(n=52,\ r^2=0.68,\ s.e.=1.14\,MJ\,m^{-2}d^{-1})$

where $L\downarrow_0$ was derived from Equation (5.9). This was tested against measured daily $L\downarrow$ from July 1987 (for which pyrgeometer measurements were available). The results (Table 5.1) gave poor r^2 and d values (0.61 and 0.79 respectively), although the MAE, MBE and RMSE were similar to those for $L\downarrow_0$ models discussed above.

TERRESTRIAL LONGWAVE RADIATION

Two approaches to the determination of terrestrial longwave radiation were tested, both using the Stefan–Boltzmann equation. Firstly, measured surface temperature (T_0) was used, thus employing the Stefan–Boltzmann equation in its theoretically proper form. Secondly, T_0 was replaced with screen-level air temperature (T) and an empirical relation derived. All results are summarized in Table 5.2.

Using Surface Temperature

Relations between measured $L\uparrow$ and σT_0^4 were examined by using Equation (5.2) and substituting different emissivity values. The results (Table 5.2) showed that agreement between the two was very close for the whole range of emissivities reflecting the very small effect of $(1-\epsilon_0)\,L\downarrow$ discussed earlier. Based upon consideration of MAE, MBE, RMSE and d values, the best agreement between $L\uparrow$ and σT_0^4 was found for $\epsilon_0=0.95$ (shown in Figure 5.6). This value of emissivity lies in the middle of the range for tundra as specified by Oke (1987), is close to the value of 0.96 estimated for Arctic tundra by Rouse (1984a) but less than the 0.97 – 1.00 range calculated (from only five hours of data) by Isard (1989) for alpine tundra.

Using Screen Level Air Temperature

1. Hourly data.

The use of screen level air temperature (T) *in lieu* of surface temperature in the Stefan–Boltzmann equation was examined. This approach has the advantage of requiring data which are routinely measured. The method can be expected to break down when divergence between surface and air temperatures exceeds their individual measurement errors. This problem is exacerbated in the alpine tundra environment as a result of the potentially

Table 5.2. Intercomparisons between hourly observed L↑ and L↑ calculated from Equation (5.2) for different emissivities for snow-free tundra from July 1987 and April to May 1988.

ϵ_0	MAE	MBE	RMSE	d
0.90	11.87	−4.28	14.89	0.971
0.91	11.58	−3.45	14.60	0.972
0.92	11.32	−2.59	14.32	0.973
0.93	11.20	−1.75	14.18	0.974
0.94	11.17	−0.88	14.10	0.974
0.95	11.19	−0.03	14.04	0.975
0.96	11.31	0.82	14.06	0.975
0.97	11.50	1.70	14.17	0.975
0.98	11.72	2.55	14.32	0.974
0.99	12.01	3.39	14.55	0.974
1.00	12.28	4.24	14.79	0.973

Results are calculated from 1105 hourly values. Mean absolute error (MAE), mean bias error (MBE), root mean square error (RMSE) and index of agreement (d) are calculated from the methods of Willmott (1981). Units are $W m^{-2}$ for all terms except ϵ_0 and d which are dimensionless.

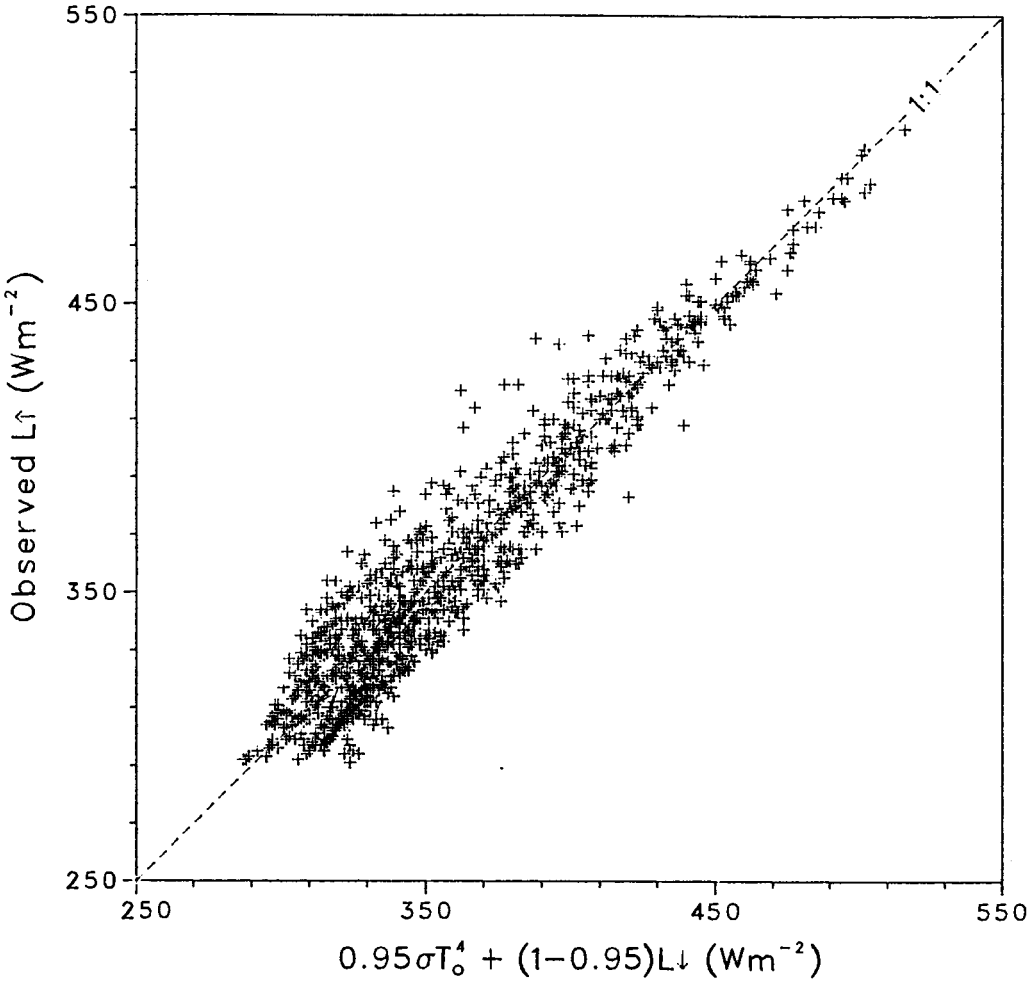

Figure 5.6. Hourly measured L↑ versus $0.95\sigma T_0^4-(1-0.95)L\downarrow$ for a snow-free surface, from July 1987 and April to May 1988.

extreme surface radiative heating (Terjung *et al.*, 1969a; Price, 1981).

A plot of ($L\uparrow - \sigma T^4$) against time for the 1988 hourly data shows the effects of divergence between surface and air temperatures (Figure 5.7). Night-time residuals are about zero, indicating similarity between T_0 and T. The daytime residuals followed a diurnal trend which mimicked the diurnal trend of solar radiation. This suggests the role of radiative surface heating. A regression between ($L\uparrow - \sigma T^4$) and global solar radiation ($K\downarrow$) for snow-free tundra (1988 data) revealed that

$$(L\uparrow - \sigma T^4) = 3.37 + 0.102\,K\downarrow \qquad (5.11)$$
$$(n=414,\ r^2=0.85,\ \text{s.e.}=13.1\,W\,m^{-2})$$

which can be simplified without significant increases in error to

$$(L\uparrow - \sigma T^4) = 0.1\,K\downarrow \qquad (5.12)$$

and the complete terrestrial longwave radiation model therefore becomes

$$L\uparrow = \sigma T^4 + 0.1\,K\downarrow \qquad (5.13)$$

This was tested on July 1987 data for which pyrgeometer measurements were available. The results gave an RMSE value of $26\,W\,m^{-2}$ and good agreement (d=0.93, Table 5.3 and Figure 5.8), although Equation (5.13) consistently overestimated (MBE=$22\,W\,m^{-2}$).

2. Daily data.

The success of Equation (5.13) found for hourly data was not duplicated for daily data. Residuals between σT^4 and $L\uparrow$ revealed no relations to T, $L\uparrow$ or $K\downarrow$. The approach adopted was to derive an empirical relation between $L\uparrow$ and σT^4 for days with pyrgeometer measurements and test it against other data. The relation derived was

$$L\uparrow = 1.55 + 1.014\,\sigma T^4 \qquad (5.14)$$
$$(n=83,\ r^2=0.92,\ \text{s.e}=0.80\,MJ\,m^{-2}d^{-1})$$

where T is screen level temperature (Kelvin) and a complete range of surface cover was encompassed (from total snow cover to snow-free tundra). This compared to measured $L\uparrow$ from the period November 1986 to June 1987. Not suprisingly, since the same site was

Table 5.3. Observed hourly and daily terrestrial longwave radiation flux densities for cloudless and cloudy skies compared to that predicted by variants of the Stefan–Boltzmann equation.

Model	n	$\bar{O}$	$\bar{P}$	s_o	s_p	r^2	a	b	MAE	MBE	RMSE	d
Hourly data – snow–free surfaces												
σT_o^4	946	362	366	49	47	0.89	9	0.966	14	3	17	0.97
Equation (5.13)	538	358	380	49	48	0.91	−10	0.970	22	22	26	0.93
Daily data – snow–free surface												
σT_o^4	45	31.90	31.10	2.03	1.71	0.79	−0.91	1.055	0.92	−0.80	1.23	0.89
Daily data – snow and snow–free surfaces												
Equation (5.14)	177	27.57	28.49	3.43	2.83	0.88	−4.85	1.138	1.30	0.94	1.55	0.94

Means of observed ($\bar{O}$) and predicted ($\bar{P}$) values, their standard deviations (s_o, s_p) coefficients of determination (r^2), constant (a) and slope (b) of regression equations are all derived from SPSSX statistical program packages for n valid cases. Measures of difference, mean absolute error (MAE), mean bias error (MBE), root mean square error (RMSE) and index of agreement (d) are derived from the methods of Willmott (1981). Units for $\bar{O}$, $\bar{P}$, s_o, s_p, a, MAE, MBE, and RMSE are $W m^{-2}$ (hourly data) and $MJ m^{-2} d^{-1}$ (daily data). Values for r^2, b and d are dimensionless.

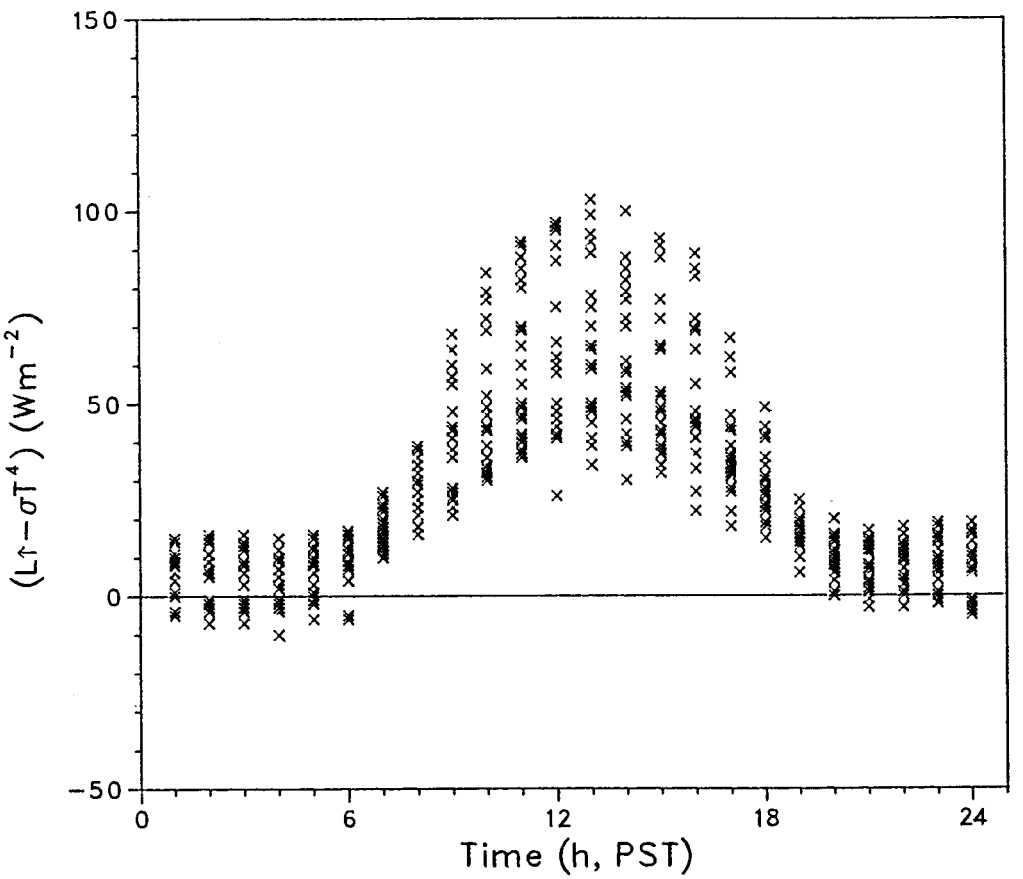

Figure 5.7. Residuals between hourly measured L↑ and σT^4 versus time for a snow-free surface, April to May 1988.

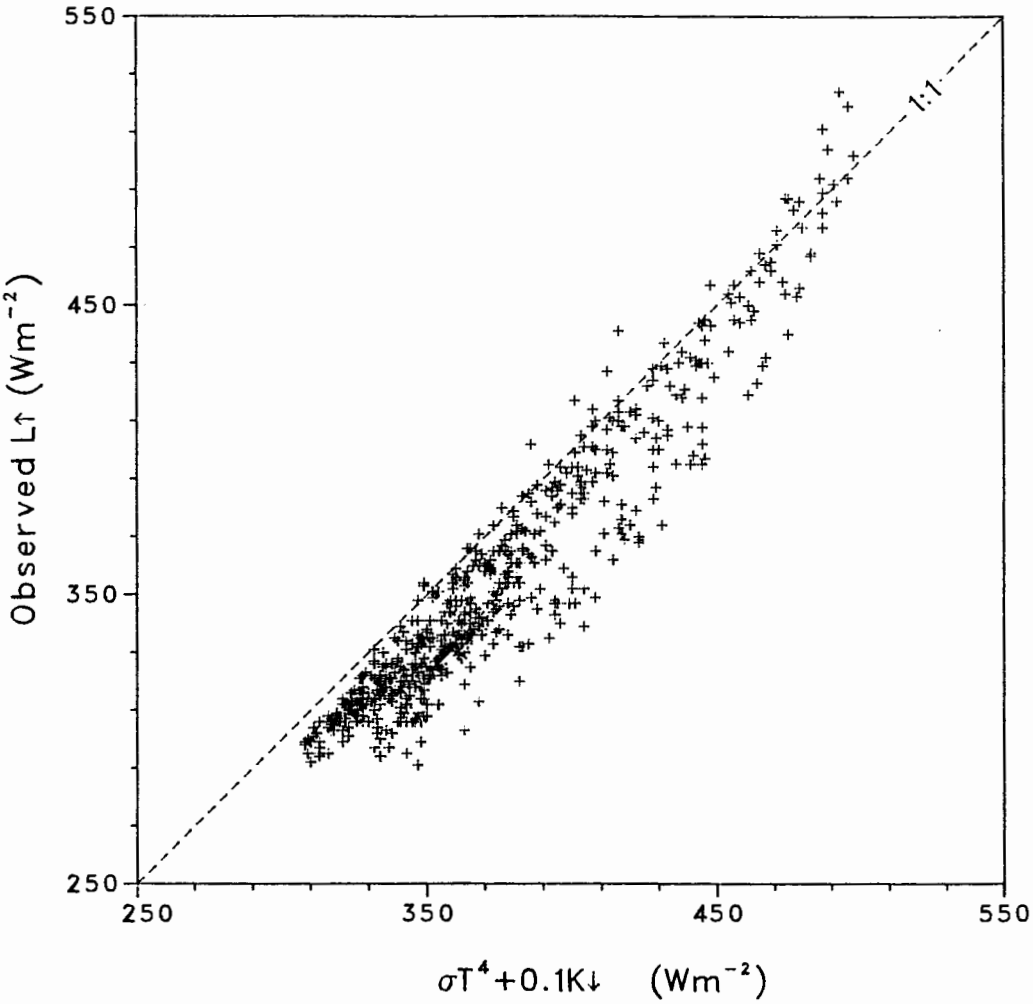

Figure 5.8. Hourly observed L↑ versus ($\sigma T^4 + 0.1K\downarrow$) for a snow-free surface under cloudy and cloudless skies, July 1987.

being used, agreement between observed and predicted fluxes was good (d = 0.94). Equation (5.14) was capable of predicting daily $L\uparrow$ to $\pm 1.58\,MJ\,m^{-2}d^{-1}$ (RMSE, Table 5.3).

NET LONGWAVE RADIATION

1. Hourly data.

For hourly data, a flux-by-flux approach was used. Equations (5.9, corrected for cloud cover) and (5.13) were used to determine $L\downarrow$ and $L\uparrow$ and estimate L^* using the longwave radiation budget (5.1). The results showed an index of agreement of 0.94 and small MAE's, MBE's and RMSE's (Table 5.4). The latter suggested model predictions of hourly L^* to within 24 W m^{-2}. Although the mean bias errors were small, the slope of the regression line indicated an overall bias in the data, such that the modelled fluxes overestimated small L^* values and underestimated large L^* losses (Figure 5.9).

2. Daily data.

A flux-by-flux approach similar to the one used for the hourly data was tested, using Equations (5.10) and (5.14) to predict $L\downarrow$ and $L\uparrow$ respectively. The results were similar to those for the hourly data, including the percentage errors and the index of agreement. Again, the data showed an overall bias indicated by the regression line slope (Figure 5.10).

An alternative approach was examined for the daily data by deriving a simple model of L^* based solely on atmospheric transmissivity. The relations between cloud cover and surface longwave radiation exchanges are implicitly assumed, such that transmissivity and L^* should be inversely related. An empirical relation between L^* and t was derived from the snow-free tundra data in May to July 1987. The small magnitudes and larger scatter of the winter data prevented the derivation on a meaningful $L^* = f(t)$ relation from the snow surface data. (The inclusion of albedo and/or air temperature did not lead to improvements.) The limitations on $L\uparrow$ imposed by a snow cover would also upset attempts to find relations between L^* and t. Additionally, there are the different timescales between the two. Transmissivity is a daylight parameter whereas L^* is 24 h.

For the snow-free tundra season in 1987

$$L^* = 1.77 - 16.65\,t \qquad (MJ\,m^{-2}d^{-1}) \qquad (5.15)$$

Table 5.4. Observed hourly and daily net longwave radiation compared to that predicted by empirical relations with σT^4 and t.

Model	n	$\bar{O}$	$\bar{P}$	s_o	s_p	r^2	a	b	MAE	MBE	RMSE	d
Hourly data												
Equations (5.9) & (5.13)	2659	−76	−79	57	45	0.84	15	1.151	19	−3	24	0.94
Daily data												
Equations (5.10) & (5.14)	202	−5.30	−5.68	3.05	2.21	0.83	1.83	1.257	1.16	−0.38	1.44	0.92
Equation (5.15)	25	−7.44	−7.99	2.02	1.62	0.70	0.88	1.042	0.96	−0.57	1.23	0.87

Means of observed ($\bar{O}$) and predicted ($\bar{P}$) values, their standard deviations (s_o, s_p) coefficients of determination (r^2), constant (a) and slope (b) of regression equations are all derived from SPSSX statistical program packages for n valid cases. Measures of difference, mean absolute error (MAE), mean bias error (MBE), root mean square error (RMSE) and index of agreement (d) are derived from the methods of Willmott (1981). Units for $\bar{O}$, $\bar{P}$, s_o, s_p, a, MAE, MBE, and RMSE are $W m^{-2}$ (hourly data) and $MJ m^{-2} d^{-1}$ (daily data). Values for r^2, b and d are dimensionless.

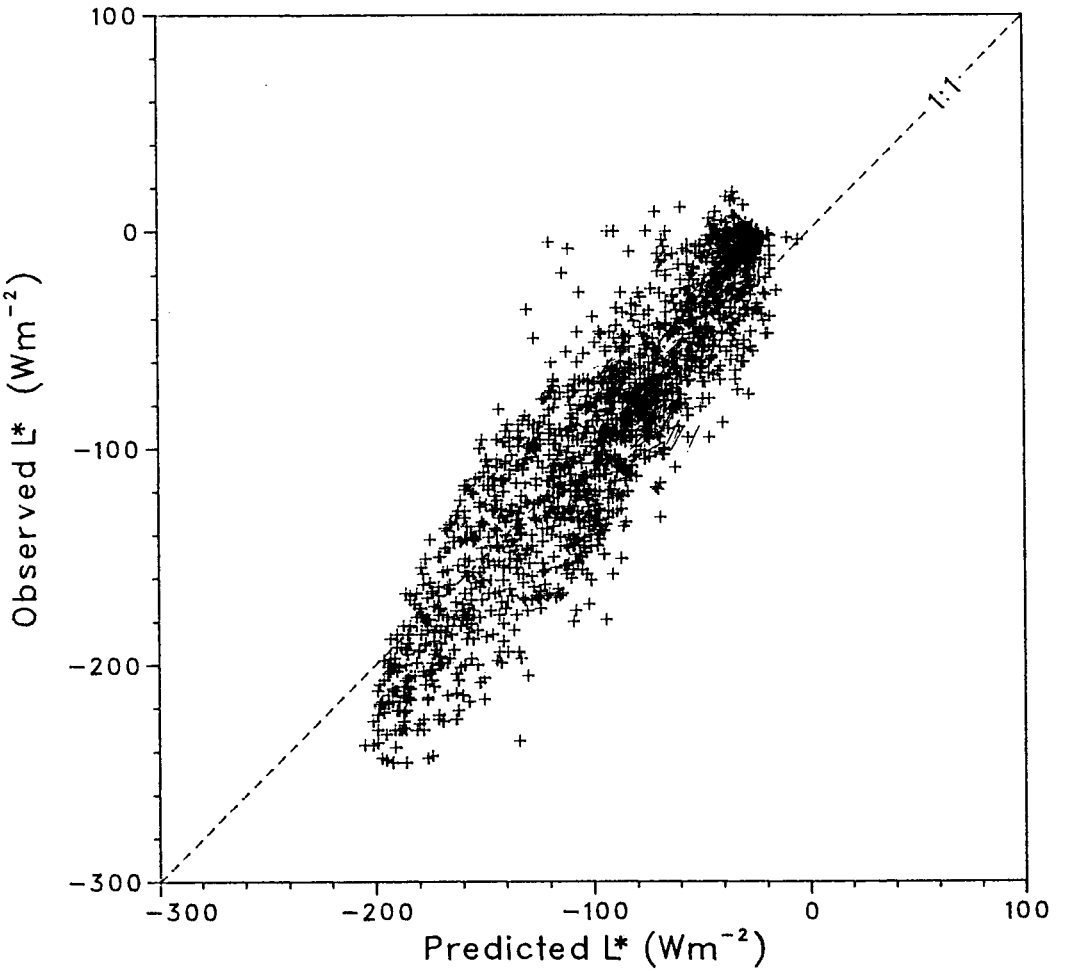

Figure 5.9. Hourly observed L* versus L* predicted from Equations (5.9) and (5.13) for snow surfaces and snow-free surfaces combined, November 1986 to June 1987.

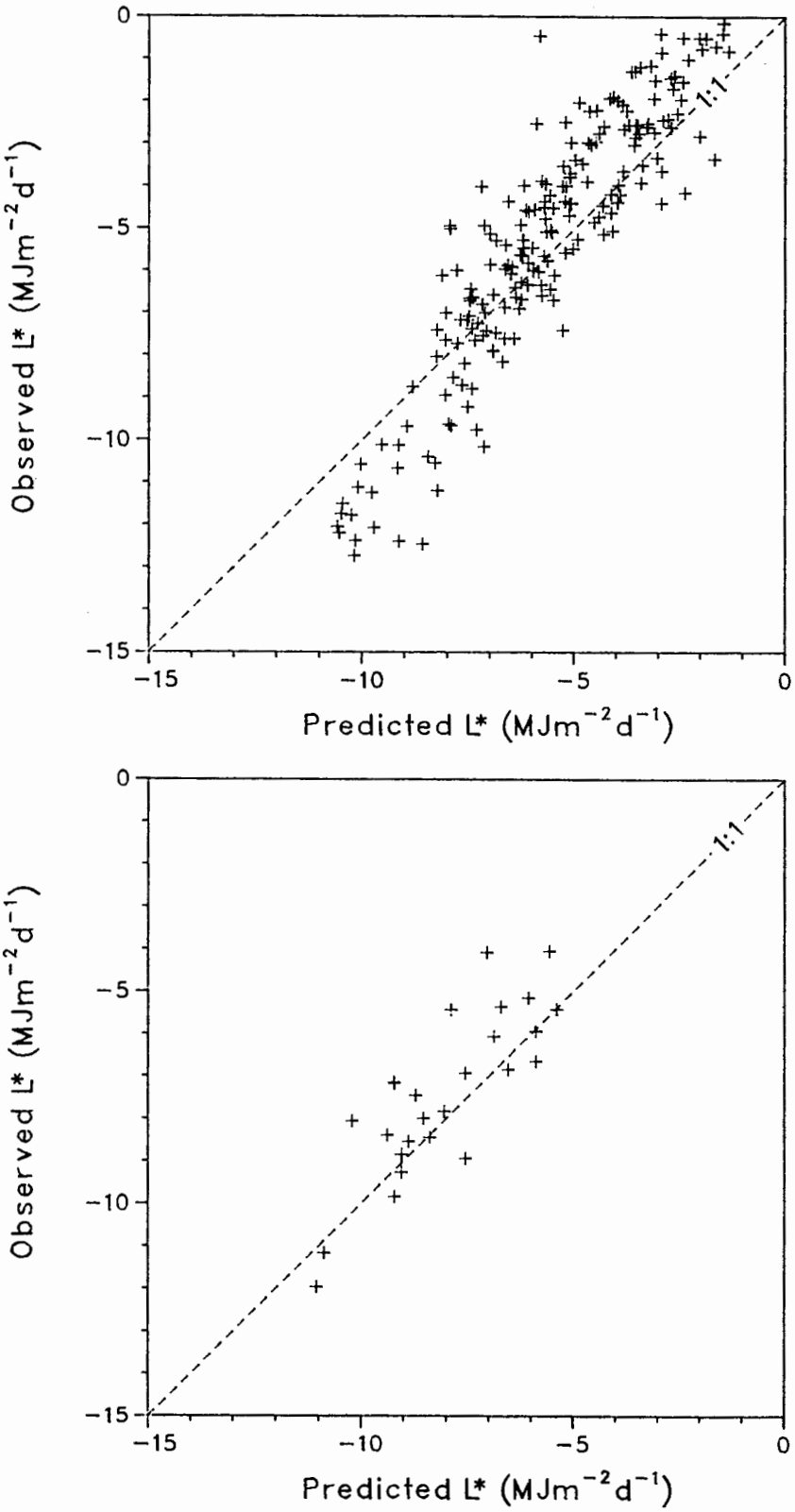

Figure 5.10. Daily observed L* versus L* predicted from (upper) Equations (5.10) and (5.14) and (lower) Equation (5.15) for a snow-free surface, April to May 1988.

$(n=76,\ r^2=0.88,\ s.e.=1.06\,MJ\,m^{-2}d^{-1})$

This was used against the 1988 snow-free tundra data. The results are shown in Table 5.4 and Figure 5.10 and compare favourably with those for the flux-by-flux approach. Equation (5.15) predicted L^* to $\pm 1.23\,MJ\,m^{-2}d^{-1}$ (RMSE) and had an index of agreement of 0.87.

DISCUSSION

For longwave radiation modelling to be of general utility in the alpine environment it should account for freezing temperatures and cloud cover and data requirements should preferably be simple. These conditions were satisfied in this study by the use of the Stefan-Boltzmann Law using $\epsilon_A = 0.75$. Although this cannot be forwarded as a generally applicable method until verified by other research, it agrees well with the proposal of Davies and Idso (1979) that $\epsilon_A = 0.70$ is a universal working value. More importantly, it suggests that hourly $L\downarrow$ can be estimated from screen temperature alone. This is in contrast to the conclusions of Aase and Idso (1974) and Hatfield *et al.* (1983) which suggested that temperature-only $L\downarrow$ models are inadequate.

The poor performance of the Swinbank model was unsurprising considering the site-specific regression approach used in its formulation (which also applies to the equations derived from Scout Mountain), and the absence of validation with cold temperature data. Deacon (1970) proposed an altitude correction to this model:

$$L\downarrow_0 = (1.20\sigma T^4 - 171) - 0.035(z/1000)\sigma T^4 \qquad (5.16)$$

where z is the altitude in metres. At Scout Mountain, assuming $z = 2350$ m a.m.s.l., the effect of Deacon's correction is to decrease $L\downarrow_0$ by 10 - 14% for the range of air temperatures experienced. It is interesting to note that this correction would worsen, and not improve, the agreement between observed and predicted $L\downarrow_0$.

The use of vapour pressure in modelling $L\downarrow$ does not necessarily improve results, despite the suggestion that it affords a better surrogate measure of the effective radiating mass of the atmosphere (Idso, 1981). LeDrew (1975a), after attempting to use a modified version of Brunt's (1932) formula in an alpine tundra with only limited success, concluded

that screen-level data were of little utility for use as determinants of longwave radiation in alpine tundra environments. This contrasts with the excellent agreement found between the Brunt formula and Kondratyev's physically based approach by Garrett (1977). It is of further interest to note that, despite LeDrew's reservations about the value of his own results, his empirical equation has been used in subsequent mountain experiments (e.g. Brazel and Hyers, 1981). The results of this study clearly refuted LeDrew's (1975a) conclusions, and confirmed the utility of screen-level measurements in estimating atmospheric longwave radiation from both cloudless and cloudy skies.

For terrestrial longwave radiation, good agreement between the observed values and σT_0^4 were found in both the daily and hourly data as, by definition, should be the case. The best estimate of surface emissivity was 0.95, but to simply assume $\epsilon_0 = 1.00$ would be justifiable considering the negligible errors incurred. The problems inherent in obtaining accurate estimates of T_0 in alpine terrain, however, seriously detract from the utility of the use of the Stefan-Boltzmann Law. Not only can snow cover cause difficulties, but the natural surface heterogeneity common in many alpine tundra landscapes compounds the problem. The use of screen-level air temperature in estimating $L\uparrow$ was found to be practical for snow-free surfaces by adding 10% of $K\downarrow$ to σT^4, thereby indirectly accounting for surface heating and the related divergence between surface and air temperatures.

The application of Equation (5.13) is invalid for continuous snow surfaces, since T_0 cannot exceed 0°C, regardless of how strong $K\downarrow$ might be and therefore the implicit considerations of surface heating are inappropriate. There is also the problem that air temperature over snow may be greater than 0°C, which would compound the errors.

For the estimation of net longwave radiation, the use of modelled $L\downarrow$ and $L\uparrow$ gave good results for hourly and daily timescales. An empirical relation between daily L^* and transmissivity also worked well. The success of the latter approach results from the simple relations between cloud cover and changes in L^* (ΔL^*). Acknowledging Paltridge and Platt's (1976) suggestion that $\Delta L^* = 60$ W m^{-2} for a change from cloudless to overcast skies is a universal working value (and supported by measurements from an alpine glacier surface by Wagner, 1980), then $\Delta L^* = 6$ W m^{-2} for each tenth of cloud cover. Therefore cloud cover, transmissivity and L^* are intrinsically related.

The present study has demonstrated the utility of estimating longwave radiation fluxes from simple data requirements. While the good results of some of the methods used are inherently a function of the site specificity of the model derivations (i.e. some models were derived from Scout Mountain data and tested on different data but from the same site), the potential to determine all longwave radiation fluxes from measurements of air temperature and global solar radiation should be recognized.

CHAPTER VI

MODELLING NET RADIATION IN AN ALPINE TUNDRA, SCOUT MOUNTAIN, SOUTHERN BRITISH COLUMBIA, CANADA

INTRODUCTION

A knowledge of net radiation is of value and has utility in a range of climatologic, hydrologic and biologic applications. Despite its importance to surface energetics, net radiation measurements in alpine environments have been sufficiently scarce to warrant calls for further research (Flohn, 1974). Most research efforts in alpine radiation and energy budget climatology have been directed to glaciological and snowmelt purposes, but the alpine environment encompasses a broad range of surface types other than snow and ice. Previous studies from surfaces other than snow or ice have been rare. Storr (1974) empirically modelled net radiation under cloudless skies for a forested mountain watershed using relations between it and global solar radiation. Empirical relations between daily net radiation and global solar radiation totals have also been reported for alpine locations by Terjung *et al.* (1969a), Isard (1989) and Bailey *et al.* (1989). The method has also been applied to sloping surfaces (Storr, 1972; Wilson and Garnier, 1975).

This study examined two approaches to net radiation modelling, one involving a consideration of the individual components which determine net radiation (the "flux-by-flux method"), and the other an empirical approach which exploits the relations between net radiation and solar radiation.

THEORETICAL BACKGROUND

There are essentially two approaches to modelling net radiation (Q^*). Firstly, the solar and longwave radiation transfers which compose the radiation budget can be individually modelled

$$Q^* = K^* + L^* = (K\downarrow - K\uparrow) + (L\downarrow - L\uparrow) \qquad (6.1)$$

where K^* and L^* are net solar and net longwave radiation, $K\downarrow$ is global solar radiation,

$K\uparrow$ is reflected solar radiation and $L\downarrow$ and $L\uparrow$ are atmospheric and terrestrial longwave radiation. The solar radiation exchange can also be expressed as $(1-\alpha)\,K\downarrow$, where α is surface albedo. A flux-by-flux approach to modelling Q^* therefore requires that four components be modelled: $K\downarrow$, $L\downarrow$, $L\uparrow$ and either $K\uparrow$ or α.

An abbreviated approach to net radiation modelling exploits the relatively conservative effect of longwave radiation on the radiation budget, by assuming that Q^* is an empirical function of $K\downarrow$ or K^*. Several models have been reported in the literature, mostly employing data from grass or crop surfaces. Commonly used daily models are those of Davies (1967)

$$Q^* = -1.01 + 0.617\,K\downarrow \qquad (MJ\,m^{-2}d^{-1}) \qquad (6.2)$$

and Fritschen (1967)

$$Q^* = -7.12 + 0.734\,K\downarrow \qquad (MJ\,m^{-2}d^{-1}) \qquad (6.3)$$

From the alpine environment, Terjung *et al.* (1969a) derived a relation from only a few hours of data for a felsenmeer surface

$$Q^* = -24 + 0.875\,K\downarrow \qquad (MJ\,m^{-2}d^{-1}) \qquad (6.4)$$

Isard (1989) determined that

$$Q^* = -66 + 0.74\,K\downarrow \qquad (W\,m^{-2}) \qquad (6.5)$$

for 31 hours of data from an alpine fellfield, and for a similar surface, Bailey *et al.* (1989) found (for 465 h of data)

$$Q^* = 0.98 + 0.514\,K\downarrow \qquad (MJ\,m^{-2}d^{-1}) \qquad (6.6)$$

and

$$Q^* = -57 + 0.680\,K\downarrow \qquad (W\,m^{-2}) \qquad (6.7)$$

For comparative purposes, the 1113 hours of Scout Mountain data (1987 only) yielded

$$Q^* = -26 + 0.664\,K\downarrow \qquad (W\,m^{-2}) \qquad (6.8)$$

and

$$Q^* = 1.10 + 0.445\,K\downarrow \qquad (MJ\,m^{-2}d^{-1}) \qquad (6.9)$$

The variance between the alpine equations might result from differences in the surfaces used, the altitude and data quality. The Bailey *et al.* and Isard equations imply that 68% and 74% of global solar radiation is used in hourly net radiation respectively. For daily Q^*, this value is 51% for Bailey *et al.*'s equation and 88% for Terjung *et al.*'s. The altitudes of Bailey *et al.*'s site was 2475 m, 3500 m for Isard's and 4270 m for Terjung *et al.*'s. The slope values of each equation thus decrease with altitude, reflecting a decreasing role of longwave radiation in the radiation budget with altitude. Part of the difference in Terjung *et al.*'s slope value may also be attributed to the different surface type.

It is of interest to note that $Q^* = f(K\downarrow)$ regressions calculated by the present author from other mountain radiation budget experiments (Kraus, 1971; Aufdemberge, 1974; Rott, 1979) were all similar to the Davies (1967) and Bailey *et al.* (1989) equations.

The transferability of these models for surfaces other than those for which they were developed depends largely upon albedo and the thermal characteristics of the surface, which govern the surface absorption of solar radiation and the radiative response. The empirical approach for alpine locations is complicated by the effects of seasonal snow cover. Not only do the correlations worsen, but the slope of the line in the model may even change sign (Dunne and Price, 1975). Assuming that they are independently measured, snow surfaces may be accommodated by modelling Q^* from K^* (Gay, 1971; Wagner, 1980), although this approach suffers from the fact that the two are not independent from each other (Equation 6.1). Furthermore, K^* becomes very small at times of low solar radiation input and high albedo, and daily totals of Q^* tend to be better predicted by longwave radiation fluxes (Serreze and Bradley, 1987). Net radiation flux modelling for snow surfaces therefore seems best performed with a flux-by-flux method.

EXPERIMENTAL PROCEDURE

Data Collection

The site (described in Chapter I) was on Scout Mountain (49° 05'N, 120° 12'W) at an altitude of 2350 m a.m.s.l., about 200 m above the local treeline. The site was approximately horizontal and consisted of grass-sedge tundra with inactive patterned ground. Measurements were made during two field seasons from November 1986 to July 1987, and April to May 1988. Global solar and reflected solar radiation was measured with an Eppley PSP Precision pyranometer and Middleton CN-7 pyranometer. Incoming net radiation was measured with a Middleton CN-1 net pyrradiometer fitted with a black-body cavity in place of the lower dome. Atmospheric longwave radiation was determined by residual throughout the measurement periods and was measured directly with an Eppley pyrgeometer during July 1987 and April to May 1988. Terrestrial longwave radiation was obtained by residual in 1986-87, but was measured with a second Eppley pyrgeometer in 1988. All data were collected and stored using Campbell Scientific CR21 and 21X dataloggers which measured sensor signals at 10 s intervals and stored hourly means. Daily data were derived from the hourly means.

The flux-by-flux method in this study used measured, and not modelled, solar radiation flux densities. This approach was adopted for two reasons. Firstly, the stringent data requirements for high quality solar radiation flux modelling, notably accurate multi-layer cloud observations and upper atmosphere radiosonde data were not available at Scout Mountain. Secondly, accurate physically based solar radiation modelling is an involved process (Atwater and Ball, 1978; Davies *et al.*, 1975; Hay and McKay, 1985) whose complexity is beyond the scope of this study but one which could be employed in future research. The present study acknowledged that the approach taken was effectively a test of the longwave radiation models, but also recognized that theoretically-based modelling could, under ideal circumstances, produce very similar results.

For the determination of $L\downarrow$ and $L\uparrow$, the following variants of the Stefan-Boltzmann equation, empirically derived at Scout Mountain (see Chapter V), were used:

$$L\downarrow = 0.75\sigma T^4(1+an^2) \qquad (W m^{-2}) \qquad (6.10)$$

$$L\downarrow = 10.76+0.866L\downarrow_0-9.82t \qquad (MJ m^{-2}d^{-1}) \qquad (6.11)$$

$$L\uparrow = \sigma T^4 + 0.1 K\downarrow \qquad (W m^{-2}) \qquad (6.12)$$

$$L\uparrow = 1.55 + 1.014 \sigma T^4 \qquad (MJ m^{-2} d^{-1}) \qquad (6.13)$$

where σ is the Stefan–Boltzmann constant, T is screen–level air temperature (in Kelvin), a is dependent upon cloud type (Oke, 1987) and n is the proportional cloud cover. These were found to estimate hourly longwave flux densities to within $\pm 25 W m^{-2}$ and daily values to $\pm 1.50 MJ m^{-2} d^{-1}$ under a broad range of atmospheric and surface conditions (Chapter V). For $L\downarrow$, the models of Brunt (1932), Idso and Jackson (1969), Brutsaert (1975) or Idso (1981) could also be employed.

For the $Q^* = f(K\downarrow)$ approach, Terjung *et al.*'s equation (Equation 6.4) was excluded on the grounds of the different surface type used and the limited data set used in it's derivation. The Davies (1967), Fritschen (1967) and Isard (1989) equations were used, however, for comparative purposes.

Intercomparisons

Comparative modelling between observed (O) and predicted (P) radiation flux densities focussed on assessing the errors between them. The mean absolute error (MAE), mean bias error (MBE), root mean squared error (RMSE) and the index of agreement (d) were calculated employing Willmott's (1981) formulae. The MAE is the mean difference between the absolute values of O and P and the MBE is the mean difference between their true values. The RMSE defines the root of the averaged squared differences between O and P and d is a dimensionless index which reflects the degree of predictive accuracy from the independent variable. Good agreement between O and P is indicated by values of d in excess of about 0.80. Linear regressions were also performed, although their limited diagnostic value for meteorological model assessment (Willmott, 1982) was recognized.

RESULTS

Results of the flux–by–flux modelling are given in Table 6.1 and those for the empirical approach in Table 6.2.

Flux- By- Flux Method

Considering all data (snow and snow-free surfaces), the flux-by-flux approach produced excellent results for both hourly and daily timescales. Indexes of agreement of 1.00 (the maximum possible value) and 0.99 were produced respectively (Table 6.1). RMSE values indicated that Q^* predictions were within $\pm 24\,W\,m^{-2}$ and $\pm 1.39\,MJ\,m^{-2}d^{-1}$. The distribution of points about the 1:1 line showed that errors had little or no dependency on the magnitude of the flux for the hourly data. For the daily data (Figure 6.2), the flux-by-flux approach underestimated Q^* at low flux densities (MBE = $-0.68\,MJ\,m^{-2}d^{-1}$) and especially when fluxes were negative. This corresponded to the winter snow data. For snow-free surfaces, the flux-by-flux approach overestimated (MBE=$0.67\,MJ\,m^{-2}d^{-1}$)

Compared to the results for snow-free tundra, the flux-by-flux method for snow covered surfaces gave slightly poorer results for both hourly and daily data, but the increases in the error terms were small (Table 6.1). However, although the MAE, MBE and RMSE values for snow-covered tundra were only slightly greater than those for snow-free conditions, they represent greater percentage errors due to the smaller net radiation flux magnitudes measured over a snow surface. The scatter in the winter snow data (Figure 6.2) at small fluxes would not suggest the good agreement between observed and predicted values as the data in Table 6.1 suggests. It is likely therefore that this is a product of the influence of the relatively few outliers from larger fluxes.

Empirical Method

For hourly predictions of Q^*, both the Bailey *et al.* (1989) and Isard (1989) equations gave very similar MAE, RMSE and d values. The bias (MBE) was greater for the Bailey *et al.* equation, but the regression line was closer to the line of equality than Isard's. For daily flux density totals, the Bailey *et al.* equation was the only one to have an index of agreement greater than 0.90, and RMSE's less than $2.00\,MJ\,m^{-2}d^{-1}$. The Fritschen equation performed least well, with d=0.87 and RMSE nearly $3.00\,MJ\,m^{-2}d^{-1}$. Errors of this magnitude would be problematic for days with small net radiation flux densities.

The hourly and daily results from the Bailey *et al.* (1989) equation are shown in Figure 6.3, and illustrate, for the hourly data, the effects of the constant in the $Q^*=a+b\,K\downarrow$

Table 6.1. Observed hourly and daily net radiation flux densities compared to values predicted from flux-by-flux methods as described in the text.

Model	n	$\bar{O}$	$\bar{P}$	s_o	s_p	r^2	a	b	MAE	MBE	RMSE	d
Hourly data												
All surfaces	2658	82	79	191	193	0.98	5	0.980	19	−3	24	1.00
Snow-free surface	1381	161	160	224	226	0.99	3	0.985	18	−1	22	1.00
Snow surface	1277	−3	−8	87	86	0.92	5	0.960	20	−6	26	0.98
Daily data												
All surfaces	202	2.36	1.99	6.06	6.60	0.96	0.57	0.900	1.13	−0.38	1.39	0.99
Snow surfaces	151	−0.69	−1.36	3.14	3.17	0.81	−0.73	0.909	1.25	−0.68	1.55	0.93
Snow-free surfaces	53	10.89	11.57	4.17	4.77	0.94	−0.51	1.109	1.13	0.67	1.43	0.97

Means of observed ($\bar{O}$) and predicted ($\bar{P}$) net radiation, their standard deviations (s_O, s_p) coefficients of determination (r^2), constant (a) and slope (b) of regression equations are all derived from SPSSX statistical program packages for n valid cases. Measures of difference, mean absolute error (MAE), mean bias error (MBE), root mean square error (RMSE) and index of agreement (d) are derived from the methods of Willmott (1981). Units for $\bar{O}$, $\bar{P}$, s_O, s_p, a, MAE, MBE, and RMSE are $W m^{-2}$ (hourly data) or $MJ m^{-2} d^{-1}$ (daily data). Values of r^2, b and d are dimensionless.

Table 6.2. Observed hourly and daily net radiation compared predicted values from the equations of Bailey *et al.* (1989), Isard (1989), Davies (1967) and Fritschen (1967) for snow-free tundra from 1987 and 1988 data.

Model	n	$\overline{O}$	$\overline{P}$	s_O	s_p	r^2	a	b	MAE	MBE	RMSE	d
Hourly data												
Bailey *et al.* (1989)	1640	234	218	207	199	0.97	12	1.018	34	−16	41	0.99
Isard (1989)	1640	234	233	207	217	0.97	16	0.936	33	−1	40	0.99
Daily data												
Bailey *et al.* (1989)	100	11.22	12.52	3.24	3.45	0.84	0.40	0.861	1.58	1.36	1.94	0.92
Davies (1967)	100	11.22	12.93	3.24	4.14	0.84	1.96	0.717	1.95	1.61	2.43	0.89
Fritschen (1967)	100	11.22	9.41	3.24	4.93	0.84	5.53	0.603	2.46	−1.78	2.94	0.87

Means of observed ($\overline{O}$) and predicted ($\overline{P}$) net radiation, their standard deviations (s_O, s_p) coefficients of determination (r^2), constant (a) and slope (b) of regression equations are all derived from SPSSX statistical program packages for n valid cases. Measures of difference, mean absolute error (MAE), mean bias error (MBE), root mean square error (RMSE) and index of agreement (d) are derived from the methods of Willmott (1981). Units for $\overline{O}$, $\overline{P}$, s_O, s_p, a, MAE, MBE, and RMSE are $W m^{-2}$ (hourly data) and $MJ m^{-2} d^{-1}$ (daily data). Values of r^2, b and d are dimensionless.

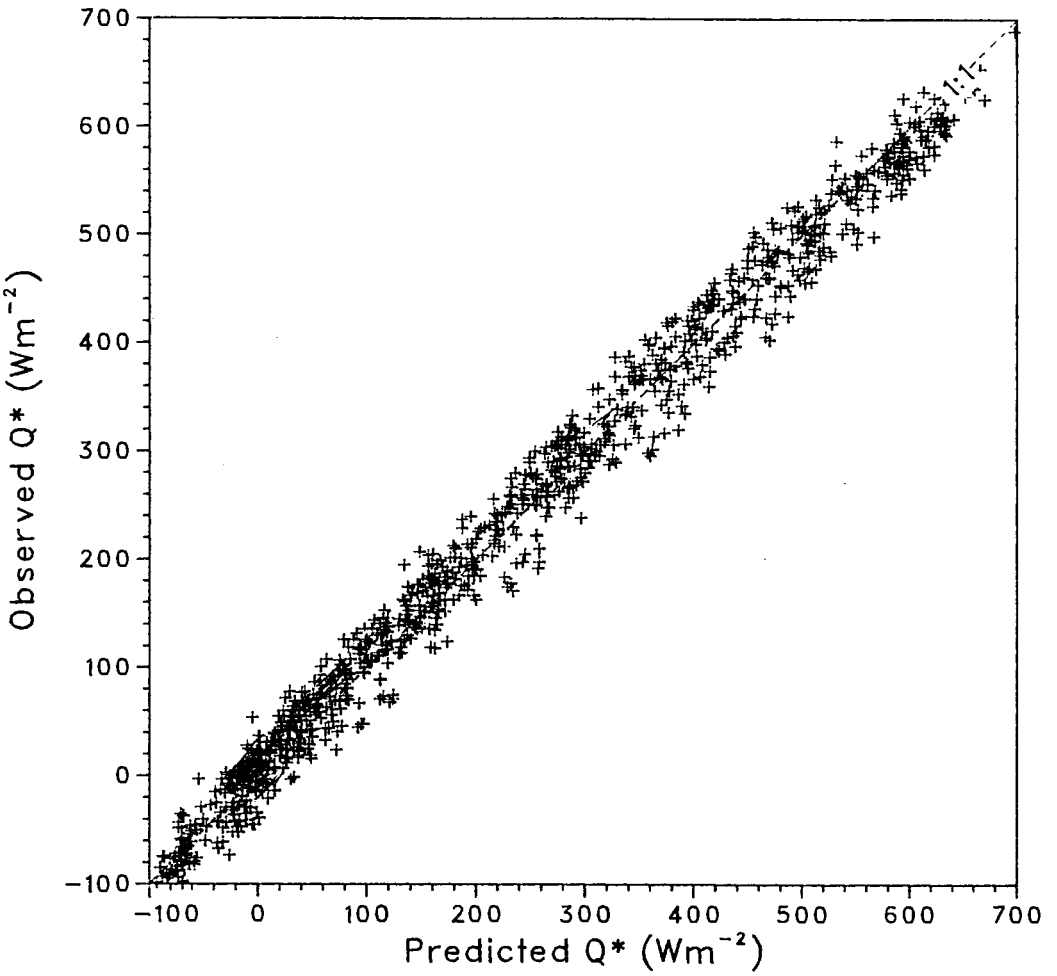

Figure 6.1. Hourly observed Q* versus Q* predicted from a flux-by-flux approach for a snow-free surface, April to July 1987.

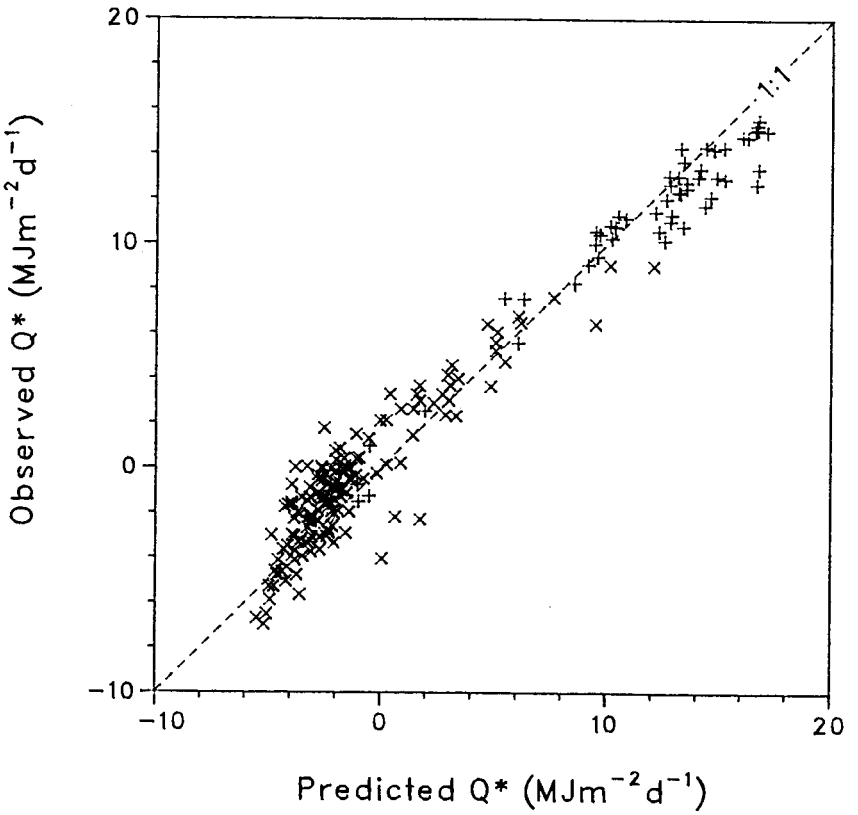

Figure 6.2. Daily observed Q* versus Q* predicted from a flux-by-flux approach, for snow-free (+) and snow-covered (x) surfaces; November 1986 to June 1987 data.

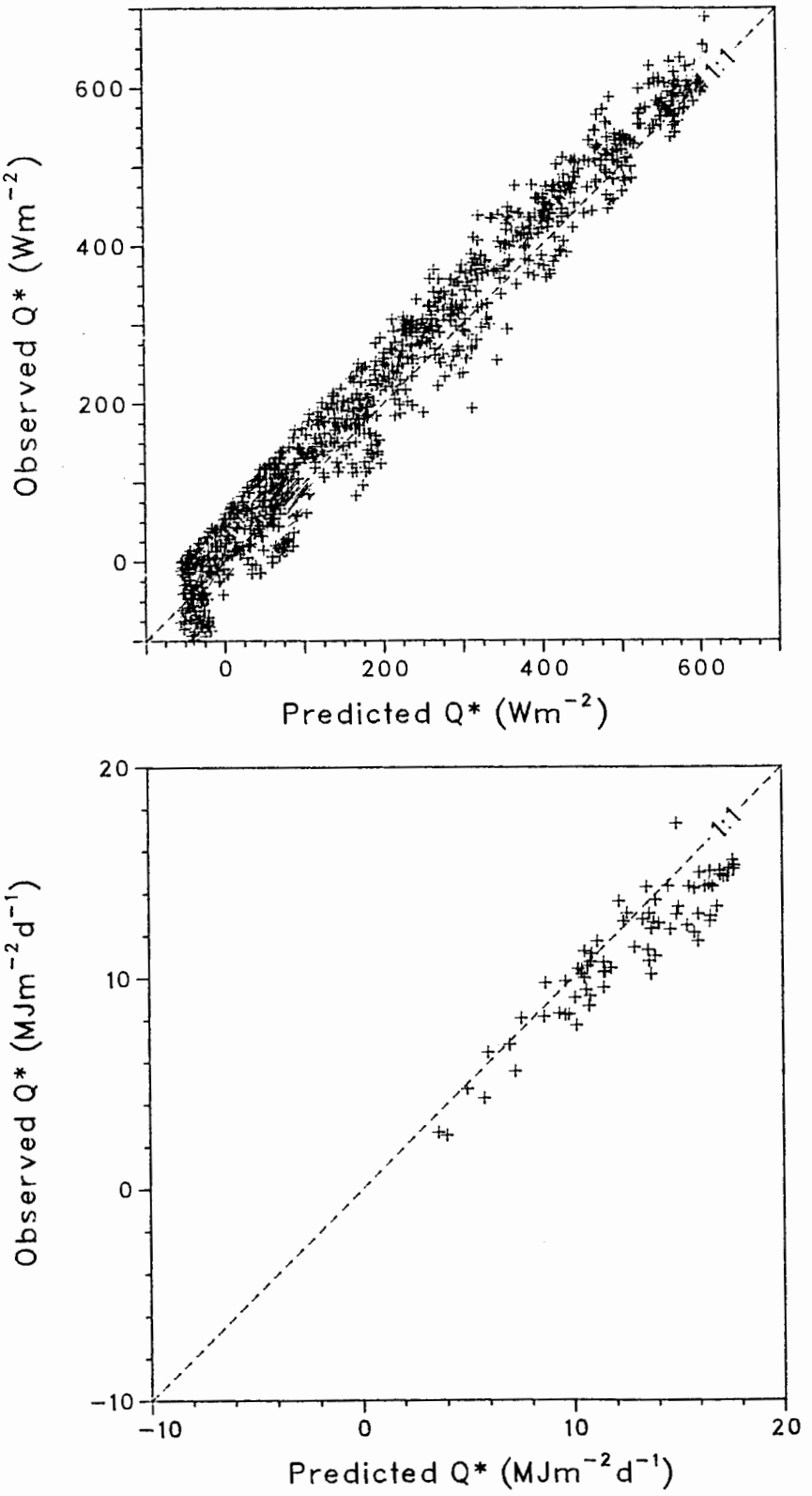

Figure 6.3. Hourly and daily observed Q* versus Q* predicted from Bailey *et al.*'s (1989) equations for a snow-free surface, May to July 1987 and April to May 1988.

equation in truncating the data set, and the greater percentage errors, at the minimum flux magnitudes.

The empirical approach to net radiation modelling breaks down with a variable albedo, as discussed earlier. Its use with snow-covered surfaces was not attempted at Scout Mountain. However, the behaviour of the $Q^* = f(K\downarrow)$ approach with different albedos was examined to simulate the effects of snow cover. Regressions between hourly Q^* and $K\downarrow$, K^* or L^* were calculated for different albedo ranges (Table 6.3). For $Q^* = f(K\downarrow)$ relations, the coefficients of determination (r^2) became worse as albedo increased above 0.50. When $\alpha \geq 0.80$, $Q^* = f(L^*)$ relations improved. The high-albedo data is derived largely from mid-winter when snow cover is greatest, solar elevation is lowest, and the daylight hours are fewest. At these times, the magnitude of net radiation is dominated by longwave radiation fluxes. This is also reflected in the sign change of the slopes of the $Q^* = f(L^*)$ regressions.

DISCUSSION

It was found that for snow-free surfaces both the flux-by-flux and empirical methods were capable of determining hourly net radiation flux densities to within about $\pm 24\,W\,m^{-2}$ or $\pm 40\,W\,m^{-2}$ respectively (based upon RMSE's). Daily predicted Q^* was within $\pm 1.50\,MJ\,m^{-2}d^{-1}$ and $\pm 3.00\,MJ\,m^{-2}d^{-1}$ for the same approaches. Overall, the flux-by-flux method estimated the larger Q^* fluxes to a similar degree of accuracy as the manufacturer's calibration of the net pyrradiometer ($\pm 5\%$).

Doubtless this good performance is partly a function of the use of measured solar radiation instead of using modelled values, and the methodological problems of modelling solar radiation were noted above. It is worth restating that the results of the flux-by-flux approach would unlikely become much poorer if solar radiation was modelled, if the data required to do this were available. Global solar radiation can be modelled with an accuracy comparable to some pyranometers. Hay and McKay (1985) show that for eight models and a range of sloping surfaces, RMSE's between observed and predicted $K\downarrow$ vary from 17 to 56 $W\,m^{-2}$.

Table 6.3. Values of coefficients of determination, intercepts and slopes of regressions for predicting hourly Q* from K↓, K* and L* for different albedo ranges.

Albedo range		K↓			K*			L*		
	n	r^2	a	b	r^2	a	b	r^2	a	b
All data	2732	0.78	−70	0.619	0.95	−42	0.805	0.34	−26	−1.825
<0.20	1078	0.97	−22	0.659	0.97	−21	0.778	0.56	40	−2.275
0.20 - 0.29	184	0.95	−62	0.635	0.95	−62	0.843	0.18	−47	−1.427
0.30 - 0.39	143	0.91	−65	0.526	0.91	−64	0.818	0.10	−11	−0.884
0.40 - 0.49	165	0.84	−38	0.402	0.84	−38	0.727	0.09	30	−0.578
0.50 - 0.59	177	0.71	−48	0.303	0.72	−49	0.687	0.01	22	−0.118
0.60 - 0.69	289	0.49	−39	0.215	0.50	−40	0.632	0.07	37	0.315
0.70 - 0.79	403	0.32	−26	0.138	0.33	−25	0.532	0.16	25	0.417
0.80 - 0.89	226	0.07	−22	0.084	0.07	−22	0.521	0.75	17	0.871
0.90 - 0.99	67	0.22	−38	0.173	0.24	−37	2.711	0.97	7	1.061

Coefficient of determination (r^2), constant (a) and slope of linear regression line (b) calculated from SPSSX statistical package programs for n valid cases. Units for a are $W m^{-2}$ and dimensionless for r^2 and b.

For the daily data, the poorer performance of the Davies and Fritschen empirical models was not surprising. The Bailey *et al.* model was derived from alpine tundra data from a similar latitude, altitude and surface type to Scout Mountain. The difference between the Bailey and Davies slope values (0.512 and 0.617 respectively) reflects a larger dependence by Q^* on solar radiation for the non-alpine data. Although the relative importance of solar and longwave radiation transfers on net radiation has been suggested to change conservatively with altitude (Barry, 1981), the difference between the two models implies otherwise.

The difference between the constants is also of interest. The positive value for Bailey *et al.*'s daily equation is anomalous amongst the $Q^* = f(K\downarrow)$ models, although it concurs with the relation derived at Scout Mountain (Equation 6.8). Again, it suggests differing roles of solar and longwave radiation in the alpine environment. It implies that daily net radiation will never be negative, which in turn suggests that L^* must be positive on days when $K\downarrow \rightarrow 0$. Over snow-free surfaces, this is unlikely.

The examination of the empirical method under different albedos (i.e. snow covers) yielded insights into how far the approach might be taken, in terms of of snow cover. The strong dependence of net radiation on longwave radiation in winter (when snow cover is at a maximum and solar radiation is at a minimum) is evidenced by the $Q^* = f(L^*)$ regressions for $\alpha > 0.80$. This has been exploited in arctic and glacial environments by using L^* as a predictor of Q^* (Petzold, 1980; Serreze and Bradley, 1987). However, the Scout Mountain data suggest that this approach is only of potential when the snow cover is complete (i.e. very high albedos).

As could be expected, relations between Q^* and $K\downarrow$ (or K^*) were best with snow-free or partial snow cover, when $\alpha < 0.50$. For these conditions the regression variables (r^2, a, b) changed little. It is interesting to note that the regressions from $Q^* = f(K^*)$ showed little difference with those for $Q^* = f(K\downarrow)$. It should be expected that K^* should be a better predictor of Q^* at higher albedos. Despite their statistical invalidity, $Q^* = f(K^*)$ relations have been used in studies of ablation of snow and ice (Munro and Young, 1982) and in examining the radiation budget over different crop surfaces (Gay, 1971).

CHAPTER VII

SURFACE ENERGY BUDGETS OF ALPINE TUNDRA, SCOUT MOUNTAIN, SOUTHERN BRITISH COLUMBIA, CANADA

INTRODUCTION

Although climatic data have long been collected in mountainous regions, there have been few complete energy budget studies from the alpine zone. Most of these have been glaciological or hydrological in purpose, and performed over snow and ice surfaces. There are presently only a few studies relating to alpine tundra environments in North America. This is probably due to a combination of logistical problems and theoretical/experimental difficulties. Many mountain research sites are inaccessible, especially in winter, and the working conditions are more extreme for both the researcher and the equipment. This study contributes to alpine climatology research by measuring the energy and mass transfers at an alpine tundra location in southern British Columbia over a period of several seasons, thereby encompassing a wide range of atmospheric and surface conditions.

THEORETICAL BACKGROUND

The Bowen ratio–energy budget (BREB) method of estimating energy partitioning between sensible heat (Q_H) and latent heat (Q_E) was used throughout the measurement periods, except when snowmelt occurred. For these times a bulk aerodynamic approach was taken. Each was discussed in more detail in Chapter III. The derivations for each are also provided by Thom (1975), Brutsaert (1982) and Oke (1987).

Assuming that advection, vegetation energy storage and photosynthetic energy fluxes are negligible, the surface energy budget is

$$Q^* + Q_G + Q_H + Q_E + \Delta Q_S + Q_M = 0 \qquad (7.1)$$

where Q^* is net radiation, Q_G is ground heat flux, Q_H is sensible heat flux, Q_E is latent heat flux, ΔQ_S is the change in snowpack energy storage and Q_M is the energy associated with snowmelt. All fluxes were considered positive when directed towards the surface.

Energy Budget Calculation for Snow-Free Tundra

In the absence of a snow cover, $\Delta Q_S = 0$ and $Q_M = 0$. The Bowen ratio-energy budget (BREB) method was used at these times, where

$$Q_E = - \frac{(Q^* + Q_G)}{1 + \beta} \tag{7.2}$$

and

$$Q_H = - \frac{(Q^* + Q_G)}{1 + \beta^{-1}} = \beta Q_E \tag{7.3}$$

where the Bowen ratio (β) is defined as

$$\beta = \frac{Q_H}{Q_E} = \gamma \frac{\Delta T}{\Delta e} \tag{7.4}$$

where ΔT and Δe are the temperature and vapour pressure changes measured over the same vertical interval and γ is the psychrometric coefficient.

Energy Budget Calculations for Snow-Covered Tundra

When the snowpack is cold and $Q_M = 0$ the BREB method can be used if ΔQ_S is known, as was the case in this study. However, in order to use the BREB method during melt periods, ΔQ_S and Q_M need to be independently measured. Due to the very thin and spatially heterogeneous snow cover which typified the Scout Mountain tundra during winter and spring, Q_M measurements were not attempted and the bulk aerodynamic method was used to independently calculate Q_H and Q_E. Melt energy was then derived by residual.

The bulk aerodynamic method is a simplification of the profile aerodynamic method which requires measurements to be made at the surface and at one level above the surface. The method is of particular interest to applications over melting snow and ice surfaces, where surface temperature and vapour pressure can be assumed (Moore, 1983b). Thus, for neutral stability

$$Q_H = \rho c_p D_H (T - T_0) \tag{7.5}$$

and

$$Q_E = \frac{\rho c_p}{\gamma} D_V (e - e_0) \qquad (7.6)$$

where D_H and D_V are bulk transfer coefficients for heat and vapour. They are assumed to be equal in accordance with the similarity between eddy diffusivities, and are defined by

$$D_H = D_V = \frac{k^2 u}{[\ln(z/z_0)]^2} \qquad (7.7)$$

where z is the reference level, z_0 is the roughness length and u is windspeed. For tundra, the zero plane displacement can be assumed to be negligible as a consequence of the very short vegetation. Moore (1983b) suggests that z_0 needs to be estimated to within an order of magnitude to ensure reliable results. This presents a problem when wind profiles are not measured, as was the case for the 1986–87 snow season. This was overcome by estimating the daily mean roughness length from the daily mean albedo. At Scout Mountain, the surface became smoother with increasing snow cover, since the snow infilled the topographic hollows between grass hummocks and between stone polygons (Figure 1.4). With increasing snow cover, albedo also increased. Using the wind profile and albedo measured from April to May 1988 an exponential relation between the two was derived. The relation covered a range of roughness lengths from 0.001 m to 0.03 m and estimated z_0 to about ±0.005 m. For the 1987 snowmelt periods, for which no wind profiles were available due to instrument problems, z_0 was estimated from measured albedo.

The other major problem to overcome was the specification of surface temperature and vapour pressure. The assumptions of 0°C and 611 Pa are only valid when the snow cover is complete and melting. When the snow cover breaks up, as was the norm at Scout Mountain, the bare grass and rock surfaces revealed will have different T_0 and e_0 values. Therefore, surface parameters were estimated by the Monteith (1963) method of fitting log–linear curves to vertical profiles of temperature and vapour pressure and then extrapolating down to the surface at z_0.

The assumption of neutrality when calculating fluxes during the snowmelt periods was a concern. As a test for the snowmelt data, hourly sensible heat calculated from the bulk aerodynamic method outlined above were compared to eddy correlation measurements. For 41 hours of data, the RMSE between the two was 10 W m^{-2} and the index of agreement

(Willmott, 1981) was 0.96, indicating close parity. Based upon these results, the bulk aerodynamic sensible heat flux densities were considered to be reasonable estimates given the measurement difficulties imposed by the heterogeneous nature of the surface.

Combination Model

The combination model considers both aerodynamic and energy budget influences on evaporation in an equation which accounts for the available energy, the saturation deficit of the air, and resistance parameters which respond to the state of turbulence and plant physiology. Monteith (1965) extended Penman's (1948) original equation by appending it with a canopy resistance term to account for the physiological response to non-saturated conditions, and defined latent heat flux density as

$$Q_E = \frac{S(Q^*+Q_G)+\rho c_p(e^*-e)/r_a}{S+\gamma+\gamma r_s/r_a} \qquad (7.8)$$

where S is the slope of the saturation vapour pressure curve, e^* is the saturation vapour pressure at T_z, e is actual vapour pressure, r_a is the aerodynamic resistance to heat and vapour and r_s is the surface resistance.

A further interpretation of the combination model has been introduced which expresses evaporation as the balance between the energy availability and aerodynamic conditions between the surface and atmosphere (McNaughton and Jarvis, 1983). It states that

$$Q_E = \Omega(Q^*+Q_G) + (1-\Omega)\frac{\rho c_p(e^*-e)}{\gamma r_s} \qquad (7.9)$$

where Ω is the decoupling coefficient, defined by

$$\Omega = [1 + \frac{\gamma}{S+\gamma}\frac{r_s}{r_a}]^{-1} \qquad (7.10)$$

The decoupling coefficient has a range from 0 to 1 and defines the relative importance of the energy term and the aerodynamic term. It is strongly dependent on the ratio of r_s/r_a. When $\Omega \rightarrow 0$, evaporation is dominated by the aerodynamic term and is governed by the surface resistance and the saturation deficit of the overlying air. Surface evaporation is therefore well coupled to the boundary layer. In contrast, when $\Omega \rightarrow 1$, Q_E tends towards equilibrium evaporation and the aerodynamic term plays a negligible role. Evaporation then becomes decoupled from the boundary layer and is instead driven by available energy.

The problems of estimating energy budget components over a surface with a thin, discontinuous snow cover are exacerbated by the presence of microscale advection. It can be reasoned that there must be horizontal transfers of energy between snow and bare ground but quantifying these at the sub–metre scale is problematic. The magnitude of advective energy (Q_A) was assumed to be zero for all energy budget data, but it should be recognized that it is likely of significance for the melt period data. Therefore the results from snowmelt periods must be considered to be the least reliable of all the data from Scout Mountain.

PREVIOUS ALPINE RESEARCH

Previous studies in alpine energy budgets were reviewed in Chapter III. Few physically based energy budgets have been reported from alpine tundra environments. In North America, studies have been undertaken in maritime mountain ranges at Chitistone Pass, Alaska (Aufdemberge, 1974; Brazel, 1974) and from drier continental regimes at Niwot Ridge, Colorado (LeDrew, 1975; Isard and Belding, 1989) and Plateau Mountain, Alberta (Bowers and Bailey, 1989). The more humid ranges produce the anticipated response from the turbulent fluxes by exhibiting strong evaporative fluxes, whereas the drier locations display strong sensible heat convection. Thus, the energy budget descriptions have revealed what could have been expected under the mesoscale climate regime.

Studies addressing the controls of surface energy budgets are rare. Rott (1979) characterized the evaporation regimes of subalpine meadows as energy–limiting and those of alpine tundra as moisture–limiting. Of particular significance to alpine tundra evaporation are measurements of physiological control on evaporation by Körner and Mayr (1981) and Bowers and Bailey (1989). The former study reported minimal restrictions on the evaporative flux from well watered vegetation. The latter documented a strong control on evaporation during moisture stress.

EXPERIMENTAL PROCEDURE

The field site (described in Chapter I) was on Scout Mountain, at (49° 05'N, 120° 12'W). at an altitude of 2350 m a.m.s.l., about 200 m above the local treeline. The site was horizontal and had adequate fetch in all directions except for the eastern quadrant, from which data were excluded. The grass–sedge tundra surface consisted of inactive patterned ground, with about 25% of the surface composed of bare rock surfaces.

Measurements at the site were taken from November 1986 to July 1987 and April to May 1988. Net radiation was measured with a Middleton CN–1 net pyrradiometer, ground heat flux with a series array of Thorthwaite heat flux plates and dry– and wet–bulb temperature gradients with shielded, aspirated thermocouples. All instruments were interrogated by Campbell Scientific CR21 or 21X dataloggers at 10 s intervals (or 120 s for Q_G) to produce hourly means.

For ground heat flux assessment, flux transducers were buried at 50 mm. The flux divergence between these and the surface was accounted for (Fuchs and Tanner, 1968; Wilson and McCaughey, 1971), where

$$Q_G = Q_{Gz} + C z \frac{\Delta T_G}{\Delta t} \qquad (7.11)$$

where Q_{Gz} is the heat flux measured by the transducers at depth z, C is soil heat capacity, T_G is the mean temperature of the surface 50 mm soil layer and t is time. Ground heat capacity (C) was determined from

$$C = C_M \chi_M + C_O \chi_O + C_W \chi_W \qquad (7.12)$$

where C_a is the heat capacity of quantity a, χ is volumetric fraction, and subscripts M, O and W refer to volumetric contents of mineral matter, organic matter and water. The heat storage of pore air in the soil is negligible and was ignored.

From 50 soil samples taken from the 0–50mm layer the weight ratio of mineral to organic matter was found to be 94:6%. Assuming a density of basalt of 2.7 kg m^{-3} and that for organic matter of 1.3 kg m^{-3} (Hillel, 1982) the volumetric fractions of mineral and organic

matter were deduced as 0.122 and 0.016 respectively. From deVries (1963) and Oke (1987), C_M = 1.926 x 10^6 J $m^{-3}K^{-1}$, C_O = 2.513 x 10^6 J $m^{-3}K^{-1}$, C_W(water) = 4.180 x 10^6 J $m^{-3}K^{-1}$, and C_W(ice) = 1.93 x 10^6 J $m^{-3}K^{-1}$. Therefore Equation (7.12) simplified to

$$C = [0.275+(C_W\chi_W)] \times 10^6 \text{ J m}^{-3}\text{K}^{-1} \quad (7.13)$$

Volumetric soil moisture content was determined gravimetrically from ten to twenty samples, employing a mean bulk density value of 0.30 derived from analysis of 50 samples. This value is low compared to soils from agricultural surfaces (Hillel, 1982) but concurs with the measurements of Bowers (1987) and reflects the organic-rich nature of the tundra surface. For most of the winter, the soil was frozen and resisted attempts at sampling. In the late- and post-snowmelt periods, samples were taken every 2-4 days when the site was occupied. For days with no samples, χ_W was estimated by linear interpolation.

In winter and spring, determination of snowpack energy parameters was problematic, due to the thin and discontinuous nature of the snow cover (Figure 1.3). Liquid water content of the snow pack (χ_{Wsnow}) was not measured, but could be assumed to be small due to the limited storage capacity of thin snow. When the snowpack temperature (T_{snow}) was less than -1°C, χ_{Wsnow} was assumed to be zero. Following Gerdel's (1954) measurements, χ_{Wsnow} was assigned a value of 0.02 when ($-1 < T_{snow} < 0$°C), and for T_{snow} > 0°C χ_{Wsnow} = 0.08. Although snow temperature cannot exceed the freezing point, measured T_{snow} did rise above 0°C on high-irradiance days when melt was occuring due to subsurface radiative heating of the thermocouples.

The measurement of vertical dry- and wet-bulb temperature profiles was accomplished using a two-level (November 1986 to May 1987) or four-level (all other periods) aspirated psychrometer system similar in design to those described by Lourence and Pruitt (1969) and Munro (1980). Bowen ratios for the four-level system were derived from the mean of the three independent values calculated for z_1-z_2, z_2-z_3 and z_3-z_4.

At sub-zero temperatures, wet bulbs were manually iced. Anti-freeze solutions were not used on the grounds that their different evaporative behaviour induces errors in the psychrometer equation (Middleton and Spilhaus, 1953), although their use has recently been found acceptable for the temperature range from -9°C to freezing point (Fritschen and

Simpson, 1989). The drawback of manual icing is that wet-bulb data are unusable when the site is unoccupied.

Hourly Bowen ratios derived from the psychrometric data were subjected to error analysis (Fuchs and Tanner, 1970; Angus and Watts, 1984) such that the relative errors in convective flux estimates can be expressed as

$$\frac{\delta Q_E}{Q_E} = \frac{(\delta Q^* + \delta Q_G)}{(|Q^* + Q_G|)} + \frac{\delta \beta}{(1+\beta)} \tag{7.14}$$

and

$$\frac{\delta Q_H}{Q_H} = \frac{(\delta Q^* + \delta Q_G)}{(|Q^* + Q_G|)} + \frac{\delta \beta}{\beta(1+\beta)} \tag{7.15}$$

where δQ^* is a function of sensor calibration (m) and accuracy of the measurement device (c) such that

$$\delta Q^* = [(c\ \delta m)^2 + (m\ \delta c)^2]^{0.5} \tag{7.16}$$

In view of the uncertainty in measuring ground heat flux parameters in patterned ground, the relative error in Q_G was assigned a generous value of 20%. In actuality, errors in the BREB equation are relatively insensitive to ground heat flux errors and most of the error arises from the vertical temperature and humidity profile measurements. The relative error in the Bowen ratio is

$$\frac{\delta \beta}{\beta} = (1+\beta)\frac{\delta \Delta T}{\Delta T} + \frac{\delta \Delta T_w}{\Delta T_w} + \frac{\delta S}{(S+\gamma)} \tag{7.17}$$

where S is the slope of the saturation vapour pressure curve. The relative errors of ΔT and ΔT_w were obtained from the total derivative in the same manner as for Q^*, and that for S from the derivative of Lowe's (1977) equation. Relative errors in ΔT increase as $\Delta T \rightarrow 0$, and are also high for sub-zero temperatures. For the differential psychrometric systems used in this study the minimum values of ΔT which could be measured with relative errors less than 25% ranged from about 0.015°C (2-level system, T>0°C) to about 0.065°C (4-level system, T<0°C).

Typical daytime relative errors in β were $\pm 10-20\%$ for summer and $\pm 30-60\%$ in winter. Errors in the turbulent fluxes were of similar magnitude, but varied with β. When $\beta<1$, $\delta Q_H/Q_H > \delta Q_E/Q_E$ and *vice versa*. The larger winter errors were attributed to the greater difficulty in resolving ΔT in freezing conditions and the very small temperature gradients consequent from an absence of strong surface heating.

Most night-time data showed large relative errors in β, commonly in excess of $\pm 100\%$. This is not atypical of nocturnal gradient measurements. As a result of the large errors, most night-time data were rejected from analyses.

Daytime totals of energy budget components were calculated from summed hourly values. Some data around sunrise or sunset were rejected during this process if they were obviously anomalous or if $\beta \simeq -1.00$. Since the magnitude of heat fluxes are minimal at this time, errors induced by this practice were small. The small nocturnal fluxes also dictate that the rejection of night-time data due to errors does not greatly affect the daily totals.

HOURLY ENERGY BUDGET RESULTS

Energy budget descriptions were subdivided into three categories: (A) snow regimes without melting, (B) snowmelt regimes, and (C) regimes for a snow-free surface. The discussion of hourly energy budgets at Scout Mountain follows this division. There was no rigidly defined temporal scale or boundary to the three types of energy regime. Type A regimes were confined to late fall and winter seasons. Type B regimes characterized the spring transition period but could also occur during summer. Type C regimes occurred in late-spring and summer only.

(A) Winter Snow Regimes

Conditions within this category were generally confined to winter and early spring, approximately November to early March in 1986-87, but until early April in 1988. About 40 days of energy budget data were derived from this period. However, vertical temperature and vapour pressure gradients were generally suppressed by the low-energy nature of the season and the minimal surface heating. This resulted in difficulties in determining Bowen ratios without large relative errors, and about one quarter of the data were of poor quality.

Indeed, the relative errors associated with all the data were generally larger than for summer days.

Typically, energy fluxes were very small and changed conservatively during the day. The most common diurnal trend which occurred in winter was not unlike that for a snow-free surface: positive daytime net radiation was offset by negative turbulent heat fluxes. Most of the days which showed this regime occurred in late winter or early spring, when radiative fluxes were increasing towards their summer magnitudes. Figure 7.1 illustrates a typical example from March 2, 1987, a windy day with complete snowcover about 0.10 m thick and overcast skies. A slight warming trend during the 24 h period was reflected by the rising snowpack temperature, which caused it to be an energy sink during the day. Hourly snowpack energy storage changes were of similar magnitude to those of sensible heat. Latent heat fluxes were generally larger and the Bowen ratio was 0.50 - 1.00. However, no turbulent energy flux density exceeded 30 $W m^{-2}$.

A variation of the above scenario occurred on several days, mostly in early spring, and was typified by a reversal of the sensible heat flux during the day. The case illustrated in Figure 7.2 for April 25, 1988 is from an overcast day with some light snow showers. Morning rime had disappeared by the afternoon. Latent heat losses dominated the dissipation of energy, probably aided by the fact that the rime was evaporating/sublimating during the morning and had disappeared by early afternoon. Sensible heat loss in the morning was replaced by a sensible heat gain in the afternoon. Thus the afternoon latent heat losses were maintained at the expense of both net radiation and sensible heat sources.

Energy and vapour transfers in mid-winter were typically positive (i.e. energy sources), driven by the negative net radiation. Figure 7.3 illustrates a case from December 10, 1986. The day was cloudless and unseasonably warm (mean daily air temperature was 0.2°C) and the snow cover did warm a little in response. However, the snowpack was always several degrees below freezing, and contributed to the strong surface temperature inversion which forced the positive turbulent fluxes. Although Q_E exceeded Q_H and was the largest flux density except for Q^*, no condensation or riming was observed. The daytime total of Q_E was only 0.97 $MJ m^{-2} d^{-1}$ or 0.4 mm water equivalent of condensation.

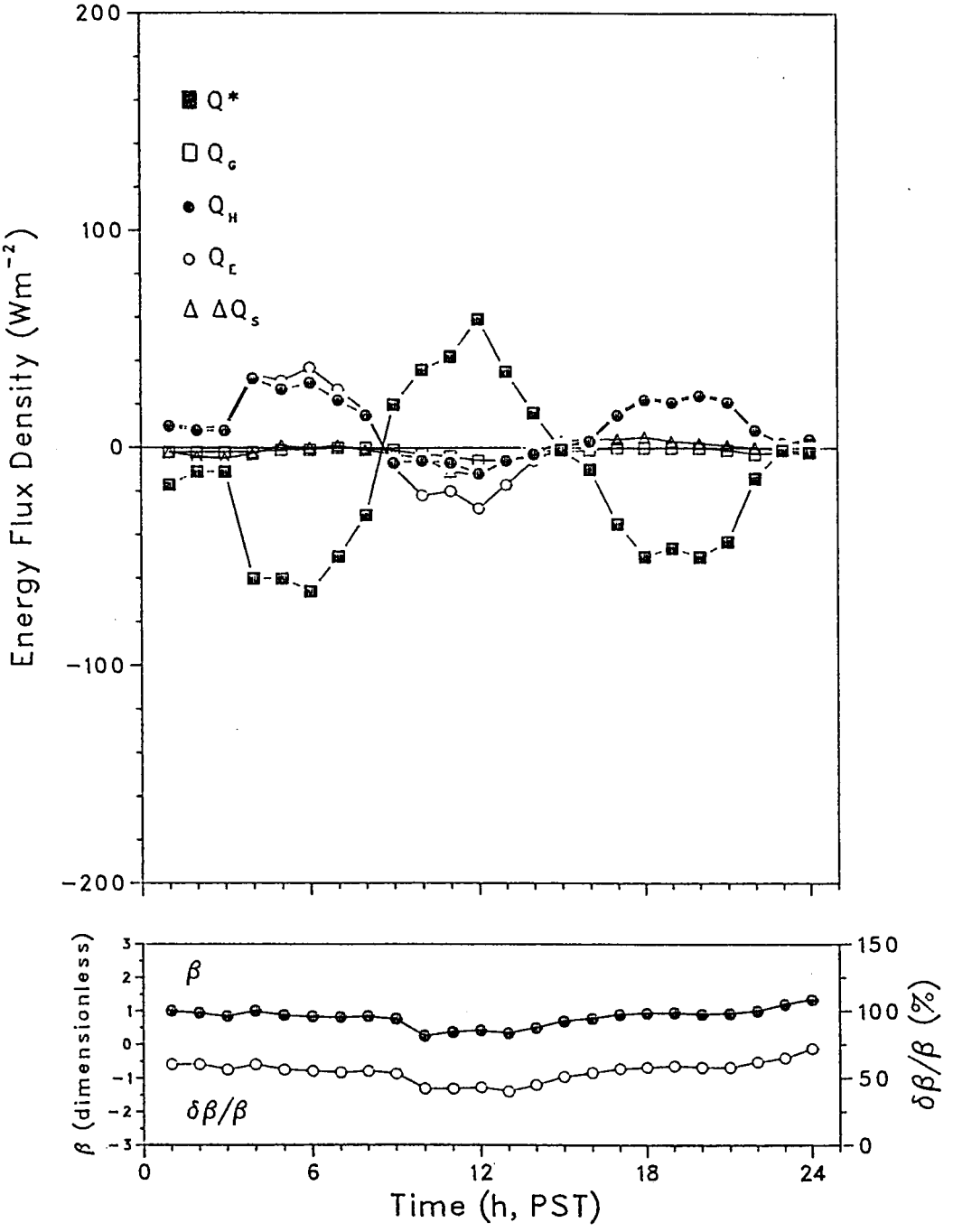

Figure 7.1. Hourly energy budget measured on March 2, 1987 for snow-covered tundra.

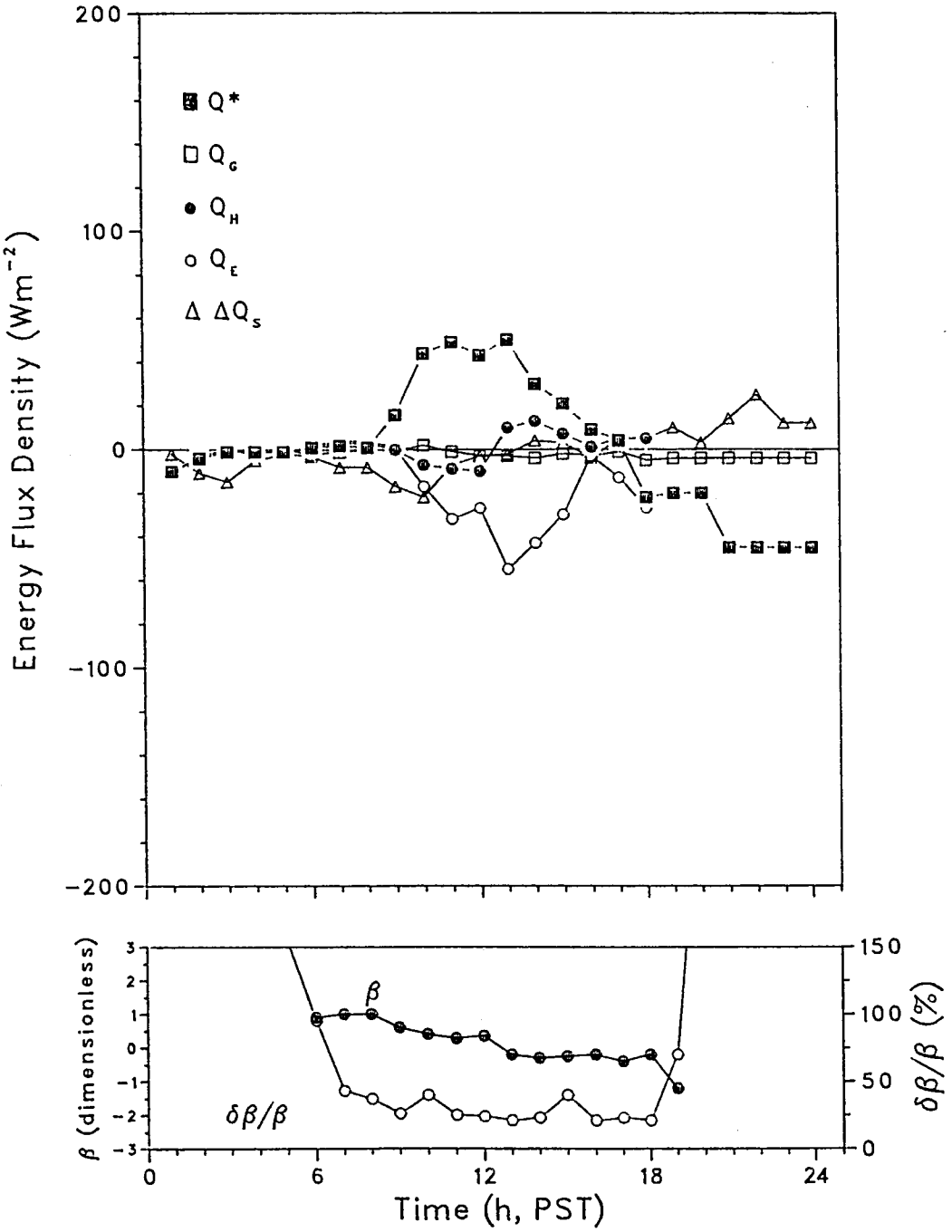

Figure 7.2. Hourly energy budget measured on April 25, 1988 for snow–covered tundra.

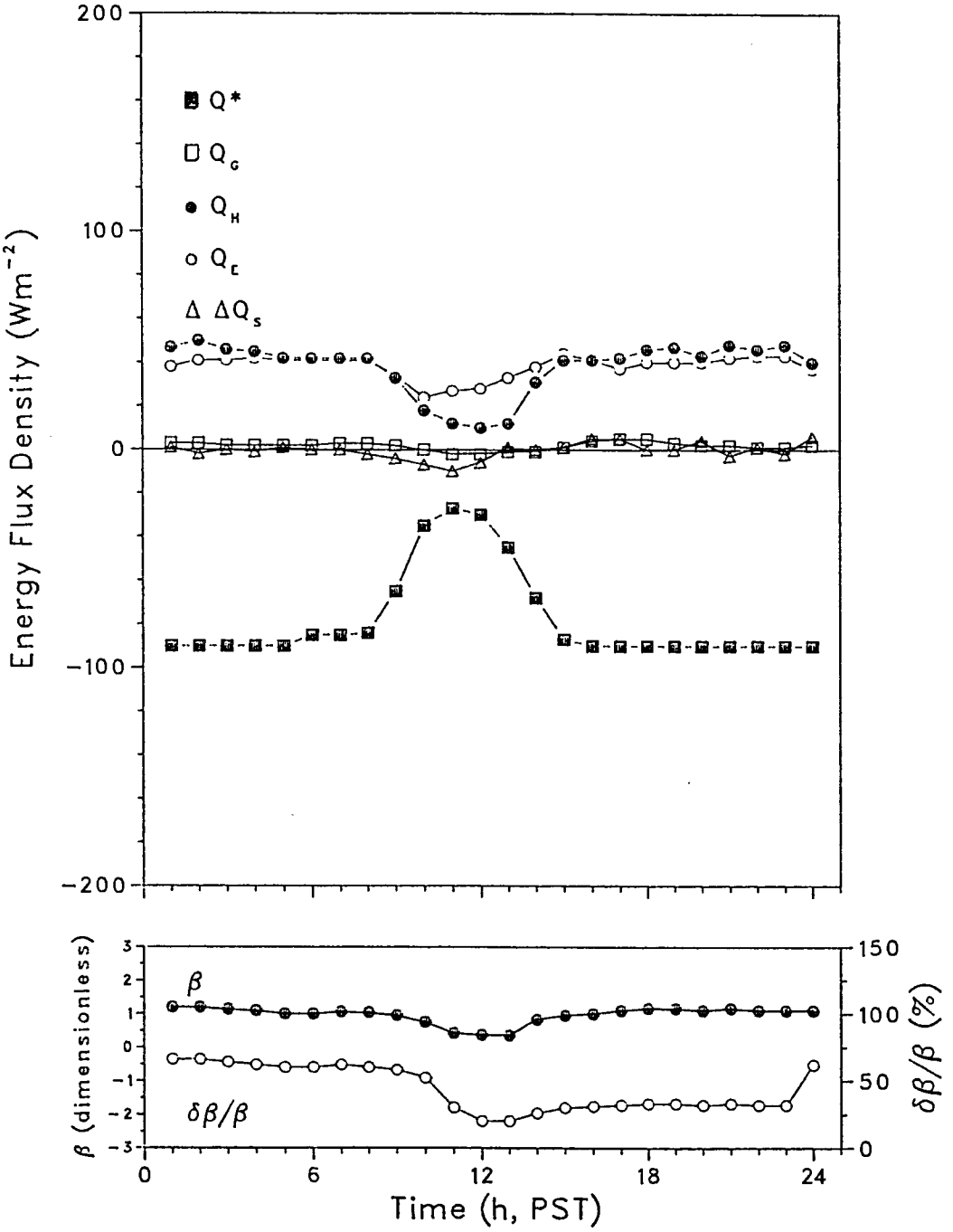

Figure 7.3. Hourly energy budget measured on December 10, 1986 for snow-covered tundra.

(B) Snowmelt Regime

Melt period durations were generally short. Because of the very thin snow cover, only a few days of cloudless or partly cloudless days without precipitation were required to change a complete snow cover to a snow-free tundra surface. Later in the spring or summer, fresh snowfalls could be melted within a couple of days, or even a few hours if conditions were favourable.

Due to the difficulties in determining the energy budget at Scout Mountain during snowmelt, only a few days from the spring of 1988 will be considered here. The energy associated with snowmelt was generally equal or greater than the turbulent fluxes. A majority of days showed that snowmelt dominated the dissipation of available energy. Latent heat was generally second in importance. Sensible heat was commonly small, and showed both positive and negative fluxes.

Figure 7.4 illustrates the energy budget for two days during a 1988 snowmelt period. Both days were partly cloudy, hence the fluctuations in Q^*. A complete, but thin, snow cover existed on the morning of April 21. On both days Q_M dominated energy disposition, and the precipitation gauges responded to the snow melt. However, by April 22 the snow cover began to break up and reveal the underlying ground surface. Snow cover thinning and breakup was initiated around prominent rocks or earth hummocks, which generally had the thinnest snow, and also could act as heat islands. Melt would occur preferentially around these nodes, and the last snow to melt would be in the bottom of the hollows between turf hummocks. Thus with increasing ablation, the surface took on a very patchy appearance, and this had occurred by April 22. The increases in the turbulent fluxes are apparent. Although practically impossible to measure and evaluate at the microscale at which it happens (on Scout Mountain), it seems likely that the high Q_M values for this day were in part fed by advective heat transfers from the bare ground (the hummocks) to the snow patches (in the hollows). This advective process has been documented for larger scale snow patches, and is known to be important (Olyphant and Isard, 1987).

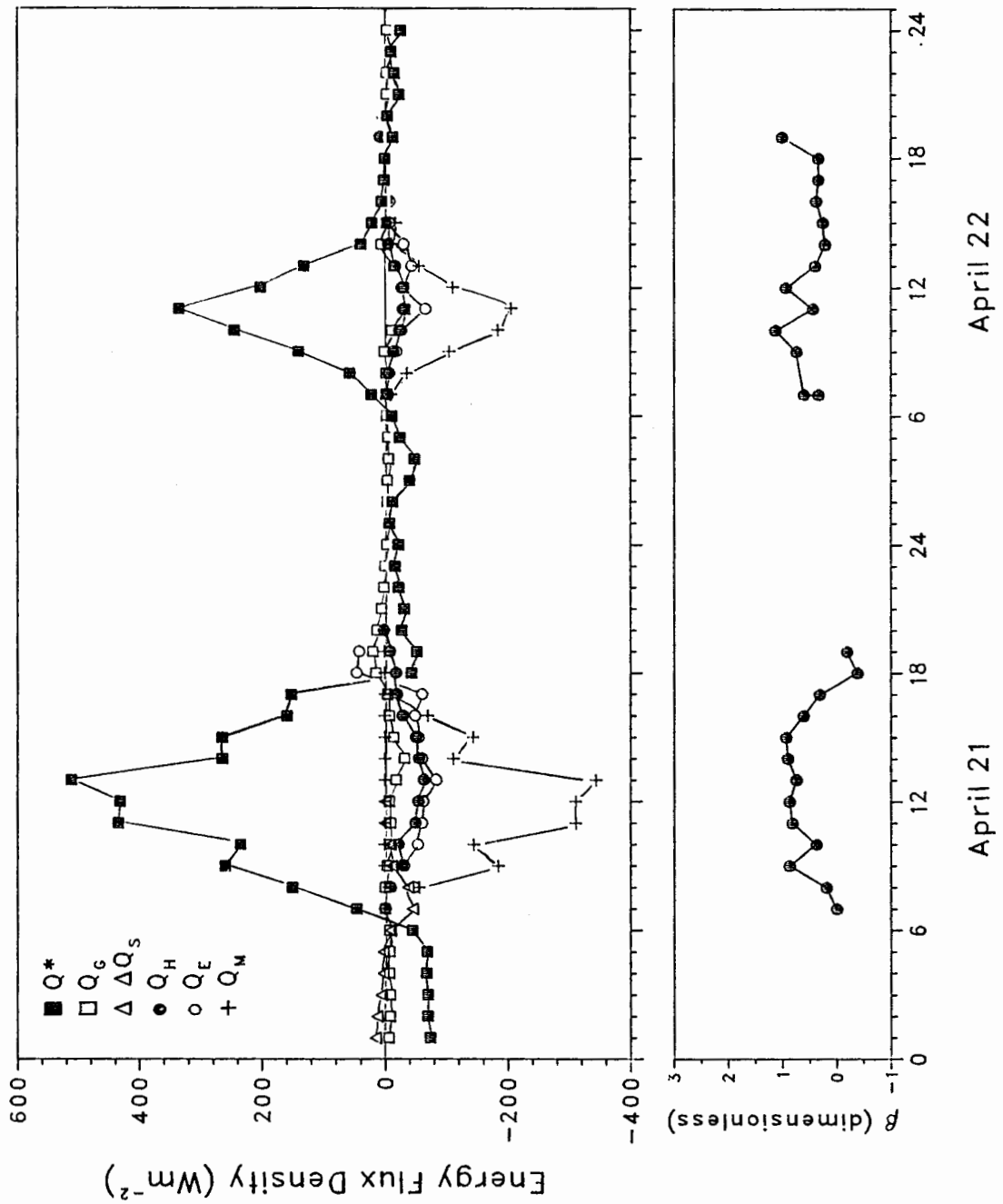

Figure 7.4. Hourly energy budget measured on April 21–22, 1988 during a snowmelt period.

(C) Snow-free Tundra

In 1987, the winter snow cover had disappeared by April 27. A snow cover existed for May 1-3 and 18-24. In 1988, an early melt produced the first snow-free conditions on April 13 but this was short-lived due to the stormier weather of that year, and not until after May 9 did a snow-free surface persist.

From the 1986-87 and 1988 measurement period about 100 days of energy budget data from snow-free tundra were obtained. About three-quarters of the days showed a diurnal trends in the Bowen ratio which were relatively small (sometimes negative) in the early morning, increased through the day, and then either decreased or remained constant in late afternoon.

Three examples derived from relatively cloudless or nearly-cloudless skies are discussed first to illustrate some typical energy budget trends without the variability introduced by cloud cover. The first two days depict straightforward energy partitioning for the two extremes of a wet and a dry surface. Many days at Scout Mountain would in fact lie somewhere between these two examples.

Figure 7.5 shows the energy budget for a day with a wet surface. The day, May 10, 1988, was preceded by several melt events from spring snowfalls and consequently the ground was very wet, and a few small pockets of snow were still ablating. This situation persisted for several days. The diurnal trends of heat fluxes show an evapotranspiration-dominated regime. Except for the early morning hours (when determination of β was problematic), the Bowen ratio displayed a conservative trend with a mean value of 0.55. The total evaporative heat loss for the daytime period was $-7.36\,MJ\,m^{-2}d^{-1}$, representing about 2.97 mm water equivalent and 52% of the available energy. The low surface resistances (calculated as residuals in Equation 7.8) are indicative of an absence of moisture stress, and are in accordance with strong evaporative fluxes.

At about the same time in the previous year, surface conditions were much drier due to sparse winter snowfall. As a result, turbulent energy dissipation was predominantly by sensible heat transfer. Figure 7.6 shows one of the days from this period, May 9, 1987. On this day only about 32% of the available energy was used in evapotranspiration and sensible

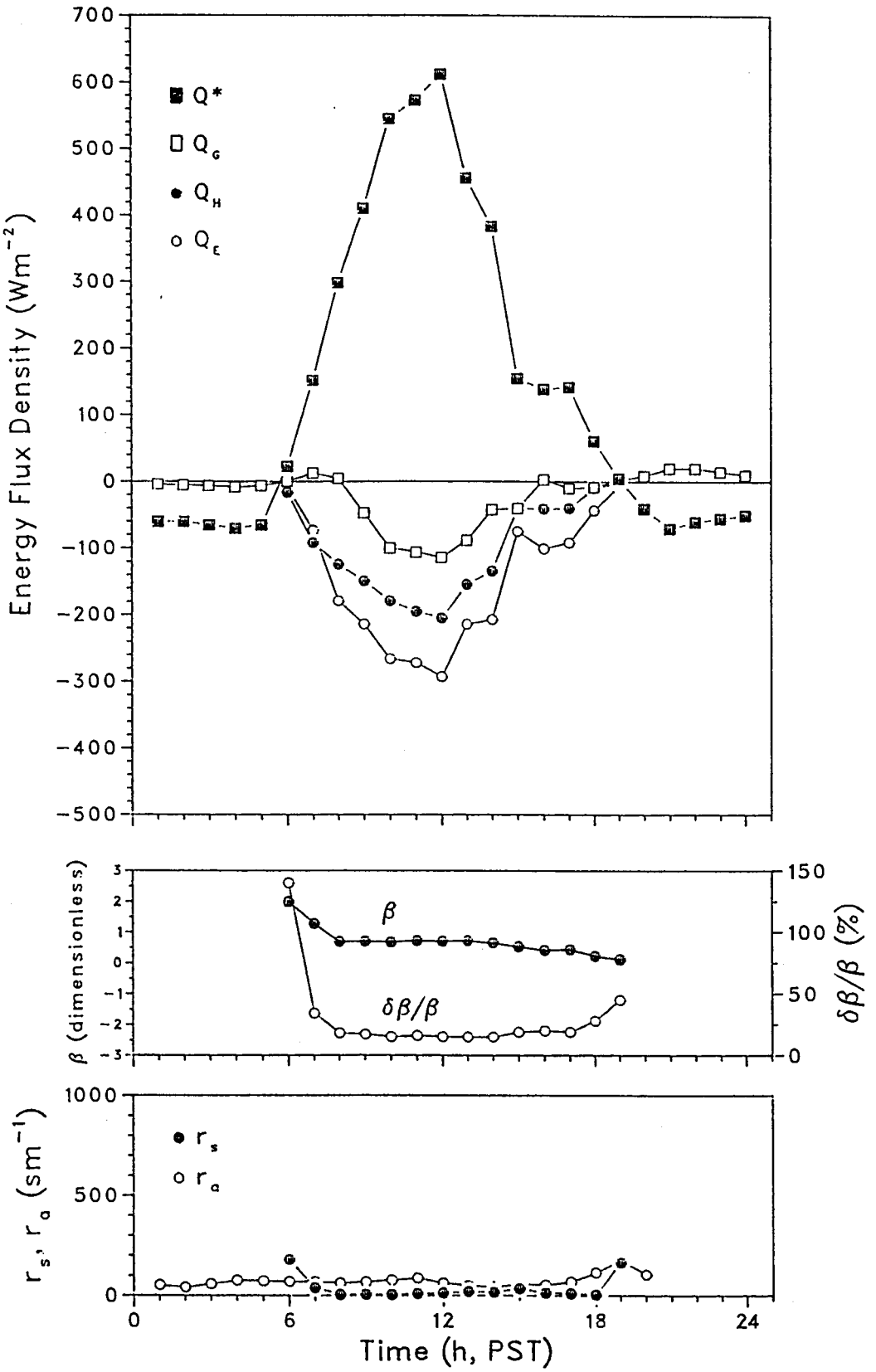

Figure 7.5. Hourly energy budget measured on May 10, 1988 for a wet snow-free tundra.

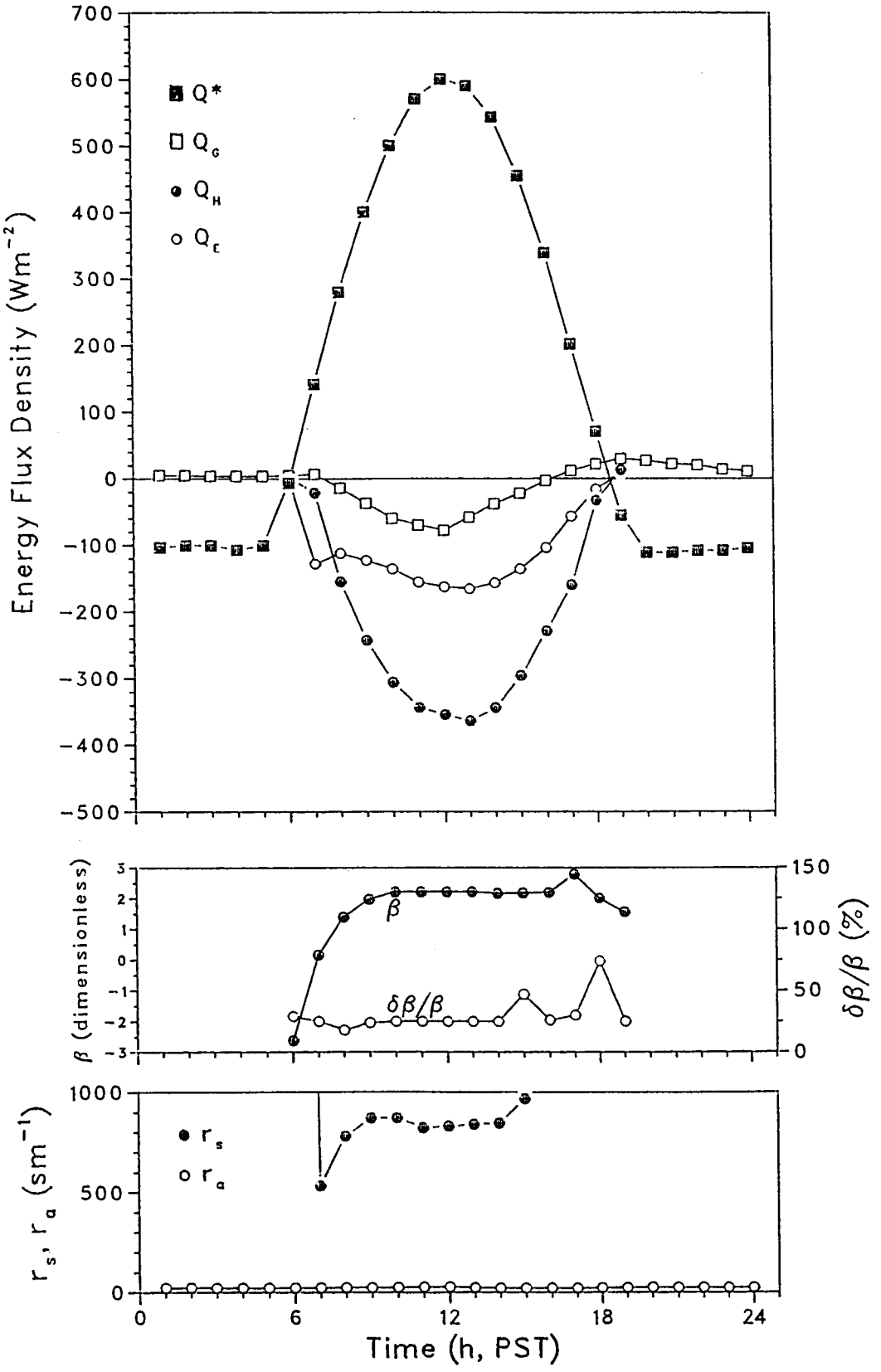

Figure 7.6. Hourly energy budget measured on May 9, 1987 for a dry snow-free tundra.

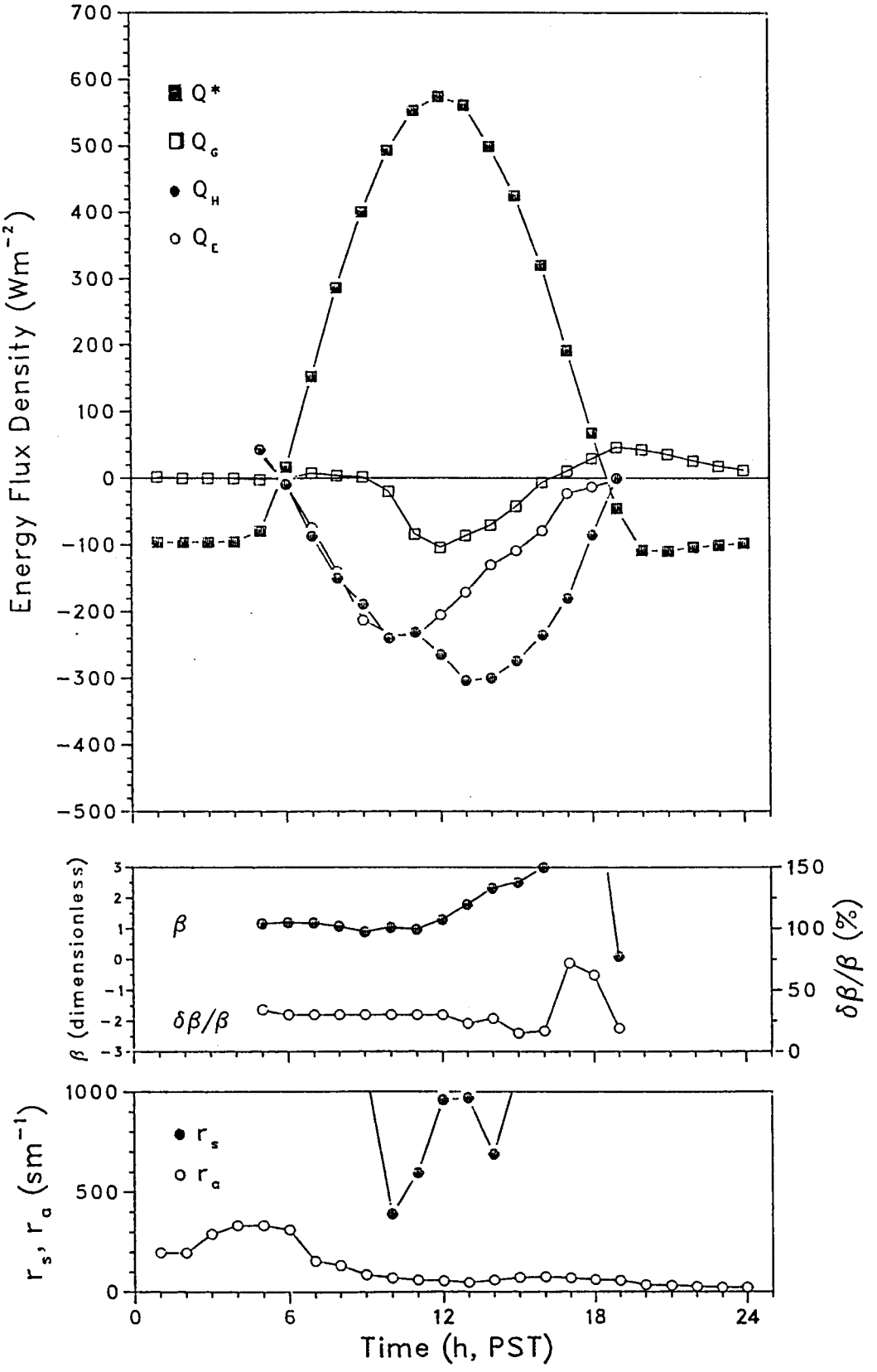

Figure 7.7. Hourly energy budget measured on May 16, 1987 for a drying snow-free tundra.

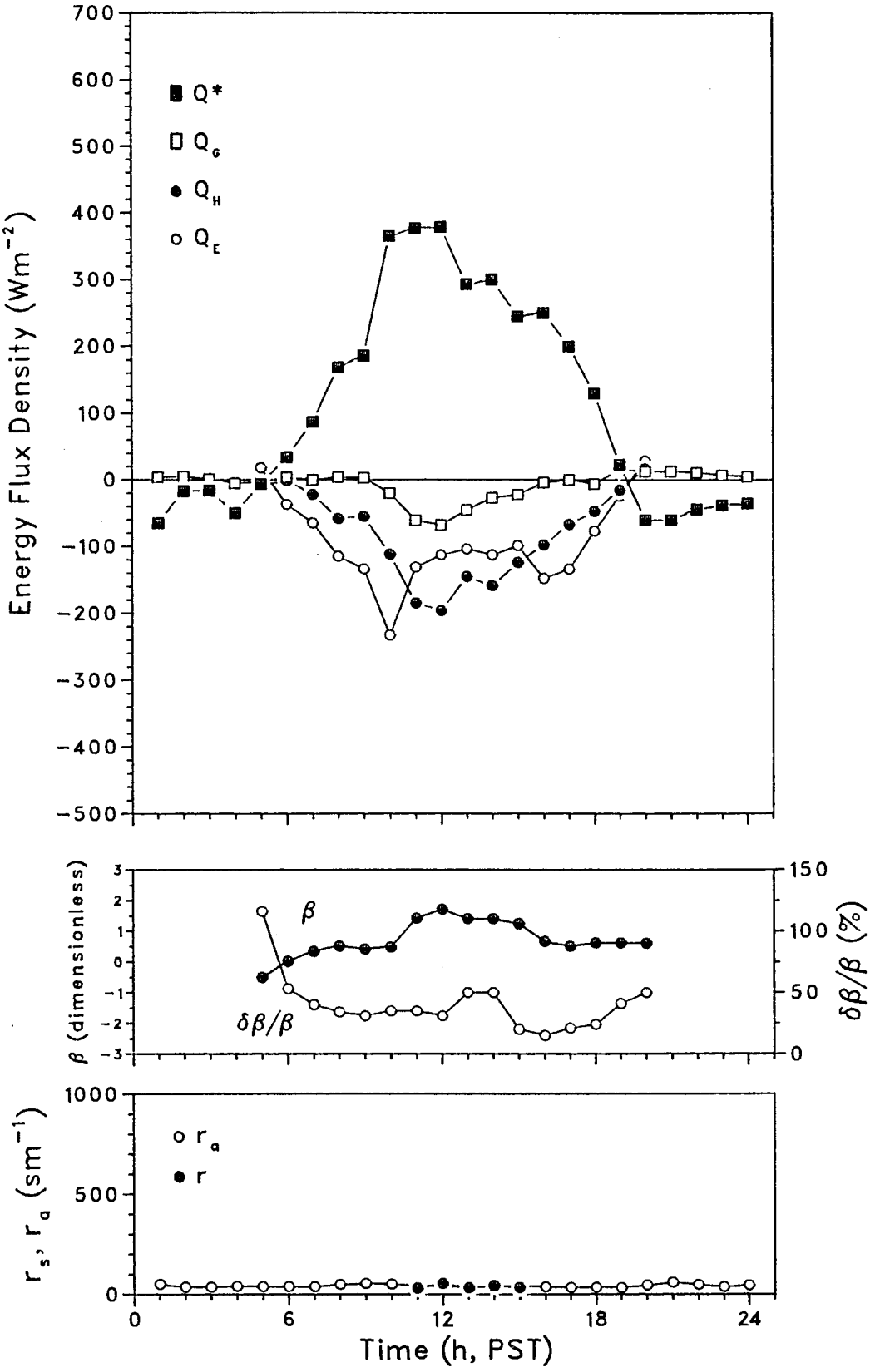

Figure 7.8. Hourly energy budget measured on May 31, 1988 for a snow-free surface and showery weather.

heat expenditure was nearly double this. After an early morning increase, the Bowen ratio stabilized at about 2.20. The aridity of the surface expressed itself in the high values of surface resistance, which confirm that the plant cover was stressed through moisture limitations and exerted a control on transpirative losses.

The third example, from May 16, 1987, is from a day somewhere between the two extremes in the previous examples, and displays a different energy regime (Figure 7.7). Three days with light rainfall had preceded this and surface moisture availablity had increased. The turbulent fluxes were approximately equal in the morning, but in the afternoon Q_H greatly exceeded Q_E. This scenario occurred several times and appears to be a result of the development of moisture-limiting conditions. This is confirmed by the r_s trend which suggests that a moisture stress on the vegetation was in effect from midday onwards.

Trends in energy partitioning similar to those discussed above were common on days without, and even on some days with, precipitation. Rainfall generally decreased the Bowen ratio, but the effects on individual days were not always comparable and on some days rainfall produced little change in the energy regimes. Most days with rain, however, did have responsive energy budgets. Figure 7.8 illustrates the energy budget for May 31, 1988. Light snow showers in the early morning were followed by a drying trend until midday. Snow showers, sometimes heavy, returned in the afternoon, and a clearing trend began after 1700 h. Overcast skies were the norm for the day and accounted for the suppressed flux magnitudes. The turbulent fluxes responded quickly to the changing surface conditions. Morning Bowen ratios were low as the trace of snow was melted and evaporated, then quickly rose at 1000 h as the surface became drier. Despite the morning precipitation, the vegetation was observed to be dry and crisp by 1030 h, less than one hour after the end of the final morning snow shower. Rapid surface dessication was commonly observed during light shower activity. The early afternoon showers had little impact on β, but the commencement of heavy precipitation drove its value down from 1600 h onwards.

Summer Drying-Cycle Behaviour

The preceding section discussed energy budgets on an individual-day basis. In reality, no one day is isolated, but forms part of a continuum of surface energy and mass transfers. No previous alpine research has detailed a progression of several days energy budget. Brazel (1974) reported the changes in daily energy totals during and after a rainy period of a few days but did not discuss it in detail. Bowers and Bailey (1989) found that evaporation on an alpine fellfield was only high immediately following precipitation as a result of the rapid drainage and drying of the predominantly stony surface, and the Bowen ratio would therefore show a quick increase in response.

Few drying periods of longer than a couple of days occurred at Scout Mountain due the frequent precipitation. The five-day period selected for discussion was for July 11 - 15, 1987. Several days with precipitation preceded this period, the final event occurring as convective shower activity on the afternoon of July 11. Overcast, showery weather resumed on July 16. The intervening period consisted of four similarly bright or cloudless days. Each day showed characteristic net radiation trends, with midday peaks of around 600 W m^{-2} (Figure 7.9). Ground heat flux tended to mimic Q^*, but at values of $\simeq$10-15% the magnitude. The interaction bewteen sensible and latent heat fluxes changed daily. On July 11 Q_E generally outweighed Q_H due to the moisture availability and precipitation, and on the following day both quantities were essentially equal. Moisture stresses became apparent on July 13, when increasing surface resistances restricted water losses. July 14 showed a similar pattern, but with sensible heat beginning to dominate the regime. By July 15, only four days after the end of the wet spell, sensible heat assumed a dominant role, and latent heat losses were typically 50-100 W m^{-2} less than the previous days. The surface resistances were persistently large, indicating surface control on the evaporative flux. This situation would continue until the next precipitation event supplied moisture to the surface.

DAILY ENERGY BUDGET RESULTS

Mean values of budget parameters are shown in Table 7.1. The trends of daily energy budget components showed much temporal variability (Figures 7.10, 7.11 and 7.12). Reasons for this included the variability of atmospheric controls (especially cloud cover) and surface

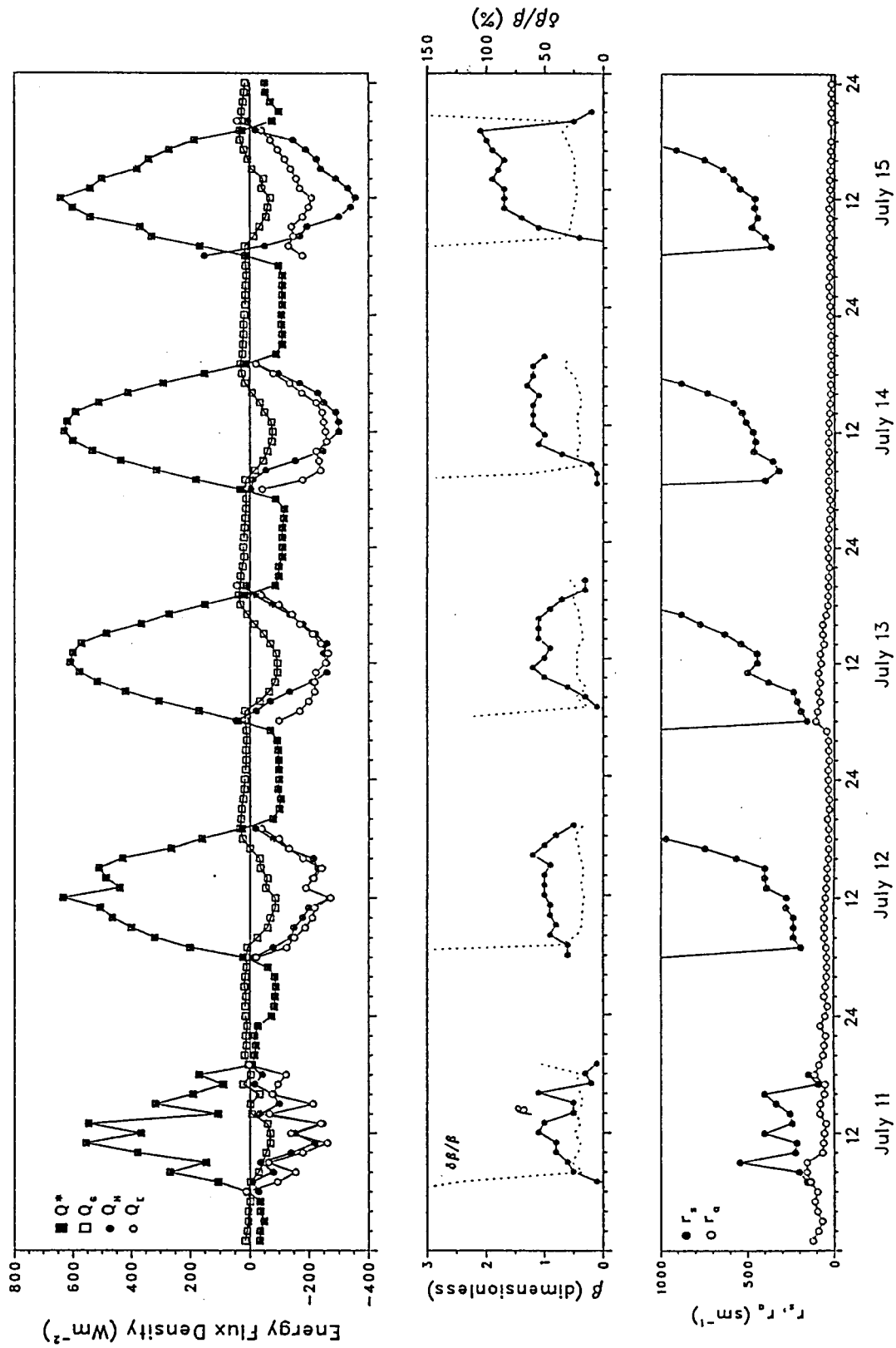

Figure 7.9. Hourly energy budget measured on July 11–15, 1987 showing the development of increasing surface dessication.

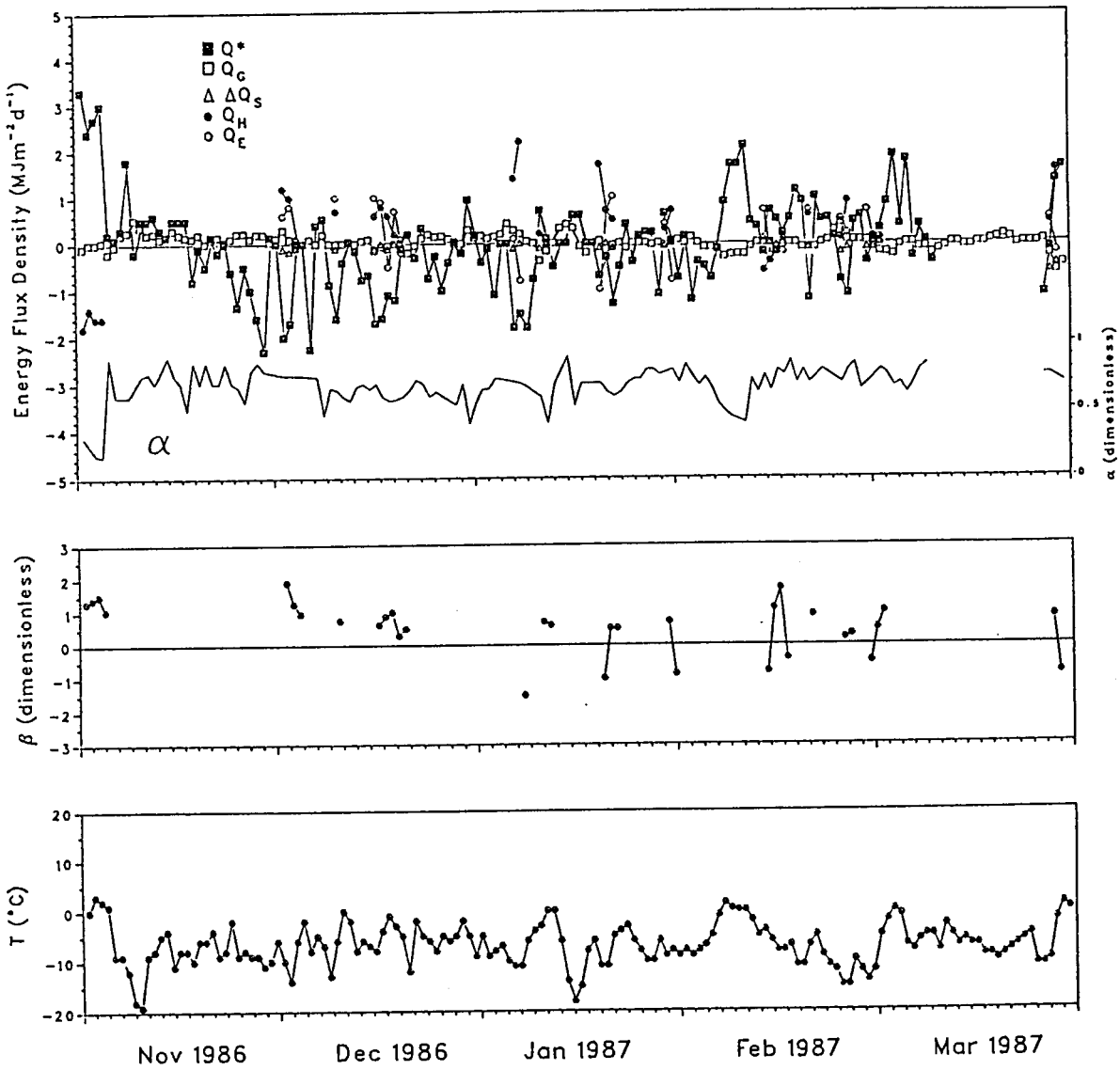

Figure 7.10. Daily energy budgets measured on November 1986 to March 1987, including surface albedo (α) and air temperature (T).

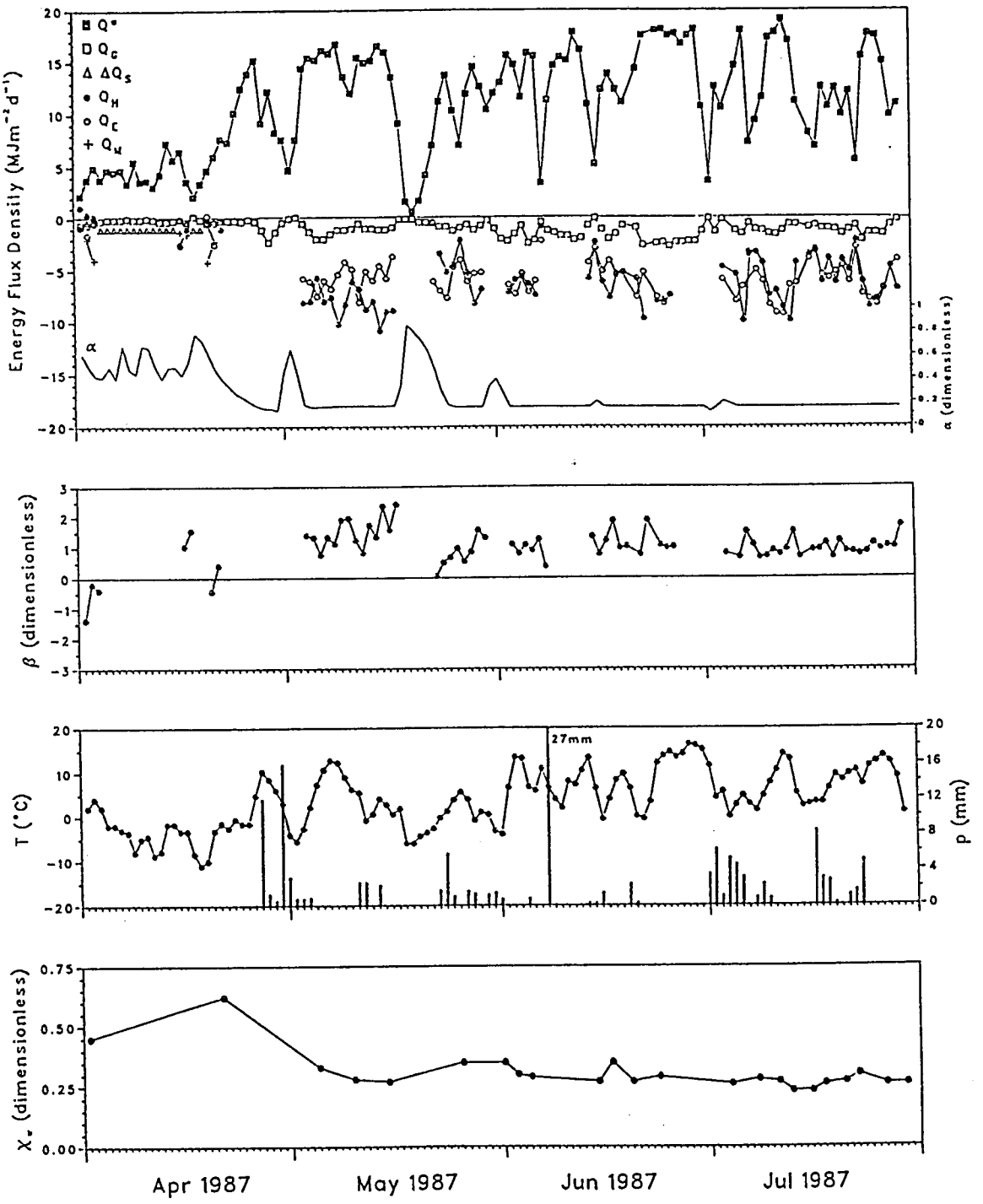

Figure 7.11. Daily energy budget, albedo (α), air temperature (T), precipitation (p) and volumetric soil moisture content (χ_W) measured from April to July 1987.

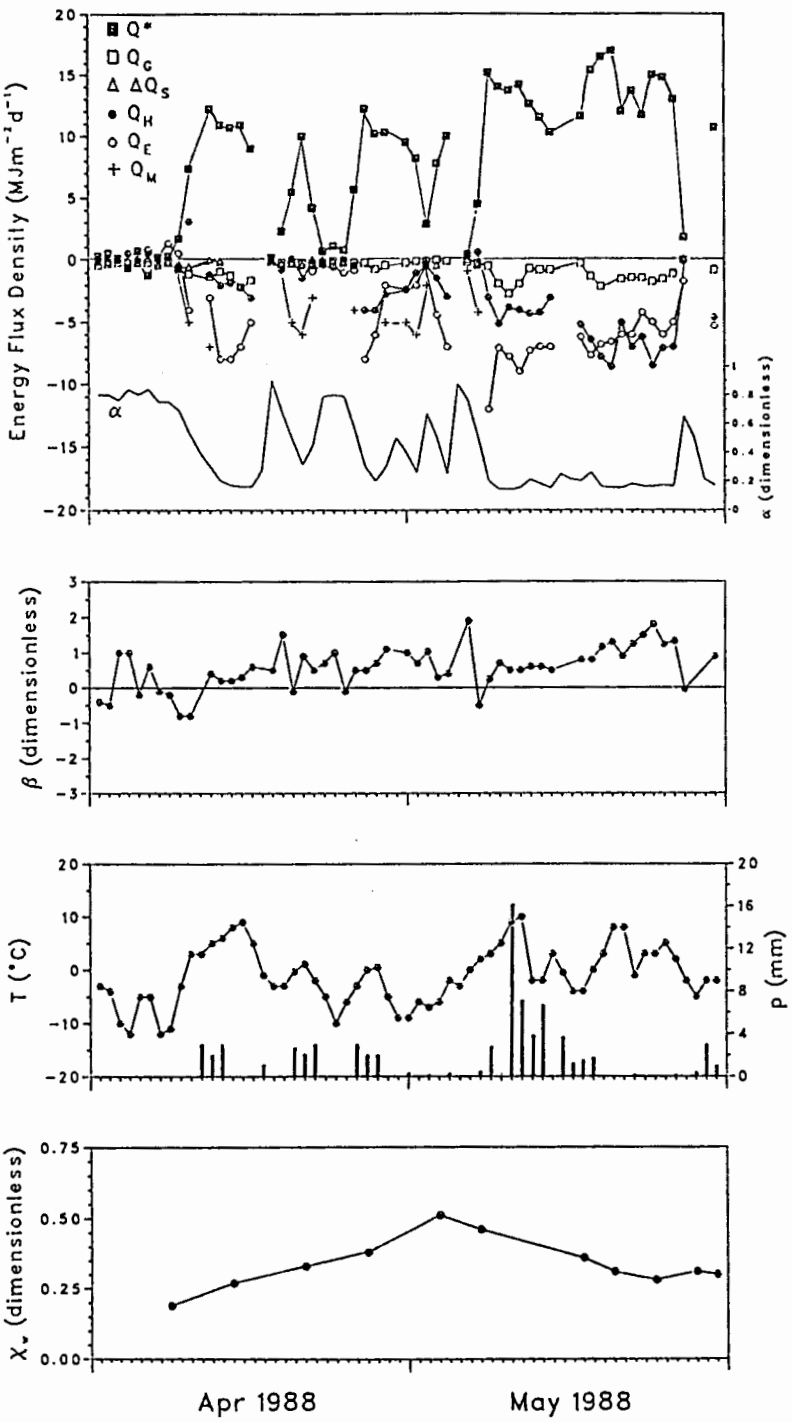

gure 7.12. Daily energy budget, albedo (α), air temperature (T), precipitation (p) and volumetric soil moisture content (χ_W) measured from April to May, 1988.

Table 7.1. Mean daytime energy flux densities for all data.

Energy Regime Type	n (days)	Q^*	Q_G	ΔQ_S	Q_H	Q_E	Q_M	β
A: Winter (snow)	43	−0.26	−0.05	−0.08	0.42	−0.09	0	−4.67
B: Snowmelt	23	5.45	−0.38	−0.27	−0.39	−1.40	−3.07	0.28
C: Snow−free tundra	114	12.06	−1.06	0	−5.47	−5.99	0	0.95

All energy flux density units are $MJ\,m^{-2}d^{-1}$.

controls (albedo and soil moisture availability). The behaviour of the turbulent fluxes was erratic. In general, β showed the greatest variability when a snow cover existed, but for snow-free tundra the simplification of $\beta = 1.00 \pm 0.50$ summarizes the results.

The 1986-87 winter-spring season (Figure 7.10) showed the sudden decrease in net radiation in early November 1986 as the winter snow cover got established. Thereafter, net radiation was generally negative and small (less than 2.00 MJ $m^{-2}d^{-1}$), forcing the sensible and latent heat fluxes to be positive at times. The ground heat flux was positive in November 1986, and then generally about zero until the snow cover melted in late April 1987 (Figure 7.11). This seasonal trend is not unlike that for subarctic tundra surfaces (Lewis and Callaghan, 1976; Rouse, 1984b).

Following snowmelt, energy and soil water availability became much greater, and Q_G, Q_H and Q_E responded by showing larger flux magnitudes. Ground heat flux losses were consistently less than 4.00 MJ $m^{-2}d^{-1}$ The evaporation regimes did not always appear to be related to the surface moisture conditions. In the second week in May 1988, immediately following snowmelt, the surface was wet and soil moisture content was at a maximum. As could be expected, latent heat fluxes dominated energy disposition. The immediate postmelt period in 1987, however, showed a somewhat different evaporation regime. The winter snow cover melted off in the last week of April, and again net radiation and soil moisture content were high. Yet during the following two weeks, only two days showed Q_E to exceed Q_H.

Thus the daily Bowen ratio trends (Figures 7.10 to 7.12) were not strongly coupled to the precipitation or soil moisture trends. This was further illustrated during July, 1987 when β was generally near unity, despite there being definite wet and dry periods. A very heavy rain storm on June 8, 1987 produced no apparent change in soil moisture content, although β did display a decrease. Soil moisture content did, however, show a general seasonality, being very high during and following snowmelt and declining thereafter. The role of spring melt in recharging soil moisture at Scout Mountain is paralleled in Arctic tundra (Rouse, 1982).

There were some drying cycles evident in the snow-free periods. Some cycles were associated with the drying of the surface following snowmelt, such as May 23-29, 1987 and

May 14–16, 1988. Other drying events were preceded by rainy periods, exemplified by May 22–25, 1988.

RELATIONS BETWEEN NET RADIATION AND GROUND HEAT FLUX

Simple linear relations between net radiation and ground heat flux are commonly found. This is advantageous for modelling boundary layer processes since Q_G can often be assumed to be a fixed proportion of Q^*, typically 10–15%, and therefore the measurement of Q^* can be converted into an estimate of available energy. The daily alpine energy budget data reviewed in Table 3.1 show a range of Q_G/Q^* values covering about 2 to 20%.

It might therefore be anticipated that similar relations between Q_G and Q^* be found for Scout Mountain, but this was not the case (Figure 7.13). Hourly data showed a non–linear trend, but daily totals were very scattered. Since flux divergence in the 0 – 50 mm soil layer was accounted for, the source of the scatter must be explained by some other phenomena.

For all the daily snow–free data (Table 7.1), the mean value of Q_G/Q^* was 0.09. The trend shown by the hourly data shows that Q_G/Q^* increased with Q^* from negligible values when Q^* is small to nearly 20% for the larger values of Q^*. The diurnal trends in energy budgets discussed above did not display consistent relations. While some days did show Q_G to vary with Q^* (such as the days shown in Figure 7.9), other days showed Q_G to have a somewhat anomalous lag time in the morning flux increases (Figures 7.7 and 7.8). This inconsistency in the diurnal behaviour of Q_G probably accounts for some of the scatter in Figure 7.13, but the causes are still uncertain.

The Scout Mountain data cover a wide range of soil moisture and temperature conditions. Soil ranged from saturated to relatively dry. Temperatures in the surface soil layer varied widely and also oscillated about 0°C on some days early in the postmelt season. Therefore the thermal conductivity of the soil (Equation 7.13) varied considerably. There are also problems in measuring ground heat flux in such heterogeneous surfaces such as the patterned ground at Scout Mountain, where lateral heat flow in the stone polygons (Figure 1.3) may occur, and where the coarse stony soils make flux plate placement problematic. The

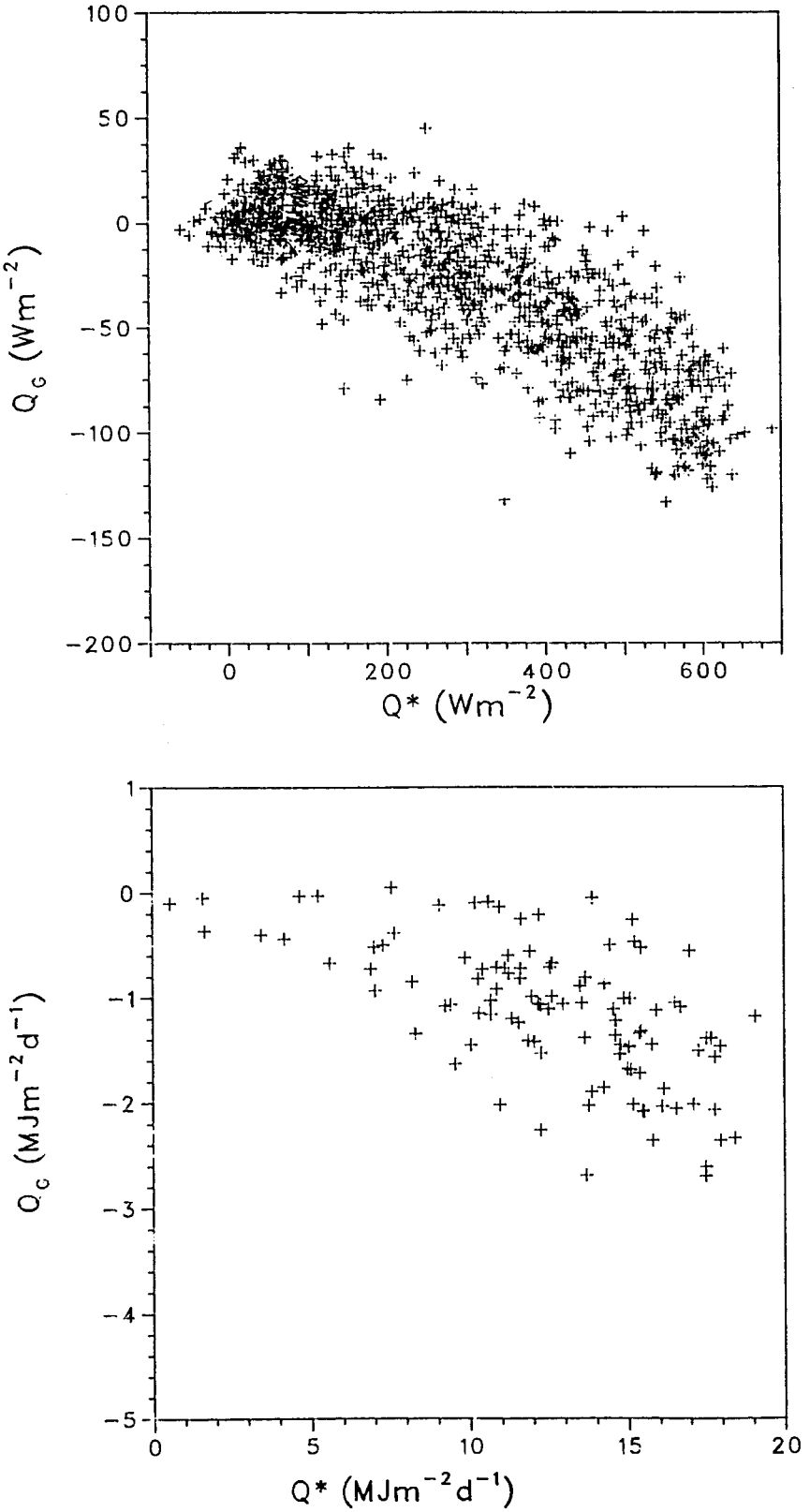

Figure 7.13. Hourly and daily net radiation (Q*) versus ground heat flux (Q_G) for a snow-free surface; 1987 and 1988 postmelt seasons.

thermal conductivity in frost-sorted alpine soils also displays microscale spatial variability (Ballard, 1973). The use of flux plates in permafrost has been criticized due to their inability to account for the significant vertical heat transfer consequent on interstitial vapour movement (Halliwell and Rouse, 1987). Although permafrost probably does not occur at Scout Mountain, the presence of frozen substrate in the early postmelt season may have incurred similar errors in Q_G measurements.

DISCUSSION

Results from the measurement of energy budgets at Scout Mountain demonstrated a strong seaonality dependent on atmospheric and surface controls. In winter and spring, the snow cover dictated the general low-energy regimes. The loss of energy through convection in winter is rather anomalous when compared to thick snowpacks, which generally have Q_H and Q_E as heat sources. Undoubtedly the sparseness of the snow cover of the tundra contributes to this. The near-permanent exposure of vegetation and rocks above the thin snow caused the surface to behave simply as a colder, whiter variant of the same summer surface, rather than as a thick mountain snowpack more typical of the subalpine and the coastal alpine zones.

In the summer, energy budgets were distinguished on the basis of energy- or moisture-limiting regimes. The patterned ground and coarse soils which characterize the site (Figures 1.2 and 1.3) promoted rapid drainage of meltwater and rain, effectively limiting the soil moisture retention to the thin organic-rich surface soil horizon. This produced a soil moisture content which was largely unaffected by precipitation or drying periods. The exception to this generalization was during and immediately after the spring snow melt periods, when the surface soil layer was saturated and occasionally had puddles of water. At these times, the subsurface layers were frozen and impermeable. Once thawed, subsurface drainage was unimpeded.

Despite the fact that soil moisture remained relatively constant for much of the postmelt season (in 1987), the evaporation regimes varied significantly. This indicated that soil moisture may not necessarily be an important control on Q_E. The conservative nature of χ_W compared to precipitation inputs and Q_E suggested that the surface energy budget was

at times decoupled from subsurface conditions. Since water typically drained or evaporated from the surface very rapidly following rainfall, it was the frequency, and not the magnitude, of rainfall events which governed the surface energy partitioning.

Further delineation between the energy- and moisture-limiting regimes at Scout Mountain can be defined using the decoupling coefficient (Ω). The decoupling coefficient has a range from 0 to 1 and expresses the relative importance of the two competing controls on evaporation, namely the energy term and the aerodynamic term (McNaughton and Jarvis, 1983). When $\Omega \rightarrow 0$, evapotranspiration is dominated by the aerodynamic term and is governed by the surface resistance and the saturation deficit of the overlying air. Surface evaporation is therefore well coupled to the boundary layer. In contrast, if $\Omega \rightarrow 1$, then Q_E tends towards equilibrium evaporation, and the aerodynamic term plays a negligible role. Evaporation becomes decoupled from the boundary layer, and is instead driven by available energy.

The contrast between the predominantly dry conditions of the 1987 snow-free season and the often wet 1988 season emerges when hourly daytime Ω and β is plotted (Figure 7.13). For the 1988 data $\Omega \rightarrow 1.0$ indicating a decoupled, energy-limiting evaporation regime. The 1987 data mostly comply with $\Omega \rightarrow 0.0$ indicating that evaporation was coupled and moisture limiting. Each evaporation regime occurs over similar ranges of the Bowen ratio. Use of Ω therefore provided insight into the response of the surface to changing moisture availability.

The extent of the data set from Scout Mountain allowed for an examination of the surface resistance under a range of conditions. Only Bowers and Bailey (1989) and Körner and Mayr (1981) have specifically considered physiological resistances in the alpine zone. The former authors deduced surface resistances by residual from the combination model. Körner and Mayr made porometer measurements of conductivity for several species in a vertical transect from 600 to 2600 m a.m.s.l. in the Alps. They contend that at altitude internal water stress is of minor importance in controlling gas diffusion, therefore allowing the high rates of evaporation observed in the alpine zone. This conflicts with Bowers and Bailey's (1989) conclusions that alpine plants play a crucial role in limiting the evaporative flux under non-saturation conditions. Of critical importance in interpreting these contrasting opinions is that Bowers and Bailey studied a very dry site whereas Körner and Mayr focussed on

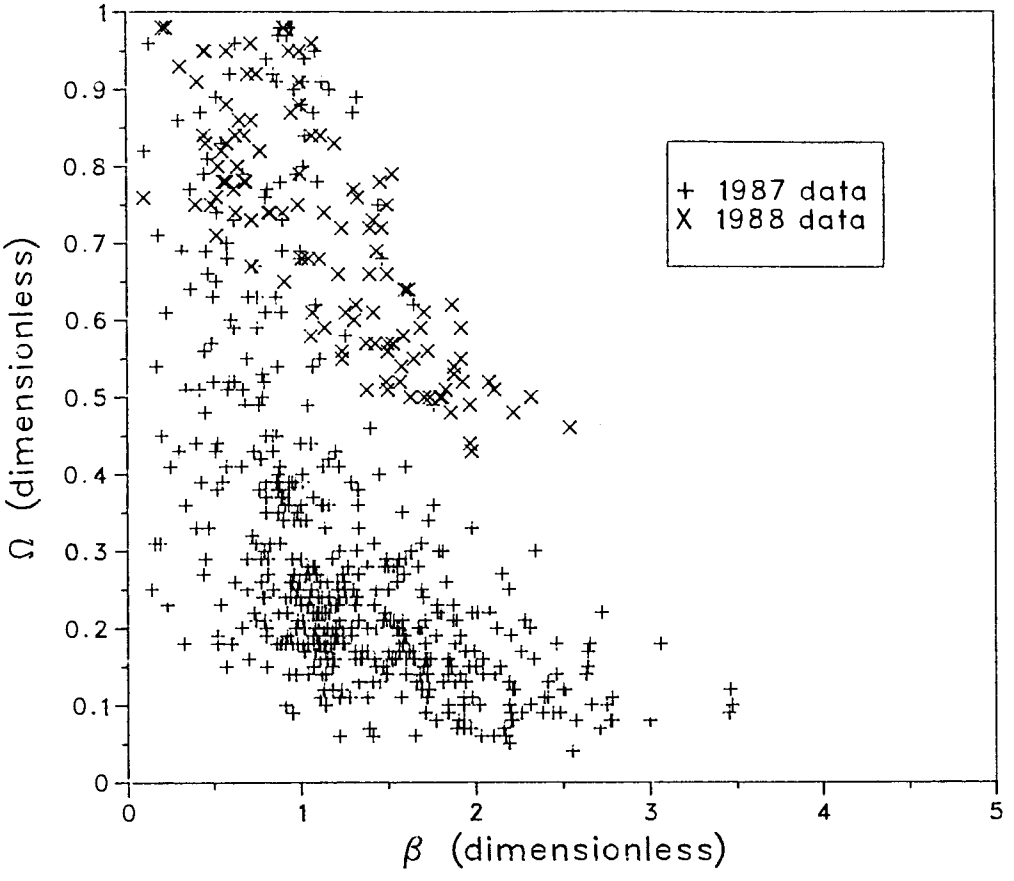

Figure 7.14. Hourly Ω versus β for a snow-free surface from the 1987 (predominantly dry) and 1988 (predominantly wet) field seasons.

wetter sites. The latter authors also confined their analyses to sunny conditions, when stomatal resistances can be expected to be lower. The decreases in r_s with increasing temperature found for a sub-Arctic sedge-grass surface by Rouse *et al.* (1987) do not appear to be paralleled at Scout Mountain. The increasing surface temperatures of the alpine tundra result in rapid dessication leading to increases in r_s. This probably outweighs the temperature effect.

The bare rock surfaces at the site were rarely wet for very long, on most occasions drying rapidly following rainfall. Since bare rocks account for at least one quarter of the surface area of the site, the moisture reservoirs available for evapotranspiration are restricted to the vegetated cores of the stone polygons. Therefore, alpine tundra energy transfers must perforce be dominated by sensible heat unless precipitation or melt wets the rock surfaces. The vegetation, which grows almost exclusively on the polygon cores, therefore played a major role in limiting evaporation and this was evidenced by the surface resistance trends. Many of the salient features of the Scout Mountain energy budgets are encapsulated in Figure 7.9 which shows the characteristics of the surface energy and mass transfers under conditions of progressive dessication. The figure shows a wet surface where evaporation losses match those of sensible heat, a drying trend with increasing Bowen ratios, the first signs of surface moisture stress and possible physiological response and finally a thoroughly dessicated state where Q_H dominates convective heat losses.

CHAPTER VIII

SENSIBLE HEAT FLUX DETERMINATIONS IN AN ALPINE TUNDRA, SCOUT MOUNTAIN, SOUTHERN BRITISH COLUMBIA, CANADA

INTRODUCTION

Physically-based sensible heat flux modelling procedures explicitly recognize atmospheric and surface controls, but their application to alpine (above treeline) environments has been very limited. Although climatic data have long been collected in mountainous regions, there have been few energy budget studies from the alpine tundra environment (Barry, 1981; Price, 1981). To date, there has been only one intercomparison of physically based sensible heat flux determinations from alpine tundra in North America (Bowers and Bailey, 1990). The reasons for this scarcity stem from the combination of logistical problems and theoretical/experimental limitations. The present study addressed this deficiency by comparing eddy correlation measurements of sensible heat fluxes to determinations made by the Bowen ratio - energy budget (BREB), aerodynamic and Ohm's Law approaches.

THEORETICAL BACKGROUND

Sensible heat flux densities were determined using two approaches. Firstly, direct measurement using the eddy correlation method was used:

$$Q_{H(EC)} = \rho c_p \overline{(w' T')} \qquad (8.1)$$

where ρ is the density of air, c_p is the specific heat of air and $\overline{(w' T')}$ is the time-averaged product of instantaneous covariances of vertical wind speed (w) and air temperature (T).

Secondly, three physically based methods which employ of surface temperature or temperature profile data were used. These were the Bowen ratio-energy budget (BREB) method, the aerodynamic method and Ohm's Law. All were discussed in more detail in Chapter III, so only the equations will be outlined here.

Bowen Ratio-Energy Budget (BREB) Method

Rearranging the energy budget equation gives

$$Q_{H(BR)} = - \frac{(Q^* + Q_G)}{1+\beta^{-1}} \qquad (8.2)$$

where Q^* is net radiation, Q_G is ground heat flux, and β is the Bowen ratio, defined as Q_H/Q_E.

Aerodynamic Method

From mass transfer equations, Thom (1975) defines the aerodynamic equation for sensible heat flux density

$$Q_{H(AE)} = \rho c_p k^2 \frac{\partial T}{\partial(\ln z)} \frac{\partial u}{\partial(\ln z)} (\Phi_M \Phi_H)^{-1} \qquad (8.3)$$

where ρ is the density of air, c_p is the specific heat of air at constant pressure, k is von Karman's constant, T is air temperature, u is wind speed and $(\Phi_M \Phi_H)^{-1}$ is a stability correction calculated from the Richardson number.

Ohm's Law Method

Exploiting the Ohm's Law relations between potential difference, flux density and resistance, the surface sensible heat flux can be defined as

$$Q_{H(OL)} = \rho c_p \frac{(T - T_0)}{r_{aH}} \qquad (8.4)$$

where T_0 is surface temperature and r_{aH} is the aerodynamic resistance to sensible heat transfer, calculated from the wind profile. The latter theoretically requires corrections to account for atmospheric stability and bluff-body resistance ("excess resistance"), but these need wind profiles to be measured. For the present study, these were only measured during the latter parts of the field program. At other times, corrections for stability and excess resistance were ignored. For an agricultural crop surface, Bailey and Davies (1981) demonstrate that the errors incurred by adopting this practice are small, provided that measurements are made sufficiently close to the surface.

In the absence of absolute values of sensible heat flux densities, the eddy correlation measurements were taken as the independent variable against which the other methods were compared. The difficulties in measuring small vertical gradients of temperature led to large errors in night-time flux determinations from profile methods, and therefore all data considered in this study were from the daytime only.

EXPERIMENTAL PROCEDURE

The site (described in Chapter I) was a grass-sedge tundra developed on the patterned ground typical of the area. Measurements were taken during two field seasons from November 1986 to July 1987 and from April to May 1988. The data which form the subject of this paper were derived from snow-free periods during May-July 1987 and April-May 1988.

Eddy correlation measurements of sensible heat used Campbell Scientific CA27 sonic anemometers interrogated by a Campbell Scientific 21X datalogger. A measurement height of one metre and a frequency of 10 Hz were used. Although the simplicity of the equipment enables rapid measurement of w' and T', robustness is compromised and the CA27 sonic anemometer cannot tolerate precipitation. Most eddy correlation data considered in this study were therefore from precipitation-free weather when the field site was supervised. However, it should also be noted that the sonic anemometers were occasionally used during light snow or rain showers without ill effect.

Vertical air temperature profiles were measured with shielded, aspirated thermopiles at two (November 1986 to May 1987) or four (all other periods) heights. Surface temperature (T_0) was measured from two arrays of fine-wire thermocouples covering an area of about 2 m^2. Periodic measurements from a hand-held infrared sensor (Barnes Instatherm) were taken to confirm the thermocouple data. Wind speed measurements were made at $z = 1.00$ m for the entire duration of the field seasons. Instrumentation problems resulted in wind speed profile being measured only during July 1987 and April to May 1988. Therefore the data base for the aerodynamic method was smaller than for the BREB method.

The data for Ohm's Law modelling were divided into two sets dependent upon whether or not wind profiles were measured. No wind profiles were measured during May to early July 1987 and therefore no stability or excess resistance corrections could be calculated for the Ohm's Law method, nor could the aerodynamic method be used. This is hereafter referred to as Period A. For the remaining data from snow-free periods, in late July 1987 and April to May 1988, wind profile measurements enabled the theoretically correct aerodynamic and Ohm's Law procedures to be followed. This is hereafter termed Period B.

RESULTS

The results of intercomparisons between flux determinations at both hourly and daily timescales are summarized in Table 8.1. It is clear from the generally d values and the error terms (MAE, MBE and RMSE) that all three methods generally showed good agreement.

For the hourly data, the best results were from the BREB method and the poorest from the Period A Ohm's Law data (which have no stability or excess resistance corrections). Based upon RMSE values, the BREB and aerodynamic methods were capable of predicting sensible heat flux densities to within approximately $50\,W\,m^{-2}$ (Figures 8.1 and 8.2) and the Ohm's Law method to within $70\,W\,m^{-2}$ (Period A) or $90\,W\,m^{-2}$ (Period B, Figure 8.3). The BREB predictions showed no large bias. The aerodynamic method tended to underestimate by $30-40\,W\,m^{-2}$ and Ohm's Law tended to overestimate by the same amount, particularly at the higher flux densities, for both Periods A and B. A marked deviation between $Q_{H(EC)}$ and $Q_{H(OL)}$ occurred at sensible heat fluxes greater than $250\,W\,m^{-2}$. This corresponds to days with the greatest Q_H fluxes, which in turn were generally synonymous with days of high atmospheric transmissivity and surface radiative heating.

The ability of each method to predict diurnal trends of sensible heat flux densities was examined. Figure 8.4 illustrates the results for two days, one with a relatively wet surface and one with a dry surface. Both days are from Period B and therefore show the higher quality Ohm's Law data. Although the two example days do not show the best agreement that was found between the different flux estimates, they are more typical of the

Table 8.1. Hourly and daily sensible heat flux densities measured with the eddy correlation method compared to predictions from the Bowen ratio–energy budget, aerodynamic and Ohm's Law methods.

Method	Data	n	$\bar{O}$	$\bar{P}$	s_O	s_P	r^2	a	b	MAE	MBE	RMSE	d
Hourly data													
$Q_{H(BR)}$	A + B	423	−170	−180	97	87	0.79	−30	0.786	37	−9	46	0.94
$Q_{H(AE)}$	B	169	−166	−131	84	70	0.80	−29	1.041	41	35	51	0.89
$Q_{H(OL)}$	A	261	−174	−219	110	142	0.89	−54	0.548	68	−45	90	0.87
$Q_{H(OL)}$	B	167	−167	−200	84	116	0.86	−49	0.590	53	−33	69	0.89
Daily data													
$Q_{H(BR)}$	A + B	27	−6.71	−7.14	1.66	1.94	0.91	0.32	1.111	0.57	−0.41	0.73	0.96
$Q_{H(AE)}$	B	12	−6.15	−4.82	1.76	1.60	0.66	−1.86	0.890	1.47	1.35	1.71	0.78
$Q_{H(OL)}$	A	17	−7.18	−8.99	1.28	2.68	0.68	−3.63	0.395	1.81	−1.62	2.26	0.60
$Q_{H(OL)}$	B	12	−6.11	−7.36	1.83	2.64	0.92	−1.22	0.665	1.19	−1.19	1.55	0.89

Means of observed ($\bar{O}$) and predicted ($\bar{P}$) flux densities, their standard deviations (s_O, s_P) coefficients of determination (r^2), constant (a) and slope (b) of regression equations are all derived from SPSSX statistical program packages for n valid cases. Measures of difference, mean absolute error (MAE), mean bias error (MBE), root mean square error (RMSE) and index of agreement (d) are derived from the methods of Willmott (1981). Units for $\bar{O}$, $\bar{P}$, s_O, s_P, a, MAE, MBE, and RMSE are $W m^{-2}$ (hourly) or $MJ m^{-2} d^{-1}$ (daily). Values for r^2, b and d are dimensionless.

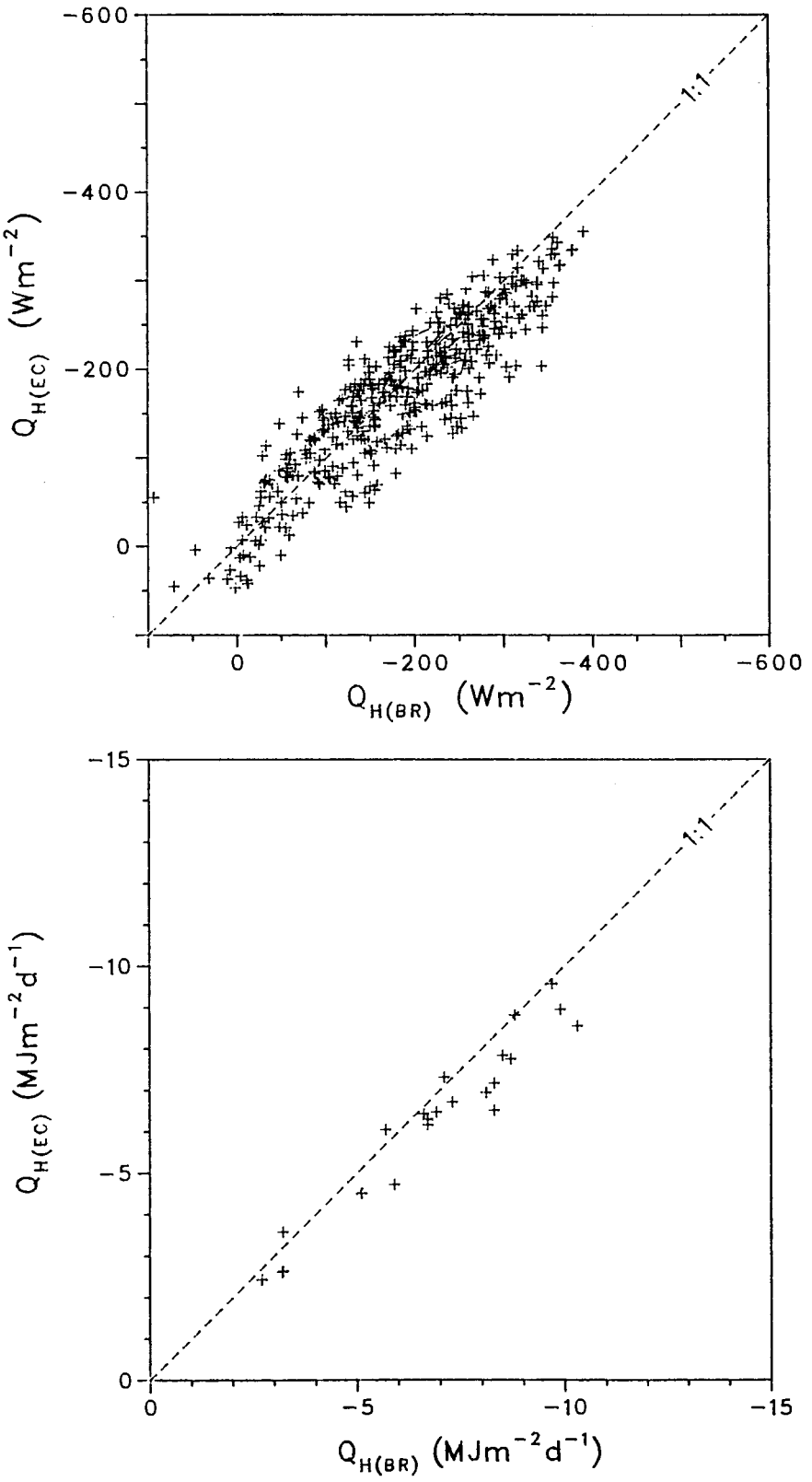

Figure 8.1. Hourly and daily $Q_{H(EC)}$ versus $Q_{H(BR)}$ for a snow-free surface, from Periods A and B combined.

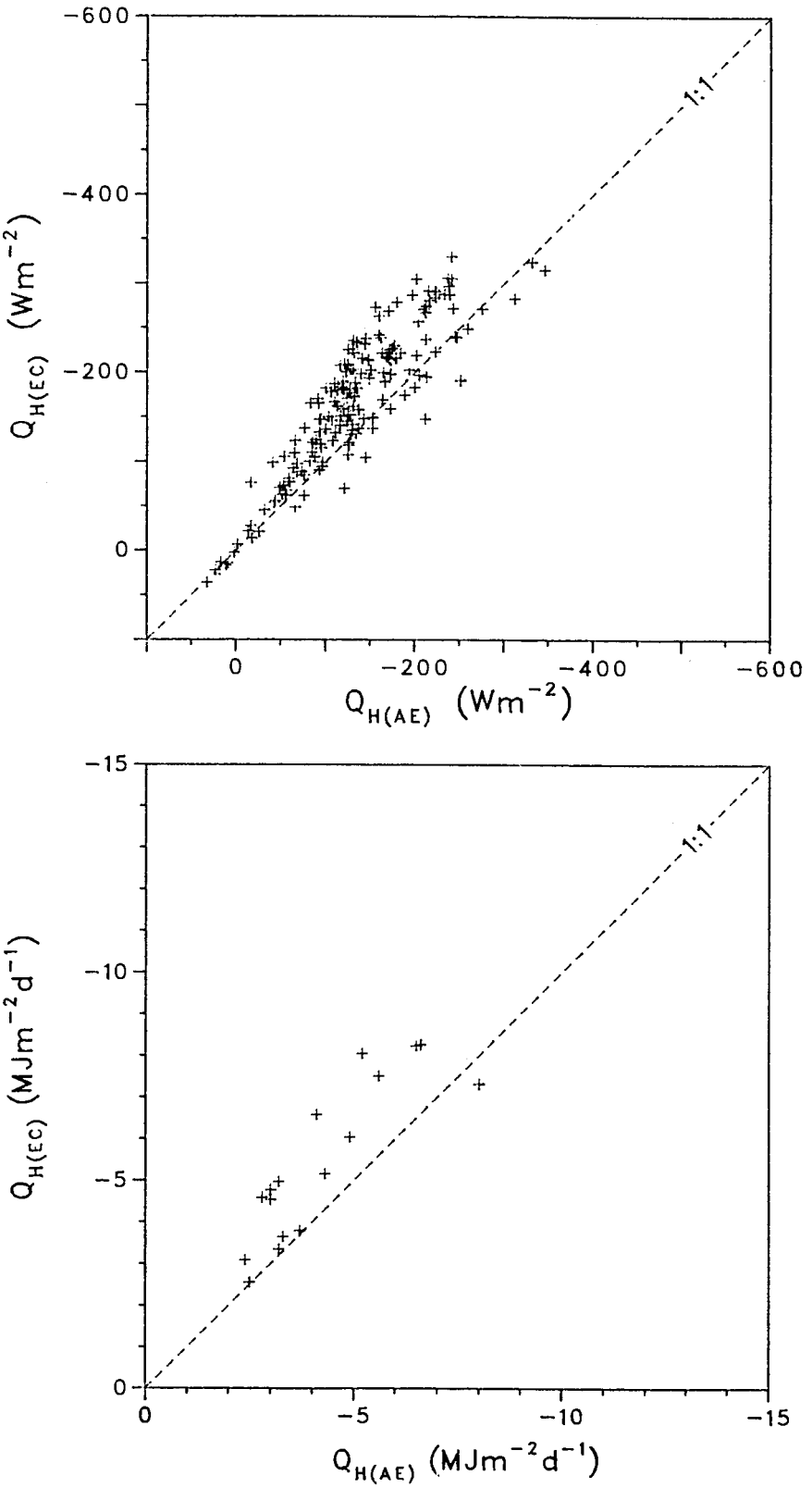

Figure 8.2. Hourly and daily $Q_{H(EC)}$ versus $Q_{H(AE)}$ for a snow-free surface, from Period B only.

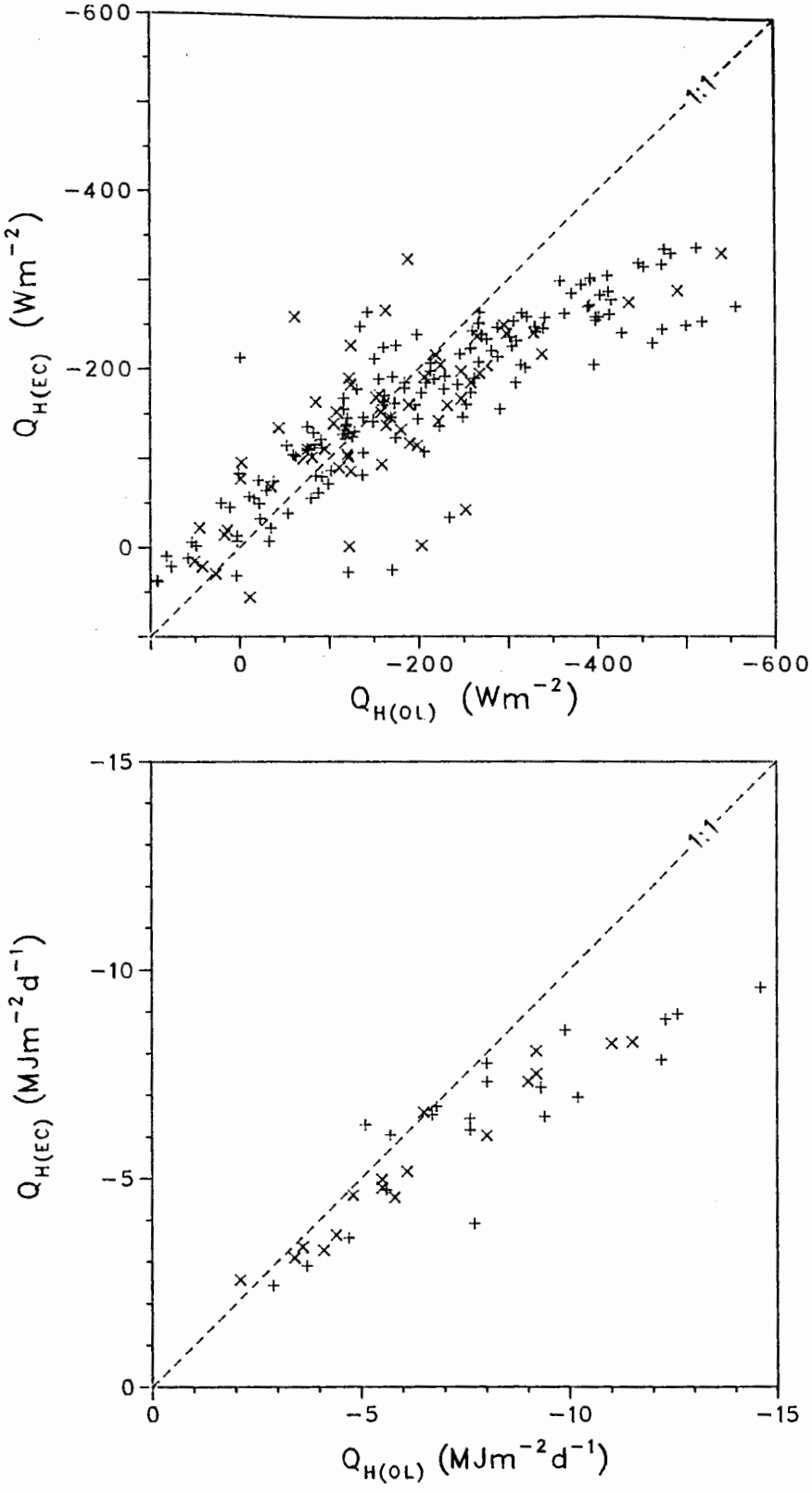

Figure 8.3. Hourly and daily $Q_{H(EC)}$ versus $Q_{H(QL)}$ for a snow-free surface, from Periods A (+) and B (x).

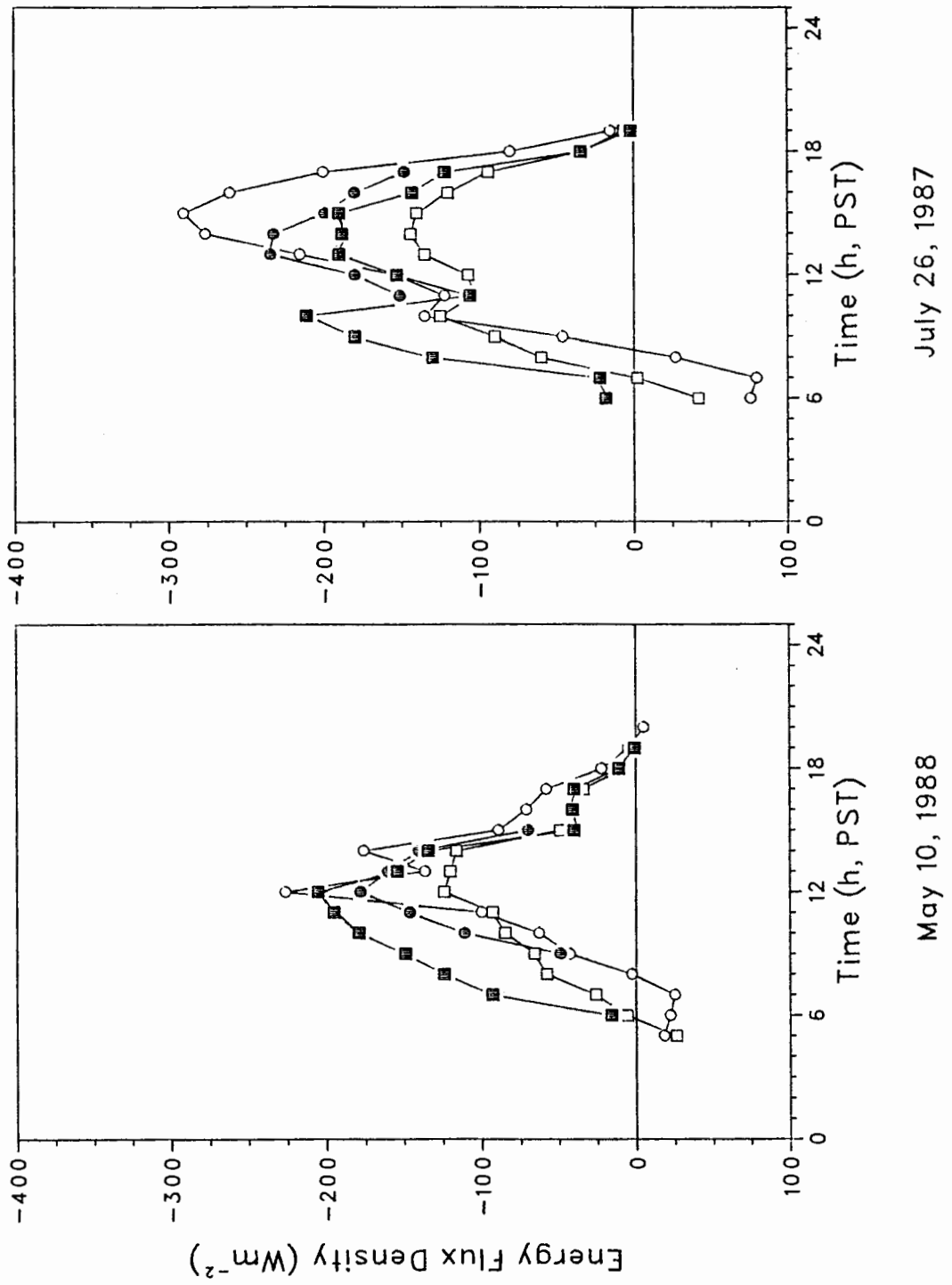

Figure 8.4. Hourly $Q_{H(EC)}$ (■), $Q_{H(BR)}$ (□), $Q_{H(AE)}$ (●) and $Q_{H(OL)}$ (o) for a day with a relatively wet surface (May 10, 1988) and a day with a dry surface (July 26, 1987).

results as a whole. The aerodynamic data tracked changes in $Q_{H(EC)}$ reasonably well, but the need for high quality temperature and wind profile measurements limited the number of hours of data collected on both of the example days. The BREB data mimicked changes in $Q_{H(OL)}$, but underestimated for most of the time. Despite using wind profile data for the determination of the aerodynamic resistances, the Ohm's Law data showed the greatest variability of all methods. The agreement between the models was better for the wet surface than for the dry, suggesting sensitivity to the greater thermal response of the dry surface. On the afternoon of the dry day (July 26, 1987), in particular, the model predictions span a range of over $150\,W\,m^{-2}$.

For daily data, similar results to those of the hourly data were obtained (Figures 8.1, 8.2 and 8.3). The indexes of agreement were about the same for the BREB and Period B Ohm's Law methods and were lower for the other two methods (Table 8.1). With respect to the mean observed flux density, the percentage errors of the RMSE's are 11% for the BREB data and 25–30% for the remaining three methods. The poorest result was that from the Period A Ohm's Law modelling. Since daily totals were derived from summed hourly data, the effects of accumulating errors was evident in this data set from the gross overestimation of Q_H at flux magnitudes greater than about $7.00\,MJ\,m^{-2}d^{-1}$.

DISCUSSION

Each of the three methods compared to eddy correlation measurements showed agreement at the smaller flux densities. At higher flux densities, the Ohm's Law data displayed a marked divergence which was worse for the Period A data than for Period B. The best results were from $Q_{H(BR)}$ and $Q_{H(AE)}$. The mean difference between the methods was about $50\,W\,m^{-2}$. This is not excessive when it is considered that errors in each method are at least 10% for $Q_{H(EC)}$ (Tanner *et al.*, 1985), typically 15–20% for $Q_{H(BR)}$ and at least the same for $Q_{H(AE)}$. At the mean flux density of the data sets (about $-170\,W\,m^{-2}$), these measurement errors account for at least half of the RMSE values in the intercomparisons.

The sensitivity of each method was indicated by the standard deviations for the data

sets (Table 8.1). The $Q_{H(EC)}$ data showed greater variability than $Q_{H(AE)}$ but less than $Q_{H(BR)}$. Given that the aerodynamic method is very sensitive to the accuracy of the temperature and wind profile measurements, this is surprising, but may be a function of the smaller data set. Visual examination of the data (Figures 8.1 and 8.2) suggests that the degree of scatter is not dissimilar. The standard deviations of $Q_{H(OL)}$ were far greater than those for $Q_{H(EC)}$, as could be expected from the poor relations between the two.

Thus, despite the potential suitability of the Ohm's Law for mountain operation, the Scout Mountain data did not wholly support it's use, as a result of the overestimation problem with the larger fluxes. A comparable study by Bowers and Bailey's between $Q_{H(EC)}$ and $Q_{H(OL)}$ did not show the same degree of disagreement as that found in this study. The source of this discrepancy may lie in systematic differences between the two experiments, such as the physical differences between the sites, the different wind profile systems employed, the measurement of surface temperatures and the differences in aerodynamic resistances.

The last two concerns are probably the more important. Bowers and Bailey (1990) defined the error in $Q_{H(OL)}$ as

$$\delta Q_{H(OL)} = \frac{\rho c_p}{r_{aH}} \delta T_0 \qquad (8.5)$$

which therefore means that errors increase directly with T_0 errors and inversely to r_{aH}. The implications for Scout Mountain are two-fold. Firstly, for a given set of wind speed and stability conditions, r_{aH} at Scout Mountain was approximately half that at Bowers and Bailey's site due to its greater roughness. The mean z_0 at Scout Mountain was 0.024 m, compared to 0.0021 m at Plateau Mountain. The effect of this increase in z_0 was a doubling in $\delta Q_{H(OL)}$ at Scout Mountain.

Secondly, errors in T_0 directly affect $\delta Q_{H(OL)}$. The poor performance of the Ohm's Law model at higher flux densities suggests that errors in the measured temperature difference $T - T_0$ are greater under conditions of strong radiative heating. Since air temperature is a conservative quantity compared to T_0, most of the errors in $Q_{H(OL)}$ can be expected to originate from inaccurate measurement of T_0. The errors would be greatest at larger sensible heat flux densities because of the associated radiative heating at the surface.

With the low values of r_{aH} typical of a windswept tundra, errors of as little as 1°C in T_0 could result in $Q_{H(OL)}$ errors of 50 – 100 W m^{-2}. Although the good relations between measured T_0 and measured $L\uparrow$ found at Scout Mountain (Chapter V) suggest that the surface thermocouple arrays are not unreliable, it is unlikely that they are capable of T_0 measurements with errors of less than ± 1°C. Furthermore, a plot of the residuals between $Q_{H(EC)}$ and $Q_{H(OL)}$ did not show that the T, T_0 or r_{aH} measurements were individually responsible.

CHAPTER IX

LATENT HEAT FLUX DETERMINATIONS IN AN ALPINE TUNDRA, SCOUT MOUNTAIN, SOUTHERN BRITISH COLUMBIA, CANADA

INTRODUCTION

The determination of latent heat flux density, and thereby the evaporation rate, is of critical importance for climatological, hydrological, agricultural and other applications, and it forms a major research objective for boundary layer meteorology. Physically-based latent heat flux modelling approaches explicitly recognize atmospheric and surface controls, but their application to alpine (above treeline) environments has been very limited. The wide range of surface energy budget regimes which characterize the alpine tundra environment dictate that empirical approaches are of limited value. This study compared two physically-based approaches to latent heat determination for an alpine tundra in British Columbia, Canada.

Previous evaporation modelling in alpine tundra environments is limited to the lysimeter-based studies of LeDrew (1975) and Isard and Belding (1989), and the Priestley-Taylor and combination model approaches to evaporation description presented by Bowers and Bailey (1989). Other studies have described energy budgets from alpine tundra sites, but have not included detailed modelling results or evaluations of surface responses or controls.

THEORETICAL BACKGROUND

Latent heat flux densities were computed from the Bowen ratio-energy budget (BREB) method, the aerodynamic equation, as a residual in the energy budget equation and from the Priestley-Taylor model. The last approach was confined to daily totals only. The aerodynamic and residual data were hourly, summed to give daily totals. The convention adopted hereafter is that energy fluxes directed away from the surface are considered negative.

A more detailed derivation of the BREB and aerodynamic methods was considered in Chapter III and will not be repeated here. Assuming all fluxes are positive when directed towards the surface, and *vice versa*, the energy budget may be defined as

$$Q^* + Q_G + Q_H + Q_E = 0 \qquad (9.1)$$

where the flux densities are those of net radiation (Q^*), ground heat (Q_G), sensible heat (Q_H) and latent heat (Q_E). When rearranged, Equation (9.1) becomes the Bowen ratio–energy budget (BREB) method of latent heat determination

$$Q_{E(BR)} = - \frac{Q^* + Q_G}{1+\beta} \qquad (9.2)$$

From mass transfer equations, Thom (1975) derives the aerodynamic equation for latent heat flux density as

$$Q_{E(AE)} = \frac{\rho c_p}{\gamma} k^2 \frac{\partial e}{\partial(\ln z)} \frac{\partial u}{\partial(\ln z)} (\Phi_M \Phi_V)^{-1} \qquad (9.3)$$

where ρ is the density of air, c_p is the specific heat of air at constant pressure, γ is the psychrometric coefficient, e is vapour pressure, u is wind speed and $(\Phi_M \Phi_V)^{-1}$ is a stability correction derived from the Richardson number.

Once rearranged to isolate Q_E, Equation (9.1) was used to determine the latent heat flux density as a residual

$$Q_{E(RE1)} = Q^* + Q_G + Q_{H(EC)} \qquad (9.4)$$

and

$$Q_{E(RE2)} = Q^* + Q_G + Q_{H(OL)} \qquad (9.5)$$

where $Q_{H(EC)}$ is the sensible heat flux measured by the eddy correlation method, and $Q_{H(OL)}$ is the sensible heat determined from the Ohm's Law approach. The former is defined as

$$Q_{H(EC)} = \rho c_p \overline{(w' T')} \qquad (9.6)$$

where $\overline{(w' T')}$ is the time-averaged product of the instantaneous deviations of vertical wind speed (w) and air temperature (T).

The Ohm's Law approach of modelling surface heat fluxes states that

$$Q_{H(OL)} = \rho c_p \frac{(T-T_0)}{r_{aH}} \qquad (9.7)$$

where T_0 is surface temperature and r_{aH} is the aerodynamic resistance to heat transfer. The latter should ideally be measured from wind profiles, as it is a function of roughness length, a stability function and friction velocity (see Chapter VIII). This was the case for only part of the study period. For the times when wind profiles were not measured, r_{aH} was calculated without corrections for stability or bluff-body resistance. These are termed Period A data. Period B data are from times when r_{aH} was calculated from wind profiles, and include late July 1987 and all 1988 data.

The Penman-Monteith combination model was defined in Chapter VII as

$$Q_E = \frac{S(Q^*+Q_G)+\rho c_p(e^*-e)/r_a}{S+\gamma+\gamma r_s/r_a} \qquad (9.8)$$

where S is the slope of the saturation vapour pressure curve, e^* is saturation vapour pressure at T_z, e is actual vapour pressure, r_s is surface resistance and r_a is aerodynamic resistance. Equation (9.8) simplifies under conditions when $e \rightarrow e^*$ or when $r_s \rightarrow 0$. Such might be the case in a saturated atmosphere (Tanner and Fuchs, 1968) or when surface moisture is non-limiting. Regardless, the simplification leads to (Slatyer and McIlroy, 1961)

$$Q_{E(EQ)} = \frac{S}{S+\gamma}(Q^*+Q_G) \qquad (9.9)$$

where $Q_{E(EQ)}$ is the latent heat flux density equivalent to equilibrium evaporation. This was considered by Slatyer and McIlroy as the evaporation rate which occurs when the surface and overlying air are in equilibrium. Under these conditions, the vapour pressure deficit in the boundary layer does not change with height. Wilson and Rouse (1972) defined equilibrium evaporation from a corn crop as occurring when $Q_E/(Q^*+Q_G)$ was in the range 0.6 to 0.8, corresponding to surface conditions which were moderately dry. For very wet and very dry surfaces, $Q_{E(EQ)}$ under- and overestimates the actual evaporative flux.

For a variety of horizontally uniform saturated surfaces in the absence of advection, Priestley and Taylor (1972) found that the evaporative flux (i.e. potential evaporation) was given by

$$Q_E = \alpha_{PT}\ Q_{E(EQ)} \qquad (9.10)$$

where the mean value of the proportionality factor α_{PT} was about 1.26. Many experiments for a wide range of surface types have since shown that maximum values of α_{PT} tend to converge at 1.26 when water is non-limiting. For dessicated surfaces, $\alpha_{PT} \rightarrow 0$, and if α_{PT} could be determined from some easily measured parameter, then Equation (9.10) becomes a very useful, yet very simple, evaporation model. Many studies have related α_{PT} to soil moisture availability. Canadian work from a wide range of surfaces was reviewed by Valentine and Bailey (1990), but these did not include alpine environments, for which few results as yet exist.

EXPERIMENTAL PROCEDURE

Data were collected at an alpine tundra site (described in Chapter I) at an elevation of 2350 m amsl on Scout Mountain, in the eastern Cascade Mountains of southern British Columbia during two field seasons from November 1986 to July 1987 and April to May 1988. The data set used in this paper was derived from snow-free periods during May to July 1987, and April to May 1988. The site was a grass-sedge tundra developed on the patterned ground (stone polygons) typical of the area. All measurements were hourly. Daytime totals of energy fluxes were calculated from the hourly data. Due to instrument problems with wind profiles and limitations in the number of $Q_{H(EC)}$ measurements, relatively few full days of simultaneous measurements of $Q_{E(BR)}$ and $Q_{E(AE)}$ or $Q_{E(REl)}$ were obtained. The daily data used in the analyses therefore include days with eight or more consecutive hours of daytime measurements.

Measurements of dry- and wet-bulb temperatures were derived from shielded, aspirated thermopiles, and used to determine vapour pressures. Problems in measuring the small vertical temperature and vapour pressure gradients at night lead to large errors in flux determination and the rejection of night-time data. All data in this study therefore refer to daytime. Net radiation was measured with a Middleton CN-1 net pyrradiometer. Ground heat flux was measured with an array of five flux transducers (Thorthwaite), corrected for flux divergence in the surface soil layer. Wind speed at $z = 1$ m was measured with a Met One cup anemometer throughout the experiment. Due to instrument problems, vertical wind profiles

were measured only during July 1987 and April to May 1988 (defined above as Period B). Climet sensitive cup anemometers were used in wind profile measurement.

Eddy correlation sensible heat was measured with a Campbell Scientific CA27 sonic anemometer mounted at one metre and interrogated by a Campbell Scientific 21X datalogger. Since this sonic anemometer includes a fragile fine-wire thermocouple and acoustic heads, it could only be used when the field site was supervised and when no precipitation was falling. Surface temperature measurements used in the Ohm's Law method were derived from thermocouple arrays affixed to the tundra surface.

Precipitation was measured with three tipping-bucket raingauges (one Sierra-Misco RG2501 and two Weathermeasure P501). Soil moisture content in the uppermost 50 mm of soil was determined gravimetrically from ten samples. In May 1987 the sampling interval was up to ten days in length, but for most of the snow-free period was two to five days.

RESULTS

The results of intercomparisons of hourly and daily $Q_{E(BR)}$, $Q_{E(AE)}$, $Q_{E(RE1)}$ and $Q_{E(RE2)}$ are summarized in Table 9.1. Both the hourly and the daily data showed relatively good agreement between $Q_{E(BR)}$ and $Q_{E(AE)}$ or $Q_{E(RE1)}$ but relatively poor agreement between $Q_{E(BR)}$ and $Q_{E(RE2)}$.

For both the hourly and the daily data, the best modelling results were those of $Q_{E(BR)}$ and $Q_{E(RE1)}$ (Figures 9.1 and 9.2), with high indexes of agreement and the smallest errors (MAE, MBE and RMSE). The RMSE values indicated that either model could predict hourly latent flux densities to ± 45 W m^{-2}. The $Q_{E(AE)}$ method underestimated, and the $Q_{E(RE1)}$ method overestimated, although the biases were not large in comparison to the mean flux densities.

The results of using Ohm's Law in the residual method gave poorer results than those when using eddy correlation, as could be expected from the results of sensible heat flux modelling in Chapter VIII (Figures 9.3 and 9.4). For Period A data (no wind profile measurements), $Q_{E(RE2)}$ was practically useless as a predictor of hourly or daily evaporation. Results were better for Period B, however, and $Q_{E(RE2)}$ gave moderate indexes of

Table 9.1. Comparisons between hourly and daily latent heat measured by the BREB method ($Q_{E(BR)}$), the aerodynamic equation ($Q_{E(AE)}$) and as a residual in the energy budget equation, using eddy correlation ($Q_{E(RE1)}$) and Ohm's Law ($Q_{E(RE2)}$) to measure sensible heat.

Observed Flux	Predicted Flux	n	$\bar{O}$	$\bar{P}$	s_o	s_p	r^2	a	b	MAE	MBE	RMSE	d
Hourly Data													
$Q_{E(BR)}$	$Q_{E(AE)}$	239	−141	−126	73	63	0.64	−24	0.929	35	15	46	0.88
$Q_{E(BR)}$	$Q_{E(RE1)}$	430	−146	−155	63	81	0.71	−46	0.650	36	−9	45	0.90
$Q_{E(BR)}$	$Q_{E(RE2)}^{A}$	800	−132	−95	87	103	0.22	−21	0.562	82	37	105	0.66
$Q_{E(BR)}$	$Q_{E(RE2)}^{B}$	394	−146	−122	96	102	0.51	−3	0.812	65	24	81	0.83
Dally Data													
$Q_{E(BR)}$	$Q_{E(AE)}$	19	−5.64	−5.07	1.72	1.46	0.65	−0.85	0.944	0.99	0.57	1.19	0.86
$Q_{E(BR)}$	$Q_{E(RE1)}$	27	−5.65	−6.10	1.58	1.57	0.83	−0.04	0.918	0.63	−0.44	0.78	0.94
$Q_{E(BR)}$	$Q_{E(RE2)}^{A}$	61	−6.09	−4.47	2.47	2.39	0.22	−1.69	0.456	2.22	1.59	2.95	0.64
$Q_{E(BR)}$	$Q_{E(RE2)}^{B}$	32	−6.36	−5.35	2.45	2.43	0.63	−0.34	0.789	1.48	0.95	1.80	0.86

Means of observed ($\bar{O}$) and predicted ($\bar{P}$) samples, their standard deviations (s_O, s_p), coefficients of determination (r^2), constant (a) and slope (b) of regression equations are all derived from SPSSX statistical program packages for n valid cases. Measures of difference mean absolute error (MAE), mean bias error (MBE), root mean square error (RMSE) and index of agreement (d) were derived from the methods Willmott (1981). Units are dimensionless for b, r^2, and d, otherwise are $W m^{-2}$ (hourly data) and $MJ m^{-2} d^{-1}$ (daily data). The A and B notations for $Q_{E(RE2)}$ refer to Period A and Period B data respectively.

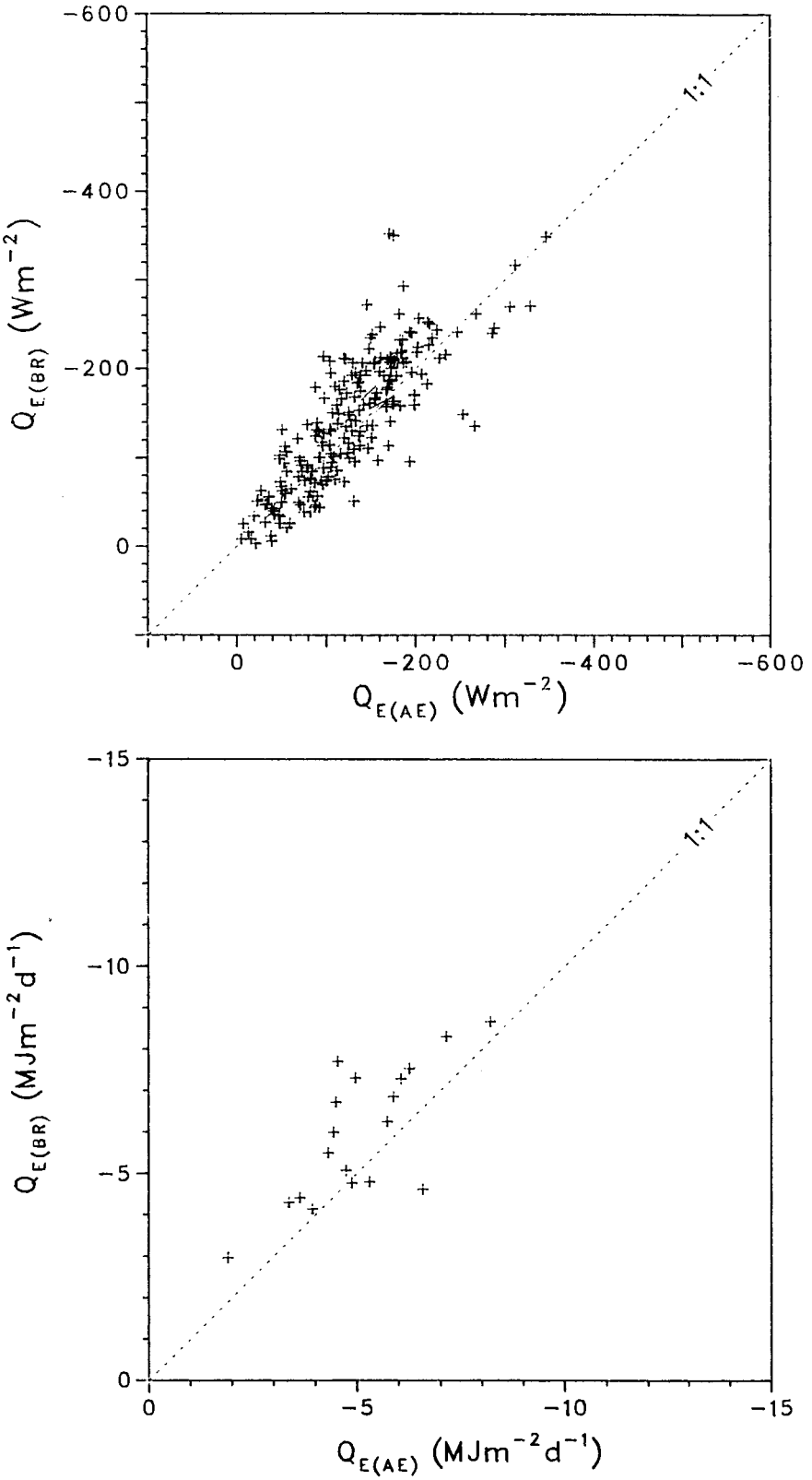

Figure 9.1. Hourly and daily $Q_{E(BR)}$ versus $Q_{E(AE)}$ for a snow-free surface, from Period B.

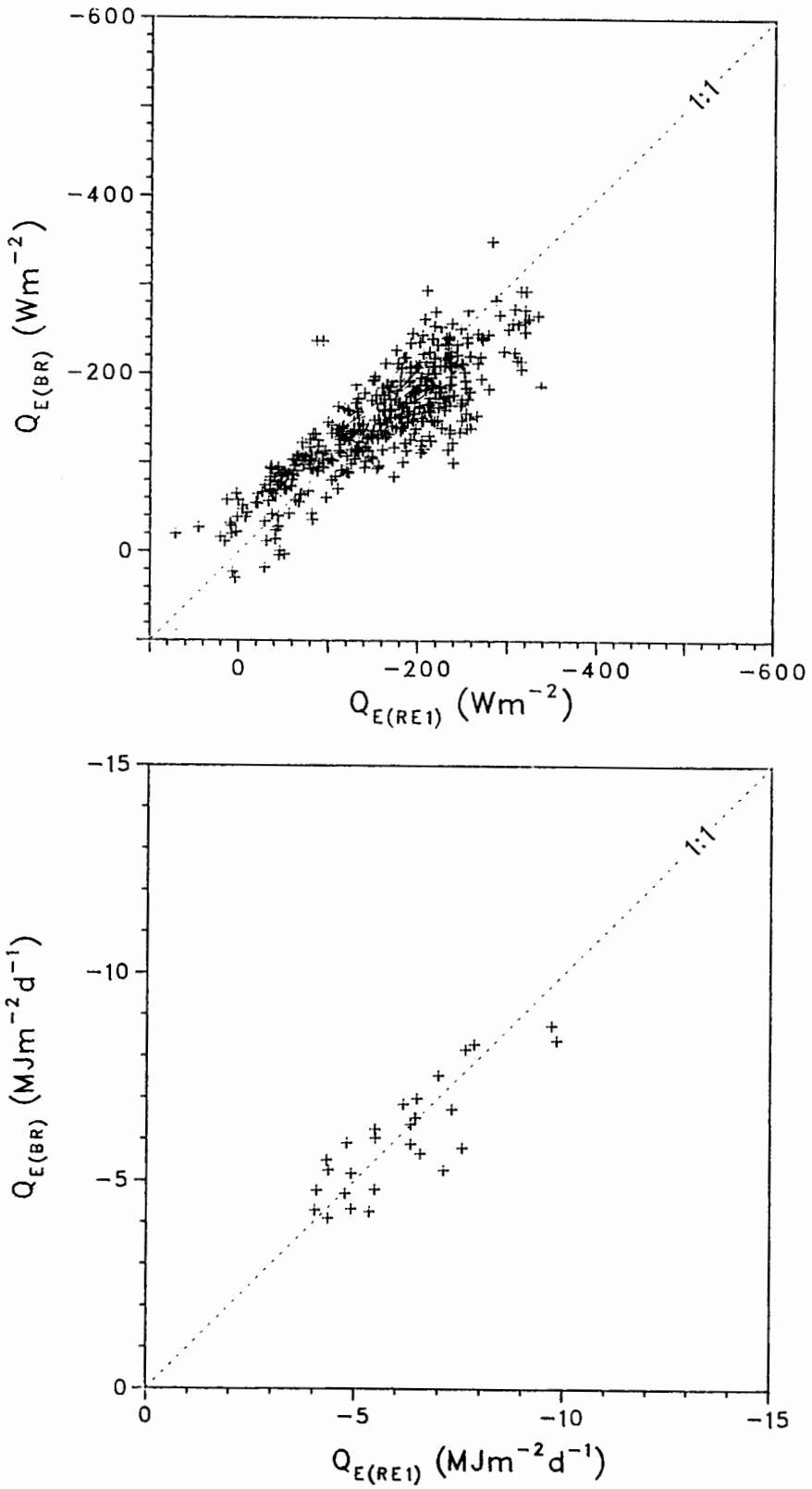

Figure 9.2. Hourly and daily $Q_{E(BR)}$ versus $Q_{E(RE1)}$ for a snow-free surface, from Periods A and B.

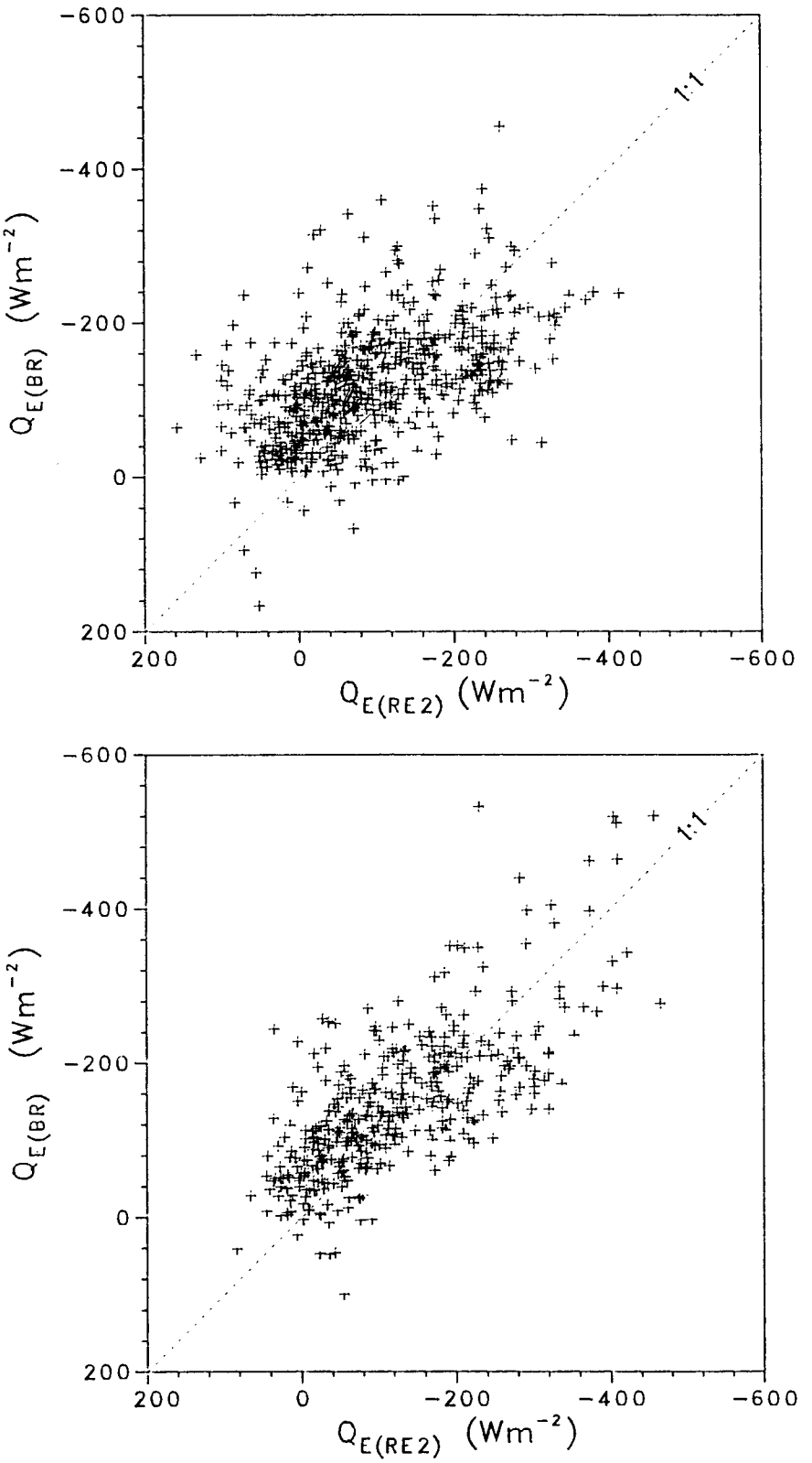

Figure 9.3. Hourly $Q_{E(BR)}$ versus $Q_{E(RE2)}$ for a snow-free surface, from Periods A (upper) and B (lower).

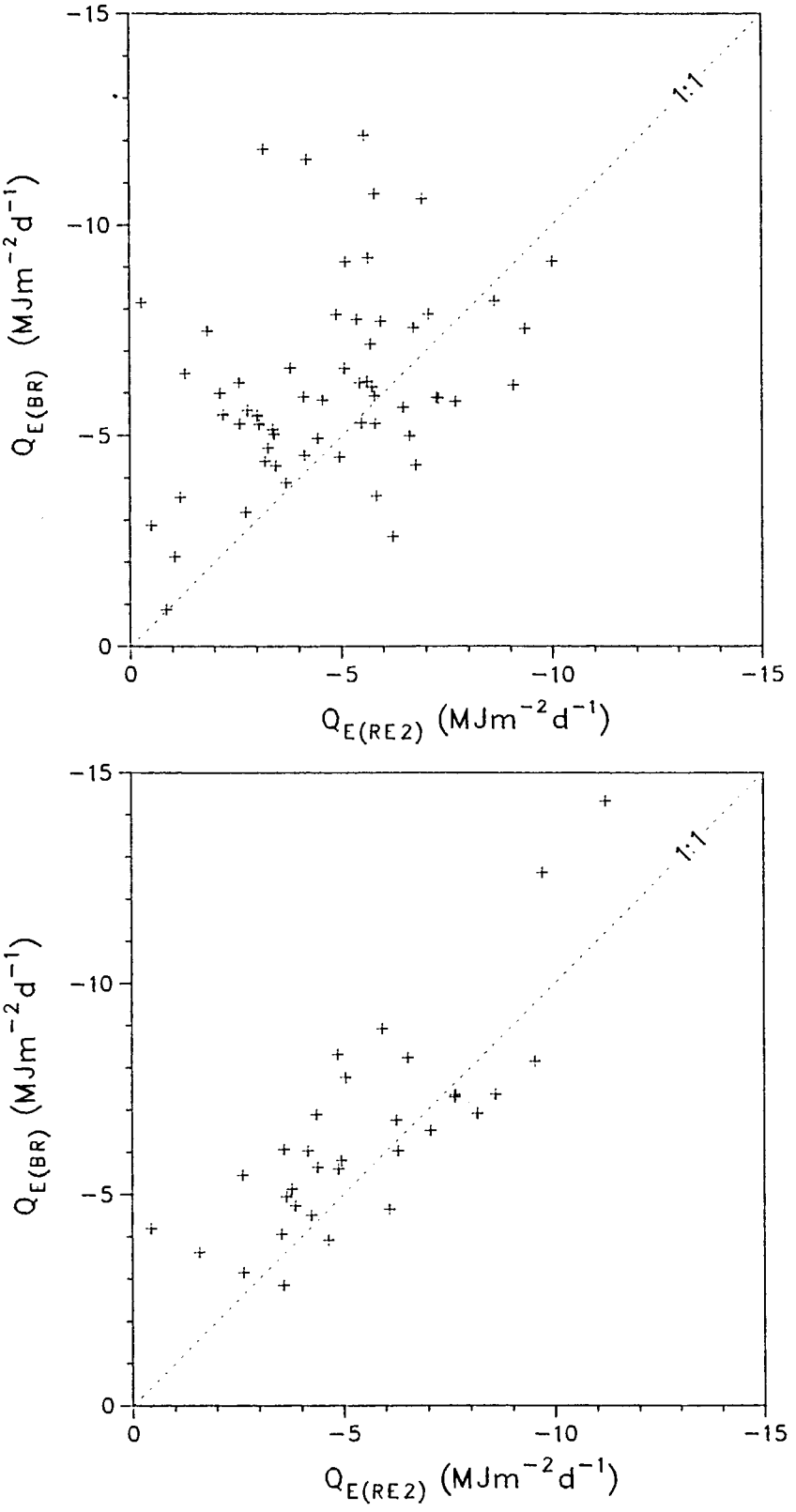

Figure 9.4. Daily $Q_{E(BR)}$ versus $Q_{E(RE2)}$ for a snow-free surface, from Periods A (upper) and B (lower).

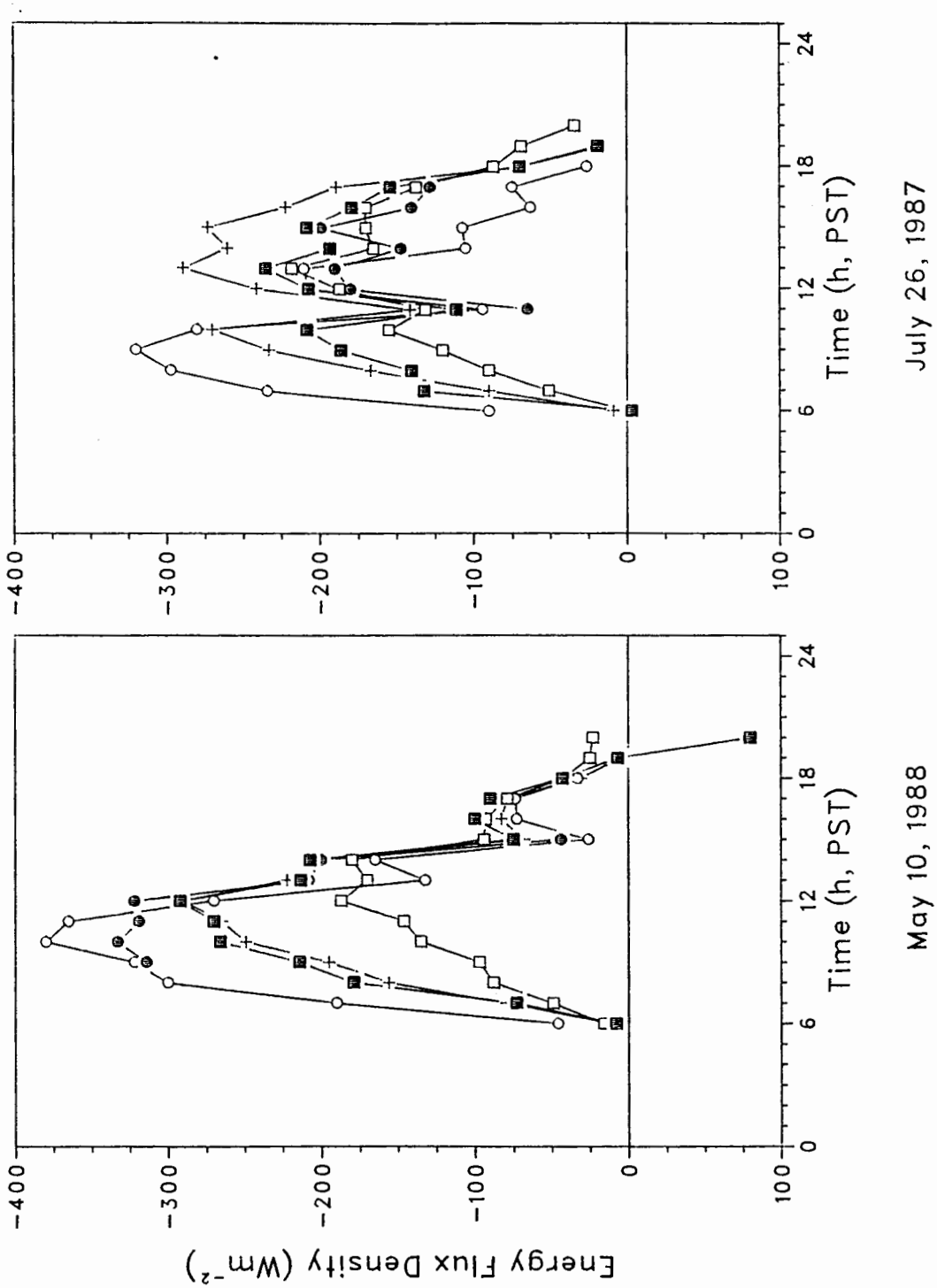

Figure 9.5. Hourly daytime $Q_{E(BR)}$ (■), $Q_{E(AE)}$ (¤), $Q_{E(RE1)}$ (o), $Q_{E(RE2)}$ (o) and $Q_{E(EQ)}$ (+) for a relatively wet surface (May 10, 1988) and a dry surface (July 26, 1987).

agreement and error terms closer to those of $Q_{E(AE)}$ and $Q_{E(RE1)}$.

The diurnal behaviour of $Q_{E(BR)}$, $Q_{E(AE)}$, $Q_{E(RE1)}$ and $Q_{E(RE2)}$ was examined for two days, one with a relatively wet surface and one with a dry surface (Figure 9.5). The equilibrium latent heat flux density ($Q_{E(EQ)}$, Equation 9.9) is also plotted for comparison. The wet day showed close agreement between $Q_{E(BR)}$ and $Q_{E(EQ)}$ but $Q_{E(EQ)}$ was much greater than $Q_{E(BR)}$ on the dry day. In fact, $Q_{E(EQ)}$ was the closest predictor of $Q_{E(BR)}$ on the wet day, for which the range of modelled latent heat flux densities was extreme in the morning. The morning of the wet day was nearly cloudless, but the skies became overcast in the afternoon. The great disagreement between the models indicated a greater sensitivity towards surface energy levels. The best agreement between the modelled and measured fluxes also occurred during the short overcast period at about 1100 h on the dry day. For both days, $Q_{E(AE)}$ seriously underestimated $Q_{E(BR)}$ in the morning, whereas $Q_{E(RE2)}$ overestimated. The performance of $Q_{E(RE1)}$ in tracking hourly $Q_{E(BR)}$ was superior to that of $Q_{E(AE)}$.

Equilibrium and Priestley-Taylor Models

Typically, the Priestley-Taylor α_{PT} values have been related to soil moisture availability in experimental studies. At Scout Mountain, no defined relation was found between α_{PT} and the volumetric soil moisture (χ_W) (Figure 9.5). However, the inclusion of Bowers' (1988) data from a dry alpine tundra at Plateau Mountain, Alberta, changed this interpretation somewhat. Taken as a whole, the data showed a general positive trend which encompasses very dry tundra (Plateau Mountain) and wetter tundra (Scout Mountain). The upper limits of the trend were not well defined, and suggest that research be focussed on very wet alpine tundras to confirm or refute the commonly accepted limiting value of $\alpha_{PT}=1.26$.

Some stratification was found in the Scout Mountain data by using daily precipitation totals as a surrogate variable. When daytime totals of actual and equilibrium evaporation were plotted, stratified by precipitation totals from the same daytime period (or the previous night), the data divided into subsets of wet and dry surfaces (Figure 9.6). For days with rainfall, α_{PT} ranges from about 0.75 to 1.30. The points are scattered for rainfall totals of 1 or 2 mm, but for days with ≥3 mm of rainfall a strong linear relation developed between $Q_{E(BR)}$ and $Q_{E(EQ)}$. The mean α_{PT} for these days was 1.08. Dry day α_{PT} values are

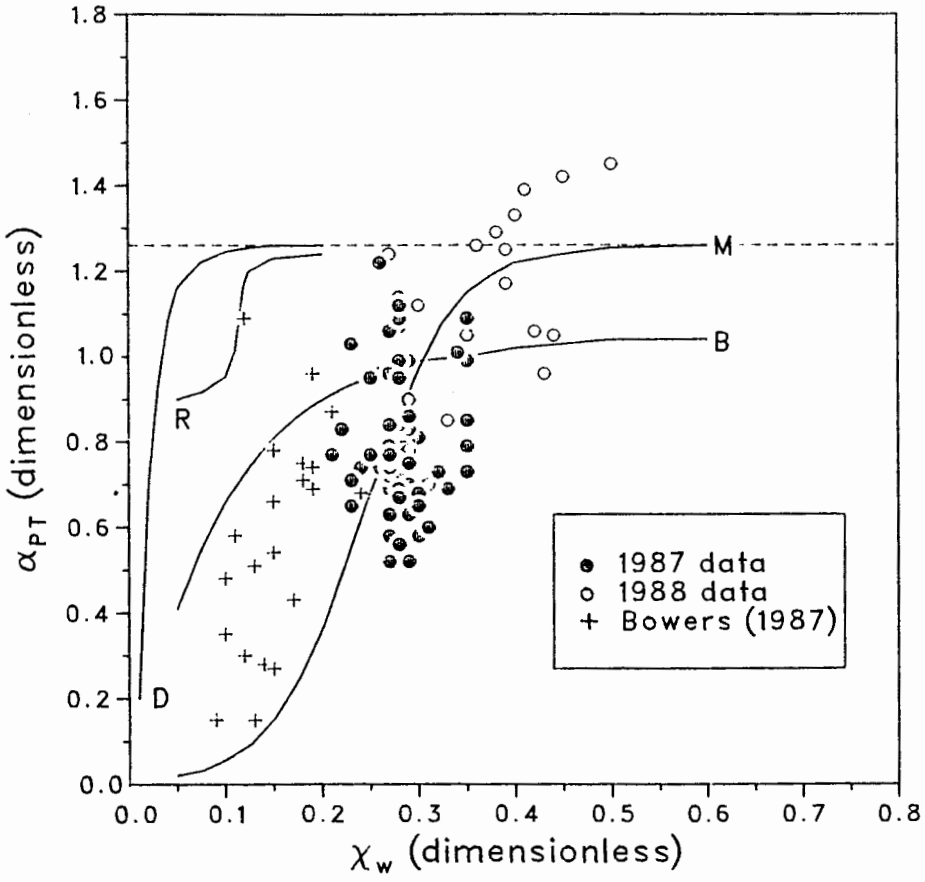

Figure 9.6. Daily α_{PT} versus χ_W for Scout Mountain, British Columbia, and Plateau Mountain, Alberta, with comparative curves from an Arctic tundra (M: Marsh *et al.*, 1981), an agricultural crop (D: Davies and Allen, 1973) and a dry grass plain (B: Barton, 1979).

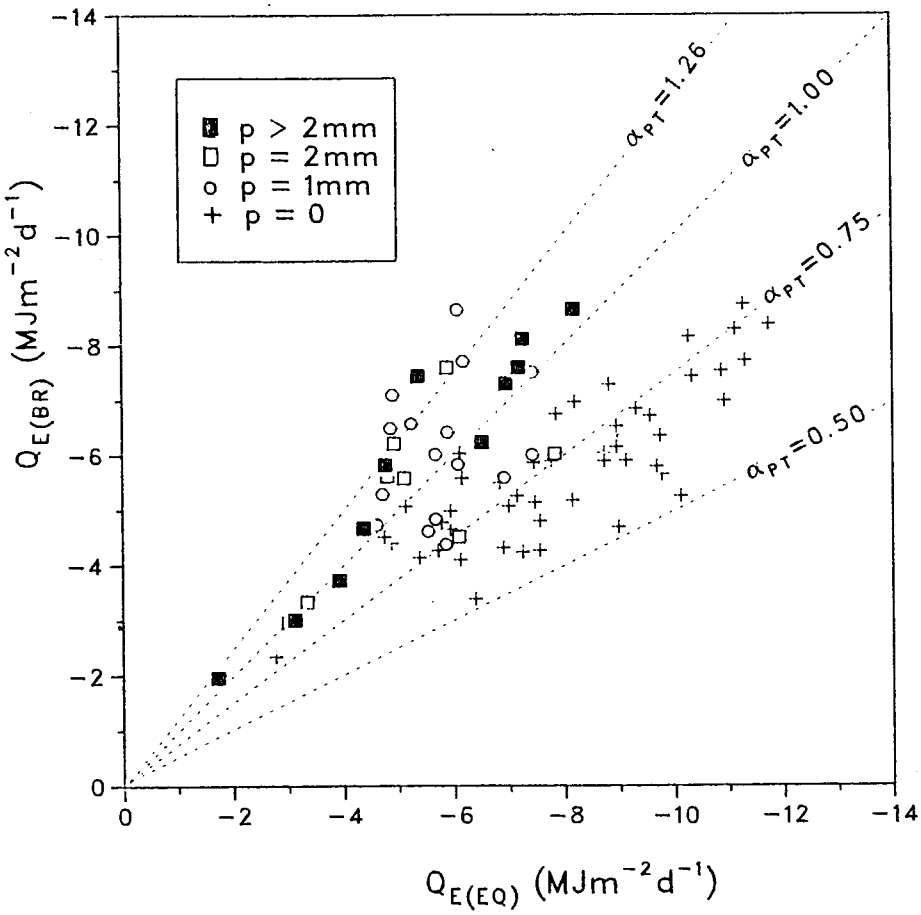

Figure 9.7. Daily $Q_{E(BR)}$ versus $Q_{E(EQ)}$ stratified by daily rainfall totals. Dashed lines show different values of α_{PT}.

exclusively less than 1.00, and the majority are between 0.50 and 0.80 with a mean of 0.73.

DISCUSSION

An important result from the model intercomparisons was the demonstration of the feasibility of determining evaporation without the need to maintain either lysimeters or measure wet-bulb temperatures, as shown by the $Q_{E(RE1)}$ results. The good performance of $Q_{E(RE1)}$ was undoubtedly due to the excellence of sensible heat measurements. If sensible heat flux densities could be determined reliably using methods which are not as sensitive as the sonic anemometer employed here, then a useful operational means of estimating evaporation results.

The use of the residual method without the eddy correlation measurements resulted in poorer results, especially for the data without wind profile measurements (Period A). Bowers (1987) also attempted to use Ohm's Law estimates of Q_H and obtained results similar to the Period B data of the present study.

The aerodynamic and residual methods used in this experiment gave evaporation measurements with accuracies which compare favourably to those from the lysimeters used in alpine tundra studies by LeDrew and Emerick (1974) and Isard and Belding (1989). The accuracy of the former's lysimeter was about ± 5.8 mm water equivalent. The accuracy of the lysimeter measurements of Isard and Belding was not specified. Based upon RMSE's the $Q_{E(AE)}$ or $Q_{E(RE1)}$ methods gave errors which were less than ± 0.50 mm d^{-1}. The daily RMSE of $Q_{E(RE2)}$ corresponded to an accuracy of 0.73 mm d^{-1}. Physically-based methods have the further advantages that they can be used with accuracy for short time scales, do not physically disturb the surface and avoid the potential errors associated with lysimeter placement.

Problems in applying the Priestley-Taylor model to the alpine tundra at Scout Mountain stemmed from difficulties in the specification of surface moisture availability. The soil moisture samples were derived exclusively from the vegetated cores of the stone polygons which characterized the microrelief of the site (Figures 1.2 and 1.3). The bare rocks of the polygons themselves retain no water, except during and immediately following

precipitation. Therefore, the χ_W measurements in Figure 9.5 overestimate the actual moisture reservoir.

Evaporation rates at Scout Mountain were high only following significant precipitation or snowmelt events. At these times, there were obvious physical sources of water which were absent during dry conditions. These sources included wet rocks, wet non-transpiring plant matter (e.g. lichens), standing water in rock hollows and in the stone-stripe hollows immediately following snowmelt when the frozen substrate restricted drainage. At all other times, these sources of water were absent, and evaporation must therefore have been derived from the vegetated soil parts of the tundra, which were primarily located in the cores of stone polygons, and the subsurface sources available. The tundra evaporation is therefore strongly controlled by snowmelt or rainfall inputs, which wet the surface. Even a light rain shower can stimulate evaporation, yet leave soil moisture contents unchanged. Similar scenarios also occur in subarctic tundras (Rouse, 1982; Wright, 1982).

It is of value to compare the Scout Mountain data with other surfaces. Figure 9.6 includes the results from an Arctic tundra, an agricultural crop and a dry grass plain. Of all these surfaces, the closest physical analogy to Scout Mountain is the barren arctic tundra studied by Marsh *et al.* (1977). The relation between their curve and the Scout Mountain data reflects this. In contrast to the crop surface, the tundra surface evaporation becomes moisture limiting even at moderate soil moisture contents, Thus a majority of data occur below the potential evaporation condition represented by $\alpha_{PT} = 1.26$. The lack of effective means of transferring subsurface moisture to the atmosphere is apparent. Contributing factors are the coarseness of the soils, which allow rapid drainage and minimize capilliary suction, and the poorly developed root systems of alpine plants.

The crop (ryegrass) surface (Davies and Allen, 1973) shows an evaporation regime which is maintained even at very low surface soil moisture contents. This is possible as a result of the potential to draw upon deeper moisture reservoirs through deep root systems, and the improved water retention of finer soils. The better developed soils of Davies and Allen's site would also promote upwards water transfer by capilliary action. The dry grass plains studied by Barton (1979) show similar response to Scout Mountain, but have a lower limiting value of α_{PT} (1.04). The use of α_{PT} values of approximately 1.00 has been found

to be of general utility in other well drained surfaces, such as subarctic tundra (Rouse and Stewart, 1972; Stewart and Rouse, 1976). Wetter tundra surfaces are well represented by $\alpha_{PT} = 1.26$ (Stewart and Rouse, 1976; Wright, 1981). More recent work, however, has shown the dependence of α_{PT} on regional airflow to be important (Rouse *et al.*, 1987).

The general trend in Figure 9.5 neither supports nor rejects the validity of $\alpha_{PT} = 1.26$ representing potential evaporation conditions in alpine tundra, but does show that surface moisture changes play a role in controlling Q_E. As such, this is at variance with Arctic tundra data, for which single values of α_{PT} have been used successfully in evaporation modelling (Rouse *et al.*, 1977). Further investigations from wetter alpine tundras, such as those found in the coastal mountains of British Columbia, would be of value in defining the behaviour of α_{PT} in mountain environments and would answer the call for further research in the behaviour of α_{PT} in Canada (Valentine and Bailey, 1990).

CHAPTER X

EPILOGUE

CONCLUSIONS FROM THE PRESENT STUDY

The present study aimed to provide descriptions and modelling results of all radiation and energy budget parameters for an alpine tundra. A total of more than twelve months of data were collected from which these aims were satisfied. The duration of the Scout Mountain data collection exceeds most experimental radiation and energy budget studies. Additionally, much of the Scout Mountain data was of higher quality than many previous studies. All components of radiation and energy budgets were measured over a total of twelve months. Given the paucity of alpine climatology research, the range of atmospheric and surface conditions encompassed represents a potentially important addition to the present state of knowledge. Noteworthy contributions from the present study included descriptions of radiation and energy transfers with broader scope than many previous studies, and modelling of hourly and daily radiation and energy flux densities using physically-based and empirical means.

Radiation Budget

The potential for very high solar radiation flux densities and topographically induced weather changes combined to produced highly variable radiation budgets at all timescales. A strong seasonal control was exerted by the presence or absence of a snow cover. Winter solar and longwave radiation transfers were of small magnitude but quickly increased with the disappearance of the snowpack. Embedded within the seasonal regime was a very variable daily radiation budget. Day to day changes in transmissivity and albedo induced many fluctuations in the radiation budget. This variability appears to characterise alpine tundra (LeDrew and Weller, 1978) and demonstrates the importance of local-scale terrain effects on mountain climates.

Radiation flux modelling focussed on the longwave and net radiation components, both of which have seen minimal attention in the alpine tundra zone. Longwave radiation in particular is in need of attention, given the inconclusive results of previous alpine research.

Hourly longwave radiation modelling at Scout Mountain used equations based upon the Stefan-Boltzmann Law for determination of all three longwave radiation fluxes. The simple approach of using an effective atmospheric emissivity of 0.75 with screen temperature worked as well as any other model.

For terrestrial longwave radiation, a surface emissivity of 0.95 appeared to be the best estimate for use with surface temperature although the errors in ignoring emissivity were negligible. Screen level temperature could also be used if the daytime divergence with the surface temperature can be accounted for, and this was achieved in this study by using 10% of $K\downarrow$. Not only are the data requirements for these approaches simple, but the foundation equation is physically sound.

The results for net radiation modelling procedures were excellent using both a flux-by-flux approach and an empirical approach. The former explicitly accounts for changing atmospheric and surface conditions but requires more stringent data, especially to model solar radiation fluxes. The longwave radiation fluxes are easier to determine, and since they are generally of secondary importance in the radiation budget, do not need to be determined with such accuracy.

Empirical $Q^* = f(K\downarrow)$ approaches recognize the conservative role of longwave radiation (and assume constant albedo) and were successfully used at Scout Mountain for snow-free conditions. By changing the regression coefficients in the $Q^* = a + b\,K\downarrow$ equation, the results suggested that the approach could be employed for partial snow cover, but for a complete snow cover and winter data the method is not useful.

In summary, the Scout Mountain longwave and net radiation modelling suggested that the complete daily radiation budget could be determined from a minimum of three measurements: $K\downarrow$, α and t. Since tundra albedo is approximately constant for snow-free conditions, and t can be calculated from $K\downarrow$ data (when combined with modelled K_{EX}), the remaining requirement is $K\downarrow$ alone.

Energy Budget

The diversity and extent of the Scout Mountain data enabled some of the atmospheric and surface controls governing surface climates to be more clearly defined. Energy budgets were measured from all seasons and demonstrated the wide range of energy transfer regimes experienced in alpine tundra. The difficulties in winter measurements resulted in few days of reliable data. The poorest data, however, were from the periods when snowmelt occurred. Problems in defining energy fluxes over a thin discontinuous snow cover were encountered. Overall, the snow-surface regimes reflected the general low-energy nature of the season and energy transfers were of very small magnitude. During the spring, complete melting of the snowcover was accomplished very quickly. Melt energy accounted for the largest proportion of available energy at these times. Microscale advection undoubtedly played a role during snowmelt, but was not quantified due to measurement difficulties.

The summer data were of generally high quality and showed that relations between Q^* and Q_G were non-linear and, for the daily data, not well defined. Potential problems included the use of flux transducers, the difficulties in determining areal ground heat flux for a spatially heterogeneous surface or the variability in thermal conductivity of the soil.

Evaporation responded rapidly to surface wetting from rainfall. Once surface dessication occurred, the lack of efficient means of transferring subsurface water to the atmosphere resulted in decreased evaporation rates. The combined effects of poor vegetation development, limited surface moisture storage and rapid drainage through the coarse substrate accumulated to give a mean Bowen ratio of about 1.00. Use of the combination model defined the controls on surface energy partitioning and the physical behaviour of the tundra surface and subsurface. The definitions of the surface resistance from the Penman-Monteith combination model suggested that evaporation was limited by stomatal closure at times of dessication. Conflicting statements that the alpine tundra energy budgets are characteristically energy limiting (Rott, 1979) or moisture-limiting (Körner and Mayr, 1981) were unified by the Scout Mountain data, which was sufficiently extensive to show the resistance changes associated with a range of surface moisture conditions. Definition of the coupling coefficient from the McNaughton-Jarvis variant of the combination model was useful in displaying the differences in evaporation controls between the drier 1987 summer and the wetter 1988 spring.

Sensible heat modelling results yielded generally good results. Of particular interest was the performance of the Ohm's Law. This physically based model has potential for applications in remote mountain locations as a consequence of its simplicity. Problems in specification of surface parameters, namely the aerodynamic resistance and surface temperature, presently limit the value of this approach but not the potential. A test of its utility in estimating evaporation (latent heat flux density) indicated that single level measurements of wind speed were insufficient. The inclusion of wind profile measurements increased the performance of the method but detracted from the model's potential for remote mountain operation.

The potential utility of the Priestley–Taylor variant of the combination model for evaporation estimation was explored. The results showed that the value of α_{PT}, the proportionality factor, could not be reliably estimated from soil moisture. The use of a single value of α_{PT} as employed at subarctic locations was not found to be viable for the alpine data. The apparent paucity of potential evaporation rates from the Scout Mountain and Plateau Mountain (Alberta) sites probably typify dry alpine tundra surfaces.

FURTHER RESEARCH

Radiation Budget

Thornthwaite (1953) introduced the term "topoclimatology" and its objective to map spatial heat and mass transfer for local regions, including the effects of terrain. This is of primary importance to mountain regions. Except for direct beam solar radiation, for which numerous models exist, relatively little research has been directed sloping surface radiation budgets in mountains. There is apparently no critical evaluation of solar radiation models from an alpine perspective. There is certainly scope for future research in verifying radiation models for complex terrain.

In the alpine zone, longwave radiation has received relatively scant attention. In the mountain environment, where snow and ice abounds, the longwave radiation transfers assume greater importance to the surface radiation budget and therefore the need for reliable modelling grows. The present study demonstrated simple yet reliable means of longwave radiation determination which could usefully be tested at other locations. In particular, the

ability to assume an effective atmospheric emissivity of 0.75 has wide-ranging implications for surface climate modelling in mountains, but needs verification. The focus in most previous alpine longwave radiation modelling has been to test various published formulae, and has been characterized by inconclusive results. More recently, the emphasis in mountain longwave radiation research has moved to examining terrain influences. However, the issue regarding the utility of longwave radiation models in alpine environments has yet to be closed satisfactorily, and the value of longwave radiation models in alpine terrain has yet to be conclusively confirmed. Further research efforts directed to longwave radiation modelling in the absence of terrain effects would therefore be of value.

A related issue of concern is the accurate determination of surface temperature (T_0). This has a two-fold value, being of relevance to terrestrial longwave radiation modelling using the Stefan-Boltzmann equation and sensible heat flux modelling with the Ohm's Law. The thermocouple arrays used at Scout Mountain gave L↑ calculations very similar to that measured with a pyrgeometer. The problems associated with contact measurements detract from the general utility of the method, and it is useless when snow lies on the ground. Radiative measurements of surface temperatures using remote sensing have recently been undertaken for an alpine tundra in Colorado and offer great potential for both radiation and energy budget applications. The use of thermal imagery in surface energy flux estimation has yet to be critically examined for alpine tundra. For many remote mountain ranges, remote sensing approaches to surface flux estimation is likely to be the most practical.

The potential utility of using a flux-by-flux approach to net radiation estimation was demonstrated in this study. A true flux-by-flux method, using modelled solar and longwave radiation, has yet to be tested in alpine terrain. This would have great value in circumventing the problems inherent in trying to use $Q^* = f(K\downarrow)$ approaches to map net radiation in a mountain basin.

Energy Budget

Several of the problems encountered in this study related to energy budget measurement relate directly to surface heterogeneity. The determination of Q_G in patterned ground, the physical sources of Q_H and Q_E and the influence of advection are obvious candidates for energy budget work. Beyond these, there are still questions regarding processes

of heat and mass transfer in alpine tundra. Probably the most important problem currently facing energy budget research in mountain regions is the lack of attention given to flux measurement and modelling for sloping surfaces. There are essentially no alpine studies addressing this concern.

Possibly the most difficult of energy budget data requirements is the determination of soil moisture availability. This has importance in the measurement of ground heat and the turbulent fluxes. The gravimetric measurements made at Scout Mountain contain inherent overestimates of uncertain magnitude. The task could not be reliably performed using neutron probes, moisture blocks or tensiometers due to the heterogeneous soils and the need for measurements from the 0 - 50 mm surface layer. The use of lysimeters has been used in alpine tundra (LeDrew and Emerick, 1974) and have recently attracted renewed interest (Isard and Belding, 1989), but the method is inappropriate in an environment as spatially heterogeneous as alpine tundra, and accuracy is also lacking. Time domain reflectometry has been used in subarctic soils (Halliwell and Rouse, 1987). Surface soil moisture has also been determined from airborne measurements for simple bare soil surfaces (Soares *et al.*, 1988) but the problems of vegetation and topography would complicate the method in alpine terrain.

The ability to determine the Priestley-Taylor proportionality factor (α_{PT}) from soil moisture data would be of great value in estimating evaporative losses from the alpine tundra. The successful parameterization of soil moisture and α_{PT} has been research for a variety of surfaces in Canada, with the exception of alpine locations. The data from Scout Mountain and Plateau Mountain (Figure 9.6) were too scattered to derive a reliable relation, but the degree of scatter is not so great as to be discouraging. Further refinement of the data collection procedures involved in this method would be worthwhile, especially as this type of approach to evaporation estimation is receiving attention (Brutsaert, 1988).

A problem not unrelated to that of soil moisture or α_{PT} determination is the question of what exactly are the sources of heat and vapour in the alpine tundra. The presence of patterned ground introduces concerns about microscale spatial variation in heat fluxes resulting from the microrelief of the surface itself and the related inhomogeneity of surface type. The spatially discrete nature of vegetation, rocks and snow which characterize the tundra surface

make assumptions of homogeneity potentially difficult to embrace at the microscale. For example, when the stone polygons are dry, they contribute no, or very little, water to the evaporative flux. This then means that the spatial distributions of the source of the sensible and latent heat fluxes are not the same, and there must be lateral advection occurring. Although the high wind speeds which characterize the alpine tundra environment ensure that the surface boundary layer is well mixed, it would be of experimental interest to evaluate the microscale contributions of energy of the vegetated and non-vegetated parts of the surface.

Related problems to this theme are the nature of the energy budget when thin, discontinuous snow lies on the ground, and when the surface is subjected to the "big leaf" analogy implicit in the derivations of surface resistance. There is apparently only one report of directly measured stomatal resistances from alpine plants (Körner and Mayr, 1981). The relations between stomatal resistance and surface resistance would be worth investigating. Theoretically, the surface resistance is the parallel sum of the stomatal resistances of all the vegetation (McNaughton and Jarvis, 1983), but for alpine tundra the vegetation cover is discontinuous and the measurements used to derive surface resistance include the rock surface as well.

In summary, it should be apparent that there remains a wide choice of further research possibilities with both experimental and operational applications. The aims of the present study were to address radiation and energy budget description and modelling for a range of ambient conditions, and this was largely achieved. The measurement and modelling of alpine tundra radiation and energy transfers still offers wide scope for future research directions, to which the present study has made several contributions.

APPENDIX A - NOTATION

Symbol	Quantity	Units
Roman Letters		
C_M	heat capacity of mineral matter	$J m^{-3} K^{-1}$
C_O	heat capacity of organic matter	$J m^{-3} K^{-1}$
C_S	heat capacity of snow	$J m^{-3} K^{-1}$
C_W	heat capacity of water	$J m^{-3} K^{-1}$
c_p	specific heat of air at constant pressure	$J kg^{-1} K^{-1}$
D_H	bulk transfer coefficient for heat	$m s^{-1}$
D_V	bulk transfer coefficient for vapour	$m s^{-1}$
e	vapour pressure	Pa
e^*	saturation vapour pressure	Pa
I_0	solar constant	$W m^{-2}$; $MJ m^{-2} d^{-1}$
K_{EX}	extraterrestrial radiation	$W m^{-2}$; $MJ m^{-2} d^{-1}$
K_H	eddy diffusivity for heat	$m^2 s^{-1}$
K_M	eddy diffusivity for momentum	$m^2 s^{-1}$
K_V	eddy diffusivity for vapour	$m^2 s^{-1}$
K^*	net solar radiation	$W m^{-2}$; $MJ m^{-2} d^{-1}$
$K\downarrow$	global solar radiation	$W m^{-2}$; $MJ m^{-2} d^{-1}$
$K\uparrow$	reflected solar radiation	$W m^{-2}$; $MJ m^{-2} d^{-1}$
k	von Karman's constant (0.41)	dimensionless
L_f	latent heat of fusion	$J kg^{-1}$
L_v	latent heat of vaporization	$J kg^{-1}$
L^*	net longwave radiation	$W m^{-2}$; $MJ m^{-2} d^{-1}$
$L\downarrow$	atmospheric longwave radiation	$W m^{-2}$; $MJ m^{-2} d^{-1}$
$L\downarrow_0$	atmospheric longwave radiation (cloudless)	$W m^{-2}$; $MJ m^{-2} d^{-1}$
$L\uparrow$	terrestrial longwave radiation	$W m^{-2}$; $MJ m^{-2} d^{-1}$
P	atmospheric pressure	Pa
p	precipitation	mm

Q^*	net radiation flux density	$W m^{-2}$; $MJ m^{-2} d^{-1}$
Q_A	advective energy flux density	$W m^{-2}$; $MJ m^{-2} d^{-1}$
Q_E	latent heat energy flux density	$W m^{-2}$; $MJ m^{-2} d^{-1}$
$Q_{E(BR)}$	Q_E from BREB method	$W m^{-2}$; $MJ m^{-2} d^{-1}$
$Q_{E(AE)}$	Q_E from aerodynamic method	$W m^{-2}$; $MJ m^{-2} d^{-1}$
$Q_{E(EQ)}$	equilibrium latent heat flux density	$W m^{-2}$; $MJ m^{-2} d^{-1}$
$Q_{E(RE1)}$	Q_E from residual method using (Equation 9.4)	$W m^{-2}$; $MJ m^{-2} d^{-1}$
$Q_{E(RE2)}$	Q_E from residual method using (Equation 9.5)	$W m^{-2}$; $MJ m^{-2} d^{-1}$
Q_G	ground heat flux density	$W m^{-2}$; $MJ m^{-2} d^{-1}$
Q_H	sensible heat flux density	$W m^{-2}$; $MJ m^{-2} d^{-1}$
$Q_{H(BR)}$	Q_H from BREB method	$W m^{-2}$; $MJ m^{-2} d^{-1}$
$Q_{H(AE)}$	Q_H from aerodynamic method	$W m^{-2}$; $MJ m^{-2} d^{-1}$
$Q_{H(EC)}$	Q_H from eddy correlation method	$W m^{-2}$; $MJ m^{-2} d^{-1}$
$Q_{H(OL)}$	Q_H from Ohm's Law method	$W m^{-2}$; $MJ m^{-2} d^{-1}$
Q_M	snowmelt energy flux density	$W m^{-2}$; $MJ m^{-2} d^{-1}$
Q_P	energy used in photosynthesis	$W m^{-2}$; $MJ m^{-2} d^{-1}$
Q_R	energy input from rainfall	$W m^{-2}$; $MJ m^{-2} d^{-1}$
ρ	density of air	$kg m^{-3}$
Ri	Richardson number (gradient form)	dimensionless
r_a	aerodynamic resistance	$s m^{-1}$
r_{aH}	aerodynamic resistance to heat transfer	$s m^{-1}$
r_{aM}	aerodynamic resistance to momentum transfer	$s m^{-1}$
r_{aV}	aerodynamic resistance to vapour transfer	$s m^{-1}$
r_b	bluff body resistance	$s m^{-1}$
r_i	climatological resistance	$s m^{-1}$
r_s	surface resistance	$s m^{-1}$
r_{st}	stomatal resistance	$s m^{-1}$
S	slope of the saturation vapour pressure curve	$Pa K^{-1}$
T	air temperature/dry-bulb temperature	K
T_G	ground temperature	K
T_w	wet-bulb temperature	K
T_{snow}	snowpack temperature	K

T'	instantaneous deviation from mean air temperature	K
T_0	surface temperature	K
t	time	s
	atmospheric transmissivity	dimensionless
u	wind speed	$m s^{-1}$
u_*	friction velocity	$m s^{-1}$
w'	instantaneous deviation from mean wind speed	$m s^{-1}$
z	height above surface	m
z_0	roughness length	m
Greek Letters		
α	albedo	dimensionless
α_{PT}	Priestley–Taylor proportionality factor	dimensionless
β	Bowen ratio	dimensionless
χ_M	volumetric soil mineral content	dimensionless
χ_O	volumetric soil organic content	dimensionless
χ_W	volumetric soil water content	dimensionless
χ_{Wsnow}	volumetric snow liquid water content	dimensionless
ΔQ_S	snowpack energy storage changes	$W m^{-2}$
ϵ_A	effective emissivity of the atmosphere	dimensionless
ϵ_0	surface emissivity	dimensionless
γ	psychrometric coefficient	PaK^{-1}
Ω	McNaughton–Jarvis coupling coefficient	dimensionless
Φ_H	stability function for heat	dimensionless
Φ_M	stability function for momentum	dimensionless
Φ_V	stability function for vapour	dimensionless
σ	Stefan–Boltzmann constant	$W m^{-2} K^{-4}$

APPENDIX B - DAILY RADIATION TOTALS

Daily radiation totals for November 1986 to July 1987 and April to May 1988.
(All flux densities are in $MJm^{-2}d^{-1}$)
Missing data is indicated by "–".

Day	K_{EX}	K↓	K↑	K*	t	α	L↓	L↑	L*	Q*
November 1986										
1	13.36	9.03	2.73	6.32	0.68	0.30	19.24	26.31	−7.07	−0.76
2	13.14	5.22	1.18	4.05	0.40	0.23	21.66	27.23	−5.56	−1.52
3	12.93	6.81	1.17	5.63	0.53	0.17	20.51	27.40	−6.89	−1.26
4	12.74	5.17	0.83	4.34	0.41	0.16	–	–	−3.37	0.96
5	12.54	3.03	2.69	0.34	0.24	0.89	25.37	25.68	−3.36	−0.03
6	12.34	8.09	4.69	3.39	0.66	0.58	–	–	−0.45	0.03
7	12.17	–	–	–	–	–	22.54	22.33	0.20	0.21
8	11.97	10.32	6.03	4.29	0.86	0.58	–	–	−2.53	1.76
9	11.78	–	–	–	–	–	–	–	−2.81	−2.31
10	11.60	5.10	3.89	1.21	0.44	0.76	22.66	23.96	−1.28	−0.07
11	11.45	2.39	1.85	0.54	0.21	0.78	23.73	23.89	−0.15	0.39
12	11.27	4.67	3.27	1.40	0.41	0.70	23.43	25.42	−1.99	−0.59
13	11.10	3.81	3.15	0.66	0.34	0.83	24.37	25.58	−1.19	−0.54
14	10.93	3.43	3.09	0.34	0.31	0.90	22.43	22.93	−0.50	−0.17
15	10.79	2.84	2.16	0.68	0.26	0.76	23.38	24.14	−0.76	−0.07
16	10.63	3.63	2.53	0.92	0.34	0.70	22.47	23.90	0.44	0.34
17	10.47	9.55	4.58	4.98	0.91	0.48	–	–	−4.94	0.04
18	10.32	3.84	3.29	0.55	0.37	0.86	23.12	25.87	−2.76	−2.21
19	10.20	3.69	2.62	1.08	0.36	0.71	22.96	25.57	−2.61	−1.53
20	10.06	4.07	3.51	0.57	0.40	0.86	24.18	26.09	−1.90	−1.34
21	9.93	4.25	2.96	1.28	0.43	0.70	–	–	−2.55	−1.27
22	9.79	4.90	3.47	1.43	0.50	0.71	–	–	−2.76	−1.33
23	9.68	1.19	1.02	0.17	0.12	0.85	25.85	26.55	−0.70	−0.52
24	9.56	5.19	3.62	1.56	0.54	0.70	21.99	25.00	−3.02	−1.47
25	9.44	6.01	4.00	2.02	0.64	0.67	21.26	26.32	−5.07	−3.04
26	9.33	7.52	4.24	3.28	0.81	0.56	–	–	−4.93	−1.65
27	9.22	4.05	3.34	0.70	0.44	0.83	21.62	24.65	−3.03	−2.33
28	9.13	4.74	4.08	0.67	0.52	0.86	19.48	23.47	−3.97	−3.32
29	9.03	6.18	4.88	1.30	0.68	0.79	19.86	26.44	−6.58	−5.29
30	8.93	–	–	–	–	–	–	–	–	–
December 1986										
1	8.84	–	–	–	–	–	–	–	–	–
2	8.75	6.27	4.78	1.49	0.72	0.76	–	–	–	–
3	8.67	5.70	4.31	1.39	0.66	0.76	20.18	26.86	−6.67	−5.28
4	8.61	2.70	2.04	0.66	0.31	0.76	23.81	26.38	−2.56	−1.91
5	8.53	–	–	–	–	–	–	–	–	–
6	8.46	–	–	–	–	–	21.54	25.61	−4.07	−4.05
7	8.40	2.38	1.80	0.58	0.28	0.75	23.48	25.00	−1.53	−0.94

8	8.34	8.15	3.79	4.36	0.98	0.46	–	–	−6.11	−1.75
9	8.28	5.57	3.72	1.85	0.67	0.67	20.77	27.40	−6.62	−4.77
10	8.23	5.70	3.68	2.03	0.69	0.65	21.91	30.63	−8.71	−6.69
11	8.19	3.75	2.26	1.49	0.46	0.60	23.63	28.31	−4.68	−3.20
12	8.14	5.55	3.15	2.40	0.68	0.57	21.42	25.40	−3.98	−1.57
13	8.12	3.50	2.39	1.12	0.43	0.68	22.63	26.84	−4.19	−3.09
14	8.09	4.48	3.13	1.34	0.55	0.70	21.66	27.14	−5.47	−4.13
15	8.06	3.92	2.57	1.36	0.49	0.66	20.86	25.97	−5.13	−3.76
16	8.04	5.35	3.71	1.64	0.67	0.69	19.58	27.73	−8.16	−6.51
17	8.02	5.61	3.36	2.25	0.70	0.60	20.69	29.91	−9.22	−6.98
18	8.00	5.13	2.91	2.22	0.64	0.57	22.28	29.15	−6.86	−4.64
19	7.99	5.08	2.93	2.15	0.64	0.58	22.05	27.69	−5.64	−3.49
20	7.98	3.03	1.78	1.24	0.38	0.59	23.03	27.18	−4.15	−2.91
21	8.00	3.11	2.03	1.09	0.39	0.65	–	–	−3.28	−2.19
22	8.00	2.38	1.74	0.63	0.30	0.73	23.35	26.93	−3.33	−3.07
23	8.00	2.56	1.80	0.76	0.32	0.70	24.41	25.24	−0.84	−0.07
24	8.02	4.14	2.57	1.57	0.52	0.62	–	–	−4.84	−3.27
25	8.03	3.04	1.94	1.09	0.38	0.64	–	–	−2.56	−1.47
26	8.05	4.44	2.70	1.74	0.55	0.61	–	–	−7.40	−5.66
27	8.07	3.27	1.88	1.39	0.41	0.57	21.54	26.59	−5.05	−3.66
28	8.11	3.76	2.04	1.72	0.46	0.54	–	–	−4.40	−2.67
29	8.14	2.63	1.90	0.73	0.32	0.72	24.08	25.59	−1.50	−0.78
30	8.18	7.24	2.99	4.24	0.89	0.41	–	–	−5.01	−0.77
31	8.22	6.01	3.35	2.66	0.73	0.56	–	–	−6.79	−4.13
January	1987									
1	8.26	2.99	1.98	1.02	0.36	0.66	–	–	−2.44	−1.43
2	8.32	3.11	2.01	1.09	0.37	0.65	23.31	25.25	−1.93	−0.84
3	8.37	2.83	2.10	0.74	0.34	0.74	–	–	−3.64	−2.90
4	8.44	–	–	–	–	–	–	–	–	–
5	8.50	–	–	–	–	–	–	–	–	–
6	8.57	5.71	4.08	1.62	0.67	0.71	–	–	−6.68	−5.05
7	8.65	5.67	4.02	1.65	0.66	0.71	–	–	−6.26	−4.60
8	8.73	6.06	4.05	2.01	0.69	0.67	–	–	−7.91	−5.89
9	8.81	5.14	3.23	1.90	0.58	0.63	–	–	−6.33	−4.43
10	8.90	1.71	1.03	0.68	0.19	0.60	–	–	−2.61	−1.93
11	8.99	5.73	2.16	3.57	0.64	0.38	–	–	−7.53	−3.96
12	9.09	2.10	1.47	0.64	0.23	0.70	–	–	−1.76	−1.12
13	9.17	–	–	–	–	–	–	–	–	–
14	9.28	1.47	1.38	0.10	0.16	0.93	–	–	–	–
15	9.39	8.60	4.57	4.02	0.92	0.53	–	–	−4.01	0.01
16	9.50	2.70	1.88	0.82	0.28	0.69	–	–	−1.01	−0.18
17	9.62	–	–	–	–	–	–	–	–	–
18	9.74	–	–	–	–	–	–	–	–	–
19	9.87	6.28	4.53	1.75	0.64	0.72	–	–	−3.78	−2.02
20	10.00	8.04	5.06	2.98	0.80	0.63	18.85	24.86	−5.99	−3.02
21	10.13	7.35	4.40	2.96	0.73	0.60	17.29	24.93	−7.65	−4.69
22	10.28	6.14	3.88	2.26	0.60	0.63	19.75	25.02	−5.26	−3.00
23	10.42	3.95	2.77	1.19	0.38	0.70	21.74	24.63	−2.85	−1.66
24	10.58	3.82	2.78	1.03	0.36	0.73	18.88	23.27	−4.40	−3.36
25	10.74	3.10	2.26	0.85	0.29	0.73	20.38	23.20	−2.82	−1.97

26	10.90	2.43	1.97	0.46	0.22	0.81	22.35	23.17	−0.81	−0.35
27	11.07	3.36	2.77	0.58	0.30	0.82	22.81	24.28	−1.45	−0.87
28	11.24	5.19	3.93	1.27	0.46	0.76	20.47	24.11	−3.64	−2.38
29	11.42	6.17	4.80	1.37	0.54	0.78	21.02	24.48	−3.46	−2.08
30	11.57	4.02	3.32	0.71	0.35	0.82	21.18	23.59	−2.41	−1.70
31	11.75	6.66	4.57	2.09	0.57	0.69	21.93	24.93	−2.98	−0.89
February 1987										
1	11.93	4.66	3.90	0.77	0.39	0.84	23.04	24.19	−1.16	−0.39
2	12.12	7.64	5.71	1.93	0.63	0.75	19.69	23.89	−4.21	−2.28
3	12.29	8.57	5.86	2.71	0.70	0.68	21.39	25.75	−4.36	−1.65
4	12.49	5.02	3.72	1.29	0.40	0.74	20.55	24.93	−4.38	−3.09
5	12.69	8.77	5.77	3.00	0.69	0.66	20.42	27.05	−6.63	−3.64
6	12.89	9.11	4.94	4.18	0.71	0.54	17.55	26.52	−8.95	−4.78
7	13.11	8.27	4.00	4.28	0.63	0.48	18.55	25.98	−7.42	−3.13
8	13.30	6.85	3.01	3.84	0.52	0.44	22.26	26.80	−4.54	−0.71
9	13.52	6.66	2.82	3.84	0.49	0.42	22.95	26.88	−3.94	−0.10
10	13.75	7.26	2.93	4.32	0.53	0.40	22.04	26.40	−4.36	−0.03
11	13.98	4.74	3.46	1.27	0.34	0.73	21.08	25.01	−3.91	−2.62
12	14.21	9.44	5.98	3.46	0.66	0.63	19.54	25.41	−5.86	−2.41
13	14.44	7.10	5.37	1.73	0.49	0.76	21.14	25.01	−3.89	−2.16
14	14.64	10.98	7.07	3.91	0.75	0.64	19.50	24.77	−5.28	−1.36
15	14.88	4.71	3.75	0.97	0.32	0.80	21.65	23.94	−2.28	−1.32
16	15.13	5.94	4.49	1.45	0.39	0.76	20.64	24.15	−3.51	−2.06
17	15.38	4.59	4.00	0.60	0.30	0.87	22.79	23.31	−0.51	0.08
18	15.64	7.53	5.39	2.15	0.48	0.72	22.11	23.42	−1.30	0.85
19	15.86	4.58	3.67	0.91	0.29	0.80	23.89	24.41	−0.50	0.41
20	16.12	12.09	8.44	3.64	0.75	0.70	18.50	25.86	−7.37	−3.72
21	16.39	5.45	4.10	1.35	0.33	0.75	21.58	23.53	−1.95	−0.59
22	16.66	4.50	3.65	0.85	0.27	0.81	23.03	23.44	−0.40	0.45
23	16.89	–	–	–	–	–	–	–	–	–
24	17.16	–	–	–	–	–	–	–	–	–
25	17.43	15.49	11.11	4.39	0.89	0.72	16.28	22.85	−6.57	−2.18
26	17.71	10.41	8.50	1.91	0.59	0.82	18.69	23.95	−5.25	−3.35
27	17.95	7.38	6.25	1.13	0.41	0.85	21.12	22.82	−1.70	−0.57
28	18.23	10.38	6.70	3.68	0.57	0.65	18.44	22.64	−4.20	−0.51
March 1987										
1	18.51	13.02	9.38	3.66	0.70	0.72	17.28	23.70	−6.43	−2.77
2	18.80	9.76	7.33	2.43	0.52	0.75	21.99	25.68	−3.68	−1.27
3	19.06	7.17	5.71	1.45	0.38	0.80	23.90	26.49	−2.59	−1.13
4	19.36	6.62	5.03	1.59	0.34	0.76	24.66	26.59	−1.93	−0.33
5	19.66	8.43	5.67	2.77	0.43	0.67	23.97	26.00	−2.03	0.73
6	19.96	12.36	8.70	3.67	0.62	0.70	19.18	24.83	−5.64	−1.96
7	20.21	16.40	10.13	6.28	0.81	0.62	16.79	23.49	−6.71	−0.43
8	20.51	12.43	8.95	3.48	0.61	0.72	19.21	25.52	−6.33	−2.84
9	20.81	9.90	8.00	1.89	0.48	0.81	22.60	24.83	−2.23	−0.33
10	21.10	8.23	6.92	1.32	0.39	0.84	22.40	25.07	−2.66	−1.35
11	21.36	–	–	–	–	–	–	–	–	–
12	21.67	–	–	–	–	–	–	–	–	–

13	21.98	–	–	–	–	–	–	–	–	–
14	22.30	–	–	–	–	–	–	–	–	–
15	22.57	–	–	–	–	–	–	–	–	–
16	22.88	–	–	–	–	–	–	–	–	–
17	23.20	–	–	–	–	–	–	–	–	–
18	23.51	–	–	–	–	–	–	–	–	–
19	23.78	–	–	–	–	–	–	–	–	–
20	24.09	–	–	–	–	–	–	–	–	–
21	24.40	–	–	–	–	–	–	–	–	–
22	24.71	–	–	–	–	–	–	–	–	–
23	24.97	–	–	–	–	–	–	–	–	–
24	25.30	–	–	–	–	–	–	–	–	–
25	25.62	–	–	–	–	–	–	–	–	–
26	25.94	–	–	–	–	–	–	–	–	–
27	26.20	–	–	–	–	–	–	–	–	–
28	26.53	–	–	–	–	–	–	–	–	–
29	26.84	19.58	14.90	4.68	0.73	0.76	18.61	25.79	−7.16	−2.48
30	27.10	17.78	12.91	4.87	0.66	0.73	20.92	27.36	−6.44	−1.57
31	27.41	20.67	14.28	6.39	0.75	0.69	19.67	27.07	−7.41	−1.03

April 1987

1	27.73	21.60	13.11	8.48	0.78	0.61	19.17	28.03	−8.75	−0.27
2	27.98	19.36	9.86	9.49	0.69	0.51	20.51	28.56	−8.04	1.44
3	28.30	15.91	6.69	9.21	0.56	0.42	22.94	28.88	−5.95	3.27
4	28.60	9.60	4.24	5.35	0.34	0.44	25.57	27.66	−2.08	3.27
5	28.85	13.82	5.69	8.14	0.48	0.41	24.18	28.18	−3.99	4.14
6	29.16	20.70	10.46	10.25	0.71	0.51	19.83	27.07	−7.24	3.01
7	29.46	18.66	7.43	11.24	0.63	0.40	20.30	27.90	−7.60	3.63
8	29.70	15.87	10.81	5.06	0.53	0.68	21.71	24.67	−2.97	2.10
9	30.01	17.25	8.25	9.00	0.57	0.48	21.59	26.60	−5.03	3.97
10	30.31	12.53	5.57	6.98	0.41	0.44	22.34	26.97	−4.62	2.35
11	30.56	18.29	12.49	5.80	0.60	0.68	22.07	24.57	−2.48	3.30
12	30.87	20.87	13.68	7.19	0.68	0.66	20.78	25.34	−4.56	2.62
13	31.16	19.44	9.55	9.89	0.62	0.49	20.24	27.83	−7.60	2.30
14	31.46	22.22	8.60	13.62	0.71	0.39	22.31	29.45	−7.16	6.48
15	31.68	18.56	9.40	9.17	0.59	0.51	23.14	27.73	−4.59	4.56
16	31.97	20.13	8.65	11.50	0.63	0.43	22.23	28.12	−5.90	5.59
17	32.25	12.35	6.73	5.62	0.38	0.55	22.71	25.45	−2.73	2.88
18	32.53	16.04	12.52	3.52	0.49	0.78	21.29	23.52	−2.23	1.29
19	32.75	26.23	19.00	7.22	0.80	0.72	19.10	24.22	−5.13	2.10
20	33.03	18.12	11.02	7.11	0.55	0.61	21.37	25.85	−4.49	2.63
21	33.32	15.32	7.25	8.07	0.46	0.47	22.69	27.09	−4.40	3.68
22	33.60	19.97	7.77	12.21	0.59	0.39	22.77	28.20	−5.45	6.76
23	33.80	16.08	5.26	10.83	0.48	0.33	21.42	27.52	−6.09	4.73
24	34.08	22.84	6.26	16.59	0.67	0.27	17.56	27.72	−10.17	6.43
25	34.34	26.76	6.55	20.21	0.78	0.24	17.80	28.99	−11.20	9.01
26	34.60	26.73	5.45	21.28	0.77	0.20	19.18	29.88	−10.67	10.58
27	34.79	27.17	4.59	22.58	0.78	0.17	21.41	31.99	−10.58	12.00
28	35.04	14.70	2.25	12.44	0.42	0.15	26.25	31.15	−4.91	7.53
29	35.29	20.61	3.12	17.49	0.58	0.15	24.66	31.31	−6.65	10.83

30	35.46	11.19	1.42	9.77	0.32	0.13	26.83	29.03	−2.21	7.56
May 1987										
1	35.63	18.49	8.55	9.94	0.52	0.46	22.44	25.97	−3.52	6.41
2	35.97	21.45	13.91	7.53	0.60	0.65	22.33	26.22	−3.88	3.65
3	36.20	18.72	8.16	10.57	0.52	0.44	22.32	26.82	−4.51	6.06
4	36.37	25.15	4.53	20.62	0.69	0.18	19.34	28.97	−9.63	11.01
5	36.61	28.86	4.66	24.19	0.79	0.16	19.61	31.67	−12.07	12.12
6	36.83	29.20	4.73	24.47	0.79	0.16	21.31	34.06	−12.74	11.71
7	37.06	29.22	4.72	24.51	0.79	0.16	22.90	34.40	−11.51	13.00
8	37.21	28.18	4.58	23.61	0.76	0.16	22.71	33.84	−11.12	12.47
9	37.42	30.36	5.08	25.29	0.81	0.17	20.28	32.67	−12.38	12.90
10	37.63	24.78	4.10	20.69	0.66	0.17	20.98	31.52	−10.55	10.15
11	37.84	18.92	2.97	15.96	0.50	0.16	25.53	30.92	−5.39	10.56
12	38.04	24.38	4.22	20.15	0.64	0.17	22.58	28.43	−5.86	14.30
13	38.17	27.18	4.52	22.65	0.71	0.17	20.28	29.94	−9.67	12.99
14	38.37	24.80	3.95	20.86	0.65	0.16	20.81	29.36	−8.54	12.31
15	38.55	30.93	5.20	25.73	0.80	0.17	18.72	31.11	−12.39	13.35
16	38.74	30.30	5.17	25.13	0.78	0.17	19.58	32.04	−12.46	12.66
17	38.93	24.61	4.07	20.54	0.63	0.17	22.32	32.09	−9.76	10.78
18	39.04	18.11	6.07	12.04	0.46	0.34	22.01	26.47	−4.45	7.60
19	39.21	12.41	10.53	1.90	0.32	0.85	25.57	25.99	−0.40	1.48
20	39.38	–	–	–	–	–	–	–	–	–
21	39.55	21.79	15.93	5.86	0.55	0.73	20.69	26.43	−5.75	0.13
22	39.70	19.00	12.23	6.76	0.48	0.64	23.61	27.38	−3.77	3.00
23	39.78	21.54	10.49	11.04	0.54	0.49	22.62	28.44	−5.81	5.23
24	39.93	24.04	7.11	16.93	0.60	0.30	22.34	30.21	−7.88	9.05
25	40.07	24.51	4.40	20.12	0.61	0.18	23.03	31.85	−8.81	11.30
26	40.21	16.86	2.61	14.25	0.42	0.15	25.60	31.62	−6.01	8.24
27	40.35	12.18	1.89	10.30	0.30	0.16	25.79	30.51	−4.72	5.57
28	40.48	18.65	3.06	15.60	0.46	0.16	24.34	28.68	−4.35	11.25
29	40.53	22.56	3.46	19.11	0.56	0.15	23.73	29.79	−6.06	13.04
30	40.64	19.30	3.10	16.22	0.47	0.16	23.48	28.55	−5.08	11.13
31	40.76	20.42	6.90	13.51	0.50	0.34	22.76	26.75	−3.99	9.53
June 1987										
1	40.87	17.88	7.17	10.71	0.44	0.40	–	–	−2.95	7.75
2	40.98	–	–	–	–	–	–	–	–	–
3	41.08	28.11	4.39	23.72	0.68	0.16	–	–	–	–
4	41.18	26.59	4.18	22.41	0.65	0.16	25.61	35.75	−10.13	12.28
5	41.19	18.77	2.94	15.84	0.46	0.16	24.96	31.38	−6.40	9.42
6	41.28	26.38	4.10	22.28	0.64	0.16	25.08	33.04	−7.01	14.33
7	41.36	27.35	4.32	23.02	0.66	0.16	24.42	34.09	−9.67	13.35
8	41.44	5.87	0.81	5.06	0.14	0.14	27.77	30.29	−2.52	2.54
9	41.51	18.05	2.85	15.20	0.43	0.16	26.15	30.90	−4.76	10.43
10	41.57	24.02	3.81	20.22	0.58	0.16	23.11	30.57	−7.47	12.75
11	41.63	25.21	3.90	21.32	0.61	0.15	25.27	32.92	−7.65	13.68
12	41.69	24.63	3.86	20.76	0.59	0.16	24.21	31.96	−7.73	13.02
13	41.65	31.24	4.91	26.33	0.75	0.16	23.20	34.45	−11.25	15.08
14	41.69	28.85	4.53	24.33	0.69	0.16	24.66	34.76	−10.12	14.22

15	41.73	18.64	3.03	15.60	0.45	0.16	26.91	32.52	−5.61	9.99
16	41.77	7.79	1.66	6.12	0.19	0.21	26.63	28.04	−1.40	4.73
17	41.79	19.18	2.96	16.21	0.46	0.15	24.90	30.36	−5.45	10.76
18	41.82	23.26	3.63	19.63	0.56	0.16	24.27	32.48	−8.20	11.42
19	41.83	20.42	3.18	17.24	0.49	0.16	25.57	32.55	−6.99	10.25
20	41.84	17.75	2.75	15.00	0.42	0.15	25.34	31.28	−5.95	9.06
21	41.85	–	–	–	–	–	–	–	–	–
22	41.85	22.24	3.59	18.65	0.53	0.16	23.18	29.16	−5.99	12.66
23	41.84	30.33	4.90	25.43	0.72	0.16	22.08	32.48	−10.40	15.04
24	41.83	–	–	–	–	–	–	–	–	–
25	41.82	32.43	5.13	27.30	0.78	0.16	23.18	34.93	−11.74	15.54
26	41.79	32.53	5.17	27.35	0.78	0.16	24.38	36.43	−12.05	15.30
27	41.77	31.55	5.00	26.55	0.76	0.16	26.42	38.22	−11.78	14.76
28	41.73	32.52	5.18	27.33	0.78	0.16	26.47	38.67	−12.20	15.13
29	41.61	30.52	4.85	25.68	0.73	0.16	26.97	38.32	−11.36	14.31
30	41.57	31.96	5.11	26.86	0.77	0.16	26.55	38.62	−12.07	14.80
July	1987									
1	41.52	32.61	5.24	27.37	0.79	0.16	25.80	37.86	−12.06	15.31
2	41.46	19.15	3.03	16.11	0.46	0.16	28.58	35.56	−6.98	9.14
3	41.40	5.11	0.64	4.47	0.12	0.12	27.96	29.76	−1.79	2.67
4	41.34	21.06	3.36	17.70	0.51	0.16	24.83	32.08	−7.24	10.45
5	41.27	15.01	3.08	11.93	0.36	0.21	26.11	28.29	−2.18	9.75
6	41.19	–	–	–	–	–	–	–	–	–
7	41.11	21.83	3.47	18.35	0.53	0.16	26.43	31.17	−4.74	13.61
8	41.03	27.17	4.20	22.98	0.66	0.15	25.05	30.71	−5.67	17.31
9	40.93	11.65	1.81	9.84	0.28	0.16	26.39	29.40	−3.01	6.84
10	40.84	14.89	2.24	12.64	0.36	0.15	26.05	30.53	−4.48	8.16
11	40.74	18.40	2.72	15.67	0.45	0.15	26.49	31.76	−5.27	10.41
12	40.64	28.37	4.40	23.98	0.70	0.16	23.49	33.17	−9.68	14.31
13	40.53	31.27	4.76	26.51	0.77	0.15	25.01	36.65	−11.65	14.86
14	40.49	32.11	5.01	27.10	0.79	0.16	23.71	35.62	−11.91	15.18
15	40.37	30.21	4.90	25.32	0.75	0.16	22.00	32.90	−10.90	14.42
16	40.25	18.36	3.07	15.30	0.46	0.17	25.50	30.63	−5.12	10.17
17	40.11	–	–	–	–	–	–	–	–	–
18	39.97	12.77	1.95	10.83	0.32	0.15	27.32	30.05	−2.74	8.10
19	39.83	9.73	1.29	8.45	0.24	0.13	27.48	29.48	−1.99	6.45
20	39.70	19.85	3.17	16.68	0.50	0.16	26.50	31.45	−4.95	11.71
21	39.54	19.06	3.01	16.06	0.48	0.16	26.01	33.38	−7.38	8.67
22	39.39	20.54	3.19	17.34	0.52	0.16	26.50	33.54	−7.04	10.31
23	39.23	17.18	2.72	14.46	0.44	0.16	26.81	32.99	−6.18	8.27
24	39.07	20.39	3.13	17.27	0.52	0.15	26.97	33.51	−6.54	10.72
25	38.90	9.36	1.32	8.05	0.24	0.14	27.22	30.97	−3.76	4.28
26	38.73	25.04	3.86	21.19	0.65	0.15	25.49	34.05	−8.57	12.61
27	38.55	29.34	4.54	24.81	0.76	0.15	24.55	34.37	−9.82	14.98
28	38.36	29.83	4.66	25.17	0.78	0.16	23.91	34.76	−10.85	14.32
29	38.18	25.50	3.98	21.52	0.67	0.16	24.92	33.88	−8.96	12.56
30	38.07	16.30	2.57	13.73	0.43	0.16	27.18	32.61	−5.43	8.31

31	37.88	16.86	2.75	14.10	0.45	0.16	24.72	28.99	−4.26	9.84
April 1988										
1	28.04	11.86	9.20	2.66	0.42	0.78	24.39	28.13	−3.74	−1.08
2	28.30	10.77	8.73	2.05	0.38	0.81	25.16	27.73	−2.57	−0.52
3	28.60	18.54	14.07	4.47	0.65	0.76	19.69	26.09	−6.40	−1.93
4	28.91	17.65	14.86	2.79	0.61	0.84	–	–	−3.47	−0.68
5	29.16	12.54	9.85	2.70	0.43	0.79	–	–	−2.07	0.63
6	29.46	14.65	12.25	2.40	0.50	0.84	24.35	28.34	−3.99	−1.59
7	29.76	20.30	15.16	5.14	0.68	0.75	20.04	25.50	−5.45	−0.31
8	30.01	15.16	11.34	3.82	0.51	0.75	20.92	25.62	−4.70	−0.88
9	30.31	23.71	16.33	7.38	0.78	0.69	19.32	27.30	−7.97	−0.59
10	30.63	21.38	11.33	10.05	0.70	0.53	23.17	28.04	−4.87	5.18
11	30.87	20.52	8.08	12.43	0.66	0.39	22.45	28.24	−5.79	6.64
12	31.16	24.15	6.90	17.25	0.78	0.29	22.80	30.51	−7.71	9.54
13	31.46	18.22	3.71	14.51	0.58	0.20	26.00	31.44	−5.44	9.07
14	31.75	20.77	3.57	17.20	0.65	0.17	24.45	33.30	−8.85	8.34
15	31.97	20.12	3.31	16.81	0.63	0.16	27.19	34.65	−7.47	9.35
16	32.25	17.96	2.96	14.99	0.56	0.16	25.56	32.49	−6.93	8.07
17	32.53	8.65	2.35	6.30	0.27	0.27	26.60	28.79	−2.19	4.11
18	32.81	11.05	10.50	0.55	0.34	0.95	25.92	26.50	−0.58	−0.03
19	33.03	17.67	12.07	5.60	0.53	0.68	22.62	27.64	−5.02	0.81
20	33.32	22.13	10.90	11.23	0.66	0.49	20.08	29.61	−9.53	2.84
21	33.60	22.32	6.99	15.33	0.66	0.31	22.22	30.60	−8.38	8.28
22	33.87	9.04	4.04	4.99	0.27	0.45	25.41	29.07	−3.67	3.45
23	34.08	13.11	10.38	2.73	0.38	0.79	23.74	27.45	−3.71	0.21
24	34.34	17.25	14.22	3.04	0.50	0.82	22.90	25.84	−2.95	0.81
25	34.60	14.03	11.04	2.99	0.41	0.79	23.20	26.71	−3.51	0.06
26	34.86	23.53	13.09	10.44	0.67	0.56	19.25	27.61	−8.36	2.89
27	35.04	23.32	6.83	16.50	0.67	0.29	21.25	29.65	−8.40	9.59
28	35.29	16.08	3.28	12.80	0.46	0.20	23.98	29.92	−5.94	8.47
29	35.54	19.83	5.53	14.30	0.56	0.28	20.22	27.72	−7.49	7.96
30	35.76	13.42	6.88	6.54	0.37	0.51	21.96	25.96	−4.00	4.56
May 1988										
1	35.98	22.38	9.09	13.28	0.62	0.41	21.29	26.32	−5.03	8.94
2	36.20	14.04	3.61	10.43	0.39	0.26	23.20	27.41	−4.21	7.61
3	36.44	19.14	12.90	6.24	0.53	0.67	22.12	26.45	−4.33	2.37
4	36.61	24.77	12.70	12.07	0.68	0.51	19.16	26.64	−7.48	6.39
5	36.83	19.05	4.81	14.24	0.52	0.25	22.59	28.66	−6.07	8.74
6	37.06	15.07	13.21	1.86	0.41	0.88	25.45	27.62	−2.16	−0.06
7	37.28	15.05	11.44	3.61	0.40	0.76	23.88	28.23	−4.36	−0.58
8	37.42	15.62	8.19	7.43	0.42	0.52	22.56	28.63	−6.07	2.74
9	37.63	24.97	4.89	20.09	0.66	0.20	22.99	30.17	−7.17	13.91
10	37.84	22.15	3.08	19.07	0.59	0.14	23.90	31.74	−7.84	12.09
11	38.04	23.12	3.29	19.83	0.61	0.14	25.12	33.57	−8.45	12.10
12	38.25	23.66	3.49	20.17	0.62	0.15	25.41	33.41	−8.00	12.97
13	38.37	20.19	4.16	16.03	0.53	0.21	24.55	28.64	−4.09	12.35

14	38.55	18.00	3.25	14.75	0.47	0.18	23.44	28.60	−5.16	10.73
15	38.74	17.70	2.73	14.98	0.46	0.15	23.72	30.37	−6.65	9.05
16	38.93	7.12	1.76	5.37	0.18	0.25	24.66	28.28	−3.63	3.09
17	39.11	17.00	3.64	13.36	0.43	0.21	21.46	27.24	−5.77	8.61
18	39.21	17.41	3.43	13.98	0.44	0.20	23.25	27.31	−4.06	10.50
19	39.38	28.47	7.46	21.01	0.72	0.26	21.01	29.08	−8.07	13.94
20	39.55	30.56	4.76	25.80	0.77	0.16	19.86	31.84	−11.98	14.05
21	39.70	30.34	4.68	25.66	0.76	0.15	22.44	33.60	−11.16	14.77
22	39.86	20.00	3.01	16.98	0.50	0.15	26.29	33.14	−6.85	10.79
23	39.93	25.45	4.71	20.74	0.64	0.18	21.59	30.14	−8.55	12.31
24	40.07	22.24	3.48	18.76	0.56	0.16	22.25	31.19	−8.94	10.25
25	40.21	26.53	4.18	22.36	0.66	0.16	21.68	31.53	−9.85	12.77
26	40.35	26.41	4.16	22.24	0.65	0.16	22.72	31.99	−9.27	13.38
27	40.48	20.63	3.29	17.34	0.51	0.16	25.03	30.41	−5.37	12.39
28	40.61	9.78	6.38	3.40	0.24	0.65	24.85	27.08	−2.24	1.52
29	40.64	20.89	10.66	10.22	0.51	0.51	21.86	26.30	−4.45	4.76
30	40.76	31.13	6.46	24.67	0.76	0.21	19.47	28.87	−9.40	15.45
31	40.88	17.46	2.89	14.58	0.43	0.17	22.72	28.25	−5.43	9.53

APPENDIX C - DAILY ENERGY TOTALS

Daily energy totals for November 1986 to July 1987 and April to May 1988.
(All flux densities are $MJm^{-2}d^{-1}$)
(Winter days without energy budget measurements have been omitted)
Missing data is indicated by "-".

Day	Q^*	Q_G	ΔQ_S	Q_H	Q_E	Q_M	β
November 1986							
1	3.28	-0.08	0	-1.81	-1.38	0	1.31
2	2.40	0.01	0	1.06	-3.13	0	-0.34
3	2.70	0.03	0	-1.65	-1.08	0	1.52
4	2.99	-0.04	0	-1.55	-1.48	0	1.05
December 1986							
2	-1.97	0.28	-0.07	1.16	0.60	0	1.92
3	-1.74	0.09	-0.16	1.00	0.81	0	1.25
4	-0.02	-0.05	-0.08	0.08	0.08	0	0.95
10	-1.61	0	-0.07	0.71	0.97	0	0.74
16	-1.68	0.14	-0.10	0.63	1.02	0	0.62
17	-1.57	-0.06	-0.01	0.77	0.87	0	0.88
18	-1.09	-0.04	-0.05	1.66	-0.48	0	-3.45
19	-1.16	0.02	0.03	0.19	0.65	0	0.29
20	-0.11	-0.12	-0.03	0.45	-0.19	0	-2.38
January 1987							
6	-1.75	0.28	-0.08	1.44	0.11	0	13.30
7	-1.53	0.20	-0.03	4.21	-2.84	0	-1.48
10	0.68	-0.38	-0.08	0.18	0.24	0	0.73
11	0.11	-0.17	-0.04	0.04	0.06	0	0.63
19	-0.69	0.04	-0.08	2.54	-2.50	0	-1.01
20	-0.27	-0.13	0.01	0.69	-0.31	0	-2.21
21	-1.32	-0.05	-0.10	0.47	1.01	0	0.46
29	-0.62	-0.04	-0.06	0.29	0.43	0	0.68
30	0.11	0	-0.02	0.74	-0.84	0	-0.88
February 1987							
13	-0.18	-0.03	0.08	-0.57	0.71	0	-0.81
14	0.66	0	0.03	-0.36	-0.33	0	1.10
15	0.48	-0.19	-0.05	-0.15	-0.09	0	1.68
16	0.18	-0.05	-0.03	0.07	-0.17	0	-0.40
20	-1.16	-0.06	-0.09	0.62	0.69	0	0.91
25	-0.82	0.42	-0.24	0.11	0.53	0	0.21

26	−1.08	0.06	−0.12	0.91	0.22	0	4.14
	March 1987						
1	−0.36	0.04	−0.05	−0.36	0.74	0	−0.49
2	0.11	−0.10	−0.09	0.13	−0.05	0	−2.40
3	0.28	−0.17	−0.03	−0.06	−0.02	0	2.83
29	−0.12	−0.26	−0.59	0.45	0.53	0	0.85
30	1.36	−0.62	−0.45	1.60	−1.89	−0.21	−0.85
	April 1987						
1	2.18	−0.64	−0.82	1.11	−0.80	−0.97	−1.38
2	3.82	−0.58	−0.30	0.40	−1.64	−1.83	−0.24
3	4.85	−0.31	−0.33	0.21	−0.49	−4.13	−0.42
16	6.46	−0.12	0.04	−2.58	−2.49	−1.32	1.03
17	3.64	−0.28	−0.30	−0.96	−0.62	−1.48	1.54
18	2.12	0.22	−0.04	−0.79	−1.52	0	0.85
20	4.67	−0.27	−0.35	−0.13	0.30	−4.22	−0.44
21	5.96	−0.35	−0.19	−0.97	−2.53	−2.20	0.38
23	7.37	−0.20	0	−1.51	−5.65	0	0.27
24	10.16	−0.23	0	−5.09	−4.84	0	1.05
25	12.49	−0.28	0	−6.31	−5.90	0	1.07
26	13.89	−0.05	0	−4.54	−9.30	0	0.49
27	15.17	−0.26	–	–	–	–	–
28	9.24	−1.08	–	–	–	–	–
29	12.24	−2.26	–	–	–	–	–
30	8.31	−1.34	–	–	–	–	–
	May 1987						
1	7.64	−0.38	–	–	–	–	–
2	4.66	−0.03	–	–	–	–	–
3	7.57	0.05	–	–	–	–	–
4	14.43	−0.50	0	−8.11	−5.82	0	1.39
5	15.41	−1.32	0	−8.01	−6.08	0	1.32
6	15.16	−2.02	0	−5.69	−7.45	0	0.76
7	16.08	−2.04	0	−8.02	−6.02	0	1.33
8	15.76	−1.45	0	−7.56	−6.75	0	1.12
9	16.69	−1.09	0	−10.22	−5.38	0	1.90
10	13.55	−1.05	0	−8.26	−4.24	0	1.95
11	11.96	−0.99	0	−6.07	−4.90	0	1.24
12	15.42	−0.53	0	−6.77	−8.12	0	0.83
13	14.87	−1.01	0	−8.77	−5.09	0	1.72
14	15.06	−1.01	0	−8.04	−6.01	0	1.34
15	16.50	−1.05	0	−10.84	−4.61	0	2.35
16	15.90	−1.12	0	−9.02	−5.76	0	1.57
17	13.50	−0.89	0	−8.91	−3.69	0	2.41
18	9.06	−0.12	–	–	–	–	–
19	1.59	−0.05	–	–	–	–	–

20	0.57	−0.10	–	–	–	–	–
21	1.65	−0.36	–	–	–	–	–
22	4.18	−0.44	–	–	–	–	–
23	7.00	−0.52	0	−0.39	−6.06	0	0.06
24	11.23	−0.77	0	−3.42	−7.04	0	0.49
25	13.67	−0.81	0	−5.18	−7.68	0	0.67
26	10.29	−1.15	0	−4.48	−4.67	0	0.96
27	7.04	−0.93	0	−2.14	−3.97	0	0.54
28	11.91	−0.56	0	−5.22	−6.13	0	0.85
29	14.54	−1.11	0	−8.18	−5.25	0	1.56
30	12.61	−0.67	0	−6.77	−5.17	0	1.31
31	–	–	–	–	–	–	–
	June 1987						
1	–	–	–	–	–	–	–
2	–	–	–	–	–	–	–
3	–	–	–	–	–	–	–
4	14.74	−1.54	0	−5.86	−7.33	0	0.80
5	11.61	−0.72	0	−5.63	−5.26	0	1.07
6	15.78	−2.36	0	−6.30	−7.11	0	0.89
7	15.47	−2.08	0	−7.44	−5.95	0	1.25
8	3.44	−0.40	0	−0.80	−2.16	0	0.37
9	11.33	−1.20	–	–	–	–	–
10	14.61	−1.36	–	–	–	–	–
11	15.37	−1.72	–	–	–	–	–
12	15.09	−1.69	–	–	–	–	–
13	17.77	−2.07	–	–	–	–	–
14	16.12	−1.87	–	–	–	–	–
15	10.85	−0.71	0	−5.81	−4.33	0	1.34
16	5.23	−0.03	0	−2.27	−2.93	0	0.77
17	12.25	−1.07	0	−6.10	−5.09	0	1.20
18	13.76	−2.03	0	−7.61	−4.12	0	1.85
19	12.26	−1.53	0	−5.27	−5.46	0	0.97
20	11.11	−0.72	0	−5.23	−5.16	0	1.01
21	–	–	–	–	–	–	–
22	14.26	−0.87	0	−5.78	−7.60	0	0.76
23	17.49	−2.61	0	−9.71	−5.17	0	1.88
24	–	–	–	–	–	–	–
25	17.97	−2.36	0	−8.04	−7.57	0	1.06
26	18.43	−2.34	0	−7.93	−8.16	0	0.97
27	17.48	−2.70	0	−7.40	−7.38	0	1.00
28	–	–	–	–	–	–	–
29	–	–	–	–	–	–	–
30	–	–	–	–	–	–	–
	July 1987						
1	–	–	–	–	–	–	–
2	–	–	–	–	–	–	–
3	–	–	–	–	–	–	–
4	–	–	–	–	–	–	–

5	10.60	−0.09	0	−4.65	−5.86	0	0.79
6	–	–	–	–	–	–	–
7	14.61	−1.22	0	−5.36	−8.02	0	0.67
8	17.97	−1.47	0	−9.90	−6.60	0	1.50
9	7.29	−0.50	0	−3.53	−3.26	0	1.08
10	9.41	−1.07	0	−3.33	−5.01	0	0.66
11	11.55	−1.24	0	−4.29	−6.11	0	0.70
12	17.26	−1.51	0	−7.37	−8.39	0	0.88
13	17.79	−1.57	0	−7.04	−9.18	0	0.77
14	19.07	−1.18	0	−8.58	−9.26	0	0.93
15	16.98	−0.56	0	−9.88	−6.54	0	1.51
16	11.22	−0.60	0	−4.31	−6.32	0	0.68
17	–	–	–	–	–	–	–
18	8.20	−0.85	0	−3.47	−3.88	0	0.90
19	6.90	−0.72	0	−2.97	−3.21	0	0.92
20	12.60	−0.99	0	−6.13	−5.48	0	1.12
21	10.66	−1.03	0	−3.88	−5.75	0	0.67
22	12.51	−1.11	0	−6.19	−5.21	0	1.19
23	10.04	−1.45	0	−3.98	−4.62	0	0.86
24	12.18	−1.06	0	−5.04	−6.07	0	0.83
25	5.59	−0.67	0	−2.12	−2.80	0	0.76
26	15.51	−2.09	0	−6.08	−7.34	0	0.83
27	17.66	−1.39	0	−8.52	−7.76	0	1.10
28	17.52	−1.39	0	−7.79	−8.34	0	0.93
29	15.03	−1.47	0	−6.84	−6.72	0	1.02
30	9.87	−0.62	0	−4.61	−4.64	0	0.99
31	10.96	−0.14	0	−6.80	−4.01	0	1.70
	April 1988						
1	0.29	−0.37	−0.06	0.23	−0.09	0	−2.60
2	0.48	−0.30	−0.08	0.09	−0.19	0	−0.46
3	0.14	−0.19	0.07	−0.01	−0.01	0	1.00
4	−0.56	−0.22	−0.14	0.41	0.18	0	2.28
5	0.73	−0.16	−0.20	0.06	−0.44	0	−0.15
6	−1.16	−0.17	0.12	0.46	0.78	0	0.59
7	0.22	−0.18	−0.35	0.03	−0.31	0	−0.10
8	0.33	−0.08	−0.15	0.31	−1.40	0	−0.22
9	1.65	−0.59	−0.66	−0.35	0.46	−0.86	−0.76
10	7.38	−1.07	−0.45	3.06	−4.06	−4.86	−0.75
11	–	–	–	–	–	–	–
12	12.24	−1.31	−0.04	−1.05	−2.80	−7.35	0.38
13	10.86	−0.92	−0.08	2.44	−12.30	0	−0.20
14	10.67	−1.16	0	−1.78	−8.19	0	0.22
15	10.94	−2.02	0	−2.24	−6.69	0	0.34
16	9.54	−1.63	0	−3.03	−4.87	0	0.62
17	–	–	–	–	–	–	–
18	0.15	−0.14	−0.13	0.04	0.08	0	0.52
19	2.34	−0.19	−0.26	−0.65	−0.43	−0.82	1.52
20	5.51	−0.23	−0.24	0.08	−0.65	−4.46	−0.12
21	9.97	−0.28	−0.39	−1.36	−1.61	−6.11	0.85
22	4.22	−0.26	0	−0.43	−0.85	−2.67	0.50

23	0.72	−0.17	−0.03	−0.27	−0.40	0	0.68
24	1.14	−0.07	−0.06	−0.50	−0.50	0	1.00
25	0.83	−0.10	−0.17	0.09	−0.85	0	−0.11
26	5.66	−0.21	−0.40	−0.38	−0.76	−3.91	0.50
27	12.21	−0.21	0	−3.95	−8.05	0	0.49
28	10.41	−0.73	0	−4.07	−5.61	0	0.73
29	10.26	−0.35	0	−2.69	−2.40	−4.82	1.12
30	–	–	–	–	–	–	–
	May 1988						
1	9.54	−0.24	0	−2.28	−2.36	−4.66	0.97
2	8.15	−0.14	0	−0.98	−1.52	−5.51	0.65
3	2.89	−0.14	−0.22	−0.39	−0.38	−1.70	1.03
4	7.77	0	−0.41	−1.41	−4.52	−1.42	0.31
5	10.18	−0.10	0	−2.88	−7.21	0	0.40
6	–	–	–	–	–	–	–
7	0.41	−0.23	−0.02	0.45	0.24	−0.86	1.88
8	4.52	−0.29	−0.37	0.63	−0.32	−4.16	−1.96
9	15.22	−0.47	0	−0.34	−14.40	0	0.02
10	13.86	−1.90	0	−5.14	−7.07	0	0.73
11	13.68	−2.69	0	−3.50	−7.49	0	0.47
12	14.24	−1.86	0	−4.02	−8.67	0	0.46
13	12.55	−0.71	0	−4.33	−7.50	0	0.58
14	11.60	−0.82	0	−4.17	−6.60	0	0.63
15	10.27	−0.82	0	−3.04	−6.55	0	0.46
16	–	–	–	–	–	–	–
17	–	–	–	–	–	–	–
18	11.64	−0.25	0	−5.17	−6.22	0	0.83
19	15.37	−1.34	0	−6.37	−7.66	0	0.83
20	16.54	−2.06	0	−7.81	−6.86	0	1.14
32	17.09	−2.02	0	−8.64	−6.64	0	1.30
22	12.05	−1.42	0	−4.99	−5.77	0	0.86
23	13.66	−1.38	0	−6.83	−5.45	0	1.25
24	11.85	−1.41	0	−6.31	−4.14	0	1.52
25	14.99	−1.68	0	−8.60	−4.72	0	1.82
26	14.76	−1.45	0	−7.33	−5.98	0	1.23
27	12.96	−1.06	0	−6.78	−5.12	0	1.33
28	1.80	−0.01	0.06	−0.06	−1.67	0	−0.04
29	–	–	–	–	–	–	–
30	–	–	–	–	–	–	–
31	10.71	−0.78	0	−4.59	−5.34	0	0.86

REFERENCES

Aase, J. K. and S. B. Idso (1978) A comparison of two formula types for calculating longwave radiation from the atmosphere, Water Resources Research, **14**, 623–625.

Aguado, E. (1985) Radiation balances of melting snow covers at an open site in the Central Sierra Nevada, California, Water Resources Research, **21**, 1649–1654.

Ambach, W. (1974) The influence of cloudiness on the net radiation balance of a snow surface with high albedo, Journal of Glaciology, **13**, 73–94.

Ambach, W. and H. Hoinkes (1963) The heat balance of an alpine snowfield, International Association of Hydrological Sciences, Publication, **61**, 24–36.

Anderson, E. A. (1976) A Point Energy and Mass Balance Model of a Snow Cover, (NOAA Technical Report NWS 19), 150 pp.

Anderton, P. W. and T. J. Chinn (1978) Ivory Glacier, New Zealand; an IHD representative basin study, Journal of Glaciology, **20**, 67–84.

Angus, D. E. and P. J. Watts (1984) Evapotranspiration — how good is the Bowen ratio method?, Agricultural Water Management, **8**, 133–150.

Atwater, M. A. and J. T. Ball (1978) A numerical solar radiation model based on standard meteorological observations, Solar Energy, **21**, 163–170.

Aufdemberge, T. P. (1974) Energy-balance studies over glacier and tundra surfaces, Chitistone Pass, Alaska, Summer 1969, in: Icefield Ranges Research Project, Scientific Results, **4**, 63–79.

Bailey, W. G. and J. A. Davies (1981) Bulk stomatal resistance control on evaporation, Boundary-Layer Meteorology, **20**, 401–415.

Bailey, W. G., E. J. Weick and J. D. Bowers (1989) The radiation balance of alpine tundra, Plateau Mountain, Alberta, Canada, Arctic and Alpine Research, **21**, 126–134.

Ballard, T. M. (1973) Soil physical properties in a sorted stripe field, Arctic and Alpine Research, **5**, 127–131.

Barry, R. G. (1981) Mountain Weather and Climate, (Methuen), 313 pp.

Barton, I. J. (1979) A parameterization of the evaporation from nonsaturated surfaces, Journal of Applied Meteorology, **18**, 43–47.

Beven, K. (1989) Changing ideas in hydrology - the case of physically-based models, Journal of Hydrology, **105**, 157–172.

Bishop, B. C., A. K. Angstrøm, A. J. Drummond and J. J. Roche (1966) Solar radiation measurements in the high Himalayas, Journal of Applied Meteorology, **5**, 94–104.

Bliss, L. C. (1956) A comparison of plant development in microenvironments of arctic and alpine tundras, Ecological Monographs, **26**, 303–337.

Bolz, H. M. (1949) Die Abhangigkeit der infraroten Gegenstrahlung von der Bewolkung, Zeitschrift für Meteorologie, **3**, 201–203.

Bowen, I. S. (1926) The ratio of heat losses by conduction and by evaporation from any water surface, Physical Review, **27**, 779–787.

Bowers, J. D. (1988) Surface radiation and energy balances at a mid-latitude alpine tundra site during the summer, (unpublished M.Sc. thesis, Simon Fraser University, Burnaby, Canada).

Bowers, J. D. and W. G. Bailey (1987) Radiation and energy balance regimes for an alpine tundra, 4th Conference on Mountain Meteorology, Preprint Volume, 6–10.

Bowers, J. D. and W. G. Bailey (1989) Summer energy balance regimes for alpine tundra, Plateau Mountain, Alberta, Canada, Arctic and Alpine Research, **21**, 135–143.

Bowers, J. D. and W. G. Bailey (1990) Comparison of sensible heat flux densities determined by eddy correlation, Bowen ratio and Ohm's Law approaches for alpine tundra, Boundary-Layer Meteorology, in press.

Boyne, H. S. and D. Fisk (1987) A comparison of snow cover liquid water measurement techniques, Water Resources Research, **23**, 1833–1836.

Brazel, A. J. (1974) Surface heat exchange at Chitistone Pass, Alaska, in: Icefield Ranges Research Project, Scientific Results, **4**, 29–32.

Brazel, A. J. and A. D. Hyers (1981) Comments on aspects of radiation transfer at high altitudes, in: Brazel, A. J. (ed), Research Papers in Climatology, (Geography Publication No. 1, Department of Geography, Arizona State University), 1–20.

Brazel, A. J. and M. G. Marcus (1979) Heat exchange across a snow surface at 5365 m, Mount Logan, Yukon, Arctic and Alpine Research, **11**, 1–16.

Brazel, A. J. and M. G. Marcus (1987) Heat enhancement by longwave wall emittance, Geographical Review, 77, 440–455.

Brunt, D. (1932) Notes on radiation in the atmosphere, Quarterly Journal, Royal Meteorological Society, **58**, 389–420.

Brutsaert, W. (1975) On a derivable formula for long-wave radiation from clear skies, Water Resources Research, **11**, 742–744.

Brutsaert, W. (1982) Evaporation into the Atmosphere. Theory, History and Applications, (Reidel; Dordrecht, Holland), 299 pp.

Brutsaert, W. (1988) The parameterization of regional evaporation – some directions and strategies, Journal of Hydrology, **102**, 409–426.

Choudhury, B. J. and A. T. C. Chang (1981) On the angular variation of solar reflectance of snow, Journal of Geophysical Research, **86**, 465–472.

Clements, W. E, J. A. Archuleta and P. H. Gudiksen (1989) Experimental design of the 1984 ASCOT field study, Journal of Applied Meteorology, **28**, 405–413.

Coulson, K. L. and D. W. Reynolds (1971) The spectral reflectance of natural surfaces, Journal of Applied Meteorology, **10**, 1285–1295.

Davies, J. A. (1967) A note on the relationship between net radiation and solar radiation, Quarterly Journal, Royal Meteorological Society, **93**, 109–115.

Davies, J. A. and C. D. Allen (1973) Equlibrium, potential and actual evaporation from cropped surfaces in southern Ontario, Journal of Applied Meteorology, **12**, 649–657.

Davies, J. A. and S. B. Idso (1979) Estimating the surface radiation balance and its components, in: Barfield, B. J. and J. F. Gerber (eds) Modification of the Aerial Environment of Plants, (American Society of Agricultural Engineers, Monograph Number 2), 183–210.

Davies, J. A., W. Schertzer and M. Nunez (1975) Estimating global solar radiation, Boundary-Layer Meteorology, **9**, 33–52.

Deacon, E. L. (1970) The derivation of Swinbank's longwave radiation formula, Quarterly Journal of the Royal Meteorological Society, **96**, 313–319.

Dirmhirn, I. and F. D. Eaton (1975) Some characteristics of the albedo of snow, Journal of Applied Meteorology, **14**, 375–379.

Dobesch, H. (1980) Die Parametrisierung der atmosparischen Gegenstrahlung im Ostalpenraum, Archiv fur Meteorologie, Geophysik und Bioklimatologie, Serie B, **28**, 365–371.

Douglas, G. W. and L. C. Bliss (1977) Alpine and high subalpine plant communities of the North Cascades Range, Washington and British Columbia, Ecological Monographs, **47**, 113–150.

Dozier, J. (1980) A clear-sky spectral solar radiation model for snow-covered mountainous terrain, Water Resources Research, **16**, 709–718.

Dozier, J. (1987) Recent research in snow hydrology, Reviews of Geophysics, **25**, 153–161.

Dunne, T. and A. G. Price (1975) Estimating daily net radiation over a snowpack, Climatological Bulletin, **18**, 40–48.

Dyer, A. J. (1967) The turbulent transport of heat and water vapour in an unstable atmosphere, Quarterly Journal of the Royal Meteorological Society, **93**, 501–508.

Dyer, A. J. (1974) A review of flux-profile relationships, Boundary-Layer Meteorology, 7, 363–372.

Dyer, A. J. and E. F. Bradley (1982) An alternative analysis of flux-gradient relationships at the 1976 ITCE, Boundary-Layer Meteorology, **22**, 3–19.

Dyer, A. J. and B. B. Hicks (1970) Flux-gradient relationships in the constant flux layer, Quarterly Journal, Royal Meteorological Society, **96**, 715–721.

Eley, F. J. (1987) Current Reseach Needs in Mountain Hydrometeorlogy, (Canadian Climate Centre Report No. 87–10), 68 pp.

Fitzharris, B. B., D. Stewart and W. Harrison (1980) Contribution of snowmelt to the October 1978 flood of the Pomahaka and Fraser Rivers, Otago, Journal of Hydrology (New Zealand), **19**, 84–93.

Flohn, H. (1974) Contribution to a comparitive meteorology of mountain areas, in: Ives, J. D. and R. G. Barry (eds) Arctic and Alpine Environments, (Methuen), 55–71.

Fohn, P. M. B. (1973) Short-term snow melt and ablation derived from heat- and mass-balance measurements, Journal of Glaciology, **12**, 275–289.

Fritschen, L. J. (1967) Net and solar radiation relations over irrigated field crops, Agricultural Meteorology, **4**, 55–62.

Fritschen, L. J. and J. R. Simpson (1989) Surface energy and radiation balance systems: general description and improvements, Journal of Applied Meteorology, **28**, 680–689.

Fuchs, M. and C. B. Tanner (1968) Calibration and field test of soil heat flux plates, Soil Science Society of America, Proceedings, **32**, 326–328.

Fuggle, R. F. (1970) A computer programme for determining direct short-wave radiation income on slopes, Climatological Bulletin, 7, 8–16.

Fuquay, D. and K. Buettner (1957) Laboratory investigation of some characteristics of the Eppley pyrheliometer, Transactions, American Geophysical Union, **38**, 38–43.

Garnier, B. J. and A. Ohmura (1968) A method of calculating the direct shortwave radiation income of slopes, Journal of Applied Meteorology, 7, 796–800.

Garrett, A. J. (1977) A comparison of the observed longwave radiation flux to calculations based on Kondratyev's and Brunt's methods, Archiv fur Meteorologie, Bioklimatologie und Geophysik, Serie B, **25**, 127–134.

Gates, D. M. and R. Janke (1966) The energy environment of the alpine tundra, Oecologia Plantarum, **1**, 39–61.

Gay, L. W. (1971) The regression of net radiation upon solar radiation, Archiv für Meteorologie, Geophysik, und Biolkimatologie, Serie B, **19**, 1–14.

Gerdel, R. W. (1954) The transmission of water through snow, Transactions, American Geophysical Union, **35**, 475–485.

Goodison, B. (1972) The distribution of global radiation over Peyto Glacier, Alberta, Environment Canada, IWD, Scientific Series, **22**, 22 pp.

Granger, R. J. and D. H. Male (1978) Melting of a prairie snowpack, Journal of Applied Meteorology, **17**, 1833–1842.

Grant, D. R. (1975) Comparison of evaporation measurements using different methods, Quarterly Journal of the Royal Meteorological Society, **101**, 543–550.

Gray, D. M. and P. G. Landine (1987) Albedo model for shallow prairie snow covers, Canadian Journal of Earth Science, **24**, 1760–1768.

Green, A. J. and T. M. Lord (1979) Soils of the Princeton area of British Columbia, (Agriculture Canada; Report No.14, British Columbia Soil Survey), 134 pp.

Greenland, D., N. Caine and O. Pollak (1984) The summer water budget and its importance in the alpine tundra of Colorado, Physical Geography, **5**, 221–239.

Häckel, H. (1978) Der Energiehaushalt einer Alnwiese dargestellt am Beispiel eines Tages aus der Trockenperiode von 1976. Schweizerische Meteorologische Zentralanstalt, Veroffentlichung, **40**, 240–242.

Halbsguth, G., M. J. Kerschgens, H. Kraus, G. Meindl and E. Schaller (1984) Energy fluxes in an alpine valley, Archiv fur Meteorlogie, Geophysik und Bioklimatologie, Serie B, **33**, 11–20.

Halliwell, D. H. and W. R. Rouse (1987) Soil heat flux in permafrost: characteristics and accuracy of measurement, Journal of Climatology, **7**, 571–584.

Hatfield, J. L., R. J. Reginato and S. B. Idso (1983) Comparison of long-wave radiation calculation methods over the United States, Water Resources Research, **19**, 285–288.

Haurwitz, G. (1948) Insolation in relation to cloud type, Journal of Meteorology, **5**, 110–113.

Hay, J. E. (1979) An analysis of solar radiation data for British Columbia, (RAB Bulletin 14, Province of British Columbia), 125 pp.

Hay, J. E. and B. B. Fitzharris (1988) The synoptic climatology of ablation on a New Zealand glacier, Journal of Climatology, **8**, 201–215.

Hay, J. E. and D. C. McKay (1985) Estimating solar irradiance on inclined surfaces: a review and assessment of methodologies, International Journal of Solar Energy, **3**, 203–240.

Hay, J. E. and P. W. Suckling (1978) Problems associated with the determination of solar radiation fluxes in the Cordilleran region of Western Canada, in: Hage, K. D. and E. R. Reinelt (eds) Essays on Meteorology and Climatology: in honour of Richmond W. Longley, (Geographical Monograph 3, Department of Geography, University of Alberta), 71–94.

Hay, J. E. and D. I. Wardle (1982) An assessment of the uncertainty in measurements of solar radiation, Solar Energy, **29**, 271–278. W. Longley, (Geographical Monograph 3, Department of Geography, University of Alberta), 71–94.

Heilman, J. L, C. L. Brittin and C. M. U. Neale (1989) Fetch requirements for Bowen ratio measurements of latent and sensible heat fluxes, Agricultural and Forest Meteorology, **44**, 261–273.

Hicks, B. B. and H. C. Martin (1972) Atmospheric turbulent fluxes over snow, Boundary-Layer Meteorology, **2**, 496–502.

Hillel, D. (1982) Introduction to Soil Physics, (Academic; New York), 364 pp.

Idso, S. B. (1981) A set of equations for full spectrum and 8- to 14-μm and 10.5- to 12.5μm thermal radiation from cloudless skies, Water Resources Research, **17**, 295–304.

Idso, S. B. and R. D. Jackson (1969) Thermal radiation from the atmosphere, Journal of Geophysical Research, **74**, 5397–5403.

Isard, S. A. (1983) Estimating potential direct insolation to alpine terrain, Arctic and Alpine Research, **15**, 77–89.

Isard, S. A. (1986) Evaluation of models for predicting insolation on slopes within the Colorado alpine tundra, Solar Energy, **36**, 559–564.

Isard, S. A. (1989) Topoclimatic controls in an alpine fellfield and their ecological significance, Physical Geography, **10**, 13–31.

Isard, S. A. and M. J. Belding (1989) Evapotranspiration from the alpine tundra of Colorado, USA, Arctic and Alpine Research, **21**, 71–82.

Ives, J. D. (1985) Mountain environments, Progress in Physical Geography, **9**, 425–433.

Ives, J. D. (1986) Mountain environments, Progress in Physical Geography, **10**, 437–445.

Karrasch, H. (1973) Microclimatic studies in the Alps, Arctic and Alpine Research, **5**, A55–A63.

Körner, Ch. and R. Mayr (1981) Stomatal behaviours in alpine plant communities between 600 and 2600 metres above sea level, in: Grace, J., E. D. Ford and P. G. Jarvis (1981) Plants and their Atmospheric Environment, Blackwell, Oxford), 205–218.

Kraus, H. (1971a) Ein Beitrag zum Wärme- und Strahlungshaushalt im Himalaya-Gebirge, Archiv fur Meteorologie, Geophysik und Bioklimatologie, Serie A, **20**, 175–182.

Kraus, H. (1971b) Der Tagesgang des Energiehaushaltes in einem Hochgebirgstal, Annalen der Meteorologie Neue Folge, **5**, 103–106.

Lang, H. (1981) Is evaporation an important component in high alpine hydrology? Nordic Hydrology, **12**, 217–224.

Latimer, J. R. (1972) Radiation Measurement, (National Research Council of Canada), 40 pp.

LeDrew, E. F. (1975a) The estimation of clear sky atmospheric emittance at high altitude, Arctic and Alpine Research, **7**, 227–236.

LeDrew, E. F. (1975b) The energy balance of a mid-latitude alpine site during the growing season, 1973, Arctic and Alpine Research, **7**, 301–314.

LeDrew, E. F. and J. C. Emerick (1974) A mechanical balance-type lysimeter for use in remote environments, Agricultural Meteorology, **13**, 253–258.

LeDrew, E. F. and G. Weller (1978) A comparison of the radiation and energy balance during the growing season for an arctic and alpine tundra, Arctic and Alpine Research, **10**, 665–678.

Lewis, M. C. and T. V. Callaghan (1976) Tundra, in: Monteith, J. L. (ed) Vegetation and the Atmosphere, Volume 2: Case Studies, (Academic), 399–433.

Lougeay, R. (1970) Microclimatological studies over the Seaward Glacier snowpack, in: Bushnell, V. C. and M. G. Marcus (eds) Icefield Ranges Research Project, Scientific Results, **4**, 17–26.

Lougeay, R. and A. Brazel (1982) A preliminary test of atmospheric emittance equations at high altitude, Archives for Meteorology, Geophysics and Bioclimatology, Series B, **30**, 227–237.

Lourence, F. J. and W. O. Pruitt (1969) A psychrometer system system for micrometeorology profile determination, Journal of Applied Meteorology **8**, 492–498.

Löve, D. (1970) Subarctic and subalpine: where and what? Arctic and Alpine Research, **2**, 63–73.

Lowe, P. R. (1977) An approximating polynomial for the computation of saturation vapour pressure, Journal of Applied Meteorology, **16**, 100–103.

Male, D. H. (1980) The seasonal snowcover. In: Colbeck, S. C. (ed) Dynamics of Snow and Ice Masses, (Academic press), 305–395.

Male, D. H. and R. J. Granger (1981) Snow surface energy exchange, Water Resources Research, **17**, 609–627.

Male, D. H. and D. M. Gray (1975) Problems in developing a physically based snowmelt model, Canadian Journal of Civil Engineering, **2**, 474–488.

Male, D. H. and D. M. Gray (1981) Snowcover ablation and runoff. In: Gray, D. M. and D. H. Male (eds) Handbook of Snow, (Pergamon Press), 360–436.

Marcus, M. G., A. J. Brazel, R. Lougeay and A. D. Hyers (1981) Long-wave radiation enhancement by cirque wall emittance, Front Range, Colorado, in: Brazel, A. J. (ed), Research Papers in Climatology, (Geographical Publication No. 1, Department of Geography, Arizona State University), 21–42.

Marks, D. and J. Dozier (1979) A clear-sky longwave radiation model for remote Alpine areas, Archiv fur Meteorologie, Geophysik und Bioklimatologie, Serie B, **27**, 159–187.

Marsh, P., W. R. Rouse and M-K. Woo (1981) Evaporation at a high arctic site, Journal of Applied Meteorlogy, **20**, 713–716.

McKay, D. and G. W. Thurtell (1978) Measurements of the energy fluxes involved in the energy budget of a snow cover, Journal of Applied Meteorlogy, **17**, 329–349.

McNaughton, K. G. and P. G. Jarvis (1983) Predicting effects of vegetation changes on transpiration and evaporation, in: Koslowski, T. T. (ed.), Water Deficits and Plant Growth, Volume III, Academic Press, New York), 1–47.

Melcon, P. Z. (1975) Tors and Weathering on McKeen Ridge, Cathedral Provincial Park, British Columbia, (unpublished M. A. thesis, Department of Geography, Simon Fraser University), 183 pp.

Middleton, W. E. K. and A. F. Spilhaus (1953) Meteorological Instruments, (Univ. Toronto), 286 pp.

Miller, D. H. (1981) Energy at the Surface of the Earth, (Academic Press), 516 pp.

Monteith, J. L. (1965) Evaporation and the Environment, Symposium, Society of Experimental Biology, **19**, 205–234.

Monteith, J. L. (1973) Principles of Environmental Physics, (Edward Arnold), 241 pp.

Monteith, J. L. and G. Szeicz (1961) The radiation balance of bare soil and vegetation, Quarterly Journal, Royal Meteorological Society, **87**, 159–170.

Moore, R. D. (1983a) Comparison of the snowmelt energy budgets in two alpine basins, Archiv fur Meteorologie, Geophysik und Bioklimatologie, Serie B, **33**, 1–10.

Moore, R. D. (1983b) On the use of bulk aerodynamic formulae over melting snow, Nordic Hydrology, **14**, 193–206.

Moore, R. D. and I. F. Owens (1984) Controls on advective snowmelt in a maritime alpine basin, Journal of Climate and Applied Meteorology, **23**, 135–142.

Morris, E. M. (1989) Turbulent transfer over snow and ice, Journal of Hydrology, **105**, 205–223.

Müller, H. (1985) On the radiation budget in the Alps, Journal of Climatology, **5**, 445–462.

Munro, D. S. (1975) Energy exchange on a melting glacier, unpublished Ph.D. thesis, McMaster University.

Munro, D. S. (1980) A portable differential psychrometer system, Journal of Applied Meteorology, **19**, 206–214.

Munro, D. S. (1989) Surface roughness and bulk heat transfer on a glacier: comparison with eddy correlation, Journal of Glaciology, **35**, 343–348.

Munro, D. S. and G. J. Young (1982) An operational net shortwave radiation model for glacier basins, Water Resources Research, **18**, 220–230.

Ohmura, A. (1970) The influence of the skyline on the incidence of direct short-wave radiation, Climatological Bulletin, **7**, 17–24.

Oke, T. R. (1987) Boundary Layer Climates, (Methuen), 372 pp.

Olyphant, G. A. (1986a) The components of incoming radiation within a mid-latitude alpine watershed during the snowmelt season, Arctic and Alpine Research, **18**, 163–169.

Olyphant, G. A. (1986b) Longwave radiation in mountainous areas and its influence on the energy balance of alpine snowfields, Water Resources Research, **22**, 62–66.

Olyphant, G. A. and S. A. Isard (1987) Some characteristics of turbulent transfer over alpine surfaces during the snowmelt-growing season: Niwot Ridge, Front Range, Colorado, U.S.A., Arctic and Alpine Research, **19**, 261–269.

Olyphant, G. A. and S. A. Isard (1988) The role of advection in the energy balance of late-lying snowfields: Niwot Ridge, Front Range, Colorado, Water Resources Research, **24**, 1962–1968.

Paltridge, G. W. (1970) Day-time long-wave radiation from the sky, Quarterly Journal, Royal Meteorological Society, **96**, 645–653.

Paltridge, G. W. and C. M. R. Platt (1976) Radiative processes in meteorology and climatology, (Elsevier: Developments in Atmospheric Science, 5), 318 pp.

Paterson, W. S. B. (1981) The Physics of Glaciers, (Pergamon), 380 pp.

Penman, H. L. (1948) Natural evaporation from open water, bare soil and grass, Proceedings, Royal Society of London, Series A, **193**, 120–145.

Petzold, D. E. (1980) An estimation technique for net longwave and net radiation over snow at Toronto, Goose Bay and Resolute, Canada, Archiv fur Meteorologie, Geophysik und Bioklimatologie, Serie B, **28**, 73–90.

Price, A. G. and D. E. Petzold (1984) Surface emissivities in a boreal forest during snowmelt, Arctic and Alpine Research, **16**, 45–51.

Price, L. W. (1981) Mountains and Man, (University of California Press), 506 pp.

Priestley, C. H. B. and R. J. Taylor (1972) On the assessment of surface heat flux and evaporation using large scale parameters, Monthly Weather Review, **100**, 81–92.

Prowse, T. D. and I. F. Owens (1982) Energy balance over melting snow, Craigieburn Range, New Zealand, Journal of Hydrology (New Zealand), **21**, 133–147.

Pruitt, W. O., D. L. Morgan and F. J. Lourence (1973) Momentum and mass transfers in the surface boundary layer, Quarterly Journal, Royal Meteorological Society, **99**, 370–386.

Ratcliffe, M. J. and R. Turkington (1987) Vegetation patterns and environment of some alpine plant communities, Lakeview Mountain, southern British Columbia, Canadian Journal of Botany, **65**, 2507–2516.

Rice, H. M. A. (1947) Geology and mineral deposits of the Princeton map-area, Geological Survey of Canada, Memoir, **243**, 136 pp.

Robinson, N. (1966) Solar Radiation, (Elsevier), 347 pp.

Rott, J. (1979) Vergleichende Untersuchungen der Energiebilanz im Hochebirge, Archiv fur Meteorlogie, Geophysik und Bioklimatologie, Serie B, **28**, 211–232.

Rouse, W. R. (1982) The water balance of upland tundra in the Hudson bay lowlands – measured and modelled, Naturaliste Canadien, **109**, 457–467.

Rouse, W. R. (1984a) Microclimate at arctic tree line. 1. Radiation balance of tundra and forest, Water Resources Research, **20**, 57–66.

Rouse, W. R. (1984b) Microclimate at arctic tree line. 2. Soil microclimate of tundra and forest, Water Resources Research, **20**, 67–73.

Rouse, W. R. and R. B. Stewart (1972) A simple model for determining evaporation from high-latitude upland sites, Journal of Applied Meteorology, **11**, 1063–1070.

Rouse, W. R., P. F. Mills and R. B. Stewart (1977) Evaporation in high latitudes, Water Resources Research, **13**, 909–914.

Rouse, W. R., S. G. Hardill and P. Lafleur (1987) The energy balance in the coastal environment of James Bay and Hudson Bay during the growing season, Journal of Climatology, **7**, 165–179.

Sauberer, F. and I. Dirmhirn (1953) Der Strahlungshaushalt horizontaler Gletscherflächen auf dem hohen Sonnblick, Geografiska Annaler, **35**, 261–290.

Sauberer, F. and I. Dirmhirn (1958) Das Strahlungsklima, in: Steinhauser, F. (ed) Klimatographie von Osterreich, (Springer-Verlag), 13–102.

Serreze, M. C. and R. S. Bradley (1987) Radiation and cloud observations on a high arctic plateau ice cap, Journal of Glaciology, **33**, 162–168.

Slatyer, R. D. and I. C. McIlroy (1961) Practical Microclimatology, (CSIRO, Australia), 310 pp.

Slaymaker, O. (1983) High mountain environments, Progress in Physical Geography, 7, 120–130.

Slaymaker, O. (1984) High mountain environments, Progress in Physical Geography, **8**, 118–128.

Smithson, P. A. (1989) Micro– and mesoclimatology, Progress in Physical Geography, **13**, 103–114.

Soares, J. V., R. Bernard, O. Taconet, D. Vidal–Madjar and A. Weill (1988) Estimation of bare soil evapration from airborne measurements, Journal of Hydrology, **99**, 281–296.

Staudinger, M. and H. Rott (1981) Evapotranspiration at two mountain sites during the vegetation period, Nordic Hydrology, **12**, 207–221.

Stewart, R. B. and W. R. Rouse (1976) Simple models for calculating evaporation from dry and wet surfaces, Arctic and Alpine Research, **8**, 263–274.

Stewart, R. B. and W. R. Rouse (1977) Substantiation of the Priestley and Taylor parameter $\alpha = 1.26$ for potential evaporation in high latitudes, Journal of Applied Meteorology, **16**, 649–650.

Storr, D. (1972) Estimating effective net radiation for a mountainous watershed, Boundary–Layer Meteorlogy, **3**, 3–14.

Storr, D. and G. Den Hartog (1975) Gamma – the psychrometer non–constant, Journal of Applied Meteorology, **14**, 1397–1398.

Swift, L. W. (1976) Algorithm for solar radiation on mountain slopes, Water Resources Research, **12**, 108–112.

Swinbank, W. C. (1951) The measurement of vertical transfer of heat and water vapour by eddies in the lower atmosphere, Journal of Meteorology, **8**, 135–145.

Swinbank, W. C. (1963) Long–wave radiation from clear skies, Quarterly Journal, Royal Meteorological Society, **89**, 339–348.

Swinbank, W. C. and A. J. Dyer (1967) An experimental study in micro–meteorology, Quarterly Journal of the Royal Meteorological Society, **93**, 494–500.

Szeicz, G. (1975) Instruments and their exposure, in: Monteith, J. L. (ed) Vegetation and the Atmosphere, (Academic Press), 229–273.

Tanner, B. D., M. S. Tanner, W. A. Ducas, E. C. Campbell, and B. L. Bland (1985) Evaluation of an operational eddy correlation system for evapotranspiration measurements. In: Proceedings, National Conference on Advances in Evapotranspiration, December 16–17, 1985, Chicago, (Am. Soc. Agr. Engr.), 87–99.

Terjung, W. H., R. N. Kickert, G. L. Potter and S. W. Swarts (1969a) Terrestrial, atmospheric and solar radiation fluxes on a high desert mountain in mid–July: White Mountain Peak, California, Solar Energy, **12**, 363–375.

Terjung, W. H., R. N. Kickert, G. L. Potter and S. W. Swarts (1969b) Energy and moisture balances of an alpine tundra in mid–July, Arctic and Alpine Research, **1**, 247–266.

Thom, A. S. (1972) Momentum, mass and heat exchange of vegetation, Quarterly Journal of the Royal Meteorological Society, **98**, 124–134.

Thom, A. S. (1975) Momentum, mass and heat exchange of plant communities, in: Monteith, J. L. (ed) Vegetation and the Atmosphere, (Academic), 57–109.

Valentine, D. A. and W. G. Bailey (1990) Application of the Priestley-Taylor evaporation model and its variants in Canada, Western Geography, **1**, 49–62.

Walton, D. W. H. (1982) Instruments for measuring biological microclimates for terrestrial habitats inpolar and high alpine regions: a review, Arctic and Alpine Research, **14**, 275–286.

Wagner, H. P. (1979) Strahlungshaushaltsuntersuchungen an einem Ostalpengletscher wahrend der Hauptablationsperiode. Teil I: Kurzwellige Strahlung. Archiv fur Meteorologie, Geophysik und Bioklimatologie, Serie B, **27**, 297–324.

Wagner, H. P. (1980) Strahlungshaushaltsuntersuchungen an einem Ostalpengletscher wahrend der Hauptablationsperiode. Teil II: Langwellige Strahlung und Strahlungsbilanz, Archiv fur Meteorologie, Geophysik und Bioklimatologie, Serie B, **28**, 41–62.

Warren, S. G. (1982) Optical properties of snow, Reviews of Geophysics and Space Physics, **20**, 67–89.

Wendler, G. and J. Kelley (1988) On the albedo of snow in Antarctica: a contribution to IAGO, Journal of Glaciology, **34**, 16–26.

Whiteman, C. D., K. J. Allwine, L. J. Fritschen, M. M. Orgill and J. R. Simpson (1989a) Deep valley radiation and surface energy budget microclimates. Part I: Radiation, Journal of Applied Meteorology, **28**, 414–426.

Whiteman, C. D., K. J. Allwine, L. J. Fritschen, M. M. Orgill and J. R. Simpson (1989b) Deep valley radiation and surface energy budget microclimates. Part II: Energy budget, Journal of Applied Meteorology, **28**, 427–437.

Willmott, C. J. (1981) On the validation of models, Physical Geography, **2**, 184–194.

Willmott, C. J. (1982) Some comments on the evaluation of model performance, Bulletin, American Meteorological Society, **63**, 1309–1313.

Wilson, R. G. and B. J. Garnier (1975) Calculated and measured net radiation for a slope, Climatological Bulletin, **12**, 1–14.

Wilson, R. G. and J. H. McCaughey (1971) Soil heat flux divergence in a developing corn crop, Climatological Bulletin, **9**, 9–16.

Wright, R. K. (1981) The Water Balance of a Lichen Tundra Underlain by Permafrost, (McGill Subarctic Research Paper No. 33), 110 pp.